Department of Civil Engineering
The University of Glasgow

UNIVERSITY
of
GLASGOW

Constitutive and Numerical Modelling of Unsaturated Soils

by

Domenico Gallipoli

Thesis submitted to the University of Glasgow
in candidature for the degree of
Doctor of Philosophy

September, 2000

A Mia Nonna Isabella

To My Grandmother Isabella

Abstract

The thesis focuses on three different areas: development of constitutive models for unsaturated soils, improvement of the finite element code "Compass" for coupled flow-deformation analysis involving unsaturated soils and application of the improved code to the simulation of pressuremeter tests in unsaturated soils.

On the constitutive side, a unique relationship is proposed between degree of saturation, suction and specific volume, by introducing dependency on specific volume in the simplified van Genuchten [48] equation. This is a significant improvement over the common assumption of a state surface expression for degree of saturation. If combined with an elasto-plastic stress-strain model predicting the variation of specific volume, the proposed relationship is capable of reproducing irreversible changes of degree of saturation and changes of degree of saturation experimentally observed during shearing. Predictions show very good agreement with experimental results from tests on compacted Speswhite Kaolin published in the literature.

On the numerical side, a number of changes to the code "Compass" have been performed. The new relationship for degree of saturation is implemented in the code and the implementation is validated against three benchmark problems. Use of the new relationship for degree of saturation results in significantly different predictions to those obtained if a conventional state surface expression for degree of saturation is used (as present in the original code).

Implementation of the water and air continuity equations in "Compass" has been corrected by expressing these equations in terms of flux velocities relative to the soil skeleton. This is the form in which the equations should be expressed if they are to be combined with Darcy's law for liquid and gas flows. The simulation of a notional laboratory test shows that the incorrect combination of Darcy's law with absolute flux velocities, as present in the original code, causes significant errors.

The convergency algorithm at constitutive level employed in the code has been corrected by introducing residual flux terms in the two flow equations, analogous to residual forces in the equilibrium equation. These terms must be taken into account if a convergency algorithm for an elasto-plastic stress-strain model is used and the relationship assumed for variation of degree of saturation involves any dependency on net stresses. A numerical study of a notional laboratory test shows that omission of residual flux terms results in substantial errors and may cause failure to converge.

The plane-strain formulation of code "Compass" has been corrected by imposing the condition of nullity only on the out-of-plane component of the total strain rate vector instead of the out-of-plane component of each single contribution to the total strain rate, as was done in the original code. Such inconsistency, due to the history of development of finite element programs, also appears in other examples published in the literature. Numerical simulations of two types of bi-axial tests show that significantly different results are generally predicted by the correct and incorrect formulations, and also provide an

explanation why this type of error was difficult to detect in codes implementing traditional models for saturated soils.

The potential of the enhanced version of code "Compass" for analysing boundary value problems is demonstrated by simulations of pressuremeter tests in unsaturated soil. This study also provides some initial insight into the interpretation of pressuremeter tests in unsaturated soil, by simulating tests at different loading rates in a normally consolidated soil. The mechanical behaviour of the soil is represented by the elasto-plastic model of Alonso, Gens and Josa [1] while the variation of degree of saturation is modelled by the new relationship proposed in the thesis. The entire range of loading rates, from undrained to fully drained (with respect to liquid), is simulated. Relatively small changes of suction are predicted even in the fastest test and the computed cavity pressure-cavity strain relationships are all very similar regardless of loading rate. It may therefore be possible to model even rapid pressuremeter tests in unsaturated soils as a drained (constant suction) process. Further work is required to investigate the generality of this conclusion.

Contents

Acknowledgements

I wish to take this opportunity to express my sincere gratitude to the following people from whom, for different reasons, I derived great benefit during the period of my study.

I am greatly indebted to my supervisors Prof. Simon Wheeler and Dr. Minna Karstunen for the high standard of their supervision throughout this research. During the weekly discussions on the progress of my work, I derived great benefit not only for the completion of the project but also for my scientific and personal enrichment in general. Their clear sense of direction and constructive criticism were influential at all stages of the work. I also wish to thank them for their valuable opinions, which were important for the choices of my career after these studies.

I am grateful to Prof. Hywel Thomas and Dr. Yang He, University of Cardiff, for providing the finite element code "Compass" and for offering their useful support during the initial period of familiarization with the code. Prof. Antonio Gens, Universitat Politecnica de Catalunya, provided inspiring discussions on a number of issues of this work during his visit to the Department of Civil Engineering at Glasgow. I also wish to thank Prof. Fernando Schnaid, Universidade Federal do Rio Grande do Sul, for his important advice and positive criticism on the part of this thesis related to the numerical simulation of pressuremeter tests in unsaturated soils. I am also grateful to Prof. Luciano Picarelli, Seconda Universitá di Napoli, for the frequent e-mail discussions throughout the period of my stay in Glasgow.

Further thanks are extended to Prof. Nenad Bicanic, Head of the Civil Engineering Department, and with him to the academic and technical staff of the Civil Engineering Department for giving me the opportunity to use the excellent facilities and for helping

me whenever I needed advice and support. In particular I wish to thank the Computer Manager Mr. Kenny McColl who always provided solutions to my requests relating to computing facilities.

I gratefully acknowledge the financial support received from the Faculty of Engineering of the University of Glasgow during the first three years of my study and from the Italian Consiglio Nazionale delle Ricerche during the last six months.

I also wish to thank people who have been part of my social life during the past three and a half years, for sharing with me unforgettable emotions in different circumstances of my life in Glasgow. In particular my thanks go to Alessandra, Alison, Amanda, Andy, Attilio, Beatrice, Cecilia, Christelle, Claire, Debbie, Egle, Eliane, Federico, Fiona, Giovanni, Lee, Linda, Lisa, Marc B., Maureen, Mynur, Rino and all the group of the FA Club (i.e. Francesco, Marc S., Pasquale, Roberto). For each of these persons there is at least one story worth telling.

My gratitude is also to the colleagues with whom I shared the office in the past years, Alan, Andrey, Chen, Chris, Kevin, Kourosh, Lim, Xiaoya and William who patiently had to bear my presence every single day! Thanks for the chats and jokes, which opportunely broke the time spent concentrating on a book or in front of a computer screen.

Finally, my deepest thanks go to my parents "papá" Martino and "mamma" Giuseppina and all the rest of my family for their encouragement and support especially in the stressful moments. In particular, I wish to thank my two brothers Giovanni and Paolo for visiting me during my stay in Scotland and for sharing with me a lot of fun on those occasions.

Notation

A_s	elastic volumetric compressibility due to a change of s
$\mathbf{B}$	differential operator of strains
$\hat{\mathbf{B}}$	strain matrix
$\mathcal{C}$	mass matrix $\left[\begin{array}{c} \mathcal{C}_f \\ \hline \mathcal{C}_u \end{array}\right] = \left[\begin{array}{ccc} \mathbf{C}_{ww} & \mathbf{C}_{wa} & \mathbf{C}_{wu} \\ \mathbf{C}_{aw} & \mathbf{C}_{aa} & \mathbf{C}_{au} \\ \hline \mathbf{C}_{uw} & \mathbf{C}_{ua} & \mathbf{C}_{uu} \end{array}\right]$
$\mathbf{D}$	elastic stiffness matrix
$\mathcal{F}$	yield locus
G	elastic shear modulus
$\mathcal{G}$	auxiliary yield locus
H	Henry's coefficient of solubility
K	elastic bulk modulus
K_{nc}	coefficient of earth pressure at rest in normally consolidated soil
K_o	coefficient of earth pressure at rest in overconsolidated soil
$\mathcal{K}$	stiffness matrix $\left[\begin{array}{c} \mathcal{K}_f \\ \hline \mathcal{K}_u \end{array}\right] = \left[\begin{array}{ccc} \mathbf{K}_{ww} & 0 & 0 \\ \mathbf{K}_{aw} & \mathbf{K}_{aa} & 0 \\ \hline 0 & 0 & 0 \end{array}\right]$
M	slope of critical state line at constant s in $(q,\bar{p})$-plane
$\mathbf{N}$	shape function vector
OCR	overconsolidation ratio
$\mathcal{Q}$	plastic potential
R_o	radius of pressuremeter
$\mathcal{R}$	residual vector $\left[\begin{array}{c|c} \mathcal{R}_f & \mathcal{R}_u \end{array}\right]^T = \left[\begin{array}{cc|c} \psi_w & \psi_a & \phi_u \end{array}\right]^T$
S_e	effective degree of saturation
S_r	degree of saturation
S_{res}	residual degree of saturation
$\hat{\boldsymbol{S}}_r$	vector of nodal values of S_r
$\mathcal{T}$	flux vector $\left[\begin{array}{c|c} \mathcal{T}_f & \mathcal{T}_u \end{array}\right]^T = \left[\begin{array}{cc|c} t_w & t_a & t_u \end{array}\right]^T$
V	volume

a	parameter for state surface relationships of Equations 2.15, 2.40 and 2.41
a	current cavity radius at mid-height of the pressuremeter membrane
a_o	initial cavity radius at mid-height of the pressuremeter membrane
b	parameter for state surface relationships of Equations 2.15, 2.40 and 2.41
$\boldsymbol{b}$	body force vector $(b_x\ b_y\ b_z)^T$
c	parameter for state surface relationships of Equations 2.15, 2.40 and 2.41
c'	cohesion in saturated conditions
c_v	coefficient of consolidation
d	parameter for state surface relationships of Equations 2.15, 2.40 and 2.41
e	void ratio
e_a	air void ratio
g	gravitational acceleration
g_2	derivative of reversible part of the change of S_r with respect to s
g_3	derivative of $S_r(v,s)$ relationship of Equation 4.5 with respect to v
g_4	derivative of $S_r(v,s)$ relationship of Equation 4.5 with respect to s
$\boldsymbol{g}_1$	derivative of reversible part of the change of S_r with respect to $\overline{\boldsymbol{\sigma}}$
h_a	gas head
h_w	hydraulic head
k	parameter controlling cohesion increase with s
k_a	coefficient of permeability with respect to gas phase
k_d	coefficient of permeability with respect to gas phase at $S_r = S_{res}$
k_s	coefficient of permeability with respect to liquid phase at $S_r = 1$
k_w	coefficient of permeability with respect to liquid phase
m	parameter for $S_r(v,s)$ relationship of Equation 4.5
$\boldsymbol{m}$	$(1\ 1\ 1\ 0\ 0\ 0)^T$
n	porosity
n	parameter for $S_r(v,s)$ relationship of Equation 4.5
$\boldsymbol{n}$	$(1\ 1\ 0\ 0\ 0\ 0)^T$
p_{atm}	atmospheric pressure
p^c	reference pressure
$\overline{p}$	mean net stress
$\overline{p}_o$	isotropic yield stress at constant s
$\overline{p}_o^*$	isotropic yield stress at $s = 0$
q	deviatoric stress
r	ratio between values of λ at $s \to \infty$ and $s = 0$
s	suction
t	time
$\boldsymbol{t}_u$	vector of nodal external force rates
u_a	pore air pressure
u_w	pore water pressure
$\boldsymbol{u}_d$	vector of soil skeleton displacement $(u_x\ u_y\ u_z)^T$
$\hat{\boldsymbol{u}}_a$	vector of nodal pore air pressure unknowns
$\hat{\boldsymbol{u}}_d$	vector of nodal displacement unknowns
$\hat{\boldsymbol{u}}_w$	vector of nodal pore water pressure unknowns

v	specific volume
v_w	specific water volume
$\boldsymbol{v_a}$	gas flux velocity $(v_{xa}\ v_{ya}\ v_{za})^T$
$\boldsymbol{v_w}$	liquid flux velocity $(v_{xw}\ v_{yw}\ v_{zw})^T$
w	water content
y	elevation

β	parameter controlling variation of λ with s
β	parameter relating ρ_a to u_a (from the gas law)
Γ_{atm}	intercept of critical state line at constant s in $(v, \ln \overline{p})$-plane at $\overline{p} = p_{atm}$
γ	fluidity parameter
$\boldsymbol{\epsilon}$	strain vector $(\epsilon_x\ \epsilon_y\ \epsilon_z\ \gamma_{xy}\ \gamma_{yz}\ \gamma_{zx})^T$
ϵ_c	cavity strain
ϵ_d	deviatoric strain
ϵ_v	volumetric strain
ϵ_w	volumetric strain of the liquid phase
η	pore size distribution index
θ	volumetric water content
$\boldsymbol{\iota}$	vector of nodal internal force rates
κ	elastic swelling index for changes of $\overline{p}$
κ_s	elastic swelling index for changes of s
λ	slope of normal compression line at constant s
μ	intercept of critical state line at constant s in $(q, \overline{p})$-plane at $\overline{p} = 0$
ν	Poisson's ratio
N	intercept of normal compression line at constant s at $\overline{p} = p^c$
N_{atm}	intercept of normal compression line at constant s at $\overline{p} = p_{atm}$
ρ_a	air density
ρ_w	water density
$\overline{\sigma}_h$	horizontal net stress
$\overline{\sigma}_v$	vertical net stress
$\overline{\sigma}_h^{nc}$	horizontal net stress in normally consolidated soil
$\overline{\sigma}_v^{nc}$	vertical net stress in normally consolidated soil
$\boldsymbol{\sigma}$	total stress vector $(\sigma_x\ \sigma_y\ \sigma_z\ \tau_{xy}\ \tau_{yz}\ \tau_{zx})^T$
$\boldsymbol{\sigma'}$	effective stress vector $\left(\sigma'_x\ \sigma'_y\ \sigma'_z\ \tau_{xy}\ \tau_{yz}\ \tau_{zx}\right)^T$
$\overline{\boldsymbol{\sigma}}$	net stress vector $(\overline{\sigma}_x\ \overline{\sigma}_y\ \overline{\sigma}_z\ \tau_{xy}\ \tau_{yz}\ \tau_{zx})^T$
τ	tolerance factor
τ_1	tolerance factor
τ_2	tolerance factor
ϕ	parameter for $S_r(v, s)$ relationship of Equation 4.5
ϕ'	friction angle at constant s
ϕ^b	friction angle controlling increase of strength with s

ψ	slope of critical state line at constant s in $(v, \ln \overline{p})$-plane
ψ	parameter for $S_r(v, s)$ relationship of Equation 4.5
$\boldsymbol{\psi}_a$	vector of nodal residual air fluxes
$\boldsymbol{\psi}_u$	vector of nodal residual forces
$\boldsymbol{\psi}_w$	vector of nodal residual water fluxes
Ω	space domain

Chapter 1

Problem statement

1.1 Introduction

In the last few years increasing research effort has been put into modelling of the mechanical behaviour of unsaturated soils. Unsaturated conditions occur in arid and semi-arid regions, where the upper soil layers never reach a state of complete saturation. Even in temperate climates there is, however, a shallow layer of unsaturated soil close to the ground surface and correct modelling of this limited zone can be relevant to the study of geotechnical design problems. Unsaturated soils are also encountered as compacted fills (for example earth dams, embankments, backfill behind retaining structures, engineered barriers for underground nuclear waste disposal). Safe and cost-effective design of these works, together with the prediction of the consequences of a change of the initial boundary conditions, can be achieved only if the behaviour of unsaturated soil is properly understood. For complex boundary value problems involving numerical analysis, this will require the use of an appropriate constitutive model for unsaturated soil.

The presence of both gas and liquid phases in the pores affects the properties of an unsaturated soil in such a way that classical models for saturated soils based on the use of effective stresses no longer apply. One of the main achievements of research in this field was the acknowledgement that, unlike the saturated case, it is not possible to postulate a constitutive model for unsaturated soils in terms of one effective stress tensor but it is necessary to introduce two independent stress variables to take into account all the features of unsaturated soil behaviour. Significant progress in constitutive modelling has been

achieved in recent years by developing elasto-plastic stress-strain models (see for example Alonso, Gens and Hight [2], Alonso, Gens and Josa [1], Wheeler and Sivakumar [3]) which are able to reproduce the main features of the behaviour of unsaturated soils.

These elasto-plastic constitutive models define a relationship between the stress state (expressed in terms of the relevant stress variables and including the previous variation of these stress parameters) and the traditional strain tensor. They do not provide, however, any information on another strain variable which is essential for a complete description of the hydro-mechanical behaviour of unsaturated soils: that is the variation of degree of saturation, S_r, or another equivalent strain variable which describes the relative proportions of gas and liquid phases inside the soil voids. Neglecting this strain variable limits the range of problems that can be considered. In fact, it is possible to carry out only analysis of uncoupled deformation problems where pore water pressure and pore air pressure remain constant or vary in a pre-defined fashion. Throughout this thesis the expressions "pore water pressure" and "pore air pressure" are equivalent to "pore liquid pressure" and "pore gas pressure" respectively, due to the assumptions that the water is the only liquid species present in the pores and that the presence of water vapour in the gas phase is negligible (the latter assumption is further discussed later).

In order to be able to carry out a coupled flow-deformation analysis it is essential to introduce a further relation between the degree of saturation and the stress parameters. In recent years, when elasto-plastic constitutive models for unsaturated soils have been applied to the study of coupled flow-deformation problems, this lack of information has been overcome by adding to the basic stress-strain model a unique (elastic) relationship, known as a state surface expression, between the variation of degree of saturation and the relevant stress state variables. This approach has severe limitations in providing accurate predictions of the variation of degree of saturation (as explained later). The approach is also inconsistent because it combines an elasto-plastic relationship for the mechanical behaviour with an elastic one for the variation of degree of saturation.

There is, therefore, scope for improvements to existing constitutive models for unsaturated soil addressing the issue of modelling the variation of degree of saturation in a more

consistent fashion with the observed experimental behaviour. In particular, the description of irreversible changes of degree of saturation occurring in unsaturated soils needs to be incorporated in the constitutive model. Irreversible changes of degree of saturation are the consequence of the combination of two different factors: one is the dependence of degree of saturation on elasto-plastic changes of void ratio, the other is the occurrence of hydraulic hysteresis. One of the aims of the research presented in this thesis was to propose an extension to existing elasto-plastic constitutive models for unsaturated soil in order to take into account the influence of the first factor mentioned above on the description of the variation of degree of saturation.

Due to the complexity of boundary conditions, application of advanced constitutive models to practical geotechnical design requires the use of numerical techniques, such as the finite element method. Consequently, in parallel with investigation of constitutive modelling of unsaturated soils, recent research has focused on implementation of the new constitutive models for unsaturated soils in computer programs which could then be used as design tools. One of the most recent contributions in this field is the finite element code "Compass" developed at the University of Cardiff, UK by a research group led by Prof. H.R. Thomas. Another aim of the work presented in this thesis was to extend the finite element code "Compass" inherited from Cardiff both by improving existing techniques for the description of variation of degree of saturation and by enhancing other aspects of the code related to the coupling of flow and deformation. Simple numerical analyses, such as simulations of the behaviour of cylindrical soil specimens, for which it was possible to calculate analytical solutions, were performed in order to verify the correctness of the modifications performed on the code and to assess the implications of the developments undertaken.

In addition to the simple numerical simulations used for verification purposes, code "Compass" was applied to the simulation of pressuremeter tests in unsaturated soil in order to show the capability of the improved code of analysing boundary value problems. These simulations involved elasto-plastic strains and coupling of gas and liquid flows with deformations. The numerical results were also used to assess the effect on a realistic

boundary value problem of changing the modelling of degree of saturation from a state surface expression, as in the original version of the code, to the improved elasto-plastic formulation proposed and implemented in code "Compass" by the author.

The simulations also provide a valuable insight into the interpretation of pressuremeter tests in unsaturated soils. Due to the costly and time-consuming nature of laboratory testing of unsaturated soils, pressuremeter tests constitute an attractive alternative for determining soil parameters values. This technique, although successfully employed in past years in saturated soils, is, however, still highly tentative in the unsaturated case due to the absence of a valid methodology for the interpretation of test results. This work provides some information on important issues for the interpretation of pressuremeter tests in unsaturated soils, such as the effects of the coupling between flow and deformation on the cavity pressure-cavity expansion relationship.

1.2 Layout of the thesis

A review of the main features of the behaviour of unsaturated soils is presented in Chapter 2. The chapter provides a detailed description of the elasto-plastic model of Alonso, Gens and Josa [1] employed in the numerical simulations presented in this thesis.

The selection of values for the various soil constants within the stress-strain model, and within both a state surface relationship for degree of saturation and relationships for the variation of liquid and gas permeabilities with degree of saturation is discussed in Chapter 3. The chosen set of parameters values, defined on the basis of laboratory test results available in the literature for compacted unsaturated Speswhite Kaolin, was employed throughout the numerical analyses performed in this work. In Chapter 3, the selected values for the state surface relationship for degree of saturation are also used to demonstrate the limitations of the approch adopted in the original version of code "Compass" to model the variation of degree of saturation.

In Chapter 4 new ideas are presented for modelling the variation of degree of saturation in an unsaturated soil. The suggested form of variation is proposed on the basis of experimental evidence available in the literature. An explicit expression for representing the

variation of degree of saturation is also presented. This equation assumes a dependency of degree of saturation on specific volume and, consequently, has the capability of predicting irreversible changes of degree of saturation when it is combined with an elasto-plastic stress-strain relationship. Values of the parameters within the suggested equation are selected from laboratory test results on compacted unsaturated Speswhite Kaolin available in the literature. Predictions of both the variation of degree of saturation for different stress paths and the variation of suction during undrained (with respect to the liquid phase) loading, arising from the proposed relationship, are compared with results from laboratory tests to demonstrate the success of the new approach.

In Chapter 5 the extensions and improvements carried out on code "Compass" are described in detail. These changes relate to the following points: implementation of the new relationship for degree of saturation proposed in Chapter 4; modifications to the equations of water and air continuity originally implemented in the code; modifications to the convergency algorithm; correction of the plane-strain deformation regime; introduction of the user option for performing mesh updating; and coding of an interface to the FEMGEN/FEMVIEW commercial software for graphical pre- and post-processing of the data. The implementation of the new relationship for degree of saturation within code "Compass" is also validated by comparison with analytical solutions for three typical stress paths.

In Chapter 6 some numerical analyses of simple problems are presented in order to demonstrate the effect of the extensions and improvements carried out on the original version of code "Compass". In particular the implications of the adoption of the new relationship for degree of saturation are assessed for a simple problem involving coupling of flow and deformation. The results are compared with simulations using the original state surface approach employed in code "Compass". Other simple numerical cases are presented in order to demonstrate the effect of the changes to the code relating to the equations of water and air continuity, the convergency algorithm and the plane-strain deformation regime.

Whereas in Chapters 5 and 6 the results from simple numerical studies are presented

in order to qualitatively assess and validate the changes carried out to code "Compass", in Chapter 7 simulations of pressuremeter tests in unsaturated soil are presented in order to demonstrate the application of the improved version of the code to a more complex boundary value problem. The work illustrated in this chapter also investigates some questions associated with pressuremeter testing in unsaturated soils. In particular the effect of rate of loading on the cavity pressure-cavity expansion response measured during a test is studied and the influence of overconsolidation on the coupling of flow and deformations is considered. Finally the effect of the modelling of the variation of degree of saturation is explored by comparing the results obtained by using the new relationship for degree of saturation proposed in this thesis and those computed by assuming the state surface approach employed in the original version of code "Compass".

Conclusions from the work presented in the thesis are given in Chapter 8. Suggestions for further work include proposals for the introduction of other features of behaviour in the current constitutive models for unsaturated soils, recommendations for further improvement and extension of code "Compass" and an indication for a methodology for the interpretation of pressuremeter test results in unsaturated soils.

Chapter 2

Constitutive Modelling of Unsaturated Soils

2.1 Introduction

This chapter provides a brief review of unsaturated soil behaviour and constitutive modelling for unsaturated soils, with particular emphasis on the elasto-plastic model of Alonso, Gens and Josa [1] which is used for the numerical modelling presented in this thesis. In Chapter 4 some suggestions for further developments for constitutive modelling of unsaturated soils are presented, concentrating in particular on the modelling of variation of degree of saturation.

In Section 2.2 the stress variables needed for modelling the mechanical behaviour of unsaturated soils are introduced and the differences with the saturated case are explained on the basis of a physical argument.

The most important aspects of the behaviour of unsaturated soil (as emerged from laboratory investigations published in the literature) are summarized in Section 2.3. In particular the variations of volume and shear strength with the stress variables are discussed. This section also provides an outline of the initial attempts to model the typical features of unsaturated soil behaviour.

In Section 2.4 the elasto-plastic model of Alonso, Gens and Josa [1] is described in detail and a summary is given of the recent experimental evidence supporting the form of behaviour predicted by the model. The main refinements to the model proposed in recent

years are also presented.

In Section 2.5 the models currently employed in numerical applications for predicting the variation of degree of saturation are introduced. The limitations of these models are also demonstrated on the basis of existing experimental evidence.

Section 2.6 introduces the laws for modelling the flows of the liquid and gas phases which were employed in the numerical analyses presented in this thesis.

2.2 Stress state variables

One of the first attempts to model the mechanical behaviour of unsaturated soils was due to Bishop [4]. He postulated that the strength and the strains could both be related to one single effective stress tensor, like in the saturated case, which could combine the total stress, the pore air pressure and the pore water pressure. If the stress-strain relations are written in a matrix form, the effective stresses proposed by Bishop [4] can be represented by:

$$\boldsymbol{\sigma'} = \boldsymbol{\sigma} - \boldsymbol{m}\left(u_a - \chi(u_a - u_w)\right) \tag{2.1}$$

where $\boldsymbol{\sigma'}$ is the effective stress vector (Equation 2.2), $\boldsymbol{\sigma}$ is the total stress vector (Equation 2.3), χ is a function of the degree of saturation, u_a is the pore air pressure, u_w is the pore water pressure and $\boldsymbol{m}$ is a vector defined by Equation 2.4.

$$\boldsymbol{\sigma'} = \left(\sigma'_x \ \sigma'_y \ \sigma'_z \ \tau_{xy} \ \tau_{yz} \ \tau_{zx}\right)^T \tag{2.2}$$

$$\boldsymbol{\sigma} = \left(\sigma_x \ \sigma_y \ \sigma_z \ \tau_{xy} \ \tau_{yz} \ \tau_{zx}\right)^T \tag{2.3}$$

$$\boldsymbol{m} = (1 \ 1 \ 1 \ 0 \ 0 \ 0)^T \tag{2.4}$$

As already mentioned in Chapter 1, the expressions "pore water pressure" and "pore air pressure" used throughout this thesis are equivalent to "pore liquid pressure" and "pore gas pressure" respectively, due to the assumption that the water is the only liquid species

present in the pores and to the disregard of the presence of water vapour in the gas phase. The latter assumption is further discussed in Chapter 5 where the equations of conservation of the water and air mass are derived.

The postulation of a single effective stress tensor implies that every constitutive model developed and tested for the saturated case could equally describe the unsaturated one, provided that the conventional effective stress tensor for saturated soils is replaced by the effective stress tensor represented in vector form of Equation 2.1.

This approach was subsequently proved to be erroneous by Jennings and Burland [5]. They carried out oedometer and isotropic tests on three different types of soils, providing evidence that the single effective stress approach, postulated by Bishop [4], could not represent the feature of collapse compression on wetting often observed during stress paths involving soaking of the unsaturated sample at constant isotropic stress or constant vertical stress. In their tests they soaked several unsaturated samples by increasing the pore water pressure from the initial value, at constant isotropic or vertical total stress and pore air pressure. According to Equation 2.1 this should have resulted in a decrease of the isotropic effective stress, given that χ is a positive number smaller than 1 for a soil in unsaturated conditions. On the basis of the effective stress principle this decrease in effective stress should be accompanied by an increase in the volume of the soil. The experimental results showed, on the contrary, that the soil sometimes underwent additional compression, suggesting that the single effective stress proposed by Bishop [4] could not be used for describing all the features of the mechanical behaviour of unsaturated soils.

One explanation for the difficulty of modelling the behaviour of unsaturated soils in terms of one effective stress tensor can be found in the analysis of the influence of pore water pressure on inter-particle forces. For a fully saturated soil, changes in the pressure of the liquid filling the voids affect the inter-particle forces in a fashion which is similar to that produced by the application of isotropic stress on the soil element boundary. The application of a total stress on the soil element boundary produces both normal and tangential forces at the inter-particle contacts, even when the applied stress is isotropic. When the tangential force exceeds the friction limit between grains, it will cause slippage

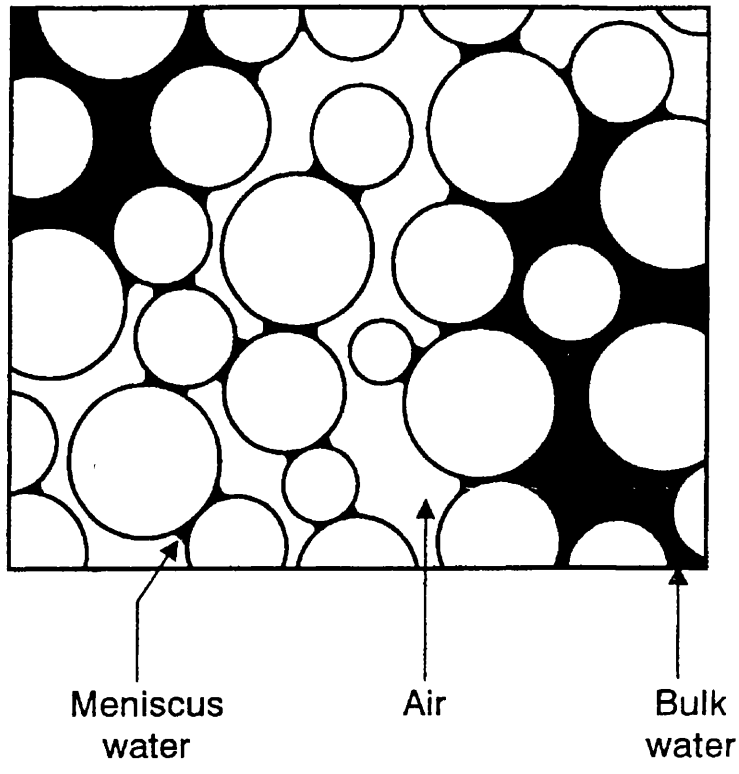

Figure 2.1: Schematic representation of bulk liquid and meniscus liquid within an unsaturated soil (after Wheeler and Karube [7])

between grains and hence plastic deformations. Changes in the pore water pressure within a saturated soil act in the same way, and therefore total stress and pore water pressure can be combined in a unique "effective stress" parameter which governs the mechanical behaviour of the soil.

The same argument does not apply for an unsaturated soil. In this case the liquid phase does not fill all the pores and some of the voids are filled by gas which is at a pressure higher than the liquid. The liquid phase can be present either as "bulk liquid", completely filling a void, or as lenses of "meniscus liquid" surrounding the inter-particle contacts that are not covered by bulk liquid (Kato, Matsuoka and Sun [6]). In Figure 2.1 a schematic representation of the microstructure of the unsaturated soil is shown for the idealized case of spherical particles.

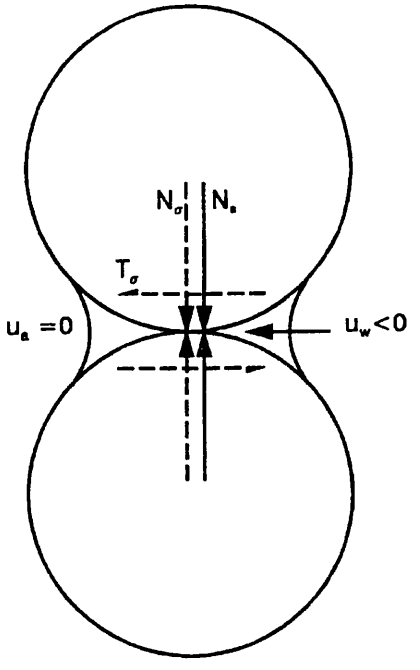

Figure 2.2: Influence of external stress and meniscus liquid on inter-particle forces (after Wheeler and Karube [7])

Negative pore water pressure within the "bulk liquid" acts as it would in the fully saturated case, whereas the negative pore water pressure within "meniscus liquid" produces only an increase of normal forces at the particle contacts, reducing the possibility of slippage and making the particle assembly more stable. To illustrate this, consider the idealised case of a lens of meniscus liquid at the contact between two spherical particles shown in Figure 2.2 , with pore liquid confined by a meniscus, and gas at a higher pressure acting outside it.

An increase in the difference $u_a - u_w$ is equivalent to an increase of isotropic total

stress acting on the soil as far as "bulk liquid" is concerned. On the contary for the liquid present as "meniscus liquid" an increase in the difference $u_a - u_w$ cannot be considered equivalent to an increase of isotropic stress because of the different effect on the inter-particle forces. An increase in the difference $u_a - u_w$ within "meniscus liquid", produces elastic compression and an increase of shear strength, both of which are equivalent to an increase of the applied isotropic total stress. However it also makes the particle assembly more stable, reducing the possibility of yielding, which is equivalent to a decrease of applied total stress. The actions of total stress, pore water pressure and pore air pressure cannot therefore be combined in one "effective stress" parameter like in the saturated case (Wheeler and Karube [7]).

Although there have been further attempts to formulate models relating the strength and the strains of an unsaturated soil to a single effective stress tensor, several researchers after Jennings and Burland [5] have shown that it is essential to consider another independent scalar stress parameter, in order to reproduce some of the most important aspects of the deformation behaviour of unsaturated soils.

Fredlund and Morgenstern [8] proposed that any two of the three stress parameters, $\overline{\overline{\boldsymbol{\sigma}}}$, $\overline{\boldsymbol{\sigma}}$ and s, defined as follows, would be suitable for a full description of the stress state:

$$\overline{\overline{\boldsymbol{\sigma}}} = (\overline{\overline{\sigma}}_x \ \overline{\overline{\sigma}}_y \ \overline{\overline{\sigma}}_z \ \tau_{xy} \ \tau_{yz} \ \tau_{zx})^T = \boldsymbol{\sigma} - \boldsymbol{m}\, u_w \tag{2.5}$$

$$\overline{\boldsymbol{\sigma}} = (\overline{\sigma}_x \ \overline{\sigma}_y \ \overline{\sigma}_z \ \tau_{xy} \ \tau_{yz} \ \tau_{zx})^T = \boldsymbol{\sigma} - \boldsymbol{m}\, u_a \tag{2.6}$$

$$s = u_a - u_w. \tag{2.7}$$

Among these three, the two stress parameters $\overline{\boldsymbol{\sigma}}$ and s, are the ones which have been most widely used in formulating constitutive models for unsaturated soils. They are usually referred to as the "net stress" and the "matrix suction" respectively.

Several constitutive models for unsaturated soils have been formulated using as stress parameters, the matrix suction s (Equation 2.7), the isotropic net stress invariant, $\overline{p}$, and

the deviatoric stress invariant, q, where $\overline{p}$ and q, are defined as:

$$\overline{p} = \frac{\overline{\sigma}_x + \overline{\sigma}_y + \overline{\sigma}_z}{3} \tag{2.8}$$

$$q = \sqrt{\frac{(\sigma_x - \sigma_y)^2 + (\sigma_y - \sigma_z)^2 + (\sigma_z - \sigma_x)^2 + 6(\tau_{xy}^2 + \tau_{yz}^2 + \tau_{zx}^2)}{2}}. \tag{2.9}$$

A review of such models is provided by Wheeler and Karube [7]. For general stress states, dependency on a third invariant of the net stress tensor or on the Lode angle may be included in the model.

The matrix suction, as defined in Equation 2.7, is, as already stated, usually used as a stress variable in formulating constitutive models for unsaturated soils. The distribution of matrix suction inside the soil also plays an important role in controlling the flow of the liquid phase within an unsaturated soil, being one of the components of the liquid phase potential, the gradient of which controls liquid flow. The definition of the suction relevant to flow problems, usually termed the "total suction"(s_{tot}), is however different from the definition of matrix suction, since the total suction is made up of two separate components: the matrix suction and the "osmotic suction" (s_{osm}) according to the following equation:

$$s_{tot} = s + s_{osm}. \tag{2.10}$$

The osmotic suction arises from the additional potential of the soil liquid due to its chemistry and, in particular, the concentration of solute inside the liquid phase.

Alonso, Gens and Hight [2] concluded that, although the chemical composition of the liquid phase can affect the mechanical behaviour of the soil due to the chemical interaction between liquid and the soil particles, the effects of matrix suction and osmotic suction on the mechanical behaviour of the soil cannot be considered equivalent. Therefore for modelling the mechanical behaviour of unsaturated soil the matrix suction is used as a stress parameter whereas the chemical composition of the pore water is taken into account in the definition of the mechanical properties of the soil. In the interest of brevity the term "suction" is used in the remaining part of this thesis to indicate only the component given by the matrix suction which is the one relevant to the formulation of the stress-strain models for unsaturated soils.

Recently, new pairs of stress state variables have been proposed by some authors. Some models introduce a stress variable which controls the shear strength having the following form:

$$\underline{\boldsymbol{\sigma}} = \left(\underline{\sigma}_x \; \underline{\sigma}_y \; \underline{\sigma}_z \; \tau_{xy} \; \tau_{yz} \; \tau_{zx}\right)^T = \boldsymbol{\sigma} - \boldsymbol{m}\, u_a + \boldsymbol{m}\, f(u_a - u_w) \tag{2.11}$$

where $f(u_a - u_w)$ is the term which takes account of the influence of suction on the shear strength. Beside this, another stress variable, usually suction, is considered to fully describe the stress-strain behaviour. Models of this type include the ones proposed by Kato, Matsuoka and Sun [6], Kohgo [9] and Modaressi, Abou-Bekr and Fry [10].

Finally, it is interesting to highlight that in a constitutive model for unsaturated soils developed using the three stress parameters q, $\overline{p}$ and s, Houlsby [11] showed that the three work-conjugate strain increment variables are: deviatoric strain increment $d\epsilon_d$, volumetric strain increment $d\epsilon_v$ and the increment of volumetric strain of the liquid phase $d\epsilon_w$ defined respectively as:

$$d\epsilon_d = \frac{2}{3}\sqrt{(d\epsilon_x - d\epsilon_y)^2 + (d\epsilon_y - d\epsilon_z)^2 + (d\epsilon_z - d\epsilon_x)^2 + \frac{3}{2}(d\gamma_{xy}^2 + d\gamma_{yz}^2 + d\gamma_{zx}^2)} \tag{2.12}$$

$$d\epsilon_v = d\epsilon_x + d\epsilon_y + d\epsilon_z \tag{2.13}$$

$$d\epsilon_w = \frac{d(eS_r)}{1+e} \tag{2.14}$$

where e is the void ratio and S_r is the degree of saturation.

2.3 Important aspects of unsaturated soil behaviour

2.3.1 Volume change

The description of volume change in an unsaturated soil due to changes of net stress and suction has received considerable attention by researchers in the past forty years. Most of the tests carried out to investigate this volumetric behaviour have been performed using

the oedometer apparatus and a smaller number of tests have used isotropic cells. Some of these tests were performed in apparatus which were modified versions of the traditional ones in order to achieve direct control of the suction parameter. In this way it was possible to subject the soil sample to stress paths which involved either loading/unloading (increase/decrease of net stress) at constant suction or wetting/drying (decrease/increase of suction) at constant net stress. The most important aspects of the volumetric behaviour of unsaturated soils which have been observed by authors in the past years will be reviewed in this section.

A well-proven pattern of the volumetric behaviour of an unsaturated soil is the relationship between the value of suction and the yield value of net stress observed during loading. This behaviour has been observed in oedometric tests, performed either at constant moisture content or at constant suction (see, for example, Dudley [12]) and also, more recently, in constant suction isotropic tests, as shown, for example, by Sivakumar [13] and Josa [14]. Figure 2.3 shows the variation of specific volume with mean net stress in isotropic tests at constant suction carried out by Sivakumar [13] on Speswhite Kaolin. The increase of yield stress with suction can be observed from these data. There is therefore a range of net stress over which the compressibility of an unsaturated sample (which has not yet yielded) is lower than the compressibility of a saturated sample (which has yielded).

In Figure 2.3 is also possible to observe that, after yielding, the soil follows separate normal compression lines for each value of suction. For the Speswhite Kaolin tested by Sivakumar [13] the slope of these lines generally increases with increasing suction, suggesting that, once the yield stress has been exceeded, the compressibility of the soil increases with increasing suction. Other authors, however, such as Alonso, Gens and Josa [1], suggested that for other soils the slope of the normal compression lines decreases with increasing suction.

If the soil is unloaded at a constant value of suction it will swell. The mechanical response of the soil during unloading is, however, stiffer if compared to the loading path along the normal compression line and it can be regarded as reversible (elastic). This result proves that the soil has experienced irreversible deformation during loading on the normal

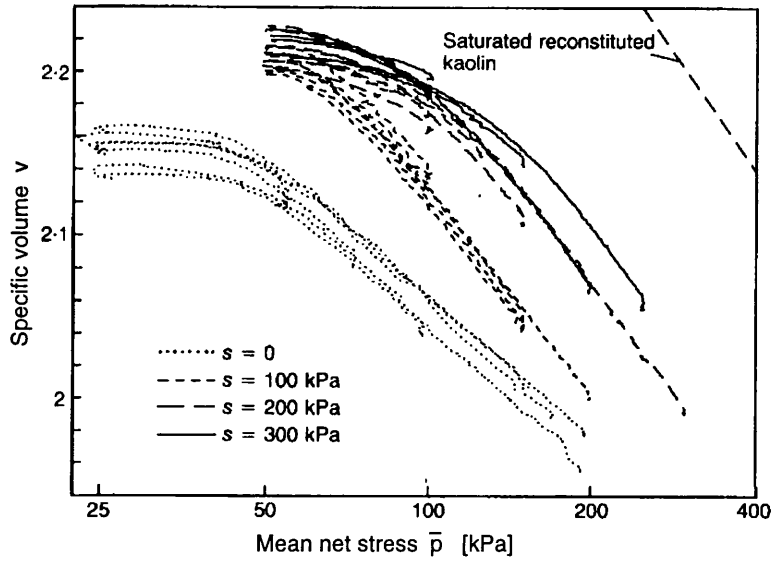

Figure 2.3: Isotropic compression tests at constant suction performed on compacted Speswhite Kaolin (after Wheeler and Sivakumar [3])

compression line. This pattern of behaviour is shown in Figure 2.4 for an isotropic loading-unloading test performed on Speswhite Kaolin by Zakaria [15] at a constant suction of 100 kPa.

Another aspect of the mechanical behaviour of unsaturated soil is the influence of the mean net stress (or the vertical net stress in oedometric tests) on the volumetric response during a wetting process. At low values of mean net stress, an unsaturated soil responds to a reduction of suction by swelling. The amount of this swelling depends on the net stress applied, tending to decrease for increasing values of net stress, as shown by authors such as Justo, Delgado and Ruiz [16] and Escario and Sáez [17]. At high values of mean net stress the same soil shows the opposite behaviour during wetting and can experience an irrecoverable volumetric compression (collapse). Yudhbir [18], who presented results for different residual soils wetted in oedometric conditions, suggested that the magnitude of collapse compression on wetting initially increases with increasing value of applied net stress, but then decreases. He showed that the value of vertical net stress for which the maximum collapse is attained depends on the type of soil and on its initial conditions.

A sample of unsaturated soil can, therefore, experience either swelling or collapse during

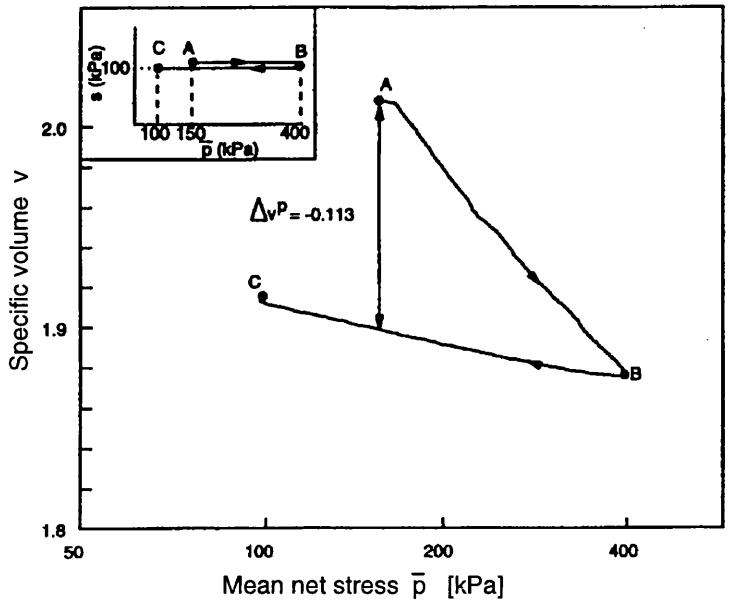

Figure 2.4: Isotropic loading-unloading test at constant suction performed on compacted Speswhite Kaolin (after Zakaria [15])

wetting, according to the intensity of mean net stress or vertical net stress to which it is subjected. It has also been shown (Escario and Sáez [17], Josa [14] and Sivakumar [13]) that, during wetting at intermediate values of net stress, the soil can swell initially and then undergo collapse compression. This is illustrated in the data from isotropic wetting tests on Speswhite Kaolin carried out by Sivakumar [13] shown in Figure 2.5.

Evidence from several experiments shows that a drying stress path (increase in suction at constant net stress) will always cause compression of the soil sample independently of the value of net stress at which the drying process occurs. The immediate consequence of this observation is that any collapse compression on wetting is a process which involves irreversible deformation. This pattern of behaviour is illustrated in Figure 2.6, which shows the volumetric strain observed during a wetting-drying cycle at constant net stress on expansive Boom clay performed by Alonso, Gens, Lloret and Yang [19]. During the wetting path D1 (suction decreasing from 100 MPa to 0.01 MPa), an initial swelling is observed followed by a greater compression (collapse). However compression is observed also during the subsequent drying D2 (suction increasing from 0.01 MPa to 0.04 MPa)

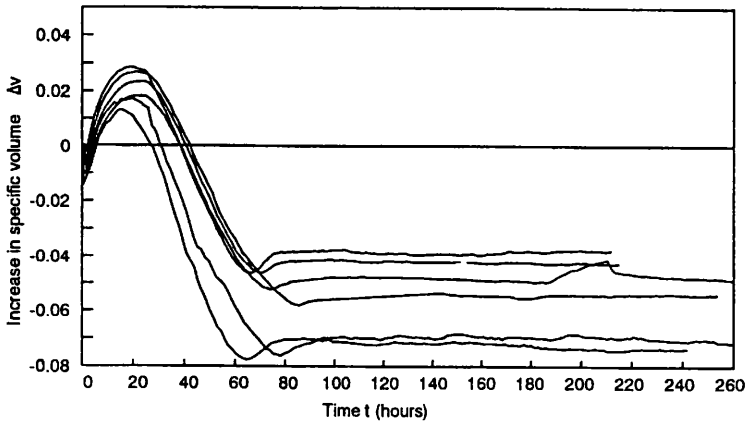

Figure 2.5: Wetting tests (decreasing suction with increasing time) performed on compacted Speswhite Kaolin (after Sivakumar [13])

which proves that an irrversible change in specific volume has occurred during the previous wetting.

Occurrence of both irreversible and reversible deformation can be interpreted on the basis of the fabric of an unsaturated compacted clay. This fabric is usually composed of clay packets, where elementary clay particles are aggregated together with small voids (microvoids) included between the single clay particles. The packets are arranged forming another level of structure with larger voids (macrovoids) enclosed between the packets. Mercury intrusion porosimetry studies carried out by Delage, Audiguier, Cui and Howat [20] suggest that large plastic reductions of volume, caused by virgin isotropic loading or wetting-induced collapse compression, are associated with a reduction in size of macrovoids due to relative slippage of packets producing a rearrangement in the pattern of the macrovoids. In contrast, elastic volume changes are likely to be associated with reversible changes in size of both macrovoids and microvoids.

Several authors have attempted to describe the swelling-collapse behaviour of an unsaturated soil by means of three dimensional plots relating void ratio to net stress and suction. This approach introduces a unique (elastic) constitutive relationship between void ratio and the stress variables and is traditionally referred to as the "state surface"

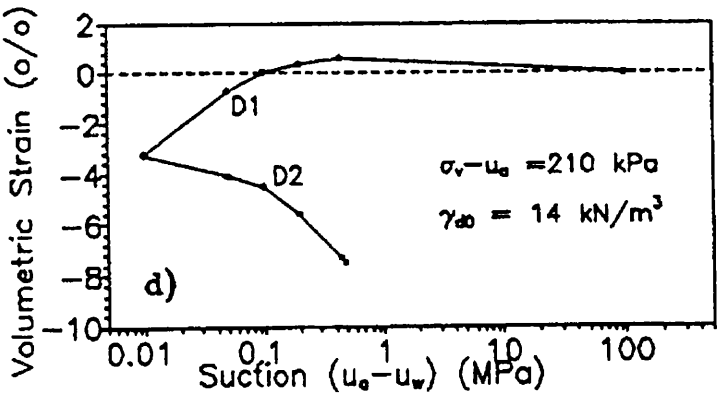

Figure 2.6: Wetting-drying test at constant net stress performed on expansive Boom clay (after Alonso, Lloret, Gens and Yang [19])

approach. The state surface represents a simple constitutive law describing the mechanical response of an unsaturated sample to change in net stress and suction. However it clearly has important shortcomings.

First of all the question of the uniqueness of this relationship arises. This approach has the limitation that no distinction is made between reversible and irreversible strains, although, as mentioned previously, experimental results have shown that unsaturated soils can undergo plastic deformations. Such models are, therefore, of interest only in the case of monotonic loading, where the stress path followed is such that, once yielding is attained, no elastic unloading takes place. Only in this case, it is possible to establish a unique relationship relating stresses and strains. A condition sufficient to guarantee such monotonic response is that the stress paths followed must not involve either increase in suction or decrease in mean net stress (or vertical net stress). This conclusion was supported by experimental evidence provided by Matyas and Radhakrishna [21]. The results from tests performed by Josa [14] and reported in Figure 2.7 provide further evidence on the non-uniqueness of the state surface for stress paths involving increase of suction. The results are from three different stress paths starting from a sample in the same initial conditions and ending at the same stress state, however the observed final specific volume is significantly different according to the stress path followed.

Further proof that the state surface is unique only for stress paths involving no increase

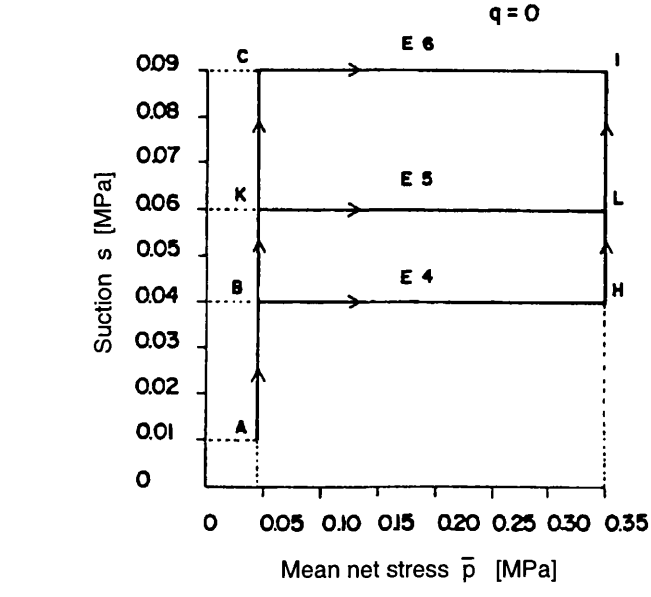

(a)

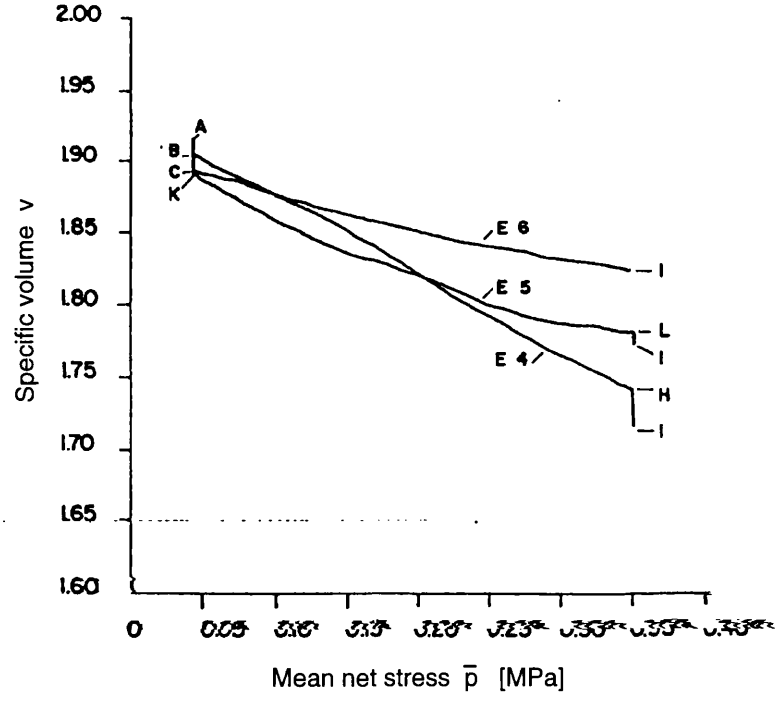

(b)

Figure 2.7: Isotropic compression-drying tests performed on low plasticity Kaolin: (a) stress paths (b) specific volume change (after Josa [14])

in suction and no decrease in net stress was presented by Lloret and Alonso [22]. These authors also proposed a possible mathematical form for the state surface relating void ratio to mean net stress (or vertical net stress) and suction for these limited conditions. In their work they analysed data from isotropic and oedometric tests on several types of unsaturated soils and interpolated them using different mathematical equations. Minimum squared error fitting techniques were used to find the coefficients of each of these proposed state surface expressions and, subsequently, predicted and measured values were compared through a conventional statistical regression. Their conclusion was that the analytical expression which appeared to give the best fit was:

$$e = a + b(\sigma - u_a) + c\log(u_a - u_w) + d\ \log(\sigma - u_a)\, log(u_a - u_w) \tag{2.15}$$

where a, b, c, d are soil parameters and σ is the relevant total stress variable (mean stress for isotropic tests and vertical stress for oedometric tests).

The importance of phenomena like hysteresis and plastic deformations for an unsaturated soil was further emphasized by Fredlund and Morgenstern [23]. They proposed an incremental elastic relationship which linked the changes of volumetric strain $\delta\epsilon_v$ to changes in mean net stress $\delta\overline{p}$ and suction δs. The strain changes predicted with the proposed constitutive law were then compared with experimental results in order to assess the uniqueness of the constitutive relationship near a stress point. Their experimental results showed, again, that an elastic relationship is successful only for monotonic deformation paths.

Another important shortcoming of the state surface approach is that it can be applied as a constitutive model only if the stress state applied to the soil is of the same type as the one imposed on the samples during the tests when the state surface was defined. State surfaces computed using, for example, oedometer tests on unsaturated soil samples can be applied to predict deformation of the same soil only if it is in an oedometric stress state. In particular, a state surface defined by data from isotropic or oedometer tests cannot be used to predict the volume changes of an unsaturated soil during shearing.

2.3.2 Shear strength

Other research has been carried out in order to investigate the relation between the shear strength τ acting on a plane, the net stress $\sigma - u_a$ normal to the plane and the suction $u_a - u_w$.

Fredlund, Morgenstern and Widger [24] analysed experimental data from triaxial tests with constant water content on clay samples, performed at the Massachusetts Institute of Technology [25] and by Bishop [26]. They proposed a planar failure criterion relating shear strength τ on a plane to net stress normal to the plane, $\sigma - u_a$ and suction, $u_a - u_w$:

$$\tau = c' + (\sigma - u_a)\tan\phi' + (u_a - u_w)\tan\phi^b \tag{2.16}$$

where c' and ϕ' are the cohesion and friction angle for the soil in a saturated or dry state and ϕ^b is the friction angle showing the increase of strength with suction. This planar failure criterion is often referred to as the "extended Mohr-Coulomb failure envelope" and it is tangential to Mohr circles representing failure conditions (see Figure 2.8). The intersection of this surface with the $s = 0$ plane coincides with the Mohr-Coulomb criterion for saturated soils.

Subsequently, Escario and Sáez [28] performed direct shear tests on three different unsaturated soils, controlling both the pore water pressure and the vertical total stress and keeping the air pressure constant at atmospheric value. They concluded that the dependence of shear strength on suction at constant net normal stress was not linear. In particular they showed that the coefficient $\tan\phi^b$ decreased for increasing values of suction. The latter conclusion was also confirmed by Gan, Fredlund and Rahardjo [27], who tested specimens of compacted glacial till in a modified shear box apparatus. Their results showed that the coefficient $\tan\phi^b$ was equal to $\tan\phi'$ at low values of suction and then tended to decrease as suction increased. The equality between $\tan\phi^b$ and $\tan\phi'$ at low values of suction can be explained by a physical argument. When the soil is at low value of suction it is likely to be fully saturated or close to fully saturated. In this condition the pore liquid is mainly present in the form of bulk liquid rather than in the form of meniscus liquid. Therefore an increase of suction can be considered to have the

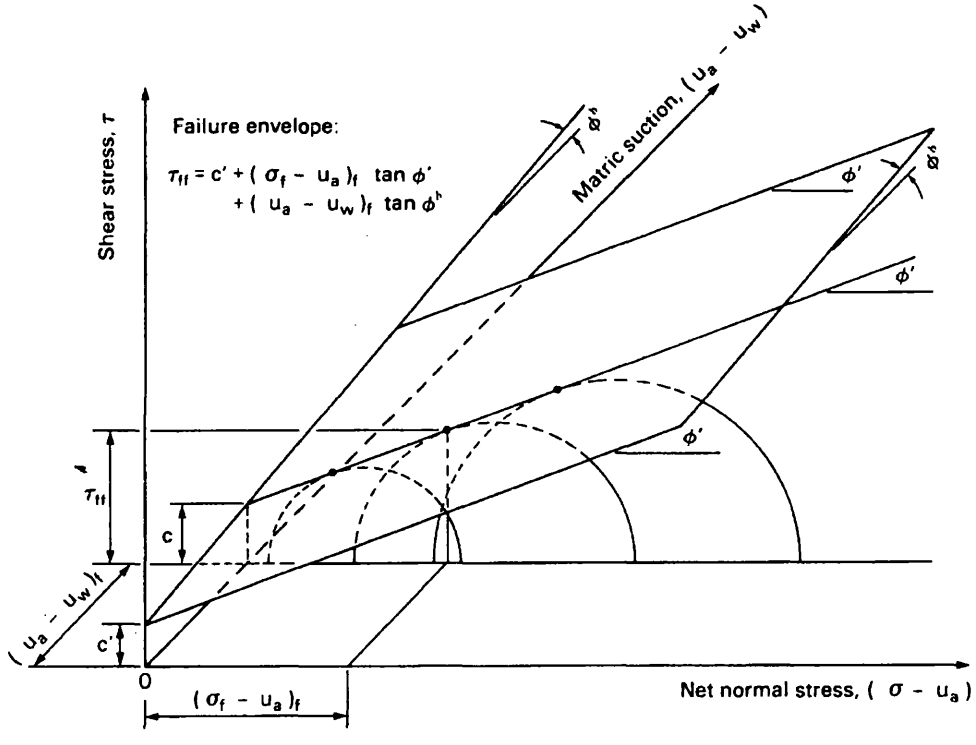

Figure 2.8: Extended Mohr-Coulomb failure envelope (after Gan, Fredlund and Rahardjo [27])

same effect on shear strength as an increase of the mean effective stress in a saturated soil.

Escario and Jucá [29] tested the same type of unsaturated soils already used by Escario and Sáez [28], but over a wider range of suction. The results confirmed the non-linear variation of shear strength with suction. Furthermore they showed that, at very high values of suction, an increase in suction can even cause a decrease of shear strength.

The fact that the parameter $\tan\phi^b$ decreases with increasing suction and its tendency to coincide with $\tan\phi'$ at low values of suction are now well-proved results. Recent experimental work by de Campos and Carrillo [30], Drumright and Nelson [31] and Röhm and Vilar [32] provided further proof of this aspect of behaviour.

Escario and Sáez [28] confirmed a linear dependence of shear strength on the normal net stress at a constant value of suction and, in addition, they also showed that the slope, $\tan\phi'$ of these linear relations was approximately constant with suction. For two of the three soils studied there was a slight tendency for $\tan\phi'$ to increase with increasing suction. Other experimental evidence proving that the coefficient $\tan\phi'$ is approximately constant, independent of the suction value, for most soils is available in the literature. Data from Wheeler and Sivakumar [3] from triaxial compression tests on compacted Speswhite Kaolin suggested that the friction angle, ϕ' increased slightly with increasing suction (by about 3.5 degrees for suctions between 0 and 200 kPa). Subsequent additional data, however, from further tests on the same soil (Wheeler and Sivakumar [33]) indicated that any variation of the friction angle, ϕ' with suction was insignificant for suctions between zero and 300 kPa.

Röhm and Vilar [32] subjected an unsaturated sandy soil to shearing at constant suction in a triaxial apparatus and the results they obtained showed that the maximum difference for the value of the friction angle, ϕ' was about 2.5 degrees for suction ranging between zero and 400 kPa.

2.4 Elasto-plastic model of Alonso, Gens and Josa [1]

2.4.1 Isotropic stress states

Elasto-plastic models have been developed recently to offer a general framework able to represent the mechanical behaviour of unsaturated soils without any of the restrictions on the type of stress paths that were necessary in the case of the elastic models reviewed in Section 2.3.1.

The first development of a complete analytical formulation of a constitutive model for unsaturated soil, which made use of the traditional framework of elasto-plasticity, was due to Alonso, Gens and Josa [1]. The model is described in terms of three stress parameters: the mean net stress, $\overline{p}$ the suction, s and the deviator stress, q whereas only two strain parameters are considered: the increment of volumetric strain, $d\epsilon_v$ and the increment of deviator strain, $d\epsilon_d$. The increment of volumetric strain $d\epsilon_v$ can be related to the increment of specific volume dv through the relation:

$$d\epsilon_v = -\frac{dv}{v} \tag{2.17}$$

where v is the specific volume. According to the principles of traditional elasto-plasticity, the soil behaves elastically inside a yield locus defined in stress space and plastic deformation starts when any stress path reaches the yield surface. In this section the elasto-plastic framework for unsaturated soils developed by Alonso, Gens and Josa [1] is reviewed. A description of the model for isotropic stress states ($q = 0$) is given in this section, whereas the next section will deal with the extension of the model to anisotropic (triaxial) stress states ($q \neq 0$).

In order to define completely the elasto-plastic stress-strain relationship, four elements have to be given: an elastic law, a yield locus, a hardening law and a plastic flow rule.

In the model considered the elastic behaviour for isotropic stress states is given by the following relation between the increment of specific volume dv^e and the increments of the two stress variables $\overline{p}$ and s:

$$dv^e = -\kappa \frac{d\overline{p}}{\overline{p}} - \kappa_s \frac{ds}{s + p_{atm}} \tag{2.18}$$

where κ and κ_s are two elastic constants and p_{atm} is atmospheric pressure. The value p_{atm} was, rather arbitrarily, included in Equation 2.18 to enable the model to be used down to zero suction (saturated conditions).

The yield locus in the $(\overline{p}, s)$-plane for isotropic stress states and the hardening law are both linked to the form of behaviour assumed during isotropic loading to virgin states. The assumption in the model is that whenever an unsaturated soil subject to an isotropic stress state behaves plastically, the soil state must fall on an isotropic normal compression surface in $(v, \overline{p}, s)$-space. Such a surface can be represented by a family of isotropic normal compression lines in the $(v, \overline{p})$-plane, each one corresponding to a different value of suction and taking the form:

$$v = N(s) - \lambda(s) \ln \frac{\overline{p}_o}{p^c} \tag{2.19}$$

where $\overline{p}_o$ represents a stress state lying on the normal compression surface (a value of isotropic yield stress), p^c is a reference pressure and the slope, $\lambda(s)$ and the intercept, $N(s)$ (measured at $\overline{p} = p^c$) are both function of suction. Alonso, Gens and Josa [1] assume that $\lambda(s)$ decreases monotonically with increasing suction according to the following relation:

$$\lambda(s) = \lambda(0) \left[(1 - r) \exp(-\beta s) + r \right] \tag{2.20}$$

where $\lambda(0)$ is the slope of the normal compression line for a value of suction equal to zero (saturated conditions) and r and β are two additional soil constants. As suction tends to infinity, the value of $\lambda(s)$ decreases towards a limiting value $r\lambda(0)$ (with r taking a value between zero and 1), and the value of β controls the rate of decay towards this limiting value. Figure 2.9 shows a schematic representation of a family of normal compression lines represented by Equations 2.19 and 2.20.

Combining the definition of such a normal compression surface with the elastic behaviour described in Equation 2.18 it is possible to define the yield locus in the $(\overline{p}, s)$-plane and the hardening law. Figure 2.10 shows two normal compression lines: one for a soil

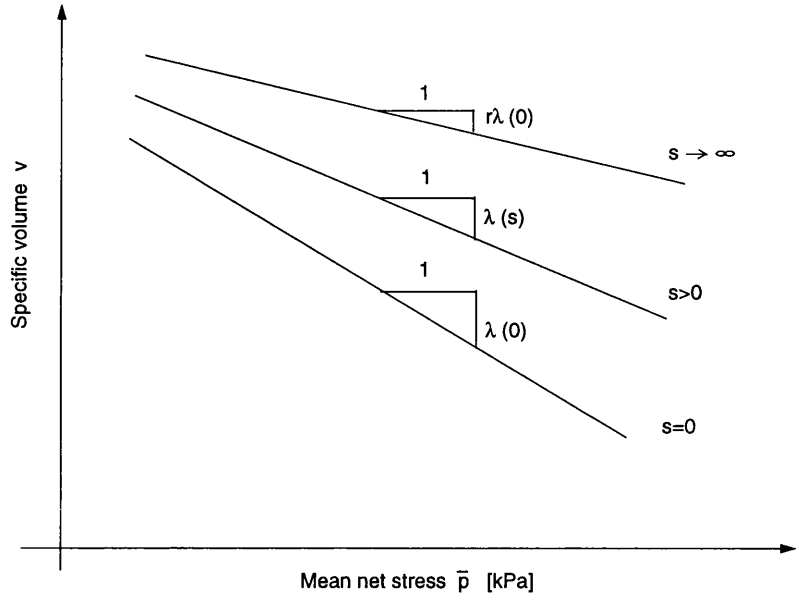

Figure 2.9: Schematic representation of normal compression lines in the $(v, \ln \overline{p})$-plane at different suctions suction according to the Alonso, Gens and Josa model [1]

in a saturated condition ($s = 0$) and another for the same soil in an unsaturated state ($s > 0$).

The yield stress for the saturated soil is indicated as $\overline{p}_o^*$ and it corresponds in Figure 2.10 to point 3 with specific volume v_3. The yield stress for the same soil at a higher level of suction is indicated as $\overline{p}_o$ and it corresponds in Figure 2.10 to point 1 with specific volume v_1. If the stress states identified by point 1 and point 3 belong to the same yield locus it must be possible to move from one point to the other through a stress path involving only elastic deformations, such as path 1→2→3 in Figure 2.10. The elastic swelling occurring along such a path (due to the reduction of $\overline{p}$ along path 1→2 and the reduction of s along path 2→3) is given by integrating Equation 2.18 as:

$$v_3 - v_1 = \kappa \ln \frac{\overline{p}_o}{\overline{p}_o^*} + \kappa_s \ln \frac{s + p_{atm}}{p_{atm}}. \tag{2.21}$$

Given, however, that points 1 and 3 lie on the normal compression lines for their respective values of suction, an alternative expression for $v_3 - v_1$ is given by Equation 2.19 as:

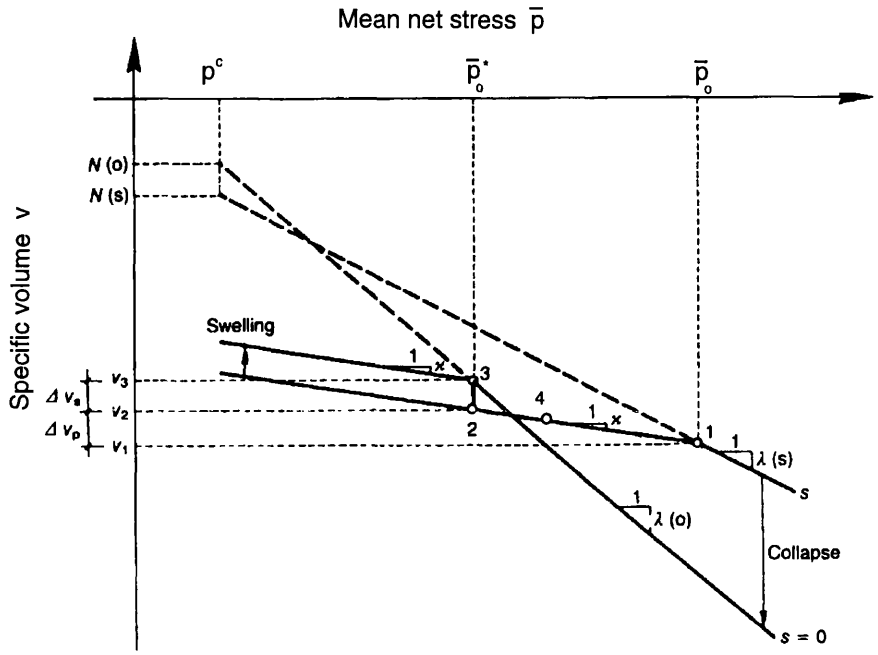

(a)

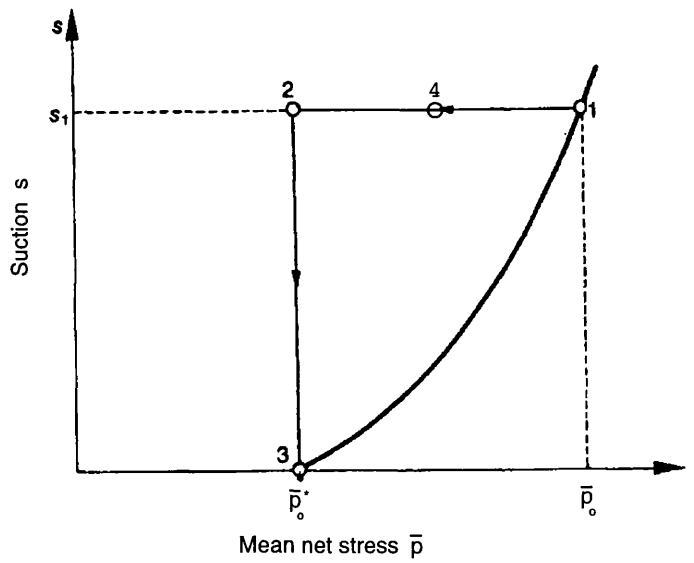

(b)

Figure 2.10: Elastic stress path from the normal compression line at $s > 0$ to that at $s = 0$ in: (a) $(v, \ln \overline{p})$-plane (b) $(\overline{p}, s)$-plane (after Alonso, Gens and Josa [1])

$$v_3 - v_1 = N(0) - \lambda(0) \ln \frac{\overline{p}_o^*}{p^c} - N(s) + \lambda(s) \ln \frac{\overline{p}_o}{p^c} \tag{2.22}$$

where $N(0)$ is the value of $N(s)$ at zero suction. Combining Equations 2.21 and 2.22:

$$N(s) - \lambda(s) \ln \frac{\overline{p}_o}{p^c} + \kappa \ln \frac{\overline{p}_o}{\overline{p}_o^*} + \kappa_s \ln \frac{s + p_{atm}}{p_{atm}} = N(0) - \lambda(0) \ln \frac{\overline{p}_o^*}{p^c}. \tag{2.23}$$

Or rearranging:

$$N(s) - (\lambda(s) - \kappa) \ln \frac{\overline{p}_o}{p^c} + \kappa_s \ln \frac{s + p_{atm}}{p_{atm}} = N(0) - (\lambda(0) - \kappa) \ln \frac{\overline{p}_o^*}{p^c}. \tag{2.24}$$

In order to simplify the expression of the yield locus given by Equation 2.24 and to reduce the number of parameters needed for its definition, the authors postulated the existence of a value of the reference pressure p^c at which one may move from a generic unsaturated normal compression line to the saturated one through a stress path which involves only elastic swelling due to change in suction. In other words they assumed that it is possible to define a value of p^c (which now becomes an additional model parameter) at which the following identity holds:

$$N(s) = N(0) - \kappa_s \ln \frac{s + p_{atm}}{p_{atm}} \tag{2.25}$$

If Equation 2.25 holds for all values of suction, this is equivalent to saying that the yield curve is a vertical straight line in the $(\overline{p}, s)$-plane for $\overline{p}_o^* = p^c$. Combining Equation 2.25 with Equation 2.24 the following relationship for the yield locus in the $(\overline{p}, s)$-plane is obtained:

$$\frac{\overline{p}_o}{p^c} = \left(\frac{\overline{p}_o^*}{p^c} \right)^{\frac{\lambda(0) - \kappa}{\lambda(s) - \kappa}}. \tag{2.26}$$

Equation 2.26 defines a family of yield curves in the $(\overline{p}, s)$-plane each one associated with a particular value of $\overline{p}_o^*$ which can be therefore considered as an hardening parameter. A qualitative representation of such family of yield curves, called Loading-Collapse (LC) yield curves, is shown in Figure 2.11, where the expansion of the yield curves with increasing values of $\overline{p}_o^*$ is evident. Figure 2.11 also illustrates the major assumption implicitly made

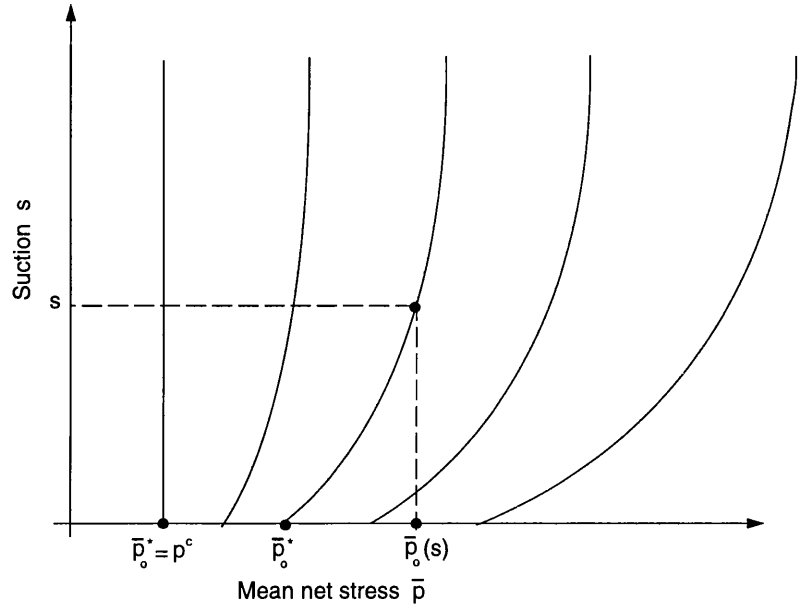

Figure 2.11: Schematic representation of the family of LC yield curves (each curve corresponds to a different value of $\bar{p}_o^*$)

in the model of Alonso, Gens and Josa [1] that there exists a value p^c of the hardening parameter $\bar{p}_o^*$ for which the yield curve is a vertical straight line.

Furthermore, due to the logic followed for their definition, each of these yield curves is related to a unique value of plastic change of specific volume Δv^p with respect to a reference state associated with a given yield locus. In terms of infinitesimal changes, the magnitude of the plastic decrement of specific volume, dv^p associated with a given increment of the hardening parameter, $d\bar{p}_o^*$, can be calculated by equating it with the value dv^p for a saturated sample (s=0) subjected to the same expansion of the yield curve:

$$dv^p = -(\lambda(0) - \kappa)\frac{d\bar{p}_o^*}{\bar{p}_o^*} \tag{2.27}$$

Equation 2.27 defines the volumetric hardening law of the constitutive model.

The Loading-Collapse yield curve defined in the $(\bar{p}, s)$-plane by Equation 2.26 for a given value of the hardening parameter, predicts an increase in the isotropic yield stress with increasing suction (see Figure 2.12). The shape of the LC yield curve and the way it expands with plastic volumetric strain are inextricably linked to the definition of the

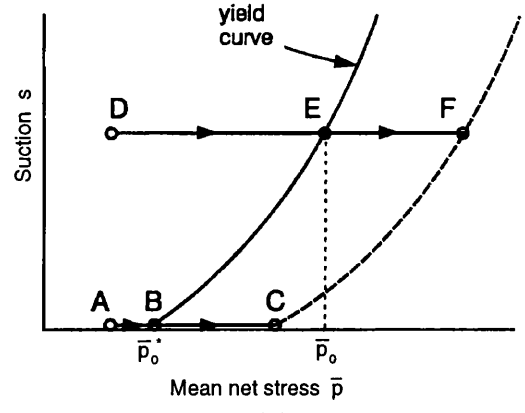

(a)

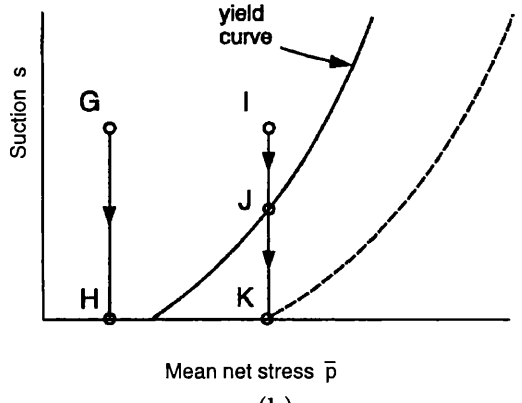

(b)

Figure 2.12: LC yield curves: (a) isotropic-loading stress paths (b) wetting stress paths (after Wheeler and Karube [7])

elastic behaviour inside the yield curve and the representation of the isotropic normal compression surface in the $(v, \overline{p}, s)$-space. In other words, once the elastic law and the normal compression lines for any value of suction have been assigned, then the shape of the LC curve and the manner in which it changes during hardening come as a consequence. From Figure 2.12 it is also evident that plastic deformations can be produced not only by an increase of mean net stress at constant suction, like in the saturated case, but also by a decrease in suction at a constant value of mean net stress (collapse compression behaviour on wetting) or even by a combination of these two effects. The model is therefore able to reproduce the mechanical response of swelling-collapse due to wetting which has been described in Section 2.3.1.

Finally from Figure 2.10, following a stress path starting at $\overline{p} = p^c$ and $s = 0$ and going through points 3-2-4 it is possible to calculate the specific volume at any general stress state 4 lying on or inside the normal compression surface at mean net stress, $\overline{p}$ and suction, s, as:

$$v = N(0) - \lambda(0) \ln \frac{\overline{p}_o^*}{p^c} - \kappa_s \ln \frac{s + p_{atm}}{p_{atm}} - \kappa \ln \frac{\overline{p}}{\overline{p}_o^*}. \tag{2.28}$$

2.4.2 Anisotropic stress states

The previous section described the model of Alonso, Gens and Josa [1] as applied to isotropic stress states. The model is extended to triaxial stress states by the authors introducing in the model a third stress parameter, the deviatoric stress q, and a second strain parameter, the increment of deviatoric strain $d\epsilon_d$. These two parameters are defined for triaxial stress states as:

$$q = \sigma_y - \sigma_x \tag{2.29}$$

$$d\epsilon_d = \frac{2}{3} (d\epsilon_y - d\epsilon_x) \tag{2.30}$$

where σ_y and σ_x are the axial and radial stresses respectively and $d\epsilon_y$ and $d\epsilon_x$ the corresponding strain increments. The model can be extended to completely general anisotropic

stress states, using the definition of deviatoric stress and deviatoric strain given in Equations 2.9 and 2.12.

In order to extend the model to anisotropic stress states, three new elements have to be introduced: an incremental link between the new strain variable, $d\epsilon_d$ and the stress increments in the elastic domain, the extension of the yield locus for isotropic stress states defined in the $(\overline{p}, s)$-plane to three-dimensional stress space $(q, \overline{p}, s)$, and the definition of a flow rule for predicting plastic components of $d\epsilon_d$.

As far as the first point is concerned, the elastic increment of deviatoric strain, $d\epsilon_d^e$ is related to the increment of deviator stress, dq through the shear modulus, G:

$$d\epsilon_d^e = \frac{1}{3G}\, dq. \tag{2.31}$$

When suction is equal to zero (soil saturated) the model is assumed to coincide with the Modified Cam-Clay model (Roscoe and Burland [34]). Therefore at zero suction the yield locus in the $(q, \overline{p})$-plane coincides with the Modified Cam-Clay elliptical curve. This elliptical shape of the yield curve is retained also in constant suction planes at values of suction different from zero. Each of such ellipses is identified by the value of the isotropic yield stress, $\overline{p}_o$ which lies on the LC curve defined in the previous section. In Figure 2.13 a qualitative plot of the yield surface in the $(q, \overline{p}, s)$-space is presented.

As in the Modified Cam-Clay (Roscoe and Burland [34]) case, the complete definition of the elliptical yield locus in each constant suction plane is obtained by specifying the value of the isotropic yield stress, $\overline{p}_o$ and the critical state line relating q and $\overline{p}$ at ultimate critical states at a given value of suction. The slope, M of such critical state lines in the $(q, \overline{p})$-plane is assumed to be constant, independent of the value of suction, whereas the intercept (μ) with the q axis is assumed to be equal to zero for a value of suction equal to zero and then increases linearly with suction (see Figure 2.14). The analytical expression of such critical state lines in the $(q, \overline{p})$-planes at a given value of suction, s is given by:

$$q = M\overline{p} + Mks \tag{2.32}$$

where k is a model parameter controlling the increase of the critical value of deviator

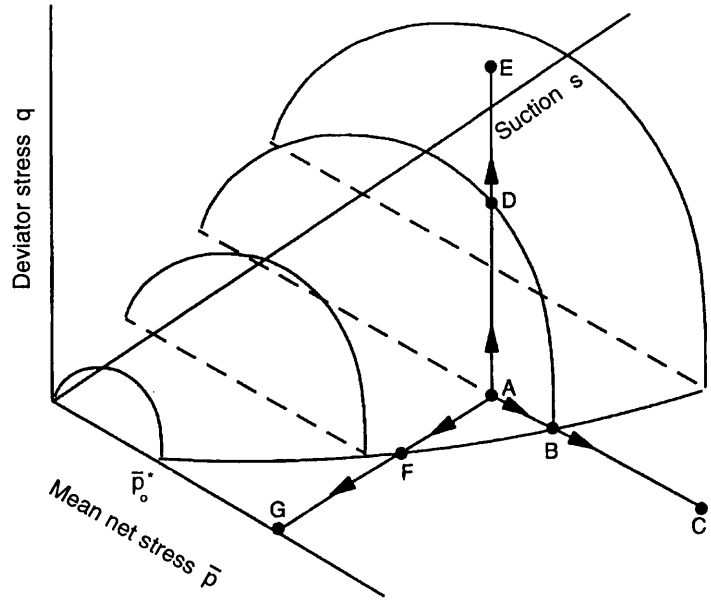

Figure 2.13: Yield surface in $(q, \overline{p}, s)$-space (after Wheeler and Karube [7])

stress with increasing suction. This assumption corresponds, for triaxial stress states, to the hypothesis of a planar failure criterion such as the one proposed by Fredlund, Morgenstern and Widger [24] and presented in Equation 2.16. Due to the linear increase with suction of the intercept of the critical state line with the q axis, the constant suction ellipses will intercept the mean net stress axis at a negative value of $-ks$.

Consequently the major axis of the ellipse in the generic constant suction plane will go from the point having coordinates $(-ks, 0)$ to the point having coordinates $(\overline{p}_o, 0)$. In Figure 2.14 two elliptical yield loci in the $(q, \overline{p})$-plane are shown for two different values of suction, $s = 0$ and $s \neq 0$.

The aspect ratio of the elliptical yield loci in the constant-suction planes is assumed not to vary with suction and it is fixed by the value of the parameter M. The equation of the yield locus in the $(q, \overline{p}, s)$-space will be therefore given by:

$$q^2 - M^2(\overline{p}_o - \overline{p})(\overline{p} + ks) = 0. \tag{2.33}$$

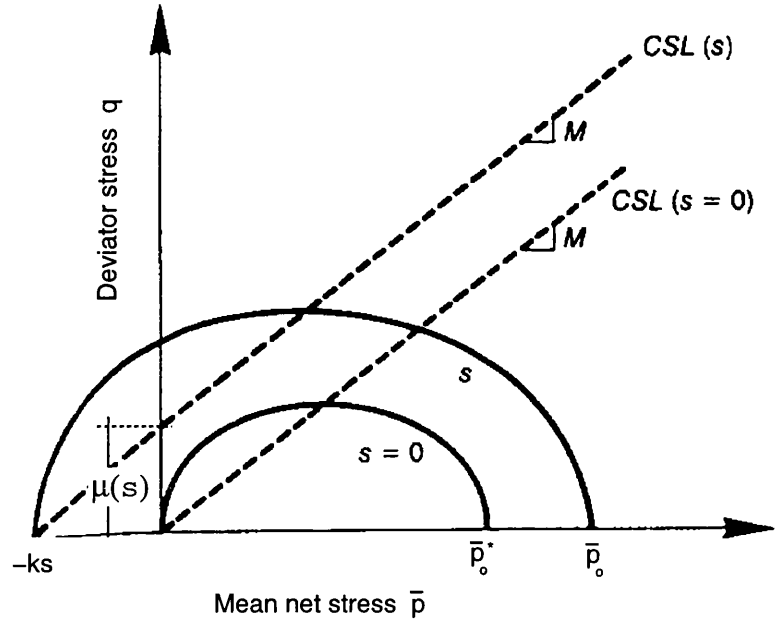

Figure 2.14: Elliptical yield loci in $(q, \overline{p})$-plane at different suctions (after Alonso, Gens and Josa [1])

The model predicts also a unique critical state surface in the $(v, \overline{p}, s)$-space. This corresponds to a series of critical state lines in the $(v, \overline{p})$-plane for different values of suction. Although not presented by Alonso, Gens and Josa [1], the expression defining these critical state lines can be derived as:

$$v = N(s) - \lambda(s) \ln \frac{\overline{p}}{p^c} - (\lambda(s) - \kappa) \ln \left(2 + \frac{ks}{\overline{p}}\right). \tag{2.34}$$

Comparison of Equation 2.34 and Equation 2.19 shows that each critical state line at a given value of suction lies, in the $(v, \overline{p})$-plane, below the normal compression line at the same value of suction. The spacing between the two lines is given by the term $(\lambda(s) - \kappa) \ln \left(2 + \frac{ks}{\overline{p}}\right)$. At high values of $\overline{p}$, this spacing tends asymptotically to $(\lambda(s) - \kappa) \ln 2$, as shown in Figure 2.15. The expression of the critical state line for s=0 reduces to the one predicted by the Modified Cam-Clay model (Roscoe and Burland [34]).

As far as the choice of the flow rule is concerned, Alonso, Gens and Josa [1] adopted a non-associated plastic flow rule in each constant suction plane. They argued for a non-

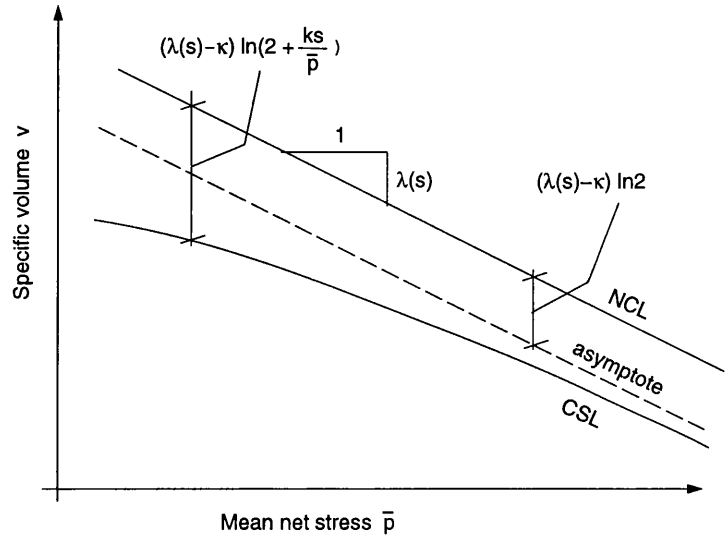

Figure 2.15: Schematic representation of normal compression line and critical state line in the $(v, \ln \overline{p})$-plane at the same suction

associated flow rule in order to get better predictions of the value of K_o during oedometric stress paths. The proposed flow rule was of the form:

$$\frac{d\epsilon_d^p}{d\epsilon_v^p} = \frac{2q\alpha}{M^2\left(2\overline{p} + ks\right)\left(\overline{p}_o - \overline{p}\right)} \tag{2.35}$$

where $d\epsilon_d^p$ and $d\epsilon_v^p$ are the plastic components of shear strain increment and volumetric strain increment respectively. Equation 2.35 gives an associated flow rule if a value of $\alpha = 1$ is assumed. The assumption of an associated flow rule is made throughout the rest of this thesis.

2.4.3 Validation, shortcomings and refinements

Experimental evidence, supporting the hypothesis of the existence of the LC yield curve for isotropic stress states and confirming its qualitative shape, has been provided by several researchers, including Josa [14], Wheeler and Sivakumar [3] and Cui and Delage [35]. The hypothesis of volumetric hardening formulated in the model of Alonso, Gens, and Josa [1] has been validated by experimental results from Wheeler and Sivakumar [3]. Volumetric hardening implies that each position of the LC yield curve is associated with a unique value of plastic volumetric strain. Wheeler and Sivakumar [3] showed that the plastic

volumetric strain during a wetting path was the same as the value calculated by considering isotroping loading at zero suction with the same increment of hardening parameter (i.e. same expansion of the yield curve).

Wheeler and Sivakumar [3] also provided experimental support for the hypothesis of a unique state boundary relationship relating specific volume v to the stress variables q, $\overline{p}$ and s for stress states on the yield surface. They considered different types of stress paths, all involving yielding and all at a fixed value of suction. They showed that, for a fixed value of suction, it was possible to plot contours of constant v in a $(q,\overline{p})$-plane that were applicable, to a reasonable approximation, to all the various types of tests, irrespective of the form of stress path.

The choice made by Alonso, Gens, and Josa [1] of an elliptical shape (with one axis of such ellipse coincident with the $\overline{p}$ axis) for the yield curves in constant suction planes, was supported by experimental data presented by Zakaria, Wheeler and Anderson [36] from tests on compacted Kaolin. Contradictory experimental evidence was offered by Cui and Delage [35], who analysed results from tests on unsaturated compacted silt, and on the basis of this proposed constant suction yield curves inclined along the K_o line. One explanation for this difference can be found in the different stress history of the samples tested: in the case of Zakaria,Wheeler and Anderson [36] the past stress history was isotropic whereas the samples tested by Cui and Delage [35] were subjected to a strongly anisotropic stress history before shearing.

Contradictory experimental evidence is also present for the form of the flow rule. While Alonso, Gens, and Josa [1] chose a non-associated flow rule for their model (Equation 2.35), Zakaria, Wheeler and Anderson [36] suggested an associated flow rule in the constant suction plane with their elliptical yield curves. In contrast Cui, Delage and Sultan [37] proposed a non associated flow rule in combination with their yield curves inclined along the K_o lines. This difference could again be attributable to the different stress histories followed in the tests before shearing.

One of the strongest assumptions made in the model of Alonso, Gens, and Josa [1] is that the LC yield curve expands during hardening in such a way that it is possible to

define a value of the hardening parameter $\overline{p}_o^* = p^c$ (the reference pressure) for which the LC yield curve reduces to a straight vertical line. This assumption noticeably simplifies the analytical expression of the LC yield curve (see Equation 2.26). However the assumption does impose a strong constraint on the shape of the LC curve as it expands. It also defines the variation of $N(s)$ with suction, according to Equation 2.25, and therefore fixes the relative locations of the normal compression lines for different values of suction in the $(v, \overline{p})$-plane, in a fashion which may not be entirely consistent with experimentally observed behaviour.

Wheeler and Sivakumar [3] proposed a refinement to the model of Alonso, Gens, and Josa [1], abandoning the hypothesis of the existence of a reference pressure at which the yield curve is a straight vertical line, and binding the definition of the LC yield curve and its hardening law to an expression of the normal compression surface in $(v, \overline{p}, s)$-space which is more consistent with experimental evidence. The analytical expression for such normal compression surface is:

$$v = N_{atm}(s) - \lambda(s) \ln \frac{\overline{p}_o}{p_{atm}} \tag{2.36}$$

where $N_{atm}(s)$ gives the values of specific volume on the normal compression surface at a reference pressure $\overline{p} = p_{atm}$ (atmospheric pressure) for varying suction and $\overline{p}_o$ represents a stress state lying on the normal compression surface. The function $N_{atm}(s)$ has to be explicitly input to the model (in contrast to the case of the Alonso, Gens, and Josa [1] model) together with the function $\lambda(s)$. The yield curve expression describing the variation of $\overline{p}_o$ with suction for a given value of $\overline{p}_o^*$ is then given, by a procedure very similar to the derivation of Equation 2.24, as:

$$(\lambda(s) - \kappa) \ln \frac{\overline{p}_o}{p_{atm}} = (\lambda(0) - \kappa) \ln \frac{\overline{p}_o^*}{p_{atm}} + N_{atm}(s) - N_{atm}(0) + \kappa_s \ln \frac{s + p_{atm}}{p_{atm}}. \tag{2.37}$$

Another weak point of the model of Alonso, Gens, and Josa [1] is that the critical states predicted in the model, in Equations 2.32 and 2.34, are not an accurate representation of observed behaviour (see Wheeler and Sivakumar [38] [39] and Maatouk, Leroueil and

La Rochelle [40]). Wheeler and Sivakumar [3] suggested that critical states could be adequately represented by the following expressions:

$$q = M(s)\overline{p} + \mu(s) \tag{2.38}$$

$$v = \Gamma_{atm}(s) - \psi(s) \ln \frac{\overline{p}}{p_{atm}}. \tag{2.39}$$

In Equation 2.38, $\mu(s)$ varies non-linearly with suction, equivalent to $\tan\phi^b$ varying with suction in a non linear fashion in Equation 2.16, and for some soils it may also be necessary to allow $M(s)$ to vary with suction, equivalent to the variation of $\tan\phi'$ in Equation 2.16 (see Section 2.3.2). $\Gamma_{atm}(s)$ and $\psi(s)$ in Equation 2.39 are also functions of suction. In the model proposed by Wheeler and Sivakumar [3], $M(s)$, $\mu(s)$, $\Gamma_{atm}(s)$ and $\psi(s)$ and their variation with suction are defined as input parameters. In other words Equations 2.38 and 2.39 are not predicted by the model, once the model parameters have been assigned, but are explicitly introduced as a further input. In this way the critical state stress state (point A in Figure 2.16) is uniquely defined in each constant suction plane and for each value of the hardening parameter, $\overline{p}_o^*$. The width and height of the constant suction yield ellipses are therefore defined by the two points A and B through which they are forced to pass. The constant aspect ratio given by the constant value of M in the model of Alonso, Gens, and Josa [1] is, therefore, lost in the model of Wheeler and Sivakumar [3]. The yield ellipses will have a variable aspect ratio given by M^* which depends on the definition of both Equations 2.38 and 2.39.

2.5 Variation of S_r

2.5.1 State surface approach

The inclusion of the change of degree of saturation, S_r, as an additional strain variable in a constitutive model for unsaturated soil is needed whenever coupling of flow and deformation has to be studied. In this kind of problem the equations of conservation of air and water mass are used, beside the equations of equilibrium, and they involve the degree of saturation (see Chapter 5). Numerical applications of constitutive models

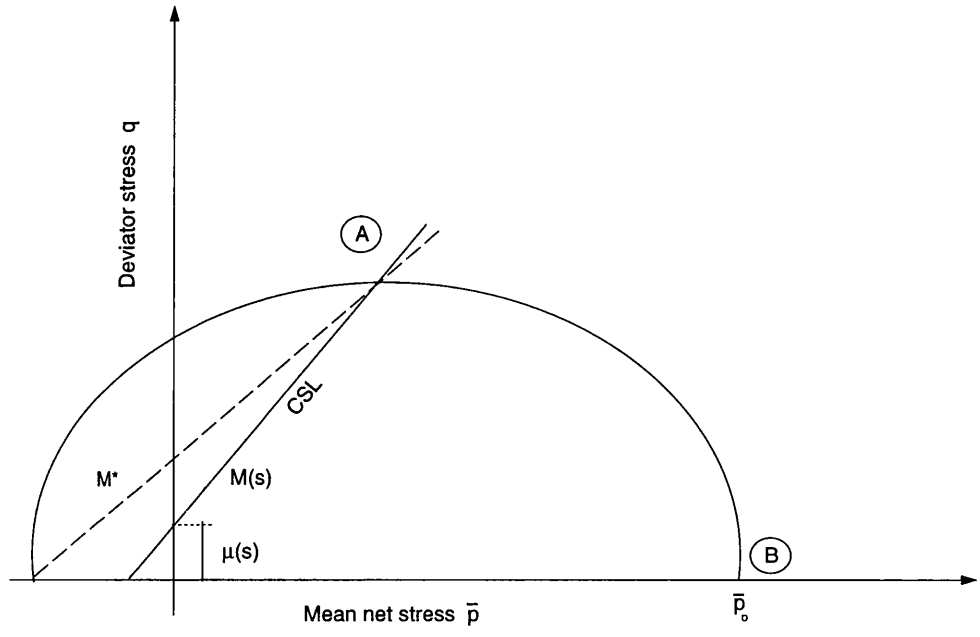

Figure 2.16: Elliptical yield locus in $(q, \bar{p})$-plane at constant suction according to the model of Wheeler and Sivakumar [3]

for unsaturated soil have taken place recently. Some of them make use of the "state surface" approach described in Section 2.3.1, in order to model the stress-strain behaviour of the soil (for example Lloret, Gens, Batlle and Alonso [41] and Alonso, Batlle, Gens and Lloret [42]). Others implement the elasto-plastic model of Alonso, Gens, and Josa [1] (for example, Thomas and He [43], Nesnas and Pyrah [44], Gatmiri, Tavakoli, Moussavi and Delage [45] and Gens, Vaunat and Ledesma [46]). All the works mentioned above are concerned with fully coupled flow-deformation analyses and, therefore, introduce the degree of saturation, as an additional parameter, within the original constitutive models for unsaturated soil. In all of them this is achieved by defining a unique relationship between degree of saturation and the stress variables, like the "state surface" approach already introduced in Section 2.3.1 for the void ratio. Matyas and Radhakrishna [21] were among the first to postulate the existence of a "state surface" for degree of saturation, linking uniquely this parameter to mean net stress (or vertical net stress) and suction. Lloret and Alonso [22] proposed a unique relationship between the degree of saturation, the net stress and suction, and suggested that one of the following two expressions would

normally provide an adequate fit to observed behaviour:

$$S_r = a - \{1 - \exp[-b(u_a - u_w)]\}[c + d(\sigma - u_a)] \tag{2.40}$$

$$S_r = a - \tanh[b(u_a - u_w)][c + d(\sigma - u_a)] \tag{2.41}$$

where a, b, c, d are soil parameters and σ is the relevant stress variable (mean stress for isotropic tests and vertical stress for oedometric tests). The experimental data and the procedure used to define Equations 2.40 and 2.41 were the same as used for the case of void ratio (see Section 2.3.1).

Many authors (see, for example, Brooks and Corey [47], van Genuchten [48], Fredlund and Xing [49]) proposed other empirical relationships linking uniquely the volumetric water content (defined as the ratio of the volume of liquid to the total volume of the soil) to the soil suction. This constitutive relationship is usually called the soil-water characteristic curve. A historical review of the contributions of several researchers to the understanding of this constitutive relationship was presented by Barbour [50]. Some of these researchers, particularly within soil science, used the pressure head of the pore liquid as a variable alternative to the soil suction. In soil science the pore air pressure within an unsaturated soil is assumed to be constant and equal to the atmospheric value, therefore the pressure head of pore liquid is an alternative measure of the soil suction. The van Genuchten [48] expression, which is widely used in unsaturated soil mechanics and which will also be used in the following part of this work (see Section 4.3), is recalled here:

$$\theta = \theta_r + (\theta_s - \theta_r)\left(\frac{1}{1 + (\alpha\, s)^n}\right)^m \tag{2.42}$$

where s is the suction (pore water pressure head, h, instead of suction, s is present in the original expression proposed by van Genuchten [48]), θ is the volumetric water content, θ_r is the residual volumetric water content, θ_s is the saturated volumetric water content, and α, m and n are model parameters. Unlike the state surface equations proposed by Lloret and Alonso [22] (Equations 2.40 and 2.41), the van Genuchten [48] expression (Equation 2.42) neglects any form of dependency of the degree of saturation on the net stress state. This is

explained by the fact that the expression proposed by van Genuchten [48] was originated and firstly employed within the field of soil science, where the assumption of a rigid soil skeleton is commonly accepted. Equation 2.42 can be rewritten in terms of degree of saturation and void ratio, e by using the following relationship:

$$\theta = S_r \frac{e}{1+e} \tag{2.43}$$

Substituting Equation 2.43 in Equation 2.42 and, due to assumption, made in soil science, of indeformable soil skeleton, Equation 2.42 may be reformulated in terms of the only degree of saturation with no dependency on the void ratio:

$$S_r = \left(\frac{1}{1+(\alpha\, s)^n}\right)^m. \tag{2.44}$$

In deriving Equation 2.44 from the original equation of van Genuchten [48] expressed in terms of volumetric water content, two additional assumptions are necessary: firstly, the soil becomes saturated at a value of suction equal to zero and, secondly, the residual value of the volumetric water content is equal to zero (i.e. the soil tends to dryness when suction tends to infinity).

The shortcomings of the state surface approach (i.e. postulation of a unique relationship between degree of saturation, suction and net stress state) already highlighted in Section 2.3.1, for the case of the void ratio, apply also for the degree of saturation. The main pitfall is that no distinction is made between reversible and irreversible change in the degree of saturation. Unsaturated soil can experience irrecoverable changes in the degree of saturation on reversal of the stress-path. This is shown in Figure 2.17 where data from an isotropic loading-unloading test at constant suction, performed by Zakaria [15] on compacted Speswhite Kaolin, have been re-plotted in terms of degree of saturation. On reversal of the stress path, the irrecoverable change in degree of saturation, indicated as ΔS_r^p, is evident.

Due to the possibility that irrecoverable changes in degree of saturation may occur, the uniqueness of the state surface formulation for degree of saturation has to be questioned, as it was for the void ratio case. This kind of approach is, therefore, applicable only

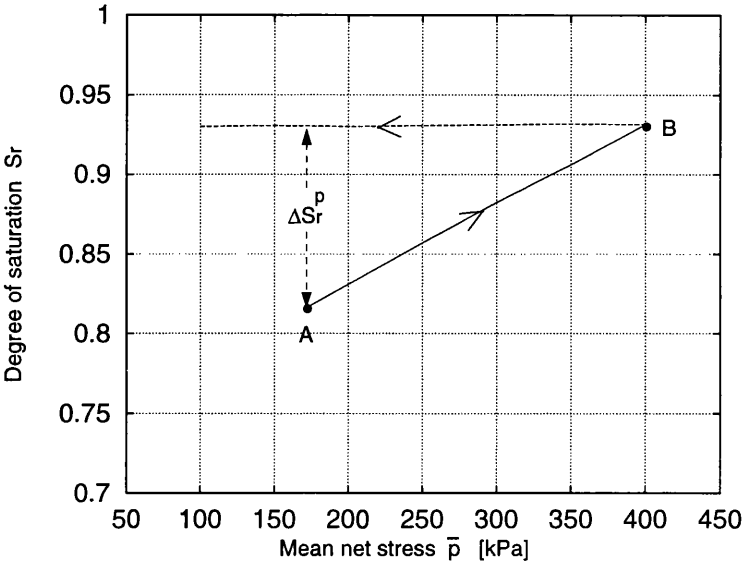

Figure 2.17: Isotropic loading-unloading test at the constant suction of 100 kPa performed on compacted Speswhite Kaolin (results computed from data published by Zakaria [15])

for monotonic loading where the stress path followed is such that it does not involve elastic unloading once yielding has taken place. Matyas and Radhakrishna [21] showed that the state surface for degree of saturation is unique and is independent of the stress path followed as long as some limitations are imposed on the nature of the stress path followed. In particular they pointed out that, like for the void ratio, the change in degree of saturation was independent of the stress path followed as long as degree of saturation was a non-decreasing parameter or, equivalently, suction was not increasing. However the uniqueness of the state surface for the degree of saturation was not as clear as it was in the case of void ratio, even for stress paths having the restriction mentioned above. Matyas and Radhakrishna [21] explained this as a consequence of testing difficulties, but an alternative explanation is the influence of hydraulic hysteresis on the variation of degree of saturation (see Section 2.5.3). Later on Lloret and Alonso [22] gave further evidence that the uniqueness of the state surface for degree of saturation is achieved only for stress paths with non-decreasing net stress and non-increasing suction. A further proof that the change of degree of saturation is stress path dependent, if the stress path involves an increase in suction, comes from Figure 2.18, which shows the results from three isotropic

tests on compacted Kaolin by Josa [14]. The three different stress paths start with a sample in the same initial condition and end at the same stress point. It is evident that the final value of degree of saturation is sensibly different depending on the stress path.

As far as practical applications are concerned, the same limitation, already highlighted for the void ratio case, applies also for the state surface of degree of saturation. The state surface approach can be applied as a constitutive model only if the initial stress state of the soil and the stress paths it follows due to the application of boundary conditions, are of the same type as those imposed on the samples during the tests when the state surface has been defined. For example, state surfaces defined in the laboratory by isotropic or oedometric tests are not able to predict change in degree of saturation due to a variation in deviator stress (as observed from tests on Speswhite Kaolin by Sivakumar [13]). In numerical applications for coupled flow-deformation analyses, the use of a state surface expression for the degree of saturation, defined by means of oedometric or isotropic tests, has been often improperly extended to problems where the stress paths experienced by the soil do not fit these restrictions.

2.5.2 Elasto-plastic variation of Wheeler [50]

Experimental data from the literature supporting the occurrence of irrecoverable changes in degree of saturation were presented in Section 2.5.1. Improved modelling of the variation of degree of saturation can therefore be achieved by using the concepts of elasto-plasticity. In the case of a change of suction (wetting and drying) the irrecoverable changes of degree of saturation observed during experiments can however be due to the combination of plastic changes of degree of saturation and the additional phenomenon of hydraulic hysteresis. A description of hydraulic hysteresis and experimental evidence from the literature supporting the occurence of such a phenomenon, will be presented in Section 2.5.3.

This section describes the ideas proposed by Wheeler [51] in order to include the elasto-plastic variation of degree of saturation, S_r in a consistent manner within an elasto-plastic framework. Wheeler's proposal was, however, expressed in terms of variations of specific water volume, v_w, rather than S_r. The specific water volume is defined as the sum of the volume of liquid and the volume of solids in a volume of soil containing unit volume of

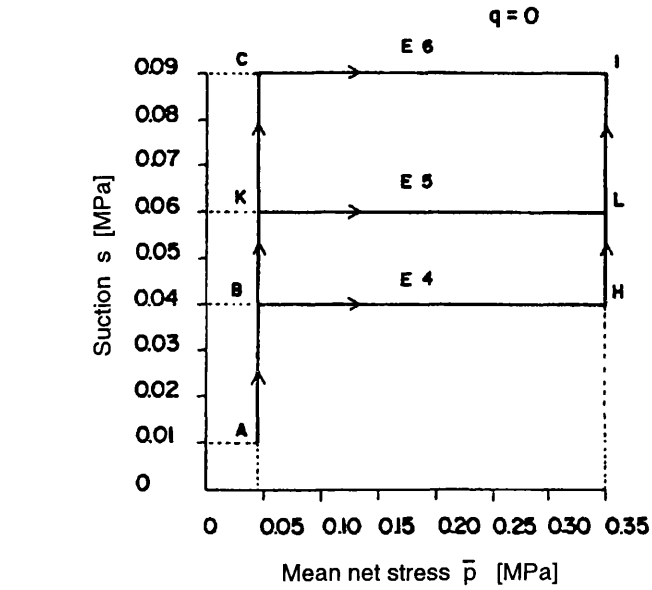

(a)

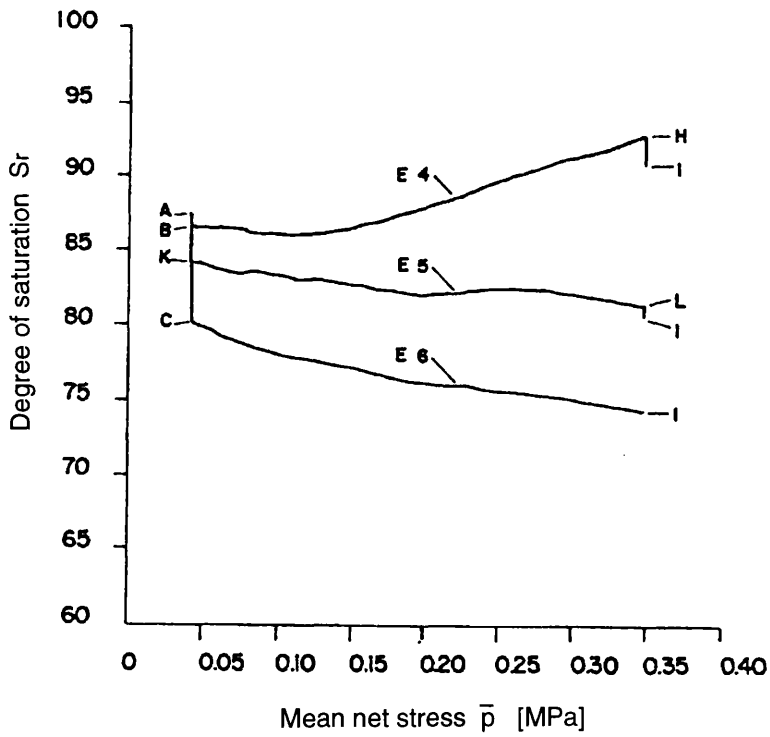

(b)

Figure 2.18: Isotropic compression-drying tests performed on low plasticity Kaolin: (a) stress paths (b) degree of saturation change (after Josa [14])

solids and its relation with specific volume, v and degree of saturation, S_r is:

$$v_w = 1 + S_r e = 1 + (v - 1)\, S_r \tag{2.45}$$

The proposals of Wheeler [51] result in a model capable of predicting the elasto-plastic variation of both v and v_w. Equation 2.45 could then be used to calculate the corresponding elasto-plastic variation of degree of saturation (which is likely to be required for implementation of the constitutive model in a finite element code, since the equations of conservation of air and water mass are usually expressed in terms of degree of saturation).

The elasto-plastic model proposed by Wheeler [51] is built on the previous model of Wheeler and Sivakumar [3] and represents an enhancement of such a model since it introduces the possibility of predicting changes of specific water volume. The main hypothesis on which this model is based is the postulation of a relationship which links the air void ratio, e_a to the value of suction, s and to the accumulated plastic volumetric strain expressed through the hardening parameter, $\overline{p}_o^*$. The air void ratio is defined as the volume of gas within an element of soil having unit volume of solids and it is related to the other soil variables by the expression:

$$e_a = (1 - S_r)e = (1 - S_r)\,(v - 1). \tag{2.46}$$

The proposed relation describing the variation of air void ratio with suction and hardening parameter is:

$$e_a(s, \overline{p}_o^*) = A(s) - \alpha(s) \ln \frac{\overline{p}_o^*}{p_{atm}} \tag{2.47}$$

where $A(s)$ and $\alpha(s)$ are two functions of suction. It is then possible to relate the value of the specific water volume v_w to the values of specific volume, v and air void ratio, e_a by means of the following relationship:

$$v_w = v - e_a. \tag{2.48}$$

In Equation 2.48 the variation of the specific volume, v is given by the elasto-plastic model of Wheeler and Sivakumar [3], while the variation of the air void ratio, e_a is given

by Equation 2.47. Therefore Equation 2.48 links the specific water volume to the stress state in an elasto-plastic fashion. It also introduces a coupling between the elastic and plastic behaviour, since the elastic variation of degree of saturation depends on the value of the hardening parameter p_o^* (i.e. on the volumetric plastic strain).

The ideas proposed by Wheeler [51] have general relevance and could equally be applied to the model of Alonso, Gens and Josa [1] in order to include in this model elasto-plastic variation of the specific water volume (and hence S_r). Finally it is worth highlighting that this approach does not represent a solution for modelling the hydraulic hysteresis of an unsaturated soil during drying-wetting cycles (see next section), because it is able to predict irreversible change in degree of saturation only for changes of suction which involve yielding but, for drying-wetting cycles within the elastic domain, the predicted variation of degree of saturation is entirely reversible.

2.5.3 Hydraulic hysteresis

Occurence of hydraulic hysteresis has been observed in wetting-drying tests on unsaturated soil performed by many authors, particularly within soil science (see, for example, Croney [52]). It consists in a difference of degree of saturation at the same value of suction during drying-wetting cycles depending on whether the stress state lies on the drying or wetting branch of the loop. A typical consequence of hydraulic hysteresis is the possibility of having unsaturated soil samples at a value of suction equal to zero. It is well known from drying tests that a finite value of suction (known as the air entry value) can be applied at the boundary of a saturated soil sample before it starts to desaturate. On the reversal of the stress path, it is possible to wet the soil up to a zero value of suction with the degree of saturation remaining significantly below unity. Figure 2.19 shows a schematic representation of the phenomenon of hydraulic hysteresis during drying-wetting tests on an initially saturated soil sample.

Hydraulic hysteresis is a qualitatively different phenomenon from plasticity since it occurs at any stress state without implying the violation of a yielding criterion. It can even occur with a rigid soil skeleton. Due to hysteresis, irreversible changes of degree of saturation arise whenever a reversal in the suction path occurs. Therefore, for drying-wetting

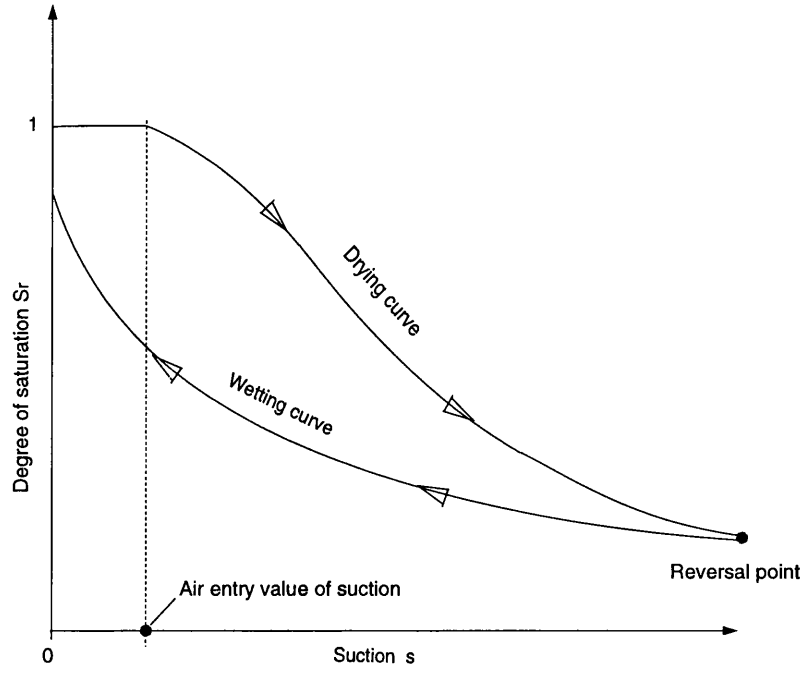

Figure 2.19: Schematic representation of hydraulic hysteresis during a drying-wetting cycle at constant net stresses

cycles even of an infinitesimal dimension, each reversal of the stress path produces irreversible changes of degree of saturation. This represents another difference with classical plasticity since during cyclic variation of the stress state, plastic changes are experienced only if the first loop of the cycle violates the initial yield and only for the first reversal in the stress path. Any subsequent part of the cycle produces reversible changes of degree of saturation since it takes place inside the yield locus.

Figure 2.20 shows the suction-moisture content relationships from tests performed by Croney [52] on two different samples of soft chalk and hard chalk. The suction is expressed on the pF scale and the moisture content, w, is used as an alternative to the degree of saturation (in much of soil science the soil skeleton is assumed to be rigid, and there is therefore a unique relationship between S_r and w). The pF scale (Schofield [53]) is defined as the logarithm (base 10) of the pressure head of the pore liquid expressed in centimetres. For both samples one main loop is reported which includes a wetting curve and a drying curve. Both these curves correspond to suction ranging between $pF = 0$

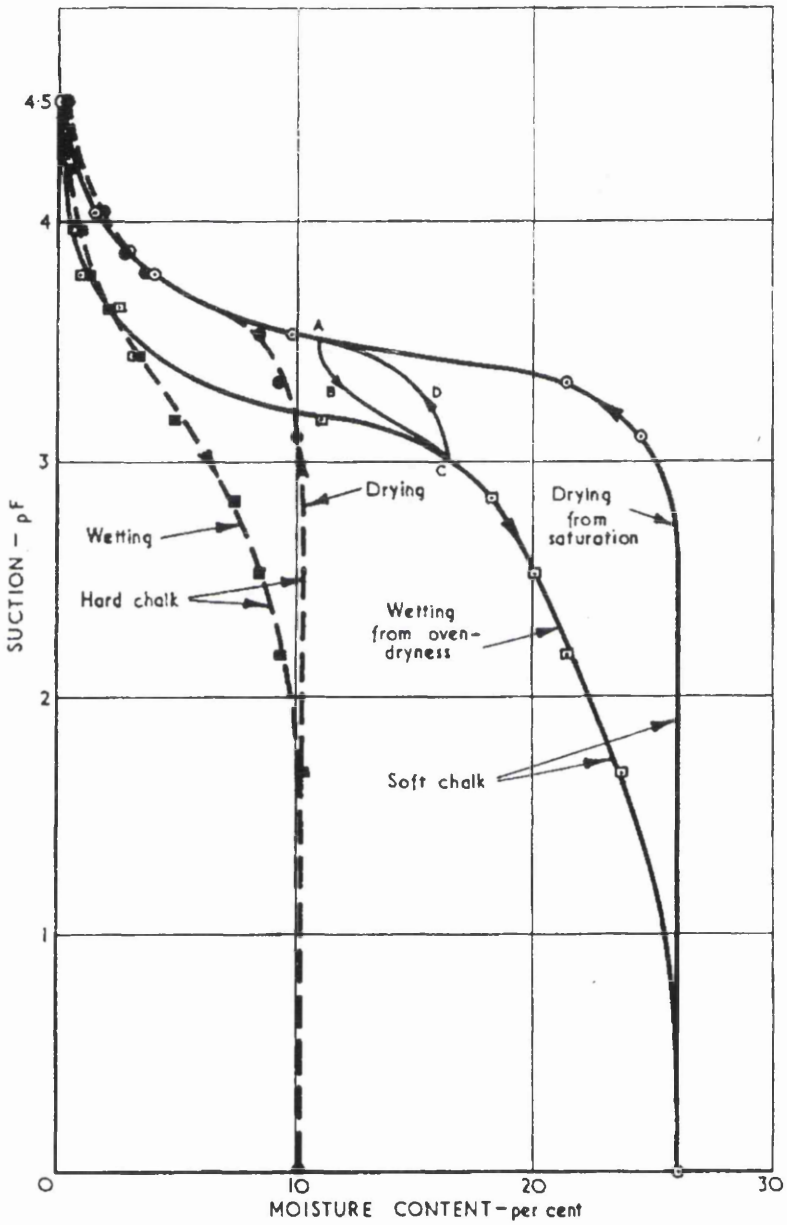

Figure 2.20: Wetting-drying test performed on hard and soft chalk (after Croney [52])

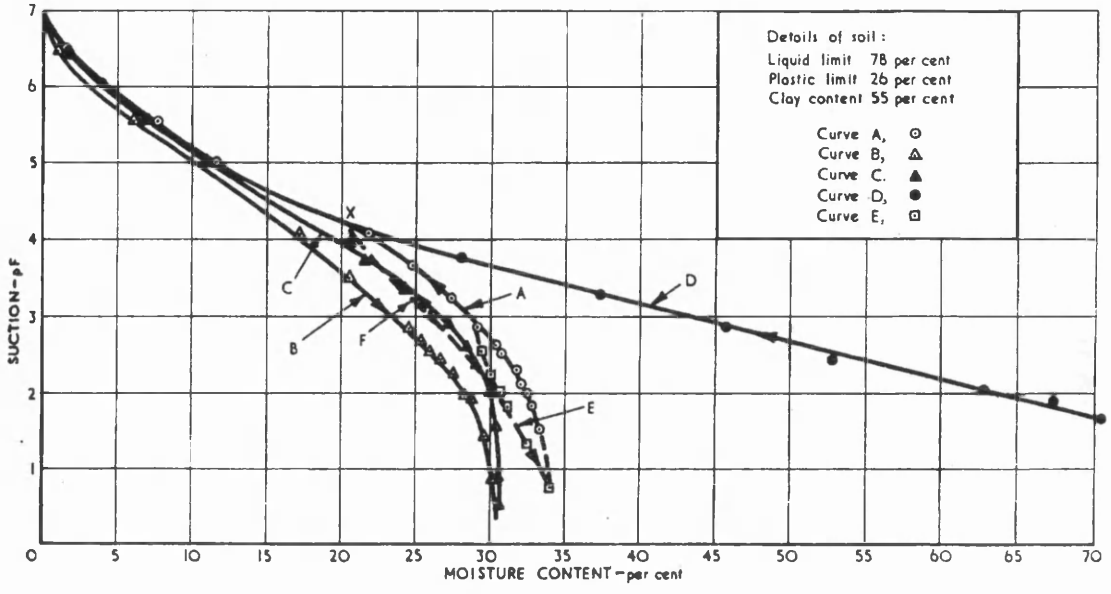

Figure 2.21: Wetting-drying test performed on an undisturbed sample of a heavy clay soil (after Croney [52])

(suction approximately null and saturated conditions) and $pF = 4.5$ (moisture content equal to oven-dryness conditions). For both samples there is a suction interval in which the soil presents, at the same value of suction, different values of moisture content. From consideration of this main loop it is clear that the variation of moisture content (or degree of saturation) is more readily represented by an hysteretic model than by classical elasto-plasticity. In fact for repetitive variations of suction between these two extremes ($pF = 0$ and $pF = 4.5$) the changes in moisture content will always follow the drying branch of the loop, for increasing suction, and the wetting branch of the loop, for decreasing suction. This pattern of behaviour is not explicable in terms of traditional isotropic hardening plasticity, where an irreversible change of moisture content would be expected only for the first reversal in suction, after violation of the initial yield locus.

The results reported in Figure 2.20 refer to a material of rigid structure like the chalk. Therefore during the wetting or drying process the soil particles do not experience any rearrangement in their structure. In the same paper Croney [52] reports also results relative to a compressible undisturbed soil sample (Figure 2.21).

In this case the initial drying path (from saturated conditions up to oven-dryness) is denoted by the letter A and the subsequent wetting path by letter B. The loop does not close and the author attributed this effect to the re-packing of the soil particles induced by the drying process. Therefore the difference between the two curves A and B is not solely attributable to hysteresis but also to plastic deformation in the soil skeleton occurring during the drying process. Curve C represents the next drying path from saturated conditions up to oven-dryness and, this time, the subsequent wetting curve follows the previous wetting curve, B, almost exactly forming a closed hysteresis loop. These results mean that, once plastic deformation occurred due to the rearrangement of soil particles during the first drying cycle, any subsequent cyclic variation of suction does not produce mechanical disturbance of the soil structure and irreversible changes of moisture content are due exclusively to hysteresis, as in a rigid material. The important conclusion is that irreversible change of moisture content (and equivalently degree of saturation) can be due to the combination of the two phenomena of hysteresis and plasticity.

The phenomenon of hysteresis may be explained by a physical argument. Consider a granular medium where pore liquid is present in the form of bulk liquid filling a soil pore. The bulk liquid is separated from the surrounding gas phase at higher pressure by menisci which act like membranes equilibrating the different pressure between the gas and liquid phases. A schematic two-dimensional representation of such a portion of soil is given in Figure 2.22 (a). If from this initial condition suction is progressively increased, the menisci at the interface between the two phases will readjust their shape increasing their curvature in order to balance the higher difference of pressure between the two phases. This will continue until a limit value of suction will be attained corresponding to the entry of gas into the soil pore (Figure 2.22 (b)). This will happen when the meniscus interface acting at the narrowest point of the widest entry throat to the pore is not able to increase further its curvature and, therefore, is no longer able to equilibrate the difference of pressure between gas and liquid.

After the emptying of the pore, a new configuration is reached with the formation, inside the pore, of new menisci (Figure 2.22 (c)). If from this condition suction is now

decreased, the pore will not immediately flood again but the menisci will rearrange their shape at their new positions (diminishing their curvatures) to adapt to the lower value of suction. Flooding of the pore will happen again when two menisci or more menisci come into contact (Figure 2.22 (d)). Therefore during a wetting path a given degree of saturation is reached at a lower value of suction than on the drying path.

2.6 Liquid and gas flows and variation of the respective permeabilities with S_r

The pores inside an unsaturated soil are filled with liquid and gas phases. These two fluid phases are at different pressures and the equilibrium between the two is maintained by the presence of the menisci at the interface between the two phases. The analysis of fluid flow requires a law which relates the flux of each of these two phases to the gradient of a driving potential using appropriate coefficients (in the same way as the liquid flux in a saturated soil is related to the gradient of hydraulic head by Darcy's law through the coefficient of permeability). Flow of liquid can also take place under a gradient of chemical concentration or electrical potential; however these aspects will not be considered in this thesis.

The driving potential which controls the liquid flow is the hydraulic head, h_w, defined as:

$$h_w = y + \frac{u_w}{\rho_w g} \tag{2.49}$$

where y is the elevation above an arbitrary datum, u_w is the pore water pressure, ρ_w is the liquid density and g is the gravitational acceleration.

Similarly the driving potential which controls the gas flow is the gas head, h_a defined as:

$$h_a = y + \frac{u_a}{\rho_{ma} g} \tag{2.50}$$

where u_a is the pore air pressure and ρ_{ma} is a reference constant gas density value. The contribution to the gas flow driving potential of Equation 2.50 due to the elevation y

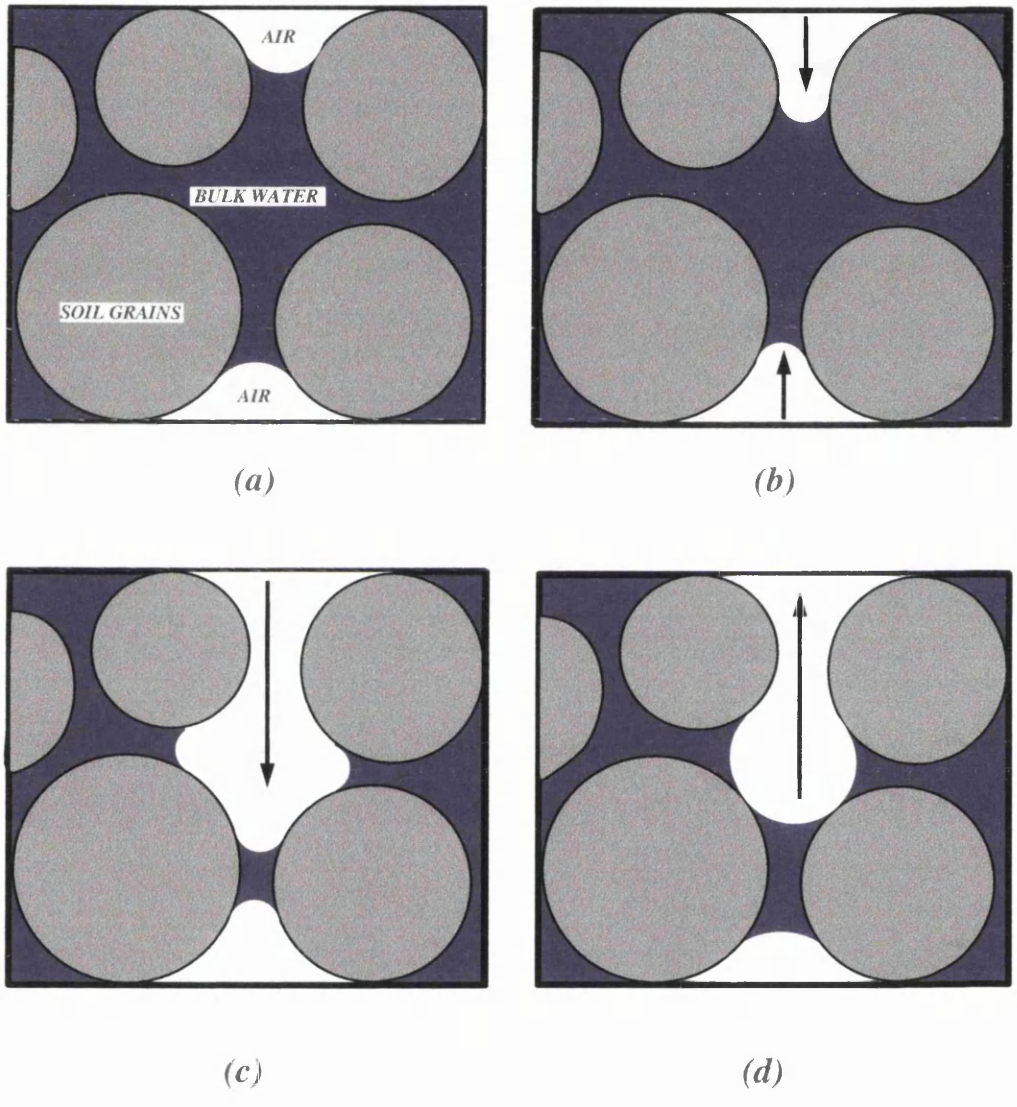

Figure 2.22: Schematic explanation of the hysteresis phenomenon for cyclic variation of suction: (a) initial conditions (drying path) (b) soil pore about to empty of liquid (drying path) (c) soil pore empty of liquid (d) soil pore about to flood with liquid (wetting path)

is, however, negligible compared to the other term, because of the small value of the air densisty, ρ_{ma}.

In a saturated medium the liquid flow is commonly described by using Darcy's law, stated as:

$$\boldsymbol{v}_{wr} = -k_w \nabla h_w \tag{2.51}$$

where $\boldsymbol{v}_{wr}$ is the liquid flux velocity relative to the soil skeleton and k_w is the coefficient of permeability with respect to the liquid phase. Equation 2.51 is also used for liquid flow through an unsaturated soil. The main difference is that the coefficient of permeability is not a constant as in the saturated case but it depends on the degree of saturation of the soil ($k_w(S_r)$).

The law for gas flow is of similar form to that for liquid flow. It introduces a relationship between the gas flow and the gradient of the relative driving potential (gas head) as follows:

$$\boldsymbol{v}_{ar} = -k_a(S_r) \nabla h_a \tag{2.52}$$

where $\boldsymbol{v}_{ar}$ is the gas flux velocity relative to the soil skeleton and $k_a(S_r)$ is the coefficient of permeability with respect to the gas phase. Again, the value of $k_a(S_r)$ depends strongly on the degree of saturation of the soil. Figure 2.23 illustrates the qualitative variation of the relative permeabilities of liquid and gas ($k_{wr}(S_r)$ and $k_{ar}(S_r)$) with degree of saturation. The relative permebilities for the liquid and gas phases are defined as:

$$k_{wr}(S_r) = \frac{k_w(S_r)}{k_s}, \quad k_{ar}(S_r) = \frac{k_a(S_r)}{k_d} \tag{2.53}$$

where k_s is the coefficient of permeability with respect to the liquid phase at full saturation (i.e. $S_r = 1$) and k_d is the coefficient of permeability with respect to the gas phase at a residual value of degree of saturation (i.e. $S_r = S_{res}$).

Figure 2.23 shows that the two relative coefficients of permeability, $k_{wr}(S_r)$ and $k_{ar}(S_r)$, assume values of zero and unity respectively when the degree of saturation is the residual one, S_{res}. Physically, the attainment of the residual value of degree of saturation, S_{res}

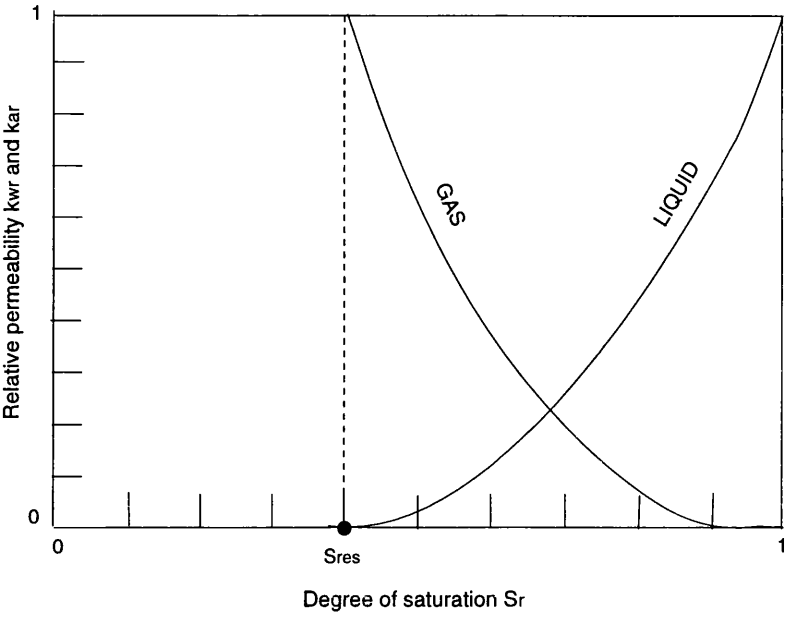

Figure 2.23: Qualitative variation of $k_{wr}(S_r)$ and $k_{ar}(S_r)$ with degree of saturation

corresponds to the situation where the liquid phase is no longer continuous, and is only present as isolated lenses at the inter-particle or inter-packet contacts.

Many authors within soil science (see, for example, Brooks and Corey [47], van Genuchten [48] and Gardner [54]) proposed relationships between the coefficients of permeability, $k_w(S_r)$ and $k_a(S_r)$, and the degree of saturation. The relationships which have been used in this work are the ones proposed by Brooks and Corey [47]. The coefficient of liquid permeability, $k_w(S_r)$, is assumed to vary with degree of saturation, S_r, according to the following relationship:

$$k_w(S_r) = k_s {S_e}^{\delta_w} \tag{2.54}$$

where S_e is the effective degree of saturation (Corey [55]) and δ_w is an empirical constant. The effective degree of satuartion, S_e in Equation 2.54 is defined as:

$$S_e = \frac{S_r - S_{res}}{1 - S_{res}}. \tag{2.55}$$

The empirical constant δ_w in Equation 2.54 is related by Brooks and Corey [47] to the

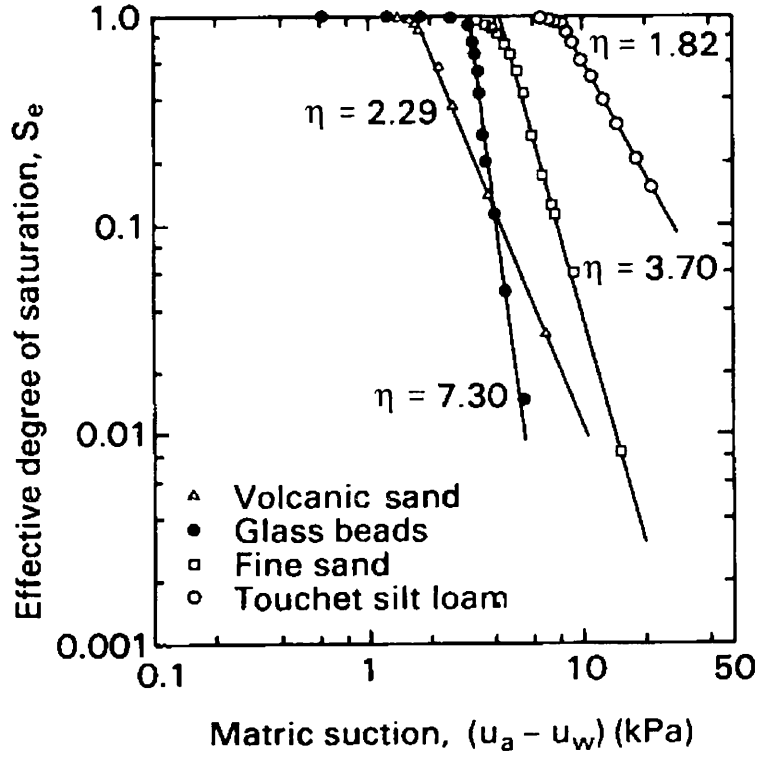

Figure 2.24: Plot of effective degree of saturation against suction for determining the pore size distribution index, η (after Fredlund and Rahardjo [56])

pore size distribution index η through the following relationship:

$$\delta_w = \frac{2+3\eta}{\eta}. \tag{2.56}$$

The pore size distribution index, η, is determined by plotting the effective degree of saturation, S_e, against suction on a logarithmic scale for a drying test on an initially saturated sample. Figure 2.24 shows typical examples of such plots for four different soils. Two lines, one horizontal and one inclined, can be fitted through the experimental data points: the slope of the inclined line defines the pore size distribution index, η. The intersection between the initial horizontal line and the inclined line gives also an estimate of the air entry value of suction.

In the same paper Brooks and Corey [47] also proposed a relationship between coefficient of gas permeability, k_a and degree of saturation, S_r having the form:

$$k_a(S_r) = k_d(1 - S_e)^2(1 - S_e{}^{\delta_a}) \tag{2.57}$$

where k_d is the coefficient of permeability with respect to the gas phase for a soil at the residual value of degree of saturation, S_{res} and δ_a is an empirical constant. The empirical constant δ_a in Equation 2.57 is related by Brooks and Corey [47] to the pore size distribution index η through the following relationship:

$$\delta_a = \frac{2 + \eta}{\eta}. \tag{2.58}$$

Chapter 3

Choice of Model Parameters

3.1 Introduction

The numerical analyses in the present work were carried out by using the finite element code "Compass" [43], which is able to perform fully coupled flow-deformation analyses in unsaturated soil. "Compass" [43] was developed by Prof. H.R. Thomas and colleagues at the University of Cardiff. An outline of the methodology of the code is given in Chapter 5.

In the code provided from Cardiff the constitutive model of Alonso, Gens and Josa [1] was implemented in order to model the mechanical behaviour of unsaturated soil (see Section 2.4 for a description of the model together with its validation and shortcomings). In order to perform coupled flow-deformation analyses, which introduced the two equations of conservation of air and water mass, in addition to the equations of equilibrium (see Chapter 5), the model of Alonso, Gens and Josa [1] was extended in the original code developed at Cardiff so that it included the change of degree of saturation, S_r, as an additional strain variable. This was achieved by using the state surface expression proposed by Lloret and Alonso [22] (Equation 2.41).

In Chapter 4 an improved model including the variation of degree of saturation in a more consistent fashion within an elasto-plastic framework is proposed. This new formulation overcomes some of the shortcomings of the state surface approach highlighted in Section 2.5.1.

The coupling of flow and deformation requires also that relationships have to be specified for the variation with degree of saturation of the coefficients of permeability with

Liquid Limit (w_L)	69%
Plastic Limit (w_P)	38%
Plasticity Index (I_P)	31%
Specific Gravity of soil particles (G_s)	2.61

Table 3.1: Index properties for Speswhite Kaolin

respect to the liquid and gas phases. For this purpose, the expressions proposed by Brooks and Corey [47], given in Equations 2.54 and 2.57, were adopted in this work.

This chapter describes the procedure used to define the set of values for the soil parameters within the elasto-plastic model of Alonso, Gens and Josa [1] (see Section 3.2), the state surface expression for degree of saturation of Lloret and Alonso [22] (see Section 3.3) and the relationships for the coefficients of permeability with respect to the liquid and gas phases of Brooks and Corey [47] (see Section 3.4). This set of model parameter values was used throughout the numerical analyses performed in this work. The model parameter values were determined using the results from tests on compacted unsaturated Speswhite Kaolin from Sivakumar [13] and from Zakaria [15]. The index properties of this material are reported in Table 3.1. In both these series of tests, triaxial samples, 50 mm in diameter and 100 mm in height, were used after compaction in a mould at a water content of 25% (4% less than the optimum from the standard Proctor compaction test). The samples were compacted in nine layers with each layer statically compacted in a compression frame at a fixed displacement rate of 1.5 mm/min up to a vertical total stress of 400 kPa.

Model parameter values matched to test results on compacted Speswhite Kaolin were selected for two different reasons. Firstly it was considered desirable to use an internally consistent set of model parameters, representing a real soil, in all the numerical analyses carried out in this work. The second reason was that the data from tests on compacted Speswhite Kaolin are used in Chapter 4 to assess the validity of the proposed extension to the constitutive model of Alonso, Gens and Josa [1]. The test results on compacted Speswhite Kaolin were selected in particular because they probably form the largest and most complete set of data on a single unsaturated soil available in the literature.

ELASTIC PARAMETERS	
Shear Modulus (G)	10000 kPa
Swelling index for changes in suction (κ_s)	0.020
Swelling index for changes in mean net stress (κ)	0.025
STRENGTH PARAMETERS	
Slope of critical state line in constant suction planes (M)	0.9
Parameter controlling cohesion increase with suction (k)	0.5
NORMAL COMPRESSION LINES AND LC YIELD CURVE	
Reference pressure (p^c)	2000 kPa
Slope of normal compression line (NCL) at zero suction ($\lambda(0)$)	0.13
Specific volume on NCL at zero suction for $\overline{p} = p^c$ ($N(0)$)	1.66
Parameter controlling ratio of NCL slopes at $s \rightarrow \infty$ and $s = 0$ (r)	1.5
Parameter controlling variation of NCL slope with suction (β)	0.01 kPa^{-1}

Table 3.2: Values of the Alonso, Gens and Josa [1] model parameters

3.2 Parameters for the Alonso, Gens and Josa [1] model

The selected set of values for the soil constants is summarized in Table 3.2. The background to the selection of these values is discussed in the following sections. In selecting the parameter values, these were often rounded within the limits which are justified by the uncertainties associated with the experimental results.

3.2.1 Choice of parameters κ, κ_s and G

The value of the elastic swelling index for changes in mean net stress, κ and the value of the elastic swelling index for changes in suction, κ_s, defined in Equation 2.18, were taken as 0.025 and 0.020 respectively, as reported in Wheeler [51] and Wheeler and Sivakumar [3].

The elastic swelling index for changes in mean net stress, κ, was chosen according to experimental evidence from Zakaria [15]. The value of 0.025 was the average value of the elastic swelling index calculated from the measured increase of specific volume in a total of eight isotropic unloading tests performed by Zakaria [15] at constant suction.

The elastic swelling index for changes in suction, κ_s, was chosen according to experimental evidence from Sivakumar [13]. It is based on the difference between the average swelling observed in several samples wetted to 200 kPa, and the average swelling observed in other samples wetted to 300 kPa.

Suction	$M(s)$	$\mu(s)$	$\frac{\mu(s)}{M(s)}$
0 *kPa*	0.813	0.0 kPa	0.0 kPa
100 *kPa*	0.933	54.2 kPa	58.1 kPa
200 *kPa*	0.959	83.5 kPa	87.1 kPa
300 *kPa*	0.910	122.0 kPa	134.1 kPa

Table 3.3: Experimental values of $M(s)$ and $\mu(s)$

The value of shear modulus G, defined in Equation 2.31, was taken as 10 MPa. This value, reported in Wheeler and Sivakumar [3], is based on constant suction shearing tests after isotropic compression to a normally consolidated state and is calculated, according to Equation 2.31, from the average value of the initial slopes of the experimental deviatoric stress-deviatoric strain curves at different values of suction and initial mean net stress.

3.2.2 Choice of parameters M and k

The slope of critical state lines in each constant suction plane, M, and the parameter controlling cohesion increase with suction, k, defined in Equation 2.32 were chosen according to experimental evidence from Sivakumar [13]. Wheeler and Sivakumar [3] proposed values of $M(s)$ and $\mu(s)$ (cohesion intercept in a $(q, \overline{p})$-plane at constant suction, see Equation 2.38), and these values are reported in Table 3.3 for four different value of suction (0 kPa, 100 kPa, 200 kPa, 300 kPa). Subsequent experimental evidence from Wheeler and Sivakumar [33] for the same material, indicated that the variation of M with suction for suctions between 0 and 300 kPa was less significant than that reported in Table 3.3 (see Section 2.3.2) and they suggested a constant value of M equal to 0.863. In the model of Alonso, Gens and Josa [1] not only is M assumed constant, but $\mu(s)$ is assumed to increase at a linear rate with suction.

In this work the values of the parameters, M and k, were chosen at 0.9 and 0.5 respectively, predicting a linear increase of shear strength with mean net stress and suction according to Equation 2.32. Figure 3.1 shows the critical state lines predicted by the model in the $(q, \overline{p})$-planes at different suctions together with experimental data points from Sivakumar [13]. Inspection of Figure 3.1 reveals that the model parameters chosen produce a reasonably good fit between experimental and predicted data at critical state in the

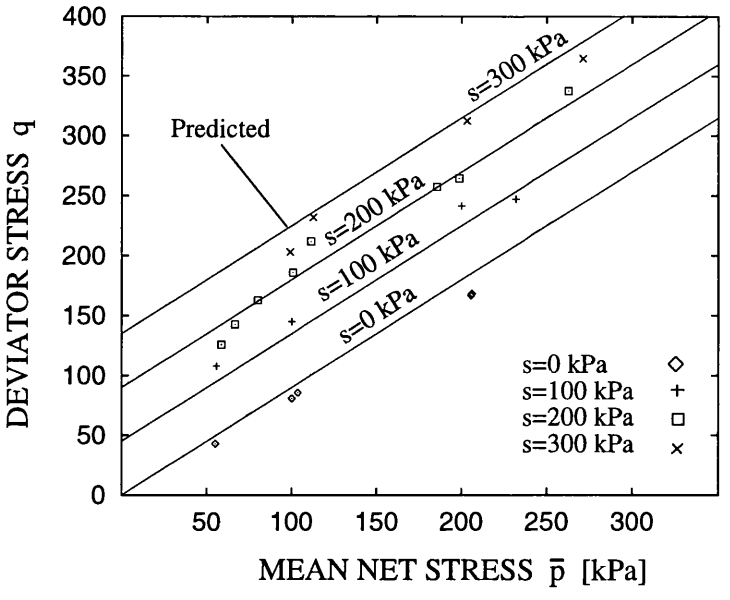

Figure 3.1: Predicted critical state lines (CSL) and experimental critical state (CS) data points in $(q, \overline{p})$-plane at different suctions

$(q, \overline{p})$-planes.

3.2.3 Choice of parameters $\lambda(0)$, r and β on the basis of NCL slopes

The parameter, $\lambda(0)$ (see Equation 2.20), is the slope of the normal compression line for a value of suction equal to zero, corresponding to saturated conditions for the soil. The parameter, r (see Equation 2.20), represents the ratio between the slope of the normal compression line for suction tending to infinity, $\lambda(\infty)$, and the slope of the normal compression line for suction equal to zero, $\lambda(0)$, (Figure 2.9). The parameter β (see Equation 2.20) controls the exponential rate of variation of the slope of the normal compression lines, $\lambda(s)$, with suction. The novelty of this work in selecting the parameters for the Alonso, Gens and Josa [1] model, is represented by the choice of a value greater than 1 for the model parameter r whereas Alonso, Gens and Josa [1] suggested values of r smaller than 1 (Section 2.4.1). The reasons and the implications of this choice will be discussed later in this section and in Section 3.2.5.

The experimental values of the slope $\lambda(s)$ of normal compression lines at constant

Suction	Experimental $\lambda(s)$	Predicted $\lambda(s)$
0 *kPa*	0.128	0.130
100 *kPa*	0.182	0.171
200 *kPa*	0.196	0.186
300 *kPa*	0.176	0.192
∞ *kPa*		0.195

Table 3.4: Predicted and experimental values of $\lambda(s)$

suction reported in Table 3.4, were presented by Wheeler and Sivakumar [3] on the basis of the average measurements of slopes from several tests at each of four values of constant suction, performed by Sivakumar [13] (Figure 2.3). Inspection of Table 3.4 reveals that the slope of the experimental normal compression lines, $\lambda(s)$, generally increases with increasing suction, except for the value of suction equal to 300 kPa, where a smaller value of $\lambda(s)$ than at a suction of 200 kPa was observed. However the value of $\lambda(s)$ corresponding to a suction of 300 kPa was based, unlike the other values, on the analysis of a single test involving only a relatively short section of normal compression line (see Figure 2.3), and it should therefore be treated with a degree of caution.

On the basis of the experimental values of $\lambda(s)$ reported in Table 3.4 a value of 0.13 was selected for $\lambda(0)$ (rounded from the measured value of 0.128) and a value of 1.5 was selected for r (to reproduce the overall pattern of increasing $\lambda(s)$ with increasing suction). This resulted in a prediction of a limiting value of $\lambda(s)$ of 0.195 as suction tended to infinity (similar to the maximum measured value of $\lambda(s)$ of 0.196, which actually occurred at a suction of 200 kPa.

As mentioned at the beginning of this section, the choice for the r parameter of a value greater than 1 may seem surprising, since Alonso, Gens and Josa [1] always assumed values smaller than 1 in developing their model. This difference is due to the fact that Alonso, Gens and Josa [1] assumed that the slopes of the normal compression lines would decrease with increasing suction (see Figure 2.9) whereas experimental evidence from Sivakumar [13] shows that, for compacted Speswhite Kaolin over the range of suctions and net stresses tested, these slopes increase with increasing suction. The choice, made in this work, of a value for the r parameter greater than 1 has to be combined with a value of

the reference pressure p^c (see Equations 2.19 and 2.26) considerably higher than the range of values of net stress that are to be modelled, in order to obtain realistic shapes of the LC yield curve. The aspects relating to the influence of the choice of a value greater than 1 for r on the shape of LC yield curves will be discussed further in Sections 3.2.4 and 3.2.5.

The range of slope variation is defined by the two limit values that $\lambda(s)$ can assume for suction equal to zero ($\lambda(0)$) and suction tending to infinity ($r\lambda(0)$). Within this range the parameter β (see Equation 2.20) controls the variation of the slope with suction. The higher the value of β, the quicker $\lambda(s)$ tends towards the limiting value $r\,\lambda(0)$ as suction is increased. In this work the value of the parameter β was assumed to be equal to 0.01 kPa^{-1}, which fits well the experimental slopes presented by Wheeler and Sivakumar [3], where most of the increase of the slope, $\lambda(s)$, takes place as the suction increases from zero to 100 kPa. Table 3.4 shows a comparison between the experimental values of $\lambda(s)$ at four different level of suction and the values predicted by the model.

3.2.4 Influence of parameters $\lambda(0)$, r and β on the shape of the LC yield curve

The values of the model parameters $\lambda(0)$, r and β introduced in Section 3.2.3, determine the variation of the slope of the normal compression lines, $\lambda(s)$, with suction. The choice of these values, however, also influences the shape of the LC yield curve, introduced in Section 2.4.1, and the way this shape develops as the yield curve expands.

In particular the parameters, $\lambda(0)$ and r , together with the parameter p^c (discussed in Section 3.2.5), control, for a LC yield curve corresponding to a given value of the hardening parameter $\overline{p}_o^*$, the difference between the limit value of $\overline{p}_o$ for suction tending to infinity and $\overline{p}_o^*$ (see Figure 3.2).

As an example, Figure 3.3 shows the influence of the variation of the r parameter on the shape of a yield curve corresponding to a value of $\overline{p}_o^* = 100$ kPa, while all the remaining model parameters are kept constant and equal to the values reported in Table 3.2. From Figure 3.3 it is evident that the difference between the value of $\overline{p}_o$ for suction tending to infinity and $\overline{p}_o^*$, increases as the value of the parameter r is increased above 1.

The choice of the parameter β influences also the shape of the LC yield curve. While

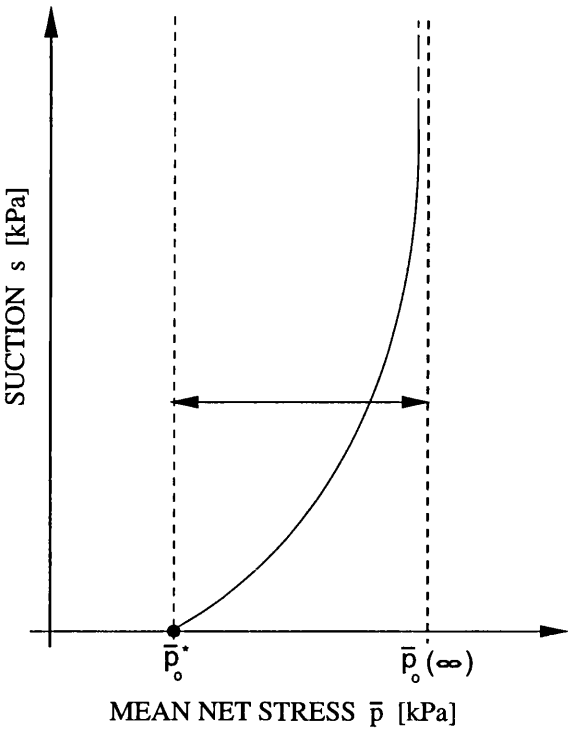

Figure 3.2: Difference between $\overline{p}(\infty)$ and $\overline{p}_o^*$ for a given LC yield curve

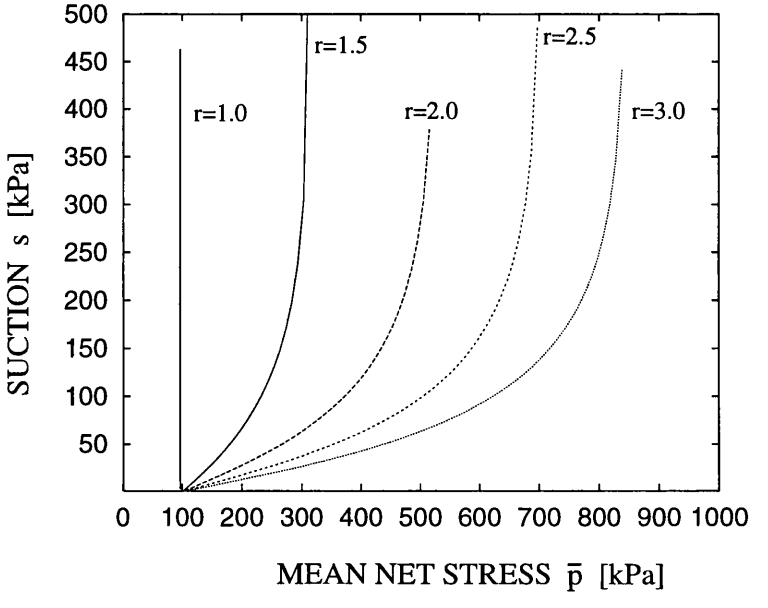

Figure 3.3: Influence of variation of the parameter r on the LC yield curve

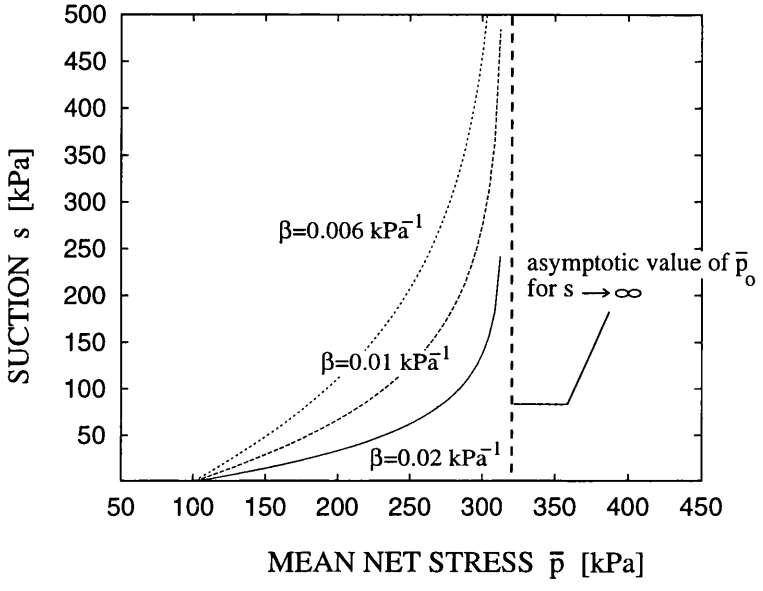

Figure 3.4: Influence of variation of the parameter β on the LC yield curve

the parameters $\lambda(0)$ and r control, for a given LC yield curve, the difference between the limit value of $\overline{p}_o$ for suction tending to infinity and $\overline{p}_o^*$, the parameter β controls the way $\overline{p}_o$ varies with suction between these two limit values. Figure 3.4 shows the influence of the variation of the β parameter on the shape of a yield curve corresponding to a value of $\overline{p}_o^* = 100$ kPa, while all the remaining model parameters are kept constant and equal to the values reported in Table 3.2.

3.2.5 Choice of parameters $N(0)$ and p^c

In presenting their model, Alonso, Gens and Josa [1] combined the choice of a value for r smaller than 1 with a value of the reference pressure p^c sensibly smaller than the range of values of interest for the hardening parameter, $\overline{p}_o^*$, in order to obtain realistic shapes of the LC yield curve. For the same reason, in this work the choice of a value for the parameter r equal to 1.5 had to be combined with a value of p^c sensibly higher than the range of values of interest for $\overline{p}_o^*$, as illustrated by Gallipoli, Karstunen and Wheeler [57]. In Figure 3.5(a) and 3.5(b) the development of the LC yield curve as it expands is plotted, to linear and logarithmic scale respectively, for the set of model parameters reported in Table 3.2.

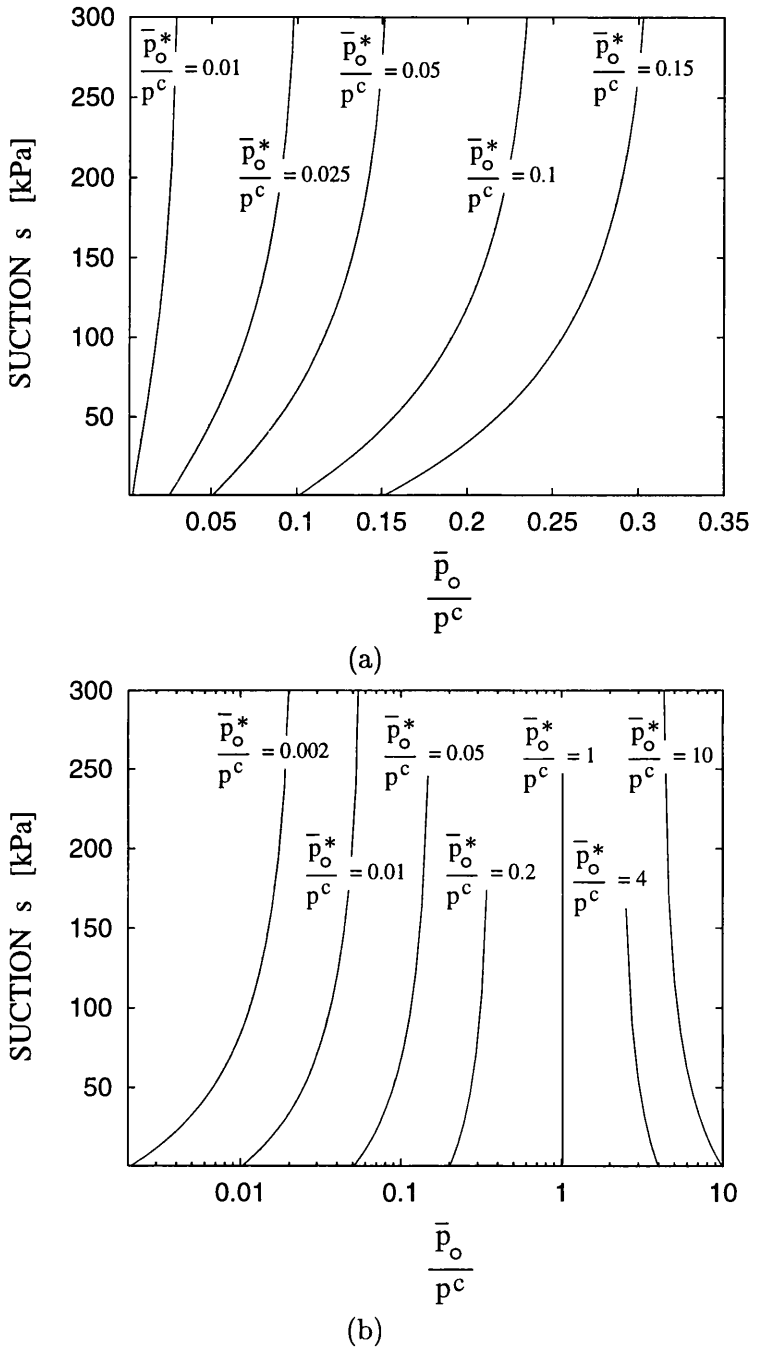

Figure 3.5: Development of shape of LC yield curve during expansion (a) linear scale (b) logarithmic scale

Figure 3.5(b) shows that the shape of the LC yield curve tends to a vertical straight line when the value of the hardening parameter, $\overline{p}_o^*$, tends to the reference pressure, p^c, and for higher values of $\overline{p}_o^*$ a yield curve with an unrealistic negative slope is predicted. However, when the LC curve is plotted to a linear scale (Figure 3.5(a)), it can be observed that, for low values of the ratio $\overline{p}_o^*/p^c$, the inclination of the LC yield curve becomes less steep as it expands, as has been observed in laboratory tests on Speswhite Kaolin (Wheeler and Sivakumar [3]). On a linear scale, the LC yield curve would be predicted to reach a minimum slope at a particular degree of expansion (corresponding to a particular value of $\overline{p}_o^*/p^c$) and then it would become steeper again on further expansion, becoming a vertical straight line for $\overline{p}_o^* = p^c$.

The choice of the value for the model parameter, p^c influences the shape of the LC yield curve. The value of p^c controls, together with the parameters r and $\lambda(0)$ introduced in Section 3.2.3, the difference, for a given LC yield curve, between the limit value of $\overline{p}$ when suction tends to infinity and $\overline{p}_o^*$ (see Figure 3.2). Figure 3.6 shows the influence of the variation of the p^c parameter on the shape of a yield curve corresponding to a value of $\overline{p}_o^* = 100$ kPa, while all the remaining model parameters are kept constant and equal to the values reported in Table 3.2.

Beside influencing the shapes of the LC yield curve, the value of the parameter p^c determines also the position of the normal compression lines at constant suction in the $(v, \ln \overline{p})$-plane. While the parameters $\lambda(0)$, r and β introduced in Section 3.2.3 define the variation of the slope of such normal compression lines with suction, the parameters $N(0)$ and p^c, together with the swelling index for changes in suction κ_s introduced in Section 3.2.1, fix the absolute positions of such normal compression lines in the $(v, \ln \overline{p})$-plane. The value of $N(0)$ represents the specific volume on the normal compression line at zero suction for a value of mean net stress $\overline{p}$ equal to the reference pressure p^c. Therefore the values of the parameters $N(0)$ and p^c fix the position in the $(v, \ln \overline{p})$-plane of the normal compression line at zero suction. The positions of the other normal compression lines at other values of suction are defined by the requirement that, for $\overline{p} = p^c$ the differences of specific volume between normal compression lines at different values of suction are equal to

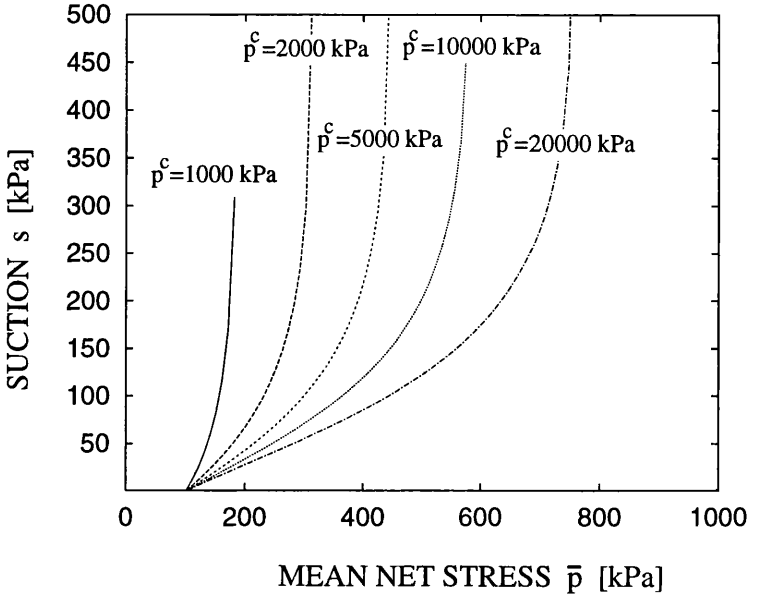

Figure 3.6: Influence of variation of the parameter p^c on the LC yield curve

the elastic variation of specific volume with suction (see Equation 2.25). Figure 3.7 shows a schematic representation of three normal compression lines at different values of suction, showing the influence of the three model parameters $N(0)$, p^c and κ_s on the position of the normal compression lines in the $(v, \ln \overline{p})$-plane.

In this work the values of the two parameters, $N(0)$ and p^c were chosen by trying to fit the predicted normal compression lines of specific volume at four different values of suction (0 kPa, 100 kPa, 200 kPa, 300 kPa) with the experimental ones presented by Wheeler and Sivakumar [3] (see Figure 2.3). The value of the parameter p^c defined in this way was subsequently used to calculate the predicted LC yield curves, to be compared with the experimental yield points observed by Wheeler and Sivakumar [3] during normal compression tests at constant suction.

The values for $N(0)$ and p^c were selected by trying to match experimental values of $N_{atm}(s)$, the specific volume on the normal compression lines at a mean net stress equal to atmospheric pressure, p_{atm} (taken as 100 kPa) from Wheeler and Sivakumar [3] at four different values of suction (0 kPa, 100 kPa, 200 kPa, 300 kPa). These experimental values were calculated by Wheeler and Sivakumar [3] taking the average value from all the tests

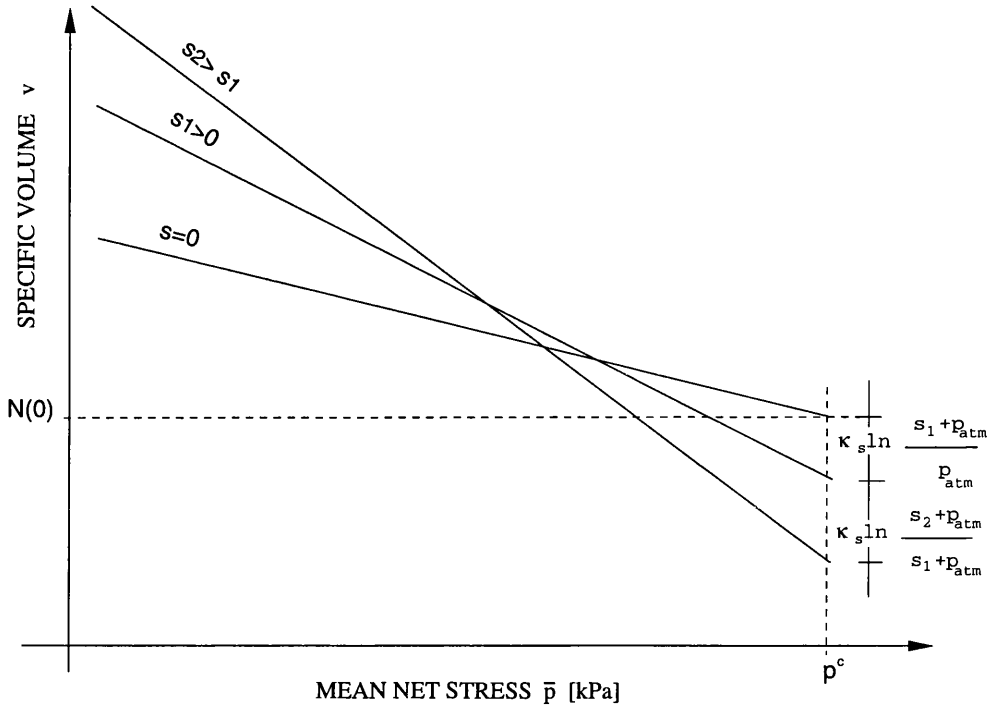

Figure 3.7: Influence of the parameters $N(0)$, p^c and κ_s on the positions of the normal compression lines (NCL) in the $(v, \ln \overline{p})$-plane at different suctions

carried out at each given value of suction. They are reported in Table 3.5.

A trial and error procedure was used, by selecting a trial value of p^c and from this a corresponding value for the parameter $N(0)$. This trial value of $N(0)$ was found by matching the predicted normal compression line at zero suction, given by Equation 2.19 for $s = 0$ kPa, to the experimental value of $N_{atm}(s) = 2.052$ at $\overline{p} = 100$ kPa. For this trial pairing of p^c and $N(0)$ it was then possible to calculate the corresponding predicted values of $N_{atm}(s)$ at the other three levels of suction, by using the following equation:

$$N_{atm}(s) = N(0) - \kappa_s \ln \frac{s + p_{atm}}{p_{atm}} - \lambda(s) \ln \frac{p_{atm}}{p^c}. \tag{3.1}$$

These predicted values of $N_{atm}(s)$ could be compared with the experimental values. In Equation 3.1 the slopes $\lambda(s)$ of the normal compression lines at the four values of suction of 0 kPa, 100 kPa, 200 kPa, 300 kPa are the ones predicted by the model reported in Table 3.4 and the value of the parameter κ_s has been defined in Section 3.2.1.

The best fit with experimental results was obtained by using a value for p^c equal to 2000

Suction	Experimental $N_{atm}(s)$	Predicted $N_{atm}(s)$
0 *kPa*	2.052	2.052
100 *kPa*	2.122	2.160
200 *kPa*	2.196	2.198
300 *kPa*	2.212	2.208
∞ *kPa*		$-\infty$

Table 3.5: Predicted and experimental values of $N_{atm}(s)$

kPa which requires a corresponding value for $N(0)$ of 1.662. Table 3.5 shows a comparison between predicted and experimental values of $N_{atm}(s)$ for the different values of suction.

Figure 3.8 shows a comparison between the predicted and experimental normal compression lines at different values of suction. Each experimental line (plotted using the values of $\lambda(s)$ and $N_{atm}(s)$ from Tables 3.4 and 3.5) represents the average of several tests conducted at the given value of suction. Figure 3.8 shows that match between predicted and measured normal compression lines is far from perfect. In particular, the predicted normal compression line at a value of suction of 100 kPa lies noticeably above the measured line. Even though the selection of a value for the r parameter greater than 1 has enabled the normal compression lines for Speswhite Kaolin to be fitted much better than would have been possible with the conventional choice of an r value less than 1, the constraints of the model of Alonso, Gens and Josa [1] mean that it is still not possible to achieve a perfect match.

A further check on the validity of the selected values for the parameters $\lambda(0)$, β, r and p^c is given by the comparison between the values of yield stress measured by Sivakmar [13] during isotropic loading test at four different levels of suctions (0 kPa, 100 kPa, 200 kPa, 300 kPa) and the corresponding LC yield curves in the $(\overline{p}, s)$-plane predicted by the model.

After compaction Sivakumar [13] subjected the unsaturated soil samples to wetting at constant mean net stress. During this stage different samples were brought from an initial unknown value of suction to the four different levels of suction of 0, 100 kPa, 200 kPa and 300 kPa. The samples brought to suctions of 200 kPa and 300 kPa showed an increase in specific volume with decreasing suction which suggests that only elastic swelling deformations took place. For the samples brought to a suction of 100 kPa, some of them

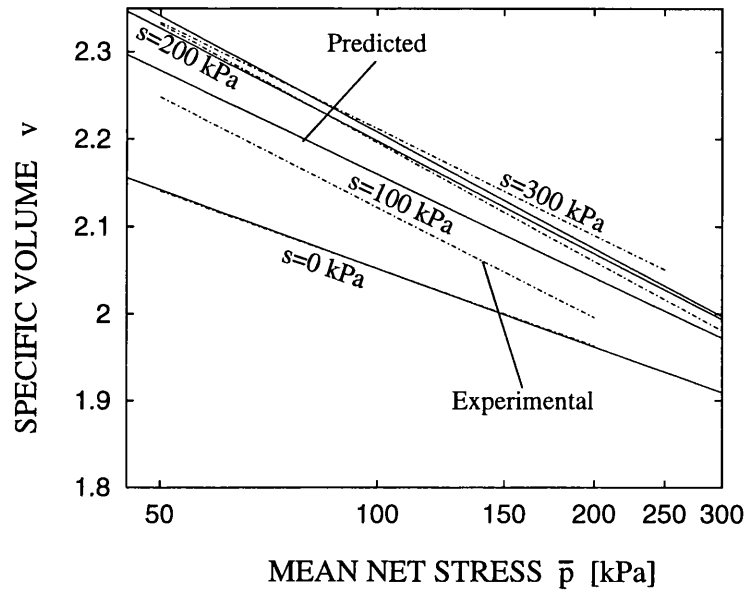

Figure 3.8: Predicted and experimental NCL in the $(v, \ln \overline{p})$-plane at different suctions

showed signs of a small amount of collapse compression at the end of wetting while others showed only an increase in specific volume, which suggests that the LC yield curve could have just been reached at the end of this wetting path. Finally the samples brought to suction of zero showed substantial collapse compression, which indicated that the LC yield curve was expanded during the wetting path. After the wetting stage the samples were isotropically loaded at a constant suction and for each test the yield stress was measured. According to the results observed during wetting, it is reasonable to expect that the yield stresses observed for the tests at suctions of 300 kPa, 200 kPa and 100 kPa belong to the same LC yield curve, which is the one corresponding to the initial state of the soil after compaction. The yield stress for the test at a suction of zero must lie instead on a LC yield curve which is expanded compared to the initial one. Figure 3.9 shows that, for the model parameter values chosen, there exists a theoretically predicted position of the LC yield curve, corresponding to a value of the hardening parameter, $\overline{p}_o^*$ equal to 18 kPa, which passes approximately through the yield stresses measured by Sivakumar [13] during isotropic loading at suctions of 100 kPa, 200 kPa and 300 kPa. In contrast, as expected, the yield stresses corresponding to isotropic tests performed at suction of zero

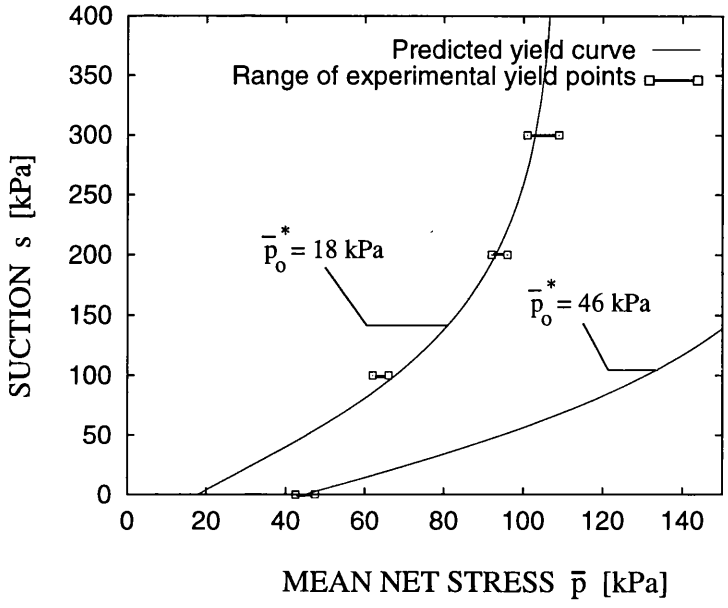

Figure 3.9: Predicted LC yield curves and experimental yield points

fall on a considerably expanded LC yield curve, corresponding to a value of the hardening parameter, $\overline{p}_o^*$ equal to 46 kPa.

3.2.6 Specific volume at critical states

The parameter values for the Alonso, Gens and Josa [1] model summarized in Table 3.2, are used in this section to compare the predicted critical state values of specific volume with the corresponding experimental data from Sivakumar [13].

Figure 3.10 shows the critical state lines predicted by the model in the $(v, \ln \overline{p})$-plane for four different values of suction (0 kPa, 100 kPa, 200 kPa, 300 kPa) together with experimental data points from Sivakumar [13]. It is evident that the agreement between predicted values of specific volume and experimental data is relatively poor at the critical state. This weakness of the Alonso, Gens and Josa [1] model has already been revealed by Wheeler and Sivakumar [3], as discussed in Section 2.4.3.

From Figure 3.10 it is evident that for suctions ranging from zero up to a limit value, the predicted critical state lines corresponding to higher values of suction lie above the ones corresponding to lower values. This trend is reversed when this limit value of suc-

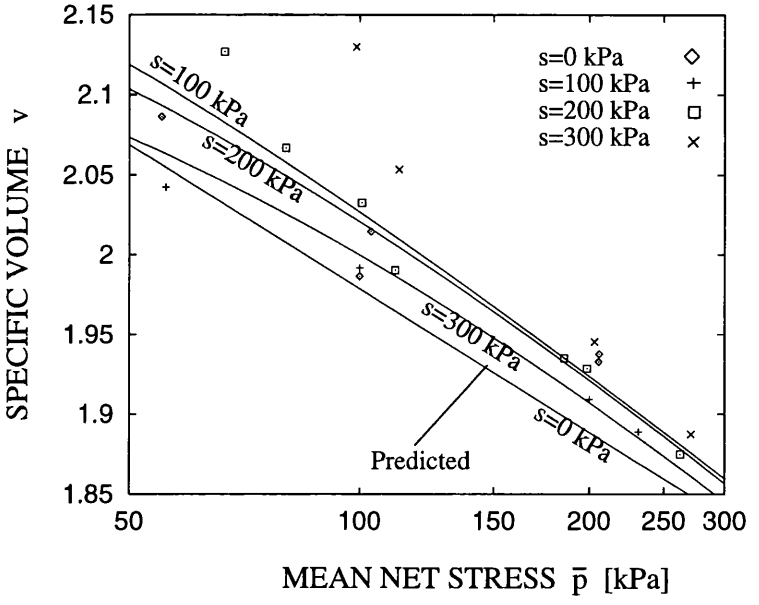

Figure 3.10: Predicted CSL and experimental CS data points in the $(v, \ln \overline{p})$-plane at different suctions

tion is exceeded. In addition, the non-linearity of the predicted critical state lines in the semilogarithmic $(v, \ln \overline{p})$-plane increases with increasing suction. These results are consistent with the general expression of the critical state lines given in Equation 2.34 and with its graphical interpretation shown in Figure 2.15, but they are not matched by the experimental data.

3.3 Parameters for the state surface for S_r

In this section the values of the model parameters for the state surface expression for degree of saturation, S_r proposed by Lloret and Alonso [22] are presented. A first set of model parameter values was obtained by fitting the experimental values of degree of saturation from Sivakumar [13] corresponding to the isotropic normal compression lines at different values of suction. However this first set of model parameters predicts an inaccurate variation of degree of saturation of the soil for stress paths within the elastic domain (see Section 6.5). Therefore a second set of model parameters was selected as a compromise between elastic and elasto-plastic behaviour in an attempt to represent the

variation of degree of saturation in a physically coherent fashion within both the elastic and elasto-plastic domains.

Lloret and Alonso [22] suggested two possible forms of state surface expression:

$$S_r = a - \{1 - \exp[-b(u_a - u_w)]\}[c + d(\sigma - u_a)] \qquad (2.40bis)$$

$$S_r = a - \tanh[b(u_a - u_w)][c + d(\sigma - u_a)]. \qquad (2.41bis)$$

Initially, both of these possibilities were considered, before selecting the expression which provided the best fit to the experimental data. In both Equations 2.40 and 2.41 the value of the parameter a was chosen as 1, in order to predict a degree of saturation of 1 at zero suction. Each of the two state surface expressions given in Equations 2.40 and 2.41 was fitted to four experimental normal compression curves for degree of saturation at constant suction (0 kPa, 100 kPa, 200 kPa, 300 kPa) calculated on the basis of test results from Sivakumar [13].

The normal compression line for degree of saturation at zero suction reduces to an horizontal line, predicting a constant value of degree of saturation of 1, due to the assumption of saturation of the soil at $s = 0$. For the remaining three values of suction (100 kPa, 200 kPa, 300 kPa), Wheeler and Sivakumar [3] provided experimental variations of specific volume, v and specific water volume, v_w on the normal compression line, and these were combined to give the corresponding experimental variation of degree of saturation, using the expression:

$$S_r = \frac{v_w - 1}{v - 1}. \qquad (2.45bis)$$

The experimental variation of specific volume v on the normal compression lines was represented by Equation 2.36, with values for the parameters $\lambda(s)$ and $N_{atm}(s)$ reported in Tables 3.4 and 3.5 (representing, for each value of suction, the average calculated from several tests). The experimental variations of specific water volume, v_w from Wheeler and Sivakumar [3] are shown in Figure 3.11. After inspection of Figure 3.11 it was assumed that, over the range of mean net stress covered by the tests, v_w was constant on a normal compression line at a suction of 100, 200 or 300 kPa. These constant values of v_w were

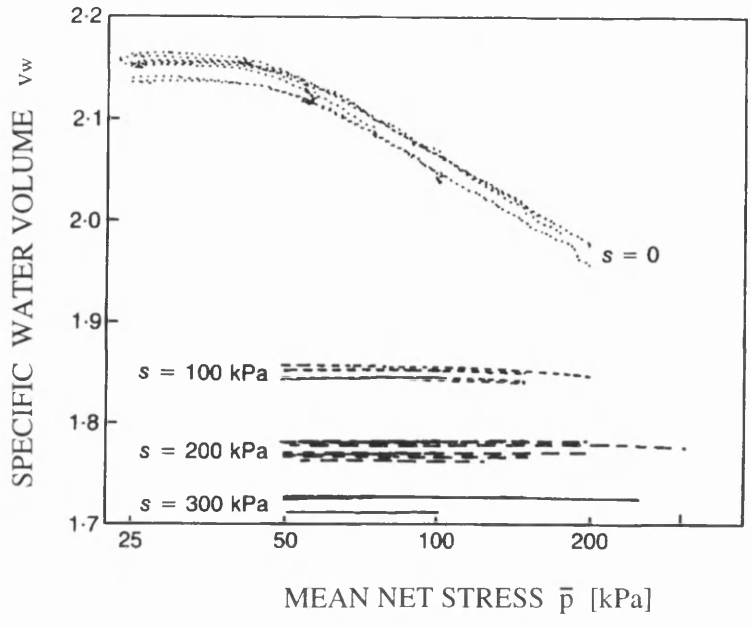

Figure 3.11: Variation of specific water volume during isotropic compression at constant suction (after Wheeler and Sivakumar [3])

assumed equal to 1.86, 1.78 and 1.73 respectively (based on the average from all the tests at the same value of suction). Therefore the explicit forms of the normal compression lines for degree of saturation at constant values of suction of 100 kPa, 200 kpa and 300 kPa were given by:

$$S_r(\overline{p}) = \frac{1}{2.279 - 0.212 \ln \overline{p}} \tag{3.2}$$

$$S_r(\overline{p}) = \frac{1}{2.691 - 0.251 \ln \overline{p}} \tag{3.3}$$

$$S_r(\overline{p}) = \frac{1}{2.770 - 0.241 \ln \overline{p}}. \tag{3.4}$$

These three curves together with the normal compression curve corresponding to a value of suction equal to zero (saturated conditions) are represented in $(\overline{p}, s, S_r)$-space in Figure 3.12. The three curves corresponding to the values of suction of 100 kPa, 200 kPa, 300 kPa are plotted in the ranges of mean net stress where experimental evidence from Sivakumar [3] is available and these ranges are 50-200 kPa, 50-300 kPa and 50-250 kPa

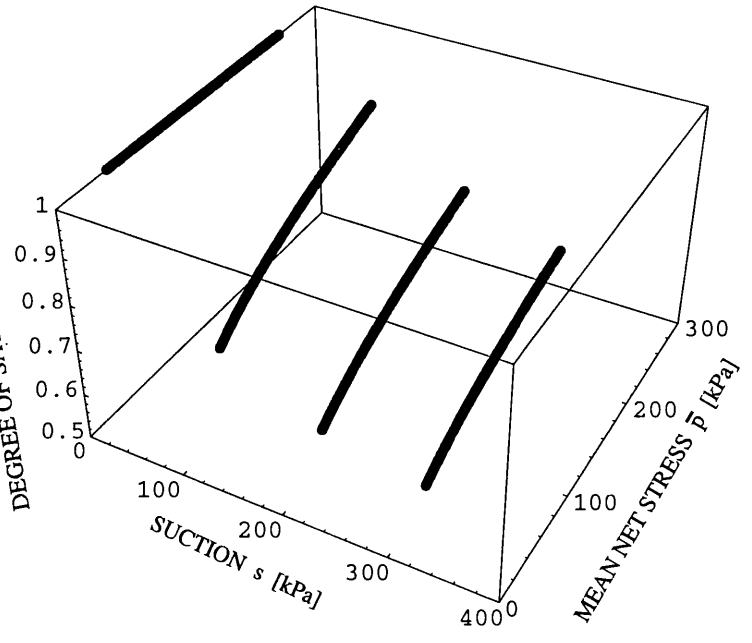

Figure 3.12: Experimental NCL at different suctions in the $(S_r, s, \overline{p})$-space

Equation type	b	c	d	χ^2	s^2
Equation 2.40	0.00588 kPa^{-1}	0.622	−0.00120 kPa^{-1}	0.0295	0.000492
Equation 2.41	0.00534 kPa^{-1}	0.554	−0.00107 kPa^{-1}	0.0288	0.000480

Table 3.6: Values of state surfaces parameters defined using experimental NCL of degree of saturation

respectively.

The fitting of the state surface expressions of Equations 2.40 and 2.41 to the experimental curves shown in Figure 3.12, was performed by using the minimum squared error technique and in Table 3.6 are reported the values of the coefficients b, c and d which were found for the two equations. The same table also shows the value of the sum of squared residuals, χ^2, and the estimated variance, s^2, which give an indication for comparing the fit with the two different equations. The best fit was achieved by using Equation 2.41 since this gives the smaller values of χ^2 and s^2 (although the difference is small). The state surface for S_r corresponding to Equation 2.41, is shown in Figure 3.13 together with the experimental normal compression curves.

Figure 3.14 shows the predicted variation of degree of saturation with mean net stress

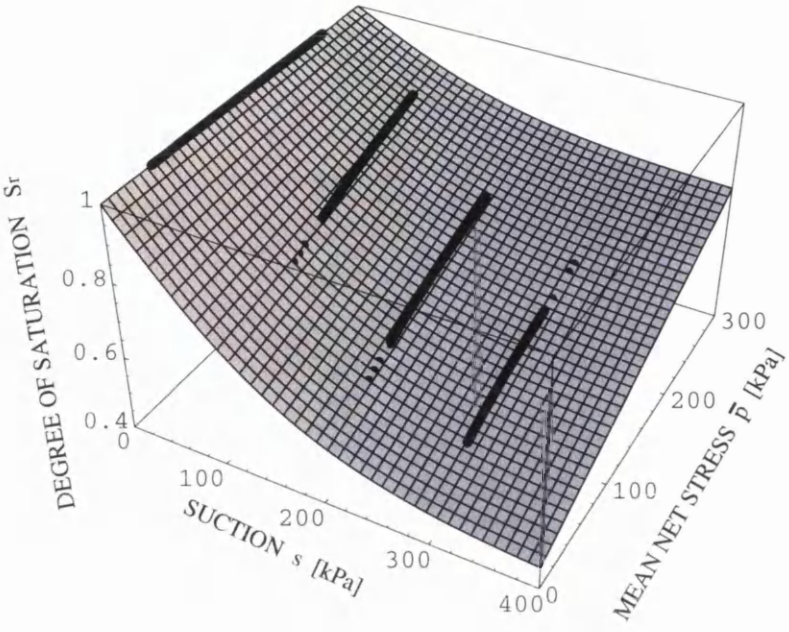

Figure 3.13: Fitting to experimental NCL at different suctions in the $(S_r, s, \overline{p})$-space

and the experimental normal compression lines in three constant suction planes (100 kPa, 200 kPa, 300 kPa). Figure 3.14 shows that the assumed state surface expression for degree of saturation provides a very good fit at a suction of 200 kPa and a worse fit for the other two values of suction of 100 kPa and 300 kPa. Figure 3.15 shows the same predicted variation of degree of saturation in the same constant suction planes compared this time with experimental data points corresponding to soil at critical state. In this case the fit between predicted and experimental data for all the three values of suction is very poor and this proves one of the limits of the state surface approach already highlighted in Section 2.5.1. State surfaces can be properly applied as constitutive models only if the initial state of the soil and the stress path followed are of the same type of the ones imposed on the soil samples in the laboratory tests. The poor fit between predictions and experimental results observed in Figure 3.15 is a consequence of the fact that the state surface of Equation 2.41, defined using results from states on isotropic normal compression lines, is unable to take into account the variation of degree of saturation observed during shearing.

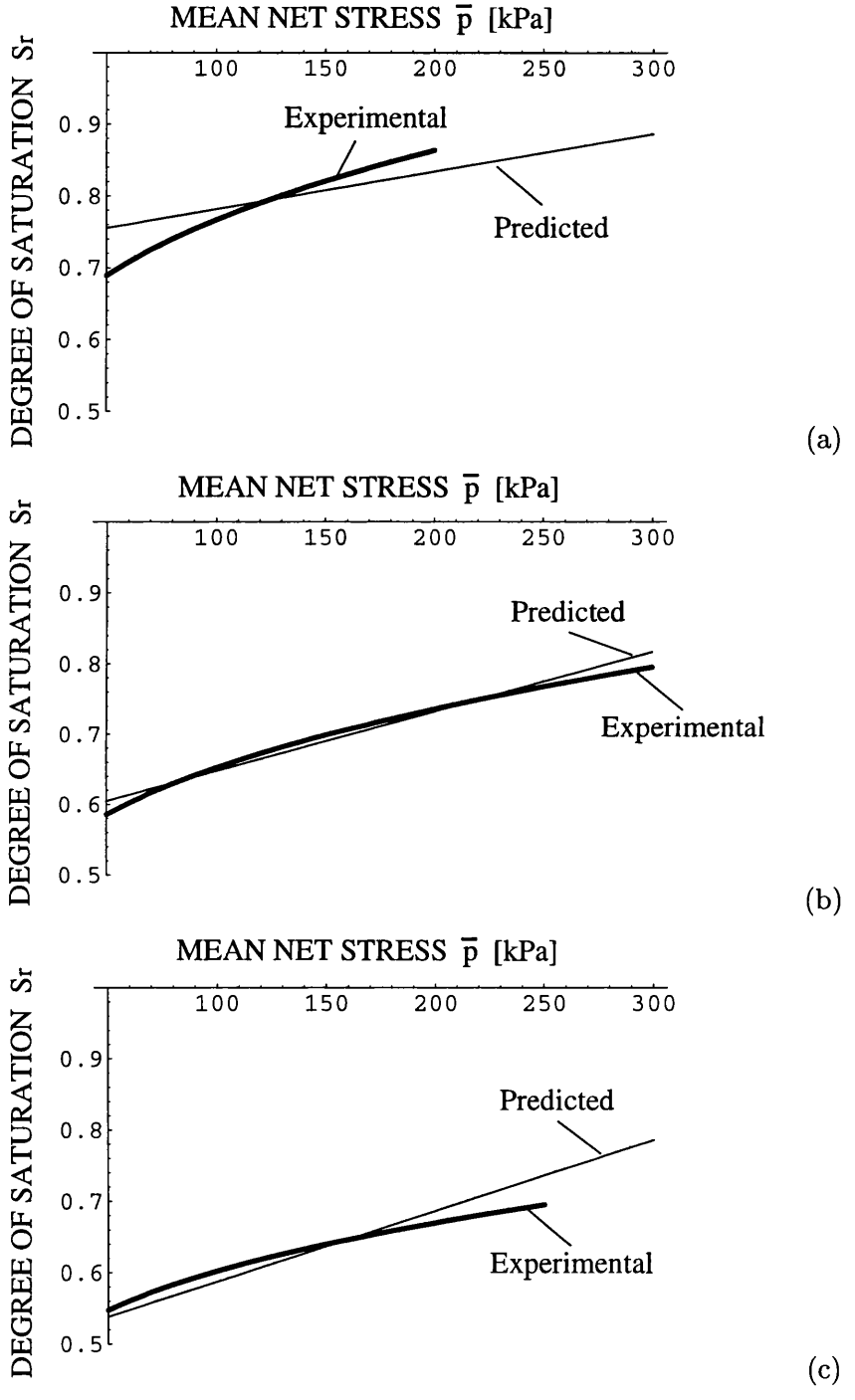

Figure 3.14: Predicted and experimental NCL in the $(S_r, \overline{p})$-planes at different suctions of: (a) 100 kPa (b) 200 kPa (c) 300 kPa

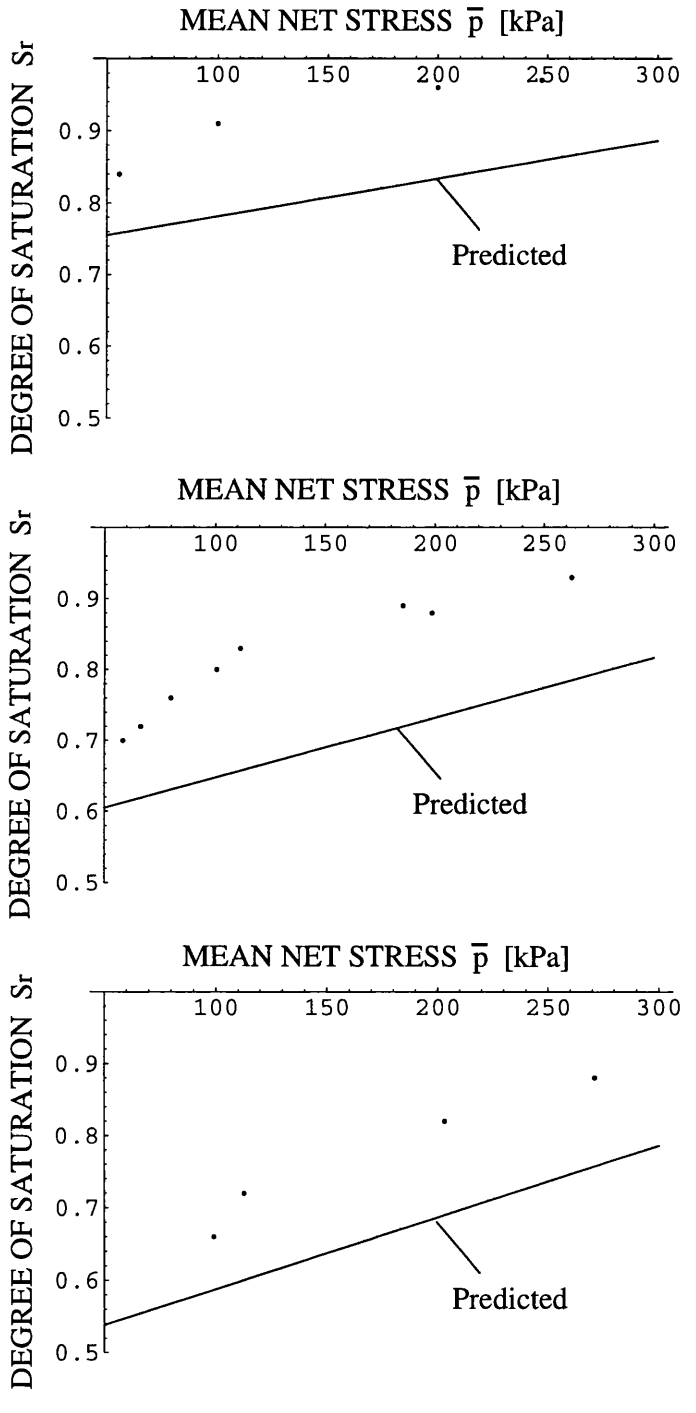

Figure 3.15: Predicted CSL and experimental CS data points in the $(S_r, \overline{p})$-planes at different suctions of: (a) 100 kPa (b) 200 kPa (c) 300 kPa

Equation type	b	c	d
Equation 2.41*bis*	0.00534 kPa^{-1}	0.554	-0.000107 kPa^{-1}

Table 3.7: Values of state surfaces parameters defined as a compromise between elastic and elasto-plastic behaviour

Since the model parameter values for the state surface of Equation 2.41 (Table 3.6) have been defined from states on isotropic normal compression lines, they are also unable to reproduce correctly the elastic variation of degree of saturation, during unloading or re-loading inside the yield locus. The variation of the degree of saturation with mean net stress observed in the elastic domain is significantly smaller than that observed during virgin (elasto-plastic) isotropic loading. This is shown in Figure 2.4 where the degree of saturation is practically constant during elastic unloading tests at constant suction from a normal consolidated state. Therefore, if a state surface for degree of saturation defined from elasto-plastic isotropic test results is employed together with an elasto-plastic constitutive model (e.g. the Alonso, Gens and Josa [1] model), the predicted response for elastic stress paths is likely to be highly unrepresentative of the actual soil behaviour. This is demonstrated by a numerical analysis presented in Section 6.5.

As an example, if the model parameter values of Table 3.6 are used for the state surface of Equation 2.41 and if the elasto-plastic model of Alonso, Gens and Josa [1] is employed to simulate elastic isotropic compression (inside the yield locus), the predicted results will show either a large influx of liquid within the sample for fully drained conditions or a large increase in suction (as shown in Section 6.5) for undrained (with respect to the liquid phase) conditions, which are not observed experimentally. In this work, in order to obtain physically sensible results in both the elastic and elasto-plastic domain by using the state surface expression of Equation 2.41, a second set of model parameter values has been chosen as a compromise between elastic and elasto-plastic behaviour, as suggested by Gallipoli, Karstunen and Wheeler [58]. In this second set of model parameter values, reported in Table 3.7, the coefficient d controlling the linear variation of the degree of saturation with mean net stress is taken equal to $1/10$ of the value reported in Table 3.6.

3.4 Parameters in the permeability relationships

The relationships proposed by Brooks and Corey [47] between the coefficients of permeability with respect to the liquid phase, k_w and gas phase, k_a and degree of saturation, S_r were introduced in Section 2.6 (see Equation 2.54 and Equation 2.57). These relationships were implemented in the code "Compass" by the author and in this section the values of the relevant model parameters are described for Speswhite Kaolin. For some of the parameters within these relationships, estimation of precise values for Speswhite Kaolin was very approximate, because of the shortage of appropriate experimental data. This was, however, not considered a serious problem because the permeability relationships only affected the coupled flow-deformation analyses presented in Chapters 6 and 7 (which were used for illustrative purposes only) and did not affect the model predictions presented in Chapter 4 (which were compared with real experimental data) referring to drained and undrained conditions.

In all the numerical simulations of this work reduced forms of the Brooks and Corey [47] relationships given by Equations 2.54 and 2.57, were used, corresponding to very high values of pore size distribution index, η. This was necessary because of the absence of enough experimental data to obtain a reliable estimate for η. In the reduced expressions the pore size distribution index, η, was assumed to be much greater than 1 in Equations 2.56 and 2.58, and this led to:

$$k_w = k_s {S_e}^3 \tag{3.5}$$

$$k_a = k_d(1 - S_e)^2(1 - S_e) \tag{3.6}$$

where S_e is the effective degree of saturation defined by Equation 2.55. Table 3.8 summarizes the values chosen for the model parameters and in the following sections the choice of the individual parameters will be discussed.

The effective degree of saturation, S_e in Equations 3.5 and 3.6 involves the residual degree of saturation S_{res} (see Equation 2.55), which corresponds to the point at which the water phase becomes discontinuous and the liquid permeability therefore falls to zero.

Residual degree of saturation (S_{res})	0.446
Coefficient of liquid permeability at saturation (k_s)	10^{-9} m/s
Coefficient of gas permeability at residual degree of saturation (k_d)	10^{-8} m/s

Table 3.8: Values of permeability relationships parameters

Brooks and Corey [47] suggested the residual degree of saturation, S_{res} could be estimated from the soil-water characteristic curve as the degree of saturation at which an increase in suction does not produce any significant change in degree of saturation. They also proposed a method for estimating the value of the residual degree of saturation, S_{res} from the experimental soil-water characteristic curve for a given soil. In this work, however, due to the deficiency of sufficient experimental data for the definition of a soil-water characteristic curve over a wide range of suction values, this value was selected by using the relation between degree of saturation, mean net stress and suction given in Equation 2.41. The residual degree of saturation was calculated, for a value of mean net stress equal to zero and suction tending to infinity, as 0.446. The same value of the residual degree of saturation was obtained regardless of which of the two sets of parameter values given in Tables 3.6 and 3.7 was employed because the value of the mean net stress in Equation 2.41 was taken equal to zero. The choice of a value of zero for the mean net stress was due to the fact that in soil science, the degree of saturation-suction curve is determined for a null value of applied stress. The selected value of 0.446 for the residual degree of saturation might seem too high for corresponding to a situation where the continuity of the liquid phase no longer exists. This is clearly due to the approximate procedure adopted for selecting the value of S_{res}, which relied on the extrapolation of Equation 2.41 to very high values of suction, whereas the parameter values in the equation were established through a fit to experimental data within a range of suction between 0 and 300 kPa.

Alternatively, if experimental measurements of the coefficient of liquid permaeability at different value of degree of saturation are available, a more rigorous approach for defining the value of S_{res} than indirect estimation by using the soil-water characteristic curve, would be the fit of Equation 3.5 to the laboratory measured values of permeability.

Determination of the saturated coefficient of pemeability, k_s, would ideally be based

on either falling head permeability tests on saturated samples or interpretation of results from step loading consolidation tests on saturated samples. Test data of this type were unfortunately not available for the compacted Speswhite Kaolin.

Sivakumar [13] did, however, perform step loading isotropic consolidation tests on unsaturated samples. Three different tests were performed and an average value of $7 * 10^{-8}$ m^2/s for the coefficient of consolidation, c_v, was proposed by Sivakumar [13]. From this it was possible to derive an average coefficient of permeability with respect to the liquid phase for the unsaturated conditions corresponding to the three samples tested.

The relationship between coefficient of permeability with respect to the liquid phase and coefficient of consolidation, differs from the well-known one used for consolidation tests on saturated samples since it is based on the different form of equation of water flow for unsaturated soils which will be derived in Section 5.2 (Equation 5.10). Assuming elastic behaviour for the soil during consolidation and neglecting, in the interest of simplicity, the term containing the gradient of degree of saturation in the equation of water flow (Equation 5.10), it is possible to derive a relationship between the coefficient of permeability with respect to the liquid phase at unsaturated condition and the coefficient of consolidation. Therefore, by using average values of specific volume, mean net stress and suction for the three soil samples tested by Sivakumar [13] of 2, 250 kPa and 200 kPa respectively, an average value of $8 * 10^{-11}$ m/s was calculated for the unsaturated coefficient of permeability with respect to the liquid phase. The corresponding average value of degree of saturation obtained by using Equation 2.41 was 0.774. Substituting this value of degree of saturation in Equation 3.5 a value of about 5 was calculated for the ratio between the saturated coefficient of permeability, k_s, and the coefficient of permeability corresponding to a degree of saturation equal to 0.774. The saturated permeability, k_s, was, therefore, estimated to be about $0.4 * 10^{-9}$ m/s.

An independent approximate estimate of the saturated coefficient of permeability was obtained by using the following empirical relationship between coeefficient of permeability and void ratio, e, proposed by Al-Tabaa for saturated Speswhite Kaolin:

$$k_s = 0.5\, e^{3.25} 10^{-9} m/s. \tag{3.7}$$

Assuming a value of 1 for the void ratio, the saturated coefficient of permeability predicted by Equation 3.7 is $0.5 * 10^{-9}$ m/s. This is very similar to the value estimated above from Sivakumar's [13] consolidation tests on unsaturated samples.

Given the uncertainty in the estimate of k_s, it was considered appropriate to select only an order of magnitude value for k_s. A value of k_s equal to 10^{-9} m/s was therefore used in all numerical modelling.

The last parameter value to be determined was the coefficient of permeability with respect to the gas phase, k_d, at the residual degree of saturation (Equation 2.57). While the coefficient of liquid permeability of fine grained soils is often measured in an indirect way through the interpretation of the consolidation curves, the coefficient of gas permeability is usually determined directly in the laboratory by applying different values of pore air pressure gradient to a soil sample and measuring the corresponding mass flow of gas. Experimental results to determine the coefficient of permeability with respect to the gas phase at residual degree of saturation were not available for the compacted Speswhite Kaolin, and therefore a value from the literature was chosen. In particular some tests on different soils were carried out by Blight [59]. He measured the gas mass flow rate corresponding to different pore air pressure gradients applied to dry soil samples. Test results for three different types of compacted soils were reported in this work; the soils in question were two kinds of compacted clays and a compacted shale. For all three the value of the coefficients of gas permeability was of the order of 10^{-8} m/s, and this value was therefore assumed in this work.

Figure 3.16 shows the variation of the coefficients of liquid and gas permeability with degree of saturation for the set of model parameter values of the Brooks and Corey [47] relationships reported in Table 3.8.

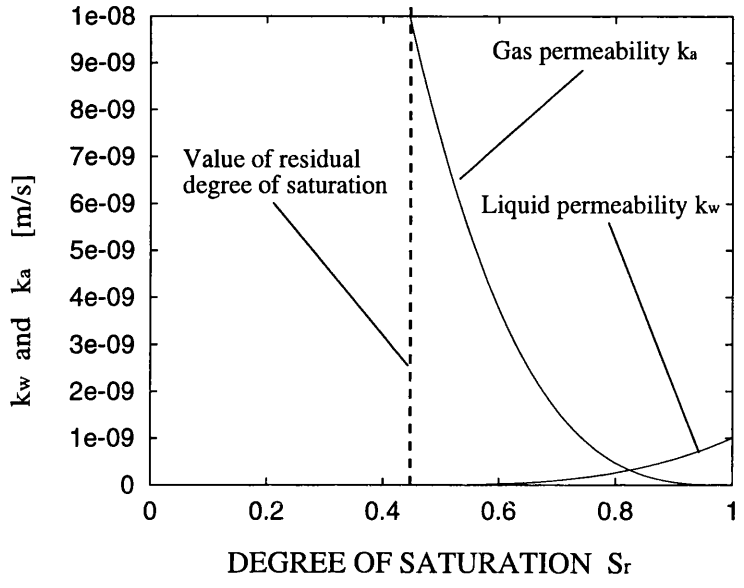

Figure 3.16: Variation of the coefficients of permeability with degree of saturation

3.5 Practical methods of selecting soil parameters

The definition of a set of soil parameter values for the elasto-plastic model of Alonso, Gens and Josa [1], for the state surface expression of degree of saturation of Lloret and Alonso [22] and for the relationships for the coefficients of permeability with respect to the liquid and gas phases of Brooks and Corey [47] was described in this chapter. The selection of these model parameter values was based on results from comprehensive testing programmes on compacted Speswhite Kaolin performed by Sivakumar [13] and Zakaria [15]. The test programmes included wetting tests at constant mean net stress, normal compression tests at constant suction, shearing under various conditions (Sivakumar [13]) and isotropic elasto-plastic loading tests followed by elastic unloading at constant suction (Zakaria [15]). Falling head permeability tests on saturated samples or step loading consolidation tests on saturated samples would have been useful additional tests in determining a more accurate value for the saturated coefficient of liquid permeability.

This approach for selecting mechanical parameter values might not be appropriate for industrial applications, due to the costly and time-consuming nature of the laboratory

testing required. Therefore there is need for alternative methods which can avoid laboratory testing or reduce the amount of necessary tests. In this regard some ideas have been recently proposed which attempt to relate various aspects of the hydro-mechanical behaviour of unsaturated soils to the soil-water characteristic curve. Therefore, once the soil-water characteristic curve has been defined over the entire suction range, it is possible to deduce from it some of the other hydro-mechanical properties of the soil. In particular Fredlund, Xing and Huang [60] presented a methodology to define the relationship between the relative coefficient of liquid permeability (i.e. the ratio between the coefficients of liquid permeability at a given value of degree of saturation and at full saturation) as an integration form of the suction versus water content relationship following a similar approach proposed previously by other reserchers (e.g. Burdine [61], Mualem [62]). Following this approach the coefficient of permeability at saturation remains the only parameter to be estimated in order to define completely the permeability versus degree of saturation relationship.

In a later paper, Fredlund, Xing, Fredlund and Barbour [63] proposed a method which can be used to relate the shear strength relationship of an unsaturated soil to the soil-water characteristic curve. According to this method the only additional parameter required to define the shear strength relationship for an unsaturated soil is the friction angle at saturated conditions. In both the previous papers the authors used, as the equation describing the soil-water characteristic curve of the soil, the one proposed by Fredlund and Xing [49]. This equation is defined over a very wide suction range (i.e. from zero to 10^6 kPa) and produces a good fit with the experimental measurements of liquid permeability and shear strength values. The ideas presented in the two papers from Fredlund, Xing and Huang [60] and Fredlund, Xing, Fredlund and Barbour [63] are general and may also be applied to cases where the variation of volumetric water content (or degree of saturation) is represented by different analytical models such as the state surfaces introduced in Section 3.3 or the more complex elasto-plastic framework which will be illustrated in Chapter 4.

Using the methodology outlined above for defining the liquid permeability and shear strength relationships, it is possible to limit the number of laboratory tests on unsaturated

soil samples necessary for the definition of the values for the soil parameters. The types of tests still required are isotropic loading/unloading tests at constant suction which have to be carried carried out at different values of suction. The test results from the elasto-plastic loading are necessary for the selection of the values of the model parameters defining the normal compression lines of specific volume at constant suction (parameters $\lambda(0)$, r, β, $N(0)$, p^c introduced in Sections 3.2.4 and 3.2.5). The results from the unloading part of these tests are used for the definition of the value of the elastic parameter κ introduced in Section 3.2.1. Some drying or wetting tests at constant mean net stress are also needed in order to define the value of the elastic parameter κ_s introduced in Section 3.2.1. The data from the isotropic loading-unloading tests may also be used for defining the values of the parameters b, c, d of the state surface expressions for degree of saturation introduced in Section 3.3. The selected state surface expression for degree of saturation may be considered as an extended form of the soil-water characteristic curve where also a dependency of degree of saturation on mean net stress is introduced. This extended form of the soil-water characteristic curve can be then used for predicting the liquid permeability and shear strength relationship as mentioned above. This approach makes it possible to reduce the amount of shear tests required to a very small number only necessary to obtain estimates of the values of the saturated critical state stress ratio M (or friction angle ϕ') and the elastic shear modulus G introduced in Section 3.2.1. Permeability or consolidation tests on saturated samples are also needed for defining the value of the saturated coefficient of liquid permeability.

Another appealing possibility for selecting the values of model parameters is represented by the interpretation of experimental results from in-situ tests, such as pressuremeter tests. This type of testing technique has been widely applied to saturated soils. Several analytical and semi-analytical methodologies have been developed which interpret pressuremter test results in the light of different constitutive models for the soil and give suggestions on how to derive the model parameter values from these results. This approach for selecting model parameter values is still highly tentative for unsaturated soils because of the difficulty in the interpretation of the test results. This is, therefore, an issue which will require further

research effort in the future (see Chapter 7).

Chapter 4

Inclusion of variation of S_r within an elasto-plastic model

4.1 Introduction

All the elasto-plastic constitutive models for unsaturated soils developed in the past years define a relationship between the stress state, the past stress history and the traditional strain tensor, but they do not provide information on another strain variable, which is essential for a complete description of the hydro-mechanical behaviour of unsaturated soils: that is the variation of degree of saturation. For fully coupled flow-deformation analyses of unsaturated soils the relationship between the variation of degree of saturation, the stress state (i.e. net stresses and suction) and past stress history is indispensable information, which needs to be added to the basic elasto-plastic stress-strain models. In all the numerical applications to date, where elasto-plastic models for unsaturated soils have been applied to fully coupled flow-deformation problems, this limitation has been overcome by assuming a unique (elastic) relationship, known as a state surface, between the variation of degree of saturation and the stress state. The shortcomings of the state surface approach were described in Section 2.5.1. In Section 3.3 the values of the model parameters for the state surface expression of Lloret and Alonso [22] (Equation 2.41), which was implemented in the original version of code "Compass" [43], were defined by fitting isotropic normal compression tests data from Sivakumar [13] and it was also shown that the predictions of degree of saturation at critical state gave a relatively poor fit to

the experimental critical state values. Since the model parameter values were selected on the basis of normal compression data (virgin loading), the state surface approach was also unable to represent the variation of degree of saturation during elastic unloading and re-loading.

A complete model for representing the variation of degree of saturation with stress state should take into account two factors which are neglected in the existing formulations: the influence of plastic deformation within the soil skeleton (along the lines proposed by Wheeler [51]) and the phenomenon of hydraulic hysteresis (see Section 2.5). In this chapter new ideas are proposed for accounting for the influence of plastic deformations on the variation of degree of saturation. The new proposals, however, do not include the representation of hydraulic hysteresis, and further work needs to be carried out on this aspect.

In this chapter comparisons are presented between experimental data from laboratory tests on compacted Speswhite Kaolin performed by Sivakumar [13] and Zakaria [15] and the predictions calculated by the proposed model. In Chapter 6 some numerical analyses of simple coupled flow-deformation cases, performed by using the code "Compass", are presented in order to assess qualitatively the difference between the predictions achieved with the new model and those by the conventional approach (with degree of saturation represented by a state surface expression). In Chapter 7 the results computed with the two different approaches are compared for the case of a more complex boundary value problem, namely the simulation of a pressuremeter test in unsaturated soil.

4.2 Formulation of a new relationship for S_r

4.2.1 Basic assumptions

The main hypothesis, on which the proposed model is based, is the postulation of a unique relationship between degree of saturation, S_r, specific volume, v, and suction, s, having the generic form:

$$S_r = S_r(s, v). \tag{4.1}$$

Equation 4.1 corresponds to the definition of a family of soil-water characteristic curves, each of them linking degree of saturation and suction at a given constant value of specific volume.

The distribution of void sizes within the soil and the spatial arrangement of these voids (including the connections between them) have a significant effect on the soil-water characteristic relationship between degree of saturation and suction. The degree of saturation is, therefore, a function of both suction and void arrangement. If a reversal of suction occurs, a complete description of the variation of the degree of saturation should also take into account the phenomenon of hydraulic hysteresis. In the present formulation the phenomenon of hydraulic hysteresis is neglected and degree of saturation is assumed to depend only on suction and the arrangement of voids within the soil. According to Equation 4.1, a single soil variable (the specific volume) is chosen to represent the influence of void arrangement on the variation of degree of saturation.

Clearly a reduction of specific volume implies a reduction in size of some of the voids, and this would be expected to shift the soil-water characteristic curve upwards, so that a higher suction is required in order to maintain a given degree of saturation (just as the suction in a fine-grained soil at a given degree of saturation is generally higher than the suction in a coarser grained soil at the same degree of saturation). Figure 4.1 shows experimental normal compression lines and critical state points from Sivakumar [13] plotted in the (S_r, v)-plane for three different values of suction (100 kPa, 200 kPa, 300 kPa). The experimental normal compression lines for degree of saturation were calculated from the corresponding plot of specific volume, v and specific water volume, v_w provided by Sivakumar [13], using the expression:

$$S_r = \frac{v_w - 1}{v - 1}. \qquad (2.45 tris)$$

The important point arising from Figure 4.1 is that, for each value of suction, the normal compression line and the critical state data points can be approximated by a single curve, providing support for the hypothesis of a unique expression between S_r, s and v (Equation 4.1). Figure 4.1 shows that critical state data points at each value of

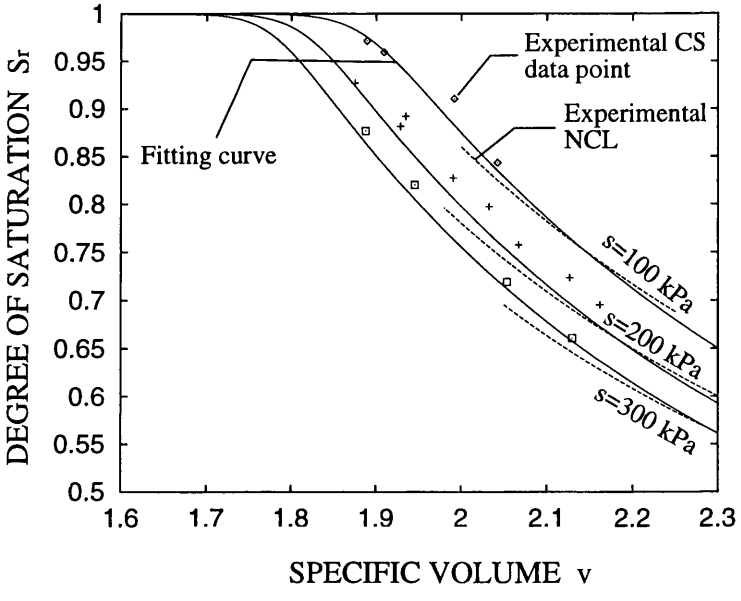

Figure 4.1: Fitting to experimental normal compression lines (NCL) and critical state (CS) data points in the (S_r, v)-plane at different suctions

suction lie slightly above the corresponding normal compression line, suggesting a possible small dependency of degree of saturation on shear strain. It is, however, possible to obtain a reasonably good fit to both critical state and normal compression data at each value of suction by means of a unique curve.

Summarizing the following assumptions are involved in the proposed relationship for the variation of degree of saturation (Equation 4.1):

1. the influence of the arrangement of voids within the soil on the soil-water characteristic curve of degree of saturation against suction is best represented by the specific volume. This means that it is assumed that the overall reduction in void volume is sufficient to characterize the associated change in distribution of void sizes. It is also assumed a variation of shape of the voids due to shear strains has no effect on the soil-water characteristic curve.

2. a change of the specific volume within the soil always has the same effect on the variation of degree of saturation, irrespective of whether the volume change is caused

by elastic or plastic deformations. Elastic strains are associated with elastic deformation of soil particles or soil packets, whereas plastic strains are associated with relative slippage of particle or packets.

3. hydraulic hysteresis on reversal of suction is neglected, so that the degree of saturation of the soil for given values of suction and specific volume is independent of whether the soil is undergoing a wetting or drying path.

If Equation 4.1 is combined with a constitutive model for unsaturated soils, which introduces an elasto-plastic variation of specific volume with the stress state (i.e. net stresses and suction), then the degree of saturation is also predicted to vary in an elasto-plastic fashion.

Another possible form of dependency was also considered in this work. This consisted of a unique relationship between degree of saturation, S_r, suction s and the plastic component of change in specific volume, Δv^p (with respect to some reference condition):

$$S_r = S_r(s, \Delta v^p) \tag{4.2}$$

Equation 4.2 is based on the hypothesis that only the plastic component of a change of specific volume is responsible for the modifications in the void arrangement within the soil which affects the soil-water characteristic relationship. The logic behind the proposal of Equation 4.2 is that plastic strains (involving slippage at inter-particle or inter-packets contacts) can produce more radical changes in void arrangement than elastic strains. Unlike Equation 4.1, the hypothesis of a form of dependency such as Equation 4.2 cannot be verified directly by the experimental data presented by Sivakumar [13], because unloading stages would be required in order to separate elastic and plastic components of volume change during a preceding loading stage. Alternatively, plastic changes of specific volume can be calculated indirectly from test results, by interpreting the data in the light of a specific elasto-plastic constitutive model.

In this work the validity of the form of dependency assumed in Equation 4.2 was assessed for the two elasto-plastic constitutive models of Alonso, Gens and Josa [1] and

Wheeler and Sivakumar [3]. For these two models the relationship of Equation 4.2 can be expressed in the following alternative form:

$$S_r = S_r(s, \overline{p}_o^*) \tag{4.3}$$

where $\overline{p}_o^*$ is the volumetric hardening parameter, which is uniquely related in the two elasto-plastic models to the plastic component of changes of specific volume (see Equation 2.27). Figure 4.2 shows the experimental normal compression lines and critical state points from tests on compacted Speswhite Kaolin by Sivakumar [13], plotted in the $(S_r, \overline{p}_o^*)$-plane at three different values of suction (100 kPa, 200 kPa, 300 kPa). Figure 4.2 refers to the two cases where the values of the hardening parameter $\overline{p}_o^*$ is calculated according to either the Alonso, Gens and Josa [1] model (Figure 4.2 (a)) or the Wheeler and Sivakumar [3] model (Figure 4.2 (b)). The model parameter values used in calculating values of $\overline{p}_o^*$ were the ones reported in Table 3.2 for the Alonso, Gens and Josa [1] model and the ones suggested by Wheeler and Sivakumar [3] for their model.

Inspection of Figure 4.2 reveals that it is possible to obtain a reasonably good fit to both critical state and normal compression data at each value of suction by means of a unique fitting curve for the case of the Wheeler and Sivakumar [3] model, whereas the fit is much worse for the case of the Alonso, Gens and Josa [1] model. This may be explained by the fact that the model of Wheeler and Sivakumar [3] is able to provide a more accurate prediction of the values of specific volume (see Section 2.4.3) and, hence, of the value of $\overline{p}_o^*$ at a given stress state. For the case of the Wheeler and Sivakumar [3] model it is even possible to obtain a unique fit to the experimental normal compression and critical state data in the $(S_r, \overline{p}_o^*)$-plane which looks slightly better than the fit in the (S_r, v)-plane reported in Figure 4.1.

In the rest of this work, however, the degree of saturation is assumed to be dependent on suction and specific volume (Equation 4.1) rather than on suction and plastic changes of specific volume (Equation 4.2) since the first form of dependency offers significant advantages.

The most important is that a relationship in terms of suction and specific volume can

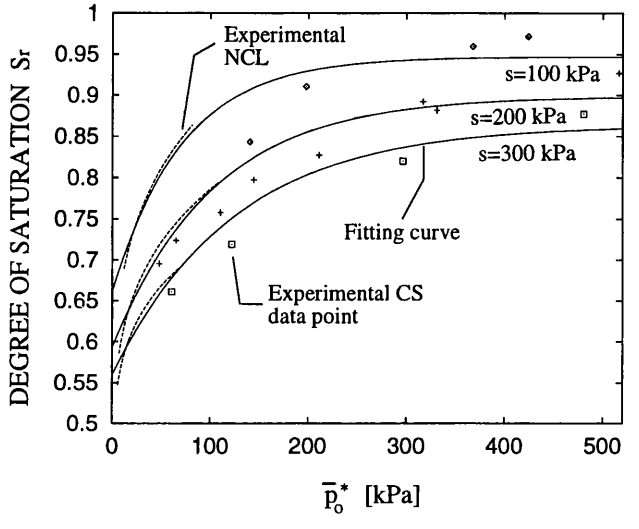

(a)

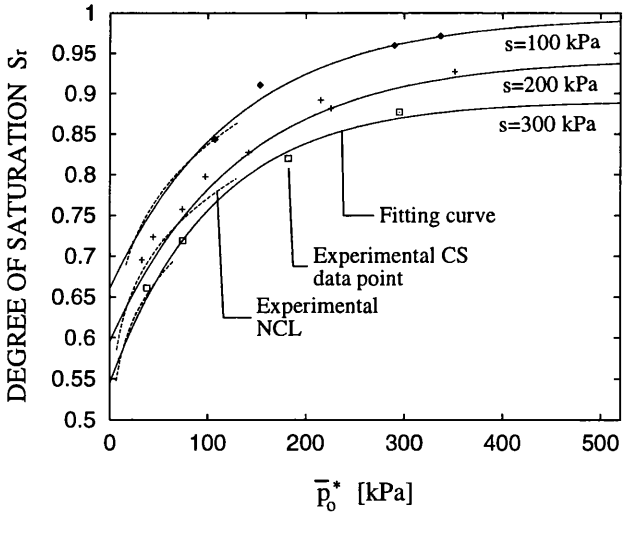

(b)

Figure 4.2: Fitting to experimental NCL and CS data points in the $(S_r, \bar{p}_o^*)$-plane at different suctions. Values of $\bar{p}_o^*$ calculated according to the: (a) Alonso, Gens and Josa [1] model (b) Wheeler and Sivakumar [3] model

be defined a priori in an explicit form valid for a given type of soil regardless of the constitutive model adopted for describing its mechanical behaviour. This relationship can then be applied to any type of stress-strain model that predicts the variation of specific volume with the stress state and stress history. In contrast, a relationship between degree of saturation, suction and plastic changes of specific volume is specific to the particular elasto-plastic constitutive model used to derive it and it cannot be combined with other types of constitutive model.

In addition, an explicit form for the soil-water characteristic curve is easier to determine in terms of suction and specific volume, because it is directly based on variables measured in laboratory tests and does not need any post-processing of the experimental data in the light of the elasto-plastic mechanical model assumed for the soil.

Finally it looks more justifiable on physical grounds because it relates degree of saturation to a soil variable rather than to an artificial model parameter.

4.3 Definition of an explicit form for the $S_r(s, v)$ relationship

In this section an explicit form for the relationship between degree of saturation, suction and specific volume is proposed and the values of the relevant model parameters are defined on the basis of the experimental results from tests on compacted Speswhite Kaolin (Sivakumar [13]).

The relationship between degree of saturation, suction and specific volume given in a generic form by Equation 4.1 could be expressed explicitly by a number of curves at constant values of suction which fit normal compression and critical state experimental data in the the (S_r, v)-plane as shown in Figure 4.1. This would provide, however, a number of relationships between degree of saturation and specific volume at given values of suction and each of these relationships could only be employed for problems where the suction remained constant. If problems involving changes of suction are to be studied, a continuous dependency on the suction value has to be introduced. One possible solution would be to use the same form of equation to fit the experimental data at constant given

values of suction in the (S_r, v)-plane and then interpolate the parameters obtained by this fitting process for intermediate levels of suction. Another approach is to use a more general equation which takes into account explicitly the dependency of degree of saturation on suction and specific volume. This equation can then be fitted to the experimental data in the (S_r, s, v)-space in order to obtain the values of the model parameters. The second approach was used in the present work.

The proposed form of variation for degree of saturation is based on the equation of the soil-water characteristic curve suggested by van Genuchten [48]. It was shown in Section 2.5.1 that, for an incompressible soil (a hypothesis typically accepted in soil science), assuming that degree of saturation tends to unity at zero suction and to zero when suction tends to infinity (i.e. residual value of the degree of saturation equal to zero), the van Genuchten expression becomes:

$$S_r = \left(\frac{1}{1 + (\alpha\, s)^n}\right)^m . \qquad (2.44bis)$$

Whereas it is usually assumed by soil scientist, such as van Genuchten, that soil is an incompressible material, in geotechnical engineering changes of soil volume are highly significant and can influence the variation of water content (or degree of saturation) within the soil (see for example Croney [52] and Horn, Baumgartl, Gräsle and Richards [64]). The objective of the work described in this section was therefore to explore whether Equation 2.44 could be modified to take account of changes of soil volume, by making one or more of the parameters m, n and α dependent on specific volume v (so providing a specific form for the general form of relationship given in Equation 4.1).

Exploration of a possible relationship between the model parameters, α, m and n, in the van Genuchten expression (Equation 2.44) and the specific volume was conducted by fitting the expression given in Equation 2.44 to the values of degree of saturation, at different values of suction and at a constant value of specific volume, calculated from the three interpolating curves relating degree of saturation and specific volume at constant suction shown in Figure 4.1. At a given value of specific volume three different data points corresponding to different values of suction were available, one value for each of the curves

Specific volume	*Parameter* α	*Parameter* n	*Parameter* m
2.4	0.2254 kPa^{-1}	3.976	0.0401
2.35	0.1893 kPa^{-1}	3.936	0.03961
2.3	0.1566 kPa^{-1}	3.882	0.03918
2.25	0.1272 kPa^{-1}	3.826	0.03871
2.2	0.1012 kPa^{-1}	3.772	0.03818
2.15	0.0786 kPa^{-1}	3.697	0.03779
2.1	0.0593 kPa^{-1}	3.615	0.03746
2.05	0.0430 kPa^{-1}	3.018	0.04342
2.0	0.0303 kPa^{-1}	4.054	0.03105
1.95	0.0200 kPa^{-1}	4.194	0.02887
1.9	0.0100 kPa^{-1}	2.779	0.0.05064
1.85	0.0063 kPa^{-1}	3.777	0.03714

Table 4.1: Parameters values in Equation 2.44

presented in Figure 4.1. This fitting in the (S_r, s)-plane at constant values of specific volume led to the determination of several sets of values for the model parameters of Equation 2.44, each set corresponding to a given value of specific volume. Table 4.1 shows the sets of model parameter values for Equation 2.44 which were found by performing the fit at each constant value of specific volume.

Inspection of Table 4.1 suggested a form of variation of each model parameter with specific volume. In particular, the values of the two parameters m and n in the van Genuchten expression varied relatively little with specific volume and in an apparently random fashion. In contrast, the parameter α decreased monotonically with decreasing specific volume, and experienced a variation of almost two orders of magnitude when the value of the specific volume varied from 2.4 to 1.85. On this basis it was decided to assume a constant value for the parameters m and n, whereas dependency on specific volume was introduced for the parameter α. In particular the following form of variation with specific volume was assumed for the parameter α:

$$\alpha(v) = \phi\,(v-1)^{\psi} \tag{4.4}$$

where ϕ and ψ are model parameters. Figure 4.3 shows a graphical representation of the fit between the values of α reported in Table 4.1 and the proposed Equation 4.4 (with $\phi = 0.03419$ kPa^{-1} and $\psi = 5.690$).

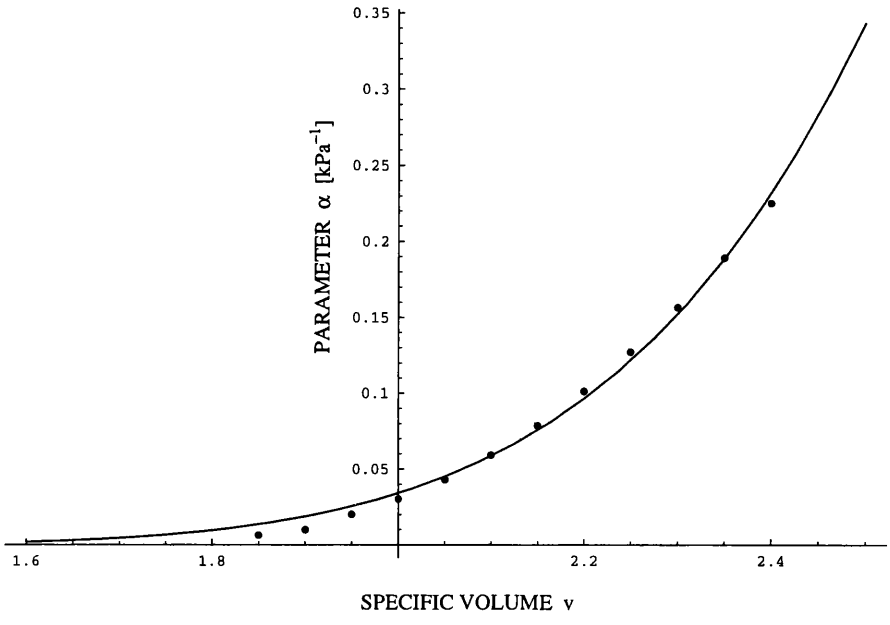

Figure 4.3: Fitting of Equation 4.4

Equation 4.4 gives a value of α equal to zero for the limit condition of specific volume equal to 1 (presence of the solid fraction only). This limit value of α, combined with Equation 2.44, predicts that the degree of saturation tends to 1 as the void ratio tends to zero (irrespective of the value of suction). Combining Equation 4.4 with Equation 2.44, the explicit form proposed for the relationship between degree of saturation, S_r suction, s and specific volume, v is:

$$S_r = \left(\frac{1}{1 + (\phi\,(v-1)^{\psi} s)^n} \right)^m \tag{4.5}$$

where selection of the values of the model parameters ϕ, ψ, m and n is required.

Four soil constants (ϕ, ψ, m and n) are incorporated in the proposed relationship for degree of saturation, only one more than needed for the state surface equation proposed by Lloret and Alonso [22] (Equation 2.41) which was implemented in the original version of the code "Compass". Values for ϕ, ψ, m and n for compacted Speswhite Kaolin were obtained by fitting, through the least squares method, Equation 4.5 to the experimental normal compression lines and critical state data points at suctions of 100 kPa, 200 kPa and 300 kPa from Sivakumar [13] in three-dimensional (S_r, s, v)-space. Figure 4.4 shows the experimental normal compression lines and critical state data points at suctions of 100

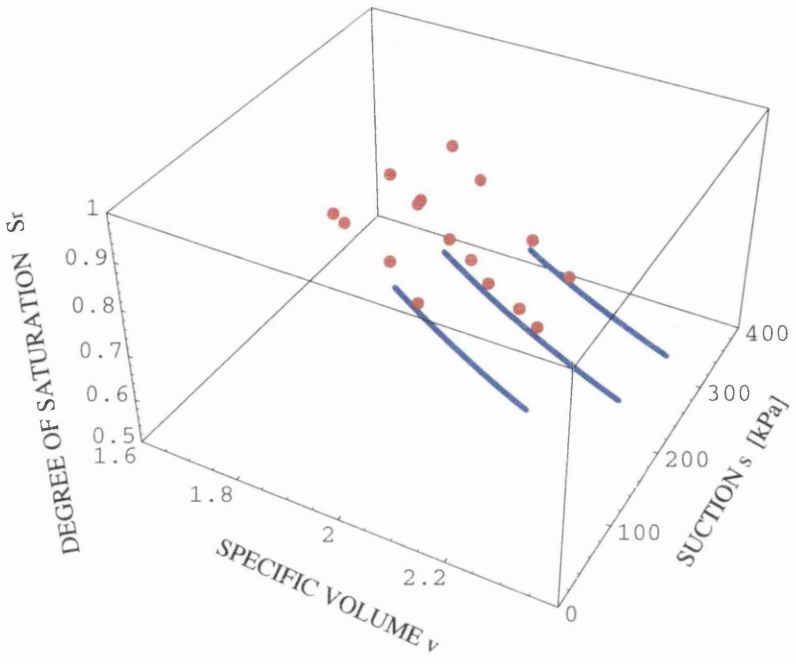

Figure 4.4: Experimental NCL and CS data points at different suctions in the (S_r, s, v)-space

ϕ	ψ	m	n
0.02691 kPa^{-1}	8.433	0.03586	3.746

Table 4.2: Parameter values for the $S_r(v, s)$ relationship

kPa, 200 kPa, 300 kPa plotted in three-dimensional (S_r, s, v)-space (the same information as presented in Figure 4.1) and Figure 4.5 shows the experimental data together with the fitting surface having the analytical form of Equation 4.5. The fit was performed using the least squares method by using the commercial package Mathematica and the values of the model parameters of Equation 4.5 are summarized in Table 4.2.

Equation 4.5 is only one possible choice for defining an analytical relationship between degree of saturation, suction and specific volume and it is therefore possible that for a material other than compacted Speswhite Kaolin or for a more complete set of experimental data, an alternative expression might provide a better fit.

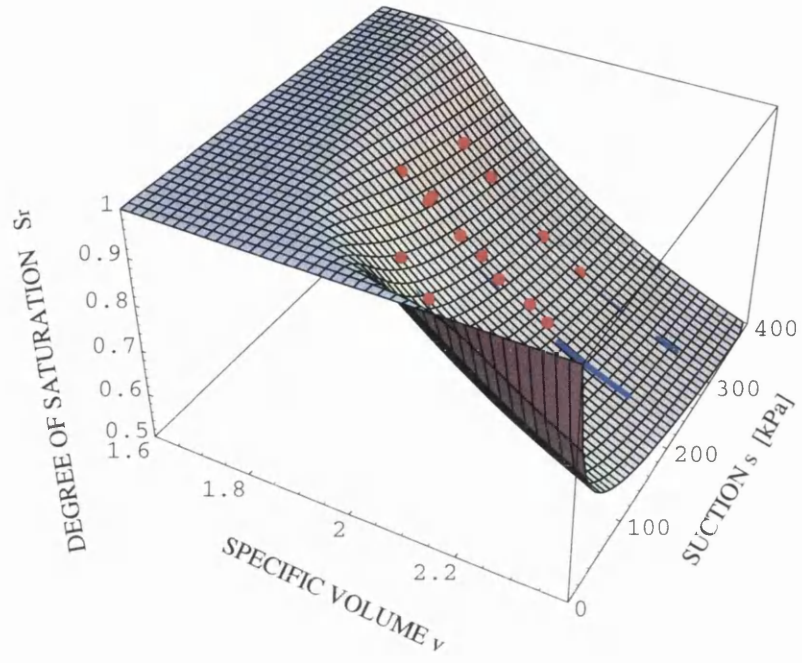

Figure 4.5: Fitting to experimental NCL and CS data points at different suctions in the (S_r, s, v)-space

4.4 Model predictions and comparison with experimental results

In this section some typical predictions of the proposed model are compared with experimental results from tests on compacted Speswhite Kaolin by Sivakumar [13] and Zakaria [15]. In all cases two different types of prediction were computed and compared with experimental data. One prediction was obtained by combining the proposed relationship for degree of saturation (Equation 4.5) with the elasto-plastic model of Alonso, Gens and Josa [1], the other was obtained by combining Equation 4.5 with the model of Wheeler and Sivakumar [3]. The model of Alonso, Gens and Josa [1] is the one implemented in the code "Compass" and it is the model employed in the remainder of this thesis. It was shown, however, in Section 3.2.6 that this model does not provide as good a match to the experimental values of specific volume, v for compacted Speswhite Kaolin as can be achieved with the model of Wheeler and Sivakumar [3]. Given that errors in the predicted values of specific volume will influence the values of degree of saturation predicted by Equation 4.5,

a fairer test of the success of Equation 4.5 is therefore achieved by combining it with the model of Wheeler and Sivakumar [3].

The values of the parameters for the Alonso, Gens and Josa [1] model are the ones summarized in Table 3.2. For the Wheeler and Sivakumar [3] model the values of the model parameters are the ones suggested by the authors of the model for compacted Speswhite Kaolin.

The following types of comparison with laboratory test results were performed and each type will be described in detail in the next sections:

1. normal compression and critical state lines of degree of saturation at constant suction.
2. shearing to critical state at constant suction.
3. isotropic loading/elastic unloading at constant suction and wetting at constant net stress under isotropic conditions.
4. contour plots of degree of saturation in the $(q, \overline{p})$-plane during yielding at constant suction.
5. undrained (with respect to the liquid phase) shearing tests.

4.4.1 Normal compression and critical state lines of degree of saturation

In this section comparisons with experimental data from Sivakumar [13] for normal compression lines and critical state lines at three different constant values of suction (100 kPa, 200 kPa, 300 kPa) are presented.

Figures 4.6 and 4.7 show the comparison between the experimental values of degree of saturation on the normal compression lines by Sivakumar [13] and the corresponding theoretical predictions when the proposed relationship for degree of saturation is combined with the elasto-plastic models of Alonso, Gens and Josa [1] and Wheeler and Sivakumar [3] respectively. The experimental normal compression lines for degree of saturation at constant suctions of 100 kPa, 200 kPa, 300 kPa are given respectively by Equations 3.2, 3.3 and 3.4, where these equations were defined from the average of all the tests

at the same value of suction performed by Sivakumar [13] (see Section 3.3). Inspection of Figures 4.6 and 4.7 reveals that, as expected, the fit between experimental and predicted results is better for the case when the Wheeler and Sivakumar [3] model is employed for the specific volume predictions. In particular the worst fit is achieved when the proposed relationship for degree of saturation is combined with the Alonso, Gens and Josa [1] stress-strain model for predicting the normal compression line of degree of saturation at a suction of 100 kPa (Figure 4.6 (a)). This result is explained by the fact that the Alonso, Gens and Josa [1] model gives less accurate predictions of the normal compression lines at constant suction in the $(v, \ln \overline{p})$-plane than the Wheeler and Sivakumar [3] model and, in particular, the worst prediction is achieved for the normal compression line at a constant suction of 100 kPa (see Figure 3.8).

Figures 4.8 and 4.9 show comparisons between the experimental critical state data points from Sivakumar [13] and the predicted critical state lines when the proposed relationship for degree of saturation is combined with the elasto-plastic stress-strain models of Alonso, Gens and Josa [1] and Wheeler and Sivakumar [3] respectively. Inspection of Figures 4.8 and 4.9 indicates that more accurate predictions are obtained by combining the proposed relationship for degree of saturation with the stress-strain model of Wheeler and Sivakumar [3]. This is consistent with the fact that the Wheeler and Sivakumar [3] model is able to provide better predictions of specific volume values at critical state. In particular the predictions computed by employing the Alonso, Gens and Josa [1] model are poorer at lower values of mean net stress, due to the fact that the critical state lines at constant suction predicted in the $(v, \ln \overline{p})$-plane by the Alonso, Gens and Josa [1] model fit poorly to experimental critical state data at lower values of mean net stress (see Figure 3.10).

Figures 4.7 and 4.9 show that, when the proposed relationship for degree of saturation is combined with the Wheeler and Sivakumar [3] model, the fit between theoretical predictions and experimental results is excellent in both normal compression and critical state conditions. This provides fundamental support to the validity of the proposed relationship for degree of saturation of Equation 4.5. In addition, while the fit is not as good in combination with the Alonso, Gens and Josa [1] model, the agreement between

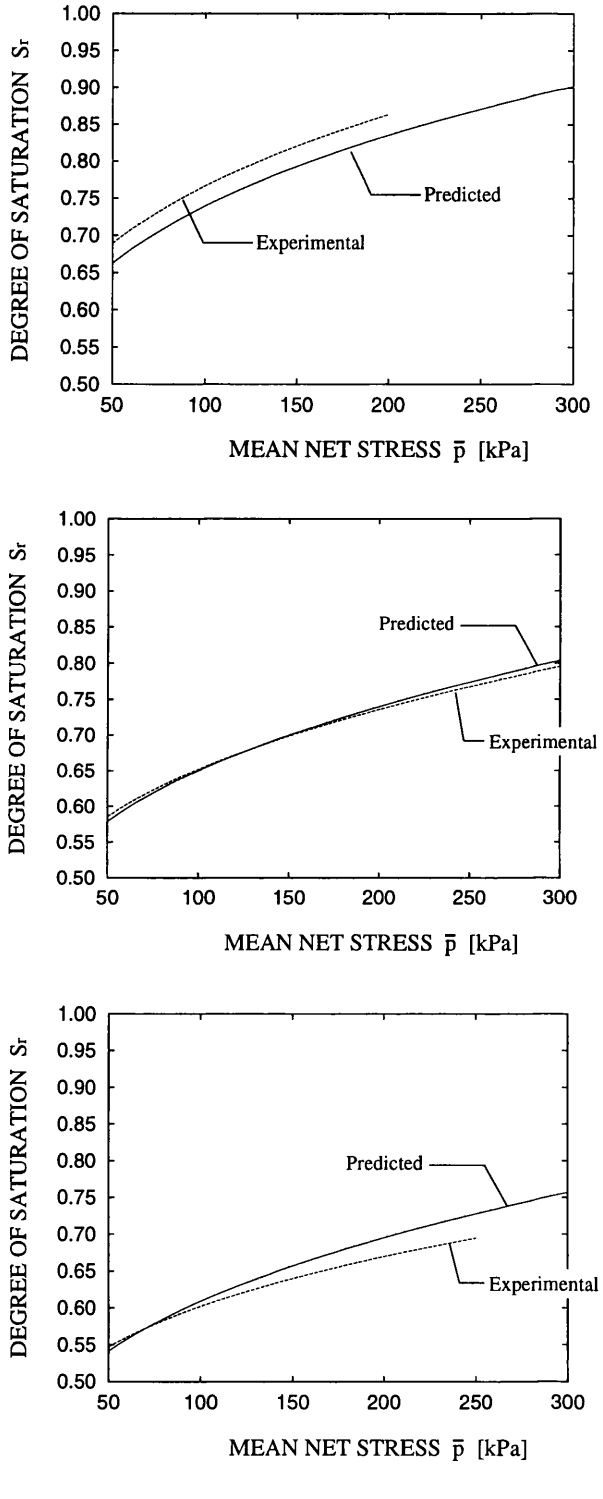

Figure 4.6: Predicted (v calculated by the Alonso, Gens and Josa [1] model) and experimental NCL in the $(S_r, \overline{p})$-plane at different suctions of: (a) s=100 kPa (b) s=200 kPa (c) s=300 kPa

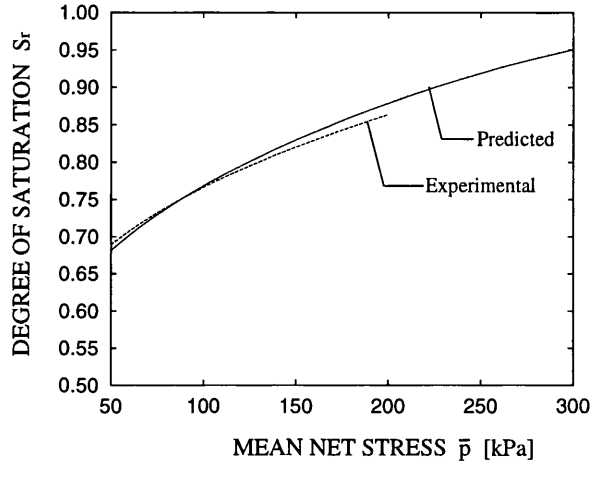

(a)

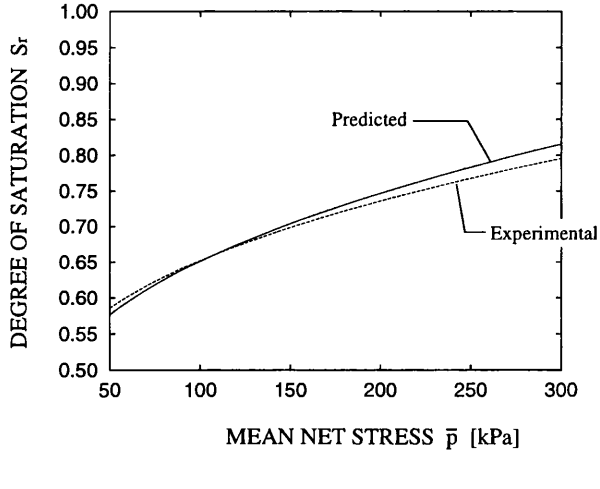

(b)

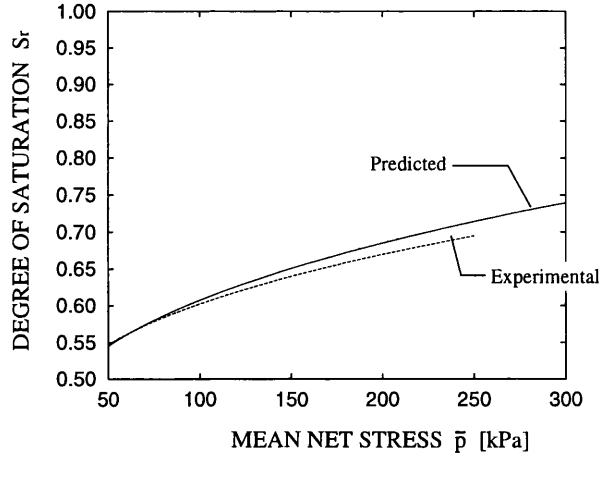

(c)

Figure 4.7: Predicted (v calculated by the Wheeler and Sivakumar [3] model) and experimental NCL in the $(S_r, \bar{p})$-plane at different suctions of: (a) s=100 kPa (b) s=200 kPa (c) s=300 kPa

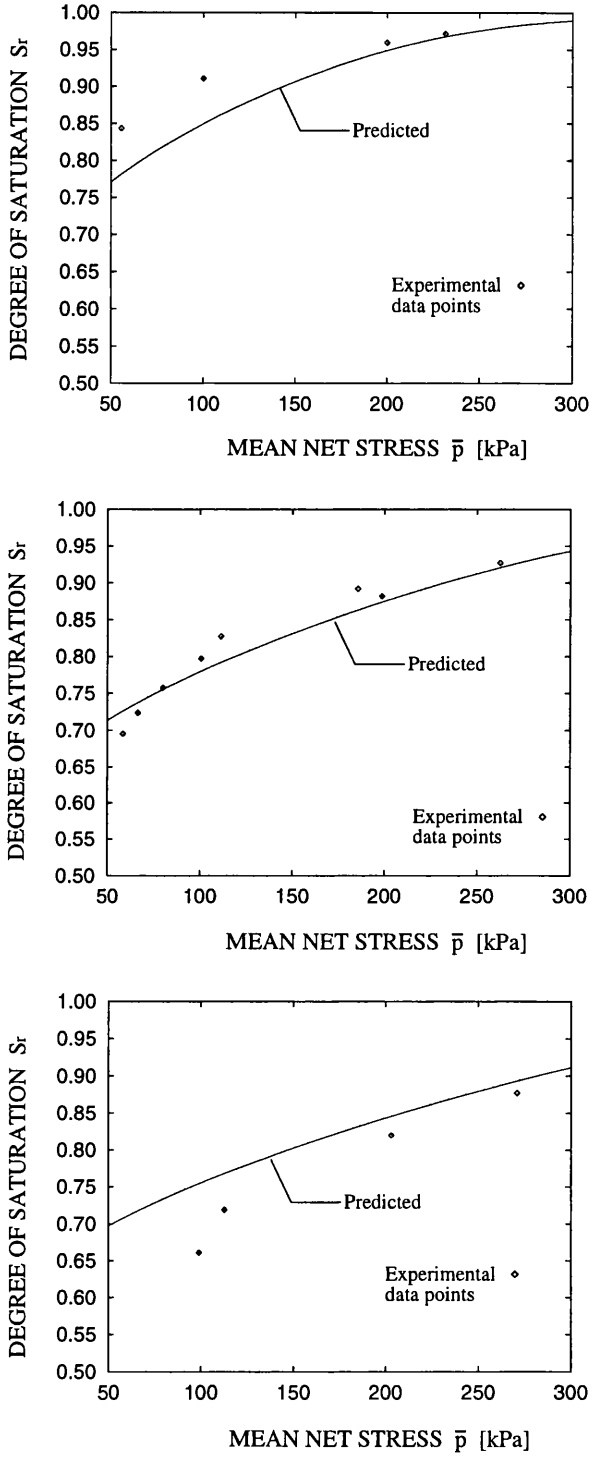

Figure 4.8: Predicted CSL (v predicted by the Alonso, Gens and Josa [1] model) and experimental CS data points in the $(S_r, \overline{p})$-plane at different suctions of: (a) s=100 kPa (b) s=200 kPa (c) s=300 kPa

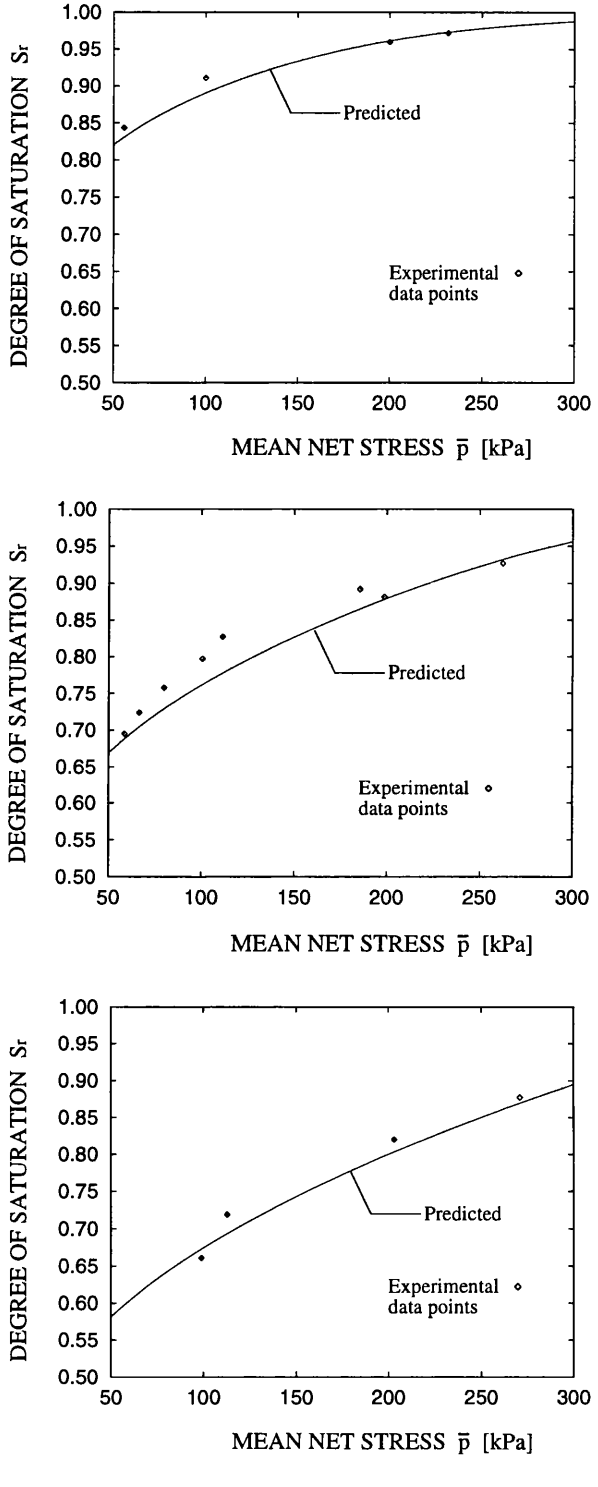

Figure 4.9: Predicted CSL (v predicted by the Wheeler and Sivakumar [3] model) and experimental CS data points in the $(S_r, \overline{p})$-plane at different suctions of: (a) s=100 kPa (b) s=200 kPa (c) s=300 kPa

theoretical predictions and experimental results is still satisfactory.

In both cases the theoretical predictions are significantly better than is achieved by employing the traditional state surafce approach (i.e. a unique relationship between degree of saturation, suction and net stress state). The state surface approach would predict the same degree of saturation for given values of suction and net stresses irrespective of whether the soil is in a normal compression condition or at critical state. Therefore, if experimental data from isotropic normal compression tests are used to define the values of the model parameters for the state surface expression, the fit at critical state between theoretically predicted values of degree of saturation and experimental ones will be significantly poorer than for the case where the proposed relationship for degree of saturation (Equation 4.5) is employed. For example, Figure 3.15 shows the poor fit, between the values of degree of saturation predicted by the state surface expression of Lloret and Alonso [22] (Equation 2.41)and experimental critical state data points from Sivakumar [13]. The relevant parameter values in Equation 2.41 were defined on the basis of isotropic normal compression tests from Sivakumar [13] (see Table 3.6).

4.4.2 Elasto-plastic shearing tests at constant suction

In the previous section it was shown that it is possible to define a unique relationship between degree of saturation, suction and specific volume which is able to give good predictions of degree of saturation for normal compression and critical state conditions provided that the specific volume is predicted with sufficient accuracy. It should, however, be remembered that experimental data of values of degree of saturation on the normal compression lines and critical state lines were used in selecting the parameter values in Equation 4.5. In this section the model performance is assessed for intermediate stress states which occur when the soil is sheared from an initial normally consolidated condition to a critical state.

The model predictions are compared with experimental tests performed by Sivakumar [13] on compacted Speswhite Kaolin. The types of test investigated were of the following two categories: constant suction/constant cell pressure shearing tests and constant suction/constant mean net stress shearing tests. The tests in question correspond

to stress paths which start from a normally consolidated condition and are therefore on the yield surface throughout the entire test path to a critical state.

Two Fortran codes were developed in order to perform simulations with the Alonso, Gens and Josa [1] model and the Wheeler and Sivakumar [3] model respectively. In both cases a large number of different shearing tests performed by Sivakumar [13] were simulated including both constant cell pressure shearing tests and constant mean net stress shearing tests, and tests at three levels of suction (100 kPa, 200 kPa, 300 kPa). In the interest of conciseness, only three constant mean net stress shearing tests (one for each value of suction) are reported here.

Figure 4.10 shows the predicted and experimental results for a shearing test performed at a constant suction of 100 kPa and a constant mean net stress of 100 kPa. The predicted results have been calculated by combining the proposed relationship for degree of saturation with the Alonso, Gens and Josa [1] stress-strain model in Figure 4.10 (a) and with the Wheeler and Sivakumar [3] model in Figure 4.10 (b). Inspection of Figure 4.10 reveals that the proposed relationship for degree of saturation is able to provide accurate predictions using either stress-strain model. Use of the Alonso, Gens and Josa [1] model actually provides a better fit to experimental data than use of the Wheeler and Sivakumar [3] model. This is, however, a fortuitous result, where the difference between the predicted and experimental results in the Wheeler and Sivakumar [3] case is offset by the error in the prediction of the specific volume caused by use of the Alonso, Gens and Josa [1] model. It is also evident from Figure 4.10 that, when the proposed relationship for degree of saturation is used in combination with the Wheeler and Sivakumar [3] stress-strain model a more accurate prediction of the critical state value of degree of saturation is obtained than with the Alonso, Gens and Josa [1] model.

Figure 4.11 shows predicted and experimental results for a shearing test performed at a constant suction of 200 kPa and a constant mean net stress of 100 kPa. Inspection shows that better fit to the experimental data is achieved with the Wheeler and Sivakumar [3] model, as would be expected. However combination of the proposed relationship for degree of saturation with the Alonso, Gens and Josa [1] model is also able to provide a

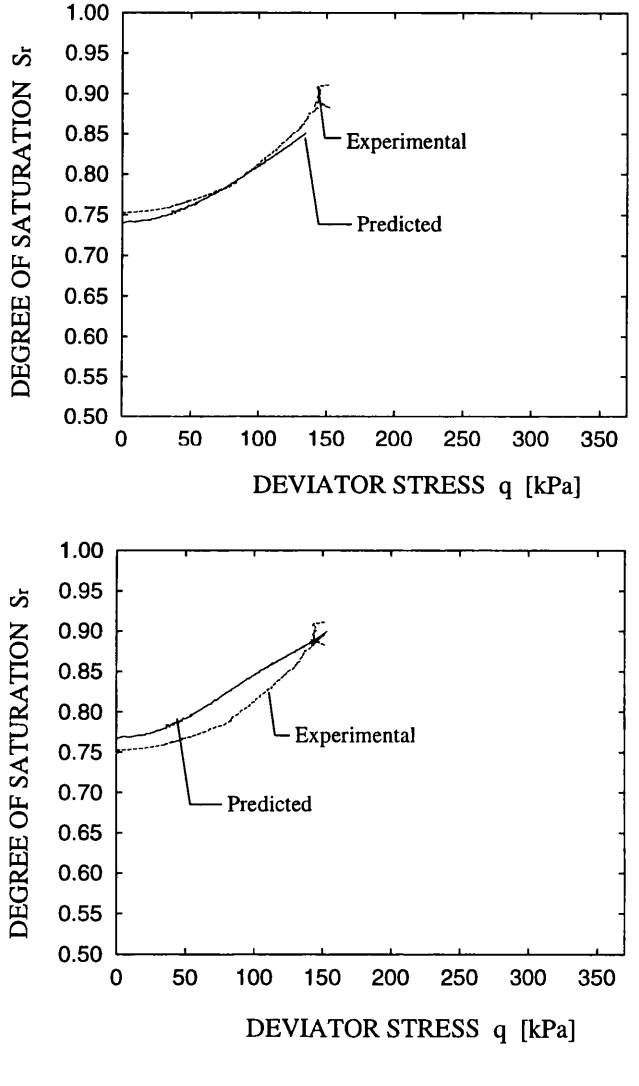

Figure 4.10: Predicted and experimental results from a constant suction (100 kPa)/constant mean net stress (100 kPa) shearing test. Predicted results used values of v calculated by: (a) the Alonso, Gens and Josa [1] model (b) the Wheeler and Sivakumar [3] model

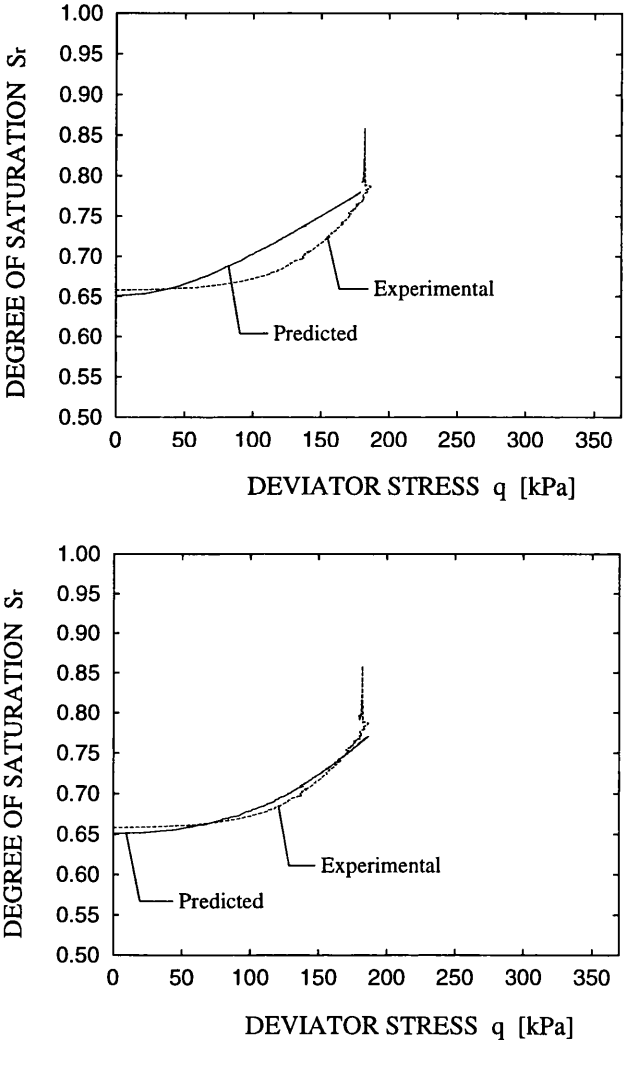

Figure 4.11: Predicted and experimental results from a constant suction (200 kPa)/constant mean net stress (100 kPa) shearing test. Predicted results used values of v calculated by: (a) the Alonso, Gens and Josa [1] model (b) the Wheeler and Sivakumar [3] model

reasonably good prediction and, in the two cases, the final critical state is predicted with approximately the same accuracy.

Figure 4.12 shows the predicted and experimental results for a shearing test performed at a constant suction of 300 kPa and a constant mean net stress of 100 kPa. Among all the constant suction shearing tests simulated, this test represents the case where the largest differences were observed between the predictions made with the Alonso, Gens and Josa [1] model and those made with the Wheeler and Sivakumar [3] model. It is clear from inspection of Figure 4.12 that the comparison between predicted and experimental results is better for the case when the Wheeler and Sivakumar [3] model is used.

The three comparisons presented in this section are only a small part of the total number of simulations performed for comparison with the experimental results from Sivakumar [13]. In all other simulations the best fit with the experimental results was achieved by combining the proposed relationship for degree of saturation with the Wheeler and Sivakumar [3] stress-strain model. Combination of the proposed relationship for degree of saturation with the Alonso, Gens and Josa [1] model provided, however, reasonably good predictions. In particular combination of the proposed relationship for degree of saturation with the Alonso, Gens and Josa [1] stress-strain model represents a significant improvement over the traditional state surface approach for degree of saturation (which predicts no change of degree of saturation during shearing at constant suction and constant mean net stress).

4.4.3 Elastic stress paths

In this section the model performance is assessed for two different elastic stress paths: isotropic unloading at constant suction and wetting at constant mean net stress under an isotropic stress state.

Zakaria [15] performed a test involving isotropic elasto-plastic loading/elastic unloading at a constant suction of 100 kPa. The experimental results from Zakaria [15] used in this comparison refer to a test on compacted Speswhite Kaolin, which is the same material as tested by Sivakumar [13], whose experimental results have been used to define the values of ϕ, ψ, m and n in Equation 4.5 used for the predictions. The compaction procedure

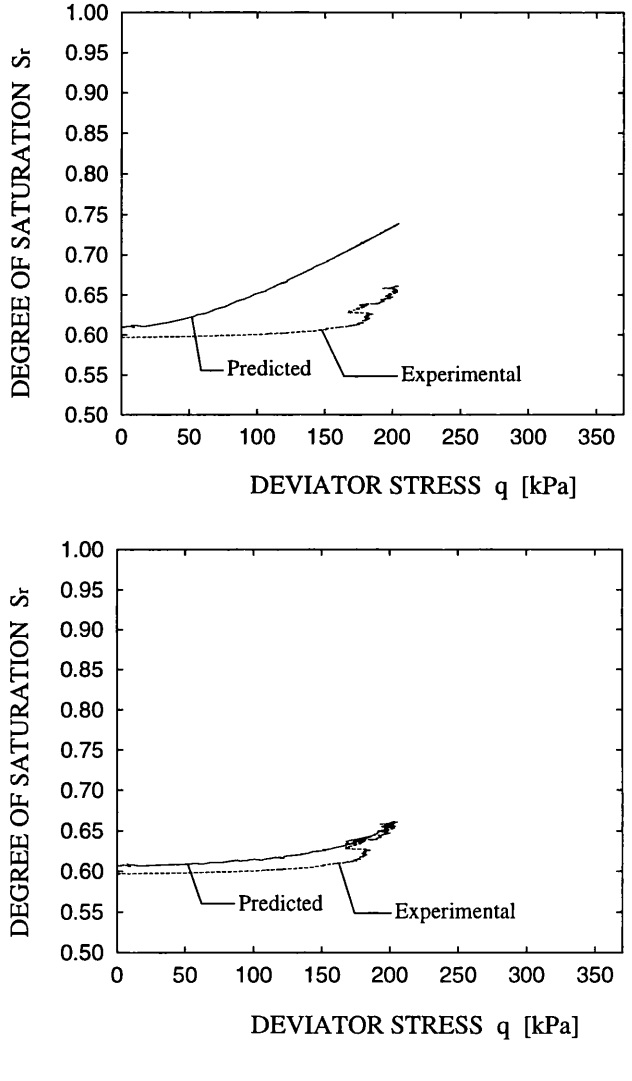

Figure 4.12: Predicted and experimental results from a constant suction (300 kPa)/constant mean net stress (100 kPa) shearing test. Predicted results used values of v calculated by: (a) the Alonso, Gens and Josa [1] model (b) the Wheeler and Sivakumar [3] model

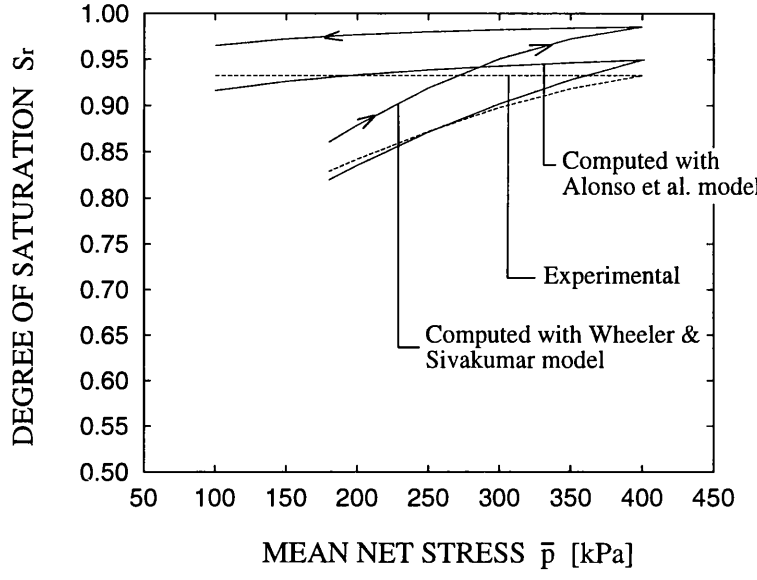

Figure 4.13: Predicted and experimental results from isotropic loading-unloading test at constant suction (100 kPa)

used by Zakaria [15] was also identical to that employed by Sivakumar [13].

Figure 4.13 shows the experimental results from the test of Zakaria [15] together with the prediction obtained by using Equation 4.5 in combination with either the Alonso, Gens and Josa [1] model or the Wheeler and Sivakumar [3] model. Inspection of Figure 4.13 shows that the general pattern of variation of degree of saturation with mean net stress during the loading-unloading path is well reproduced by the proposed model in both cases. The discrepancy in Figure 4.13 between the experimental and predicted results for the case of the Wheeler and Sivakumar [3] model, is probably attributable to the fact that the experimental values are from a test series using different equipment and performed by a different individual than the tests employed to calibrate the model. Therefore, despite the fact that the material tested in the two series was ostensibly the same, some differences are to be expected, due to lack of repeatability of the experiments. This is supported by the fact that in Figure 4.13 the predicted normal compression curve (the loading branch) using the Wheeler and Sivakumar [3] model is approximately parallel to the corresponding experimental curve but significantly offset (the difference between the two is certainly

more significant than in Figure 4.7 where a comparison with the experimental values of Sivakumar [13] is reported). The comparison for the case when the proposed relationship for degree of saturation is used in combination with the Alonso, Gens and Josa [1] model shows a better fit between predicted and experimental data. This is, however, a fortuitous result where the less accurate prediction of specific volume happens to offset the discrepancy between experimental and predicted curves caused by the lack of repeatability of the experiments.

For the unloading part of the test, the experimental pattern of variation of degree of saturation during elastic unloading is well reproduced by the proposed relationship for degree of saturation in both cases. In particular, the predicted variation of degree of saturation during elastic unloading is much less than during plastic loading (because of the smaller variation of specific volume), and this agrees with observed behaviour. Although the experimental results suggest an almost constant value of degree of saturation during unloading while the model predicts a decrease of degree of saturation with decreasing mean net stress, the predicted reduction of degree of saturation is relatively small and does not exceed a value of 0.03 for a decrease of mean net stress from 400 kPa to 100 kPa. The measured constant value of degree of saturation during the unloading part of the test is actually more consistent with the other form of variation of degree of saturation proposed in Equation 4.2, which would indeed predict a constant value of degree of saturation during elastic unloading at constant suction due to the absence of plastic changes of specific volume. However the differences between the predictions of the two Equations 4.1 and 4.2 for the unloading branch are relatively small and both are able to model adequately the pattern of variation of degree of saturation during elastic unloading.

Again in this case the theoretical predictions, obtained combining the proposed relationship for degree of saturation (Equation 4.1) with either the Alonso, Gens and Josa [1] model or the Wheeler and Sivakumar [3] model, are significantly improved with respect to the case where the traditional state surface approach is employed. For the test reported in Figure 4.13 the state surface approach would predict entirely reversible changes of degree of saturation during the loading and unloading paths. In other words it would predict the

same value of degree of saturation at a given suction and net stress irrespective whether the soil is subject to an elasto-plastic or elastic stress path. Therefore, if experimental data from isotropic normal compression tests are used to define the values of the model parameters for the state surface expression, the fit between theoretically predicted values of degree of saturation and experimental data for the elastic unloading path would be significantly poor. In contrast, if experimental data from elastic tests are used to define the values of the model parameters for the state surface expression, the theoretical predictions of degree of saturation during the elasto-plastic stress path would be significantly in error.

The second elastic stress path simulated is a wetting test at constant mean net stress. Sivakumar [13] performed wetting of several samples of compacted Speswhite Kaolin from an initial condition after compaction to four different suction levels (300 kPa, 200 kPa, 100 kPa, 0 kPa). Immediately following compaction the degree of saturation was reported as 0.54, and the value of suction was subsequently measured in a pressure plate apparatus by Sivakumar and Wheeler [65] as approximately 700 kPa. The samples wetted to suctions of 300 kPa, 200 kPa and 100 kPa were isotropically loaded and at a constant value of mean net stress of 50 kPa. The samples brought to a level of suction of zero were forcibly saturated at an average mean net stress within the sample of 32.5 kPa. The samples brought from the initial suction of 700 kPa to final values of suctions of 300 kPa and 200 kPa showed swelling throughout the wetting process. In contrast, the samples wetted to a value of suction of 100 kPa and to saturated conditions (zero suction) presented, in the first case, a small amount of collapse compression and, in the latter case, larger values of collapse compression at the end of wetting. These experimental results indicate that the three stress states corresponding to suctions of 200 kPa, 300 kPa, 700 kPa are lying inside the initial yield locus (i.e. the yield locus corresponding to the soil state immediately after compaction), whereas the stress state corresponding to a suction of 100 kPa lies on a slightly expanded yield surface respect to the initial one (as suggested by the occurrence of small values of collapse compression). Finally the stress state corresponding to saturated conditions lies on a significantly expanded yield locus, which corresponds to a noticeably greater value of the hardening parameter, $\overline{p}_o^*$ than the initial one. For the model

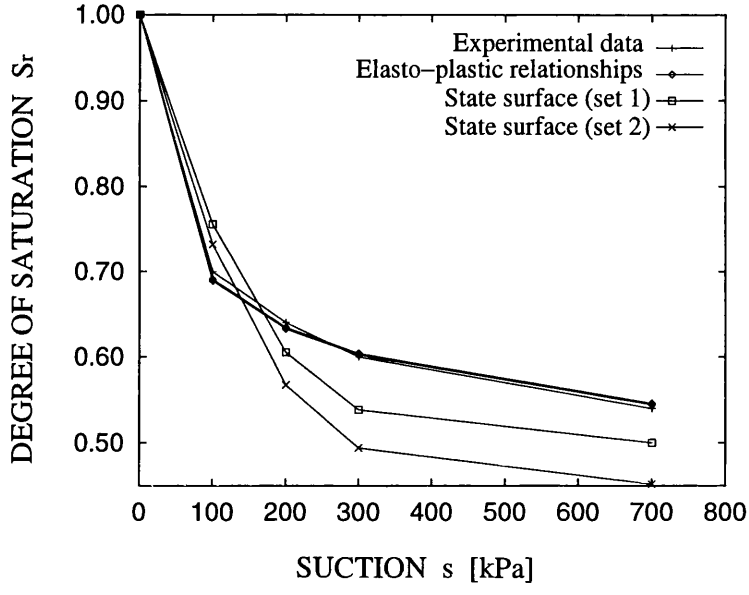

Figure 4.14: Predicted and experimental results from wetting test at constant mean net stress (50 kPa)

predictions the initial value of the hardening parameter $\overline{p}_o^*$ for both stress-strain models was assumed equal to 18 kPa. This value was selected for the Alonso, Gens and Josa [1] model in Section 3.2.5 as the value corresponding to the soil condition after compaction (see Figure 3.9). The same value was suggested for the Wheeler and Sivakumar [3] model by the authors.

Figure 4.14 shows the comparison between experimental (Sivakumar [13]) and predicted values of degree of saturation during the wetting tests. The experimental data points are the average from all the wetting tests at the same level of suction. Inspection of Figure 4.14 shows that the two predictions obtained by combining the proposed relationship for degree of saturation with the Alonso, Gens and Josa [1] stress-strain model or the Wheeler and Sivakumar [3] model are very close. The two predicted curves practically overlap and they are indicated with the same entry in the legend (i.e. Elasto-plastic relationships). The computed results show an exact fit to the experimental point at zero suction because Equation 4.1 predicts full saturation of the soil when a null value of suction is attained and Sivakumar [13] forcibly saturated his samples at zero suction, by flushing with water.

The other four predicted data points at values of suction of 700 kPa, 300 kPa, 200 kPa and 100 kPa are in very good agreement with the experimental results.

The proposed relationship for degree of saturation provides also in this case improved predictions of degree of saturation in comparison with the traditional state surface approach. The important difference between the two methods is that the state surface approach predicts always the same soil-water characteristic curve for degree of saturation at a given constant value of net stress, whereas the proposed relationship for degree of saturation, introduces a dependency on suction and specific volume which accounts for both the net stress state and the past stress history (i.e. past occurence of plastic changes of specific volume). Therefore different soil-water characteristic curves at constant net stress may be predicted depending on the initial value of specific volume of the soil and/or if volumetric plastic deformations occur during wetting.

Figure 4.14 also shows the predictions obtained with the state surface expression of Equation 2.41 for both the sets of parameter values given by Tables 3.6 (set 1) and 3.7 (set 2). Inspection of Figure 4.14 clearly suggests that better predictions are obtained by using the elasto-plastic relationship for degree of saturation rather than the state surface approach. In particular the two curves computed by using the state surface approach tend to noticeably underestimate the value of degree of saturation over most of the suction range relevant to the experimental data. The values of degree of saturation corresponding to stress states lying inside the yield locus (i.e. at values of suction of 200 kPa, 300 kPa, 700 kPa) are smaller when the state surface approach is employed than when the elasto-plastic relationship for degree of saturation is used. This is explained by the fact that, at any given value of suction and net stresses, the state surface expression refers to a normally consolidated soil (due to the particular choice of parameter values) whereas the elasto-plastic relationship correctly accounts for overconsolidation by considering the occurrence of irreversible changes of specific volume.

4.4.4 Contour plot of S_r in the $(q, \overline{p})$-plane at constant suction

In this section the predicted contour plots of degree of saturation in the $(q, \overline{p})$-plane during yielding at a constant suction of 200 kPa are compared with Sivakumar's [13] experimental

results.

When the soil is on the yield surface it is possible to define a unique relationship between degree of saturation, mean net stress, deviator stress and suction. The experimental contour plot in Figure 4.15 was estimated on the basis of all the elasto-plastic tests at a constant suction of 200 kPa performed by Sivakumar [3] (i.e normal compression tests and shearing tests). Inspection of Figure 4.15 shows that the predicted and experimental constant degree of saturation curves are very close. Similar results were also obtained for the contour plots at the other two levels of suction of 100 kPa and 300 kPa but the relevant figures are not reported here. It is interesting to note that the predicted contour plots of degree of saturation reported in Figure 4.15 coincide with the contour plots of specific volume at the constant suction of 200 kPa for an element of soil which is yielding. This is due to the assumed dependency of the degree of saturation (Equation 4.1) on suction and specific volume.

The proposed relationship for degree of saturation provides, also in this case, improved predictions in comparison with traditional state surface expression, such as the one proposed by Lloret and Alonso [22] (Equation 2.41) which was originally implemented in the code "Compass". In particular the state surface expression of Equation 2.41 would predict contours of degree of saturation which are vertical lines due to the fact that no dependency of degree of saturation on the deviator stress is included in the expression.

4.4.5 Elasto-plastic shearing tests undrained with respect to the liquid phase

In this section experimental results from three shearing tests, undrained with respect to the liquid phase, performed by Sivakumar [13] are compared with model predictions. Shearing of the samples was achieved by keeping the radial cell pressure of the triaxial apparatus constant while the axial stress was increased. The restraint imposed on the specific water volume (or water content), which had to remain constant, caused a change of suction during the shearing process. Two of the three tests started from an initial value of suction of 100 kPa and from initial isotropic condition at a value of mean net stress of 100 kPa or 200 kPa. The third test started from an initial value of suction of 200 kPa and

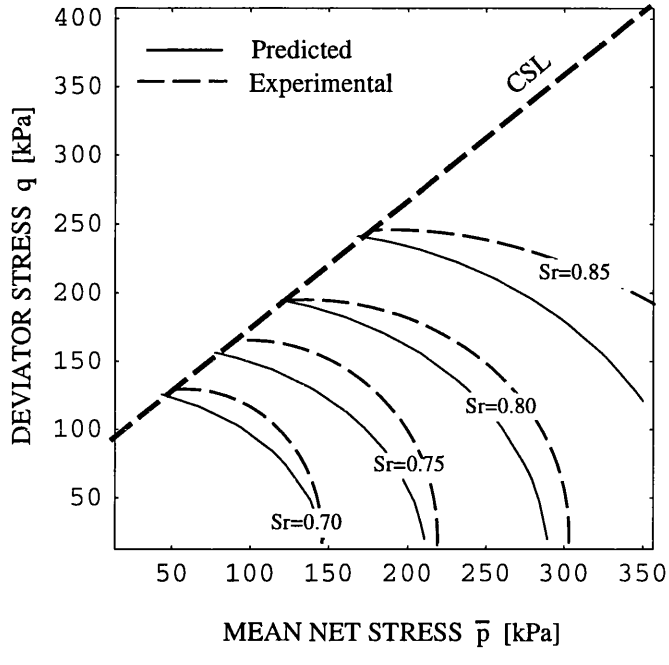

(a)

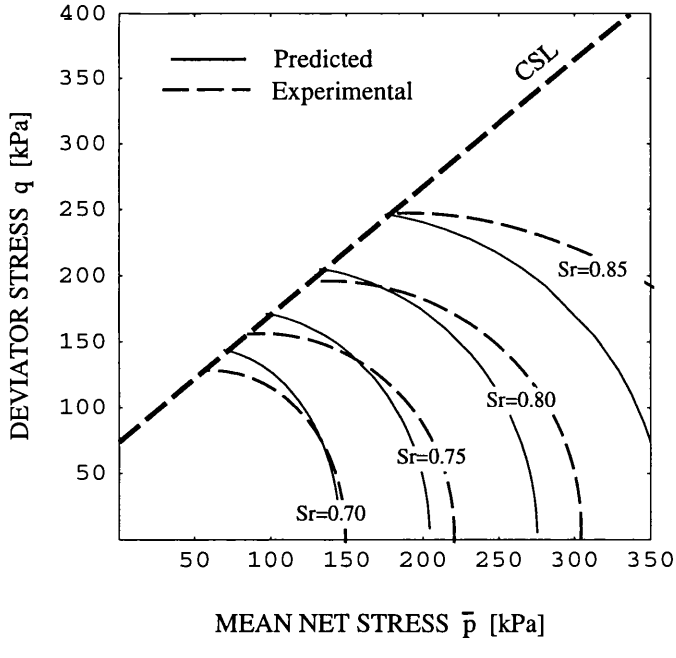

(b)

Figure 4.15: Predicted and experimental contour plots of degree of saturation in the $(q, \bar{p})$-plane for yielding at a constant suction of 200 kPa. Predicted results used values of v calculated by: (a) the Alonso, Gens and Josa [1] model (b) the Wheeler and Sivakumar [3] model

from initial isotropic condition at a value of mean net stress of 100 kPa.

In order to calculate the predicted variation of suction both the proposed relationship for degree of saturation (Equation 4.5) and, for comparison, the state surface expression of Lloret and Alonso [22] (Equation 2.41) were combined with the constitutive models of Alonso, Gens and Josa [1] and Wheeler and Sivakumar [3]. The restraints of constant specific water volume and the imposed stress path in the $(q, \overline{p})$-plane were enforced in the model. This process led to a system of two non-linear equations to be solved for the unknowns of specific volume and suction. Two Fortran codes were developed, one for each stress-strain model, to solve iteratively the set of equations with the possibility of considering both the relationships for degree of saturation. For the model of Wheeler and Sivakumar [3], because the values of suction-dependent soil parameters for compacted Speswhite Kaolin were provided by the authors at discrete values of suction (0 kPa, 100 kPa, 200 kPa, 300 kPa), linear interpolation was used in solving the system of equations for the intermediate values of suction.

For the state surface of Equation 2.41 the set of parameters values reported in Table 3.6 was employed. The tests considered in this section involve elasto-plastic deformations from the beginning of loading and, therefore, the choice of the first of the two sets of parameters values, selected in Section 3.3 for the state surface of Equation 2.41, seemed appropriate.

The comparisons between experimental and computed results are reported in Figures 4.16 and 4.17. Inspection of Figures 4.16 and 4.17 reveals that the proposed relationship for degree of saturation used in combination with both models, correctly predicts an increase in suction during shearing for two of the three tests but the magnitude of this increase was significantly underestimated. In the third test (see Figures 4.16 (b) and 4.17 (b)), the predicted value of suction, by using both models, is approximately constant during most of the shearing process with a drop towards the final stages of the test. The experimental results instead showed an increase of suction at the end of the shearing process after the suction remained approximately constant during the previous part of the test. These are the only cases among all the tests investigated in this work where significant discrepancies between the predictions of the proposed relationship

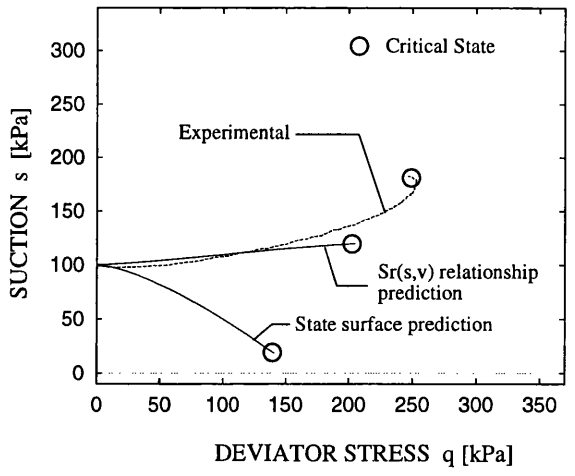

(a)

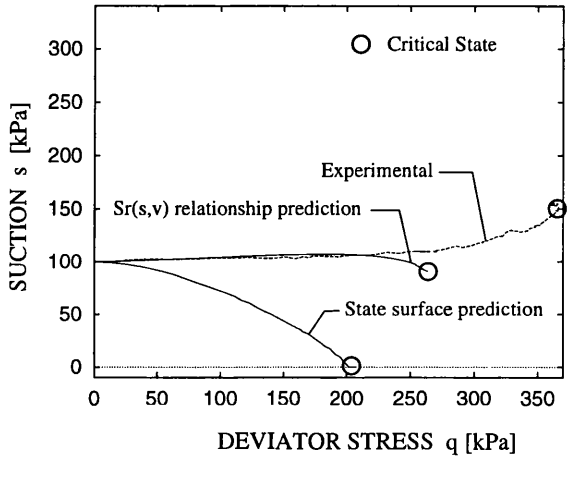

(b)

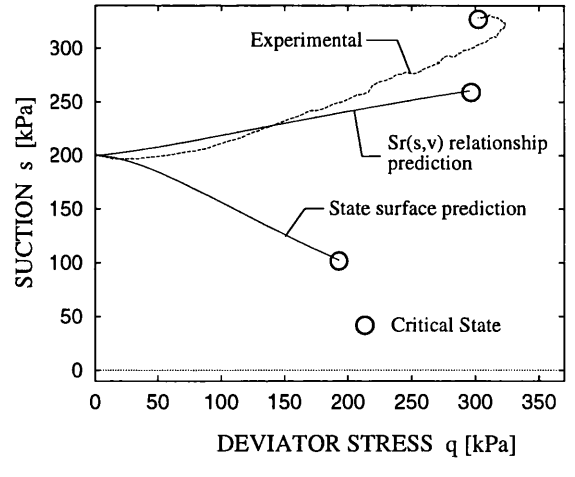

(c)

Figure 4.16: Predicted (v calculated by the Alonso, Gens and Josa [1] model) and experimental results from undrained shearing tests. (a) Initial s=100 kPa, initial $\overline{p}$=100 kPa (b) Initial s=100 kPa, initial $\overline{p}$=200 kPa (c) Initial s=200 kPa, initial $\overline{p}$=100 kPa

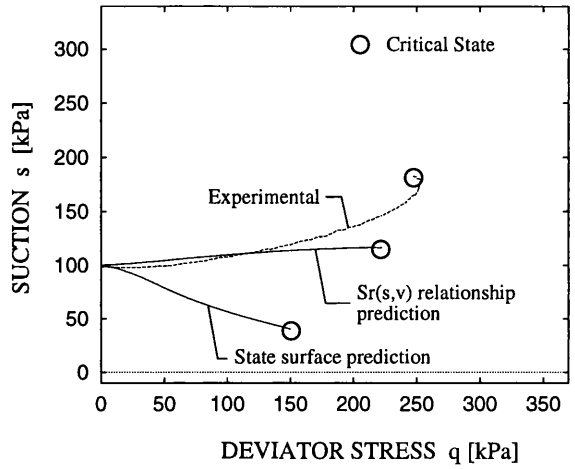

(a)

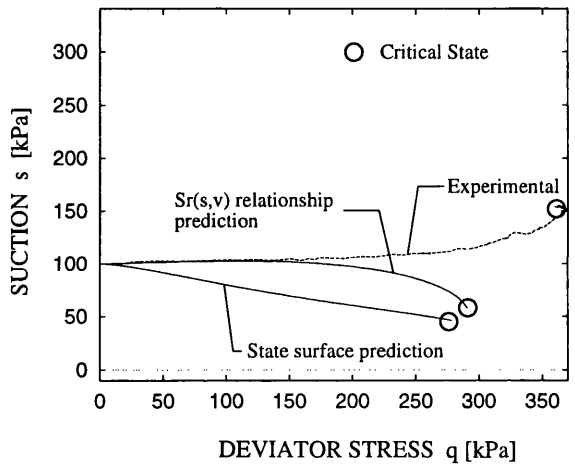

(b)

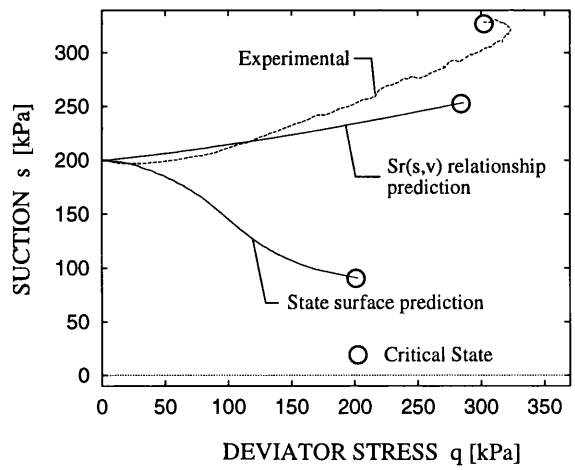

(c)

Figure 4.17: Predicted (v calculated by the Wheeler and Sivakumar [3] model) and experimental results from undrained shearing tests. (a) Initial s=100 kPa, initial $\overline{p}$=100 kPa (b) Initial s=100 kPa, initial $\overline{p}$=200 kPa (c) Initial s=200 kPa, initial $\overline{p}$=100 kPa

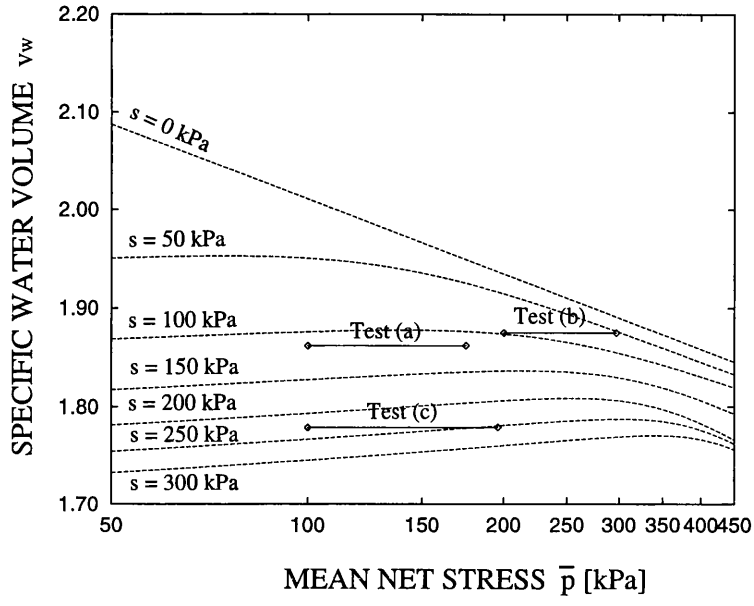

Figure 4.18: Predicted CSL (v calculated by the Wheeler and Sivakumar model [3]) in the $(v_w, \ln \overline{p})$-plane at different suctions

for degree of saturation and experimental results were observed.

One possible explanation for these discrepancies is the fact that critical state lines for specific water volume at different values of suction tend to be very close to each other at the relatively high values of mean net stress relevant to the test simulations. This is illustrated in Figure 4.18, which shows the critical state lines of specific water volume at different levels of suction together with the projection on the $(v_w, \ln \overline{p})$-plane of the stress paths for the three tests investigated. The critical state lines of specific water volume reported in Figure 4.18 have been plotted by combining the proposed relationship for degree of saturation with the Wheeler and Sivakumar [3] stress-strain model, using linear interpolation to calculate the values of the suction-dependent parameters at the intermediate values of suction of 50 kPa, 150 kPa and 250 kPa. If the critical state lines for v_w at different suctions are very close together, a small variation of specific water volume can produce relatively large changes in suction or, analogously, a small error in the prediction of the critical state lines of specific water volume may result in more significant errors in the prediction of the suction values.

As the predicted specific water volume is dependent on predictions of both degree of saturation and specific volume, potential errors in the predicted critical state lines of specific water volume may be due to two different causes. These are the incorrect prediction of degree of saturation at critical state from the proposed relationship for degree of saturation and the incorrect prediction of specific volume at critical state from the stress-strain model. Therefore the inaccuracy in the results may not be due exclusively to the proposed relastionship for degree of saturation but it could be partly caused by imprecise prediction of specific volume at critical state by the stress-strain model employed.

Inspection of Figures 4.16 and 4.17 reveals, however, that, as in the previous examples of this chapter, the predictions computed by the proposed relationship for degree of saturation in combination with both stress-strain models and for any test simulation, are significantly better than those obtained with the state surface expression.

4.5 Concluding remarks

In this chapter a new relationship for the prediction of the variation of degree of saturation in an unsaturated soil has been presented. The proposed relationship assumes that the degree of saturation is dependent on suction and specific volume. An explicit form for this relationship has been proposed, given by Equation 4.1. This is based on the soil-water characteristic expression proposed by van Genuchten [48] and reported in Equation 2.44. The dependency on specific volume is introduced by relating the parameter α of the original van Genuchten expression to the specific volume v through the relationship reported in Equation 4.4.

When combined with an elasto-plastic constitutive model predicting changes of specific volume with the stress state, the proposed relationship for degree of saturation is able to reproduce irreversible changes in degree of saturation after yielding (due to the occurrence of irreversible changes in specific volume). An alternative form of relationship has also been considered, where degree of saturation is assumed to be dependent on suction and plastic changes of specific volume. This other option, however, has subsequently been disregarded in favour of the first one which presents some advantages. The most important

advantage is that a relationship between degree of saturation, suction and specific volume could generally be defined for a given soil regardless of the constitutive model adopted for describing its mechanical behaviour. Instead a relationship between degree of saturation, suction and plastic changes of specific volume is specific to the particular elasto-plastic constitutive model used to derive it.

Model performances have been assessed by comparing the predictions with experimental results from laboratory tests on compacted Speswhite Kaolin from Sivakumar [3] and Zakaria [15]. The predictions have been calculated by combining the proposed relationship for degree of saturation with the predicted changes of specific volume computed according to the two elasto-plastic stress-strain models of Alonso, Gens and Josa [1] and Wheeler and Sivakumar [3]. The agreement between predicted and experimental results has generally been very good and better results have generally been obtained by using the proposed relationship for degree of saturation in combination with the Wheeler and Sivakumar [3] stress-strain relationship. This is due to the fact that the Wheeler and Sivakumar [3] model is able to give more accurate predictions of the changes in specific volume with stress state than the Alonso, Gens and Josa [1] model.

The proposed relationship for degree of saturation represents a significant improvement over the traditional method used to model the variation of degree of saturation with net stress state and suction (i.e. the state surface approach). It is able to distinguish between elastic and plastic (irreversible) changes of degree of saturation, providing also a means to model the changes of degree of saturation observed during shearing in laboratory tests (see, for example, Figure 4.15). Further research is, however, needed to extend the proposed model in order to incorporate the phenomenon of hydraulic hysteresis.

Chapter 5

Improvements to the FE code "Compass"

5.1 Introduction

This chapter describes the improvements and developments undertaken by the author on the finite element code "Compass" [43] (originally developed by Prof. H.R. Thomas and co-workers at the Cardiff University). The version of code "Compass" [43] used in this study is able to perform coupled flow-deformation analyses in unsaturated soils for bi-dimensional problems (plane-strain, axi-symmetric, plane-stress). In the code provided by the Cardiff University the constitutive model of Alonso, Gens and Josa [1] was implemented. An outline of the methodology of discretization and computational procedures adopted in the code is given in Section 5.3.

The main improvements and extension introduced in code "Compass" [43] by the author are summarized below.

1. ***Implementation of the new relationship for the variation of degree of saturation proposed in Chapter 4 (Equation 4.5).*** The new relationship represents the variation of degree of saturation in an elasto-plastic fashion, consistent with the rest of the stress-strain model. The aspects associated to the numerical implementation of this new relationship for degree of saturation are discussed in Section 5.4.3.

2. ***Correction of the equations of continuity of water and air implemented***

in the code. These equations were originally expressed in terms of absolute flux velocities, whereas in the modified version of the code the governing equations were implemented in terms of flux velocities relative to the soil skeleton. This is necessary because it is the relative flux velocities that are related to the gradient of the hydraulic head through Darcy's law. The equations of continuity of water and air expressed in terms of flux velocities relative to the soil skeleton are derived in Section 5.2. Issues associated with the numerical implementation of the modified forms of the equations of continuity of water and air are discussed in Section 5.4.4.

3. ***Modifications to the convergency algorithm for elasto-plastic load steps.*** The modifications involve two different aspects. Firstly, the original convergency algorithm was corrected by taking into account residual flux terms in the two equations of flow. These residual terms, neglected in the original version of the code, must be considered during the convergency process, analogous to residual forces in the equilibrium equation. Secondly, a new convergency criterion for the Alonso, Gens and Josa [1] stress-strain relationship was introduced, replacing the one present in the original version of the code. The reasons for these changes and the practices employed are explained in detail in Section 5.4.2.

4. ***Correction of the implementation of the plane-strain formulation for an elasto-plastic unsaturated soil.*** Details about this part of the work are given in Section 5.4.5.

5. ***Introduction of the optional mesh updating for analyses involving large displacements***, in order to take into account geometrical non-linearity.

6. ***Coding of an interface to the FEMGEN/FEMVIEW [66] commercial software*** for graphical pre- and post-processing of the data.

Item number 1 in the list above represents a significant improvement, that would benefit all finite element codes for coupled hydro-mechanical analyses in unsaturated soils. In the codes available to date the variation of degree of saturation is related to the net

stress state and suction (or only to suction) by a simple elastic relationship, known as a state surface, whose shortcomings were highlighted in Section 2.5.1. For example, in the original version of code "Compass" [43] the state surface expression of Lloret and Alonso [22] (Equation 2.41) is present. In other finite element codes for coupled thermo-hydro-mechanical analyses, other relationships are employed: "CODE_BRIGHT" [67], developed at Universitat Politecnica de Catalunya in Barcelona implements the soil-water characteristic curve of van Genuchten [48] whereas in code "HMTRA-DEF" [68], developed at Università di Padova in Padova a number of alternative "elastic" relationships for degree of saturation are available (e.g. Safai and Pinder [69], Brooks and Corey [70]).

Numerical simulations of notional laboratory tests were performed with two different versions of code "Compass": the original one implementing the state surface equation of Lloret and Alonso [22] and the modified one implementing the new relationship for degree of saturation (proposed in Chapter 4), with values of model parameters taken from Section 3.3 and Section 4.3, respectively. The results of these simulations, presented in Section 6.5, demonstrate that substantially different predictions (not only in terms of degree of saturation but also of displacement and suction) are obtained in the two cases.

Items number 2, 3, and 4 above refer to correction of faulty features in the original version of code "Compass". It is, however, likely that these are general issues that may be relevant also to other finite element codes. For all three points, simple numerical studies have been performed with both the original and the amended versions of code "Compass" in order to demonstrate the potential significance of such errors. The results of these numerical analyses are presented in Sections 6.2, 6.3 and 6.4.

Item number 5 relates to the introduction of the possibility to activate updating of the nodal coordinates during the analysis. The updating of the nodal coordinates is performed at the beginning of each time step, according to the displacements that occurred in preceding time steps. This option was included in the code for taking into account geometrical non-linearity in those cases where large displacements are predicted, however it does not represent a full large-strain formulation of the problem. In particular, this feature was considered necessary for the simulations of pressuremeter tests presented in

Chapter 7, where large values of displacement at the borehole wall were computed.

Item number 6 refers to the development of two pieces of code interfacing the input and output of code "Compass" to the FEMGEN/FEMVIEW [66] commercial package in order to achieve effective graphical pre- and post-processing of the data. The FEMGEN [66] pre-processor allows fast and easy input of data by enabling graphical definition of the mesh geometry and boundary conditions and the package outputs this information in the form of a text file. The interface developed reads this file and rewrites it in a form which, after minor manual editing, can be understood by code "Compass". Conversely, the post-processor interface creates a number of text files, containing numerical results from the analysis performed by code "Compass", which can be recognized by the FEMVIEW [66] post-processor and represented in graphical form (e.g. graphs, contour plots, deformed mesh plots, vector plots) to aid subsequent interpretation and analysis of numerical results. The results which can be displayed through the FEMVIEW post-processor for a selected number of time steps are: (a) displacements and pore pressures (water and air) at nodes, (b) suction at nodes, (c) extrapolated net stresses at nodes, (d) total and net stresses at Gauss points, (e) degree of saturation and specific volume at Gauss points, (f) stress invariants ($\overline{p}$ and q) at Gauss points, (g) averaged values of net stresses over each element.

5.2 Governing equations

The governing differential equation for the isothermal problem of coupled flow-deformation in unsaturated soils can be derived from considerations of static equilibrium, mass balance of water and mass balance of air.

The static equilibrium equation is:

$$\frac{\partial}{\partial x_j}\frac{d\overline{\sigma}_{ij}}{dt} + \frac{\partial}{\partial x_i}\frac{du_a}{dt} - \frac{db_i}{dt} = 0 \quad \text{with} \quad i,j = \{x,y,z\} \tag{5.1}$$

where $\overline{\sigma}_{ij}$ is the appropriate component of the net stress vector (compression positive), u_a is the pore air pressure, b_i is the appropriate component of the body force vector and x_i is the appropriate spatial co-ordinate.

The following part of this section relates to the formulation of the equations of continuity of water and air for the case where the liquid and gas flux velocities are considered

relative to the soil skeleton. This is the form in which the continuity equations should be presented if the flux velocities are to be subsequently combined with Darcy's law, which relates the flux velocity of the liquid or gas phase relative to the soil skeleton (rather than the absolute flux velocities) to the relevant potential gradient. In the original version of code "Compass" (Thomas and He [43], Thomas and He [71]), however, the continuity equations expressed in terms of absolute flux velocities were incorrectly combined with Darcy's law. Moreover such an error is apparently also present in other numerical formulations published in the literature (Nesnas and Pyrah [44], Gatmiri and Delage [72] and Gens, Vaunat and Ledesma [46]).

The incorrect combination of absolute flux velocities with Darcy's law can lead to two possible mistakes in the governing equations of flow. The first possible mistake applies equally to saturated or unsaturated conditions. This is often (sometimes inadvertantly) corrected by an additional compensating mistake (following the logic of Terzaghi [73]), as was the case in the original version of code "Compass". The second error relates to the distinction between Lagrangian and Eulerian temporal derivatives of degree of saturation and air density, and is only present for unsaturated conditions.

In deriving the governing equation for water transfer, the movement of water in the form of vapour has been neglected. The significance of the movement of water in the form of vapour is equally relevant as that of liquid water in cases where gradients of temperature occur in the soil domain (see Philip and de Vries [74]). For isothermal problems, the vapour contribution to the water transfer equation is significant only in very dry soils as, under these circumstance, the continuity of the liquid phase in the medium is minimal and liquid water is present mainly in the form of isolated lenses at the inter-particle contacts (see de Vries [75], Philip [76]). In this thesis isothermal problems are considered, with values of degree of saturation greater than the range where transfer of water in the form of vapour becomes significant in comparison with the movement of liquid water, and, therefore, it is admissible to neglect any transfer of water vapour.

In the derivation of the governing equation for air transfer, the presence of dissolved air in the liquid phase is initially disregarded in order to express the equation of air

continuity in a more concise form. Subsequently, the additional terms arising from the presence of dissolved air are introduced and a more general form of the air continuity equation accounting for the advective flux of dissolved air is given. This form of the air continuity equation is implemented in the code.

If water vapour and dissolved air are ignored, the continuity equations can be regarded either as mass balances of each single species, water, air and soil minerals, (a "compositional" approach, see for example Olivella, Carrera, Gens and Alonso [77], Panday and Corapcioglu [78]) or, as mass balances of each phase: liquid, gas and solid (see for example Lewis and Schrefler [79]). This is because when water vapour and dissolved air are ignored, each species now identifies a single phase: the liquid phase is composed only of water, the gas phase is composed only of dry air and the solid phase is made up only of soil minerals.

In order to derive the equations of continuity for water and air in terms of relative flux velocities, the mass balance of water or air is applied to an infinitesimal element of soil containing at each instant of time the same solid fraction (a Lagrangian approach). The volume dV of an element of soil containing at each instant of time the same solid fraction is given by:

$$dV = (1 + e)dV_s \tag{5.2}$$

where e is the void ratio, which may vary with time, and dV_s is the volume of solid fraction. dV_s is a constant if the soil particles are assumed incompressible. The volume of liquid water dV_w within such an element of soil at a generic time is given by:

$$dV_w = eS_r dV_s \tag{5.3}$$

where S_r is the degree of saturation.

The rate of change of liquid water volume within the element of soil containing the solid fraction dV_s is obtained by differentiating Equation 5.3 with respect to time. This gives:

$$\frac{\mathrm{D}(dV_w)}{\mathrm{D}t} = \left(S_r \frac{\mathrm{D}e}{\mathrm{D}t} + e \frac{\mathrm{D}S_r}{\mathrm{D}t} \right) dV_s \tag{5.4}$$

where the symbol $\mathrm{D} \bullet / \mathrm{D}t$ denotes a Lagrangian or material derivative with respect to time. The Lagrangian derivative of dV_w must be considered since the temporal derivative

is not calculated at a constant point in space but for a given element of soil associated to the same solid fraction. The Lagrangian derivatives in Equation 5.4 may, however, be rewritten in terms of Eulerian derivatives[1], using the general relation between Lagrangian and Eulerian derivatives (see, for example, Olivella, Carrera, Gens and Alonso [77]):

$$\frac{\mathrm{D}\bullet}{\mathrm{D}t} = \frac{d\bullet}{dt} + \frac{d\boldsymbol{u}_d}{dt}\nabla\bullet \tag{5.5}$$

where the symbol $d\bullet/dt$ denotes an Eulerian derivative with respect to time and $\boldsymbol{u}_d$ is the displacement vector for the soil skeleton.

Therefore, the right-hand side of Equation 5.4 can be converted from Lagrangian to Eulerian temporal derivatives by using Equations 5.5:

$$\frac{\mathrm{D}(dV_w)}{\mathrm{D}t} = \left(S_r\frac{de}{dt} + S_r\frac{d\boldsymbol{u}_d}{dt}\nabla e + e\frac{dS_r}{dt} + e\frac{d\boldsymbol{u}_d}{dt}\nabla S_r\right)dV_s. \tag{5.6}$$

If the water is assumed to be incompressible and the presence of water in the form of vapour is neglected, as explained above, the mass balance of the water requires that the rate of change of liquid water volume within the element of soil containing the solid fraction dV_s, given by Equation 5.6, must be equal to the net influx of liquid water through the element boundaries. This net influx is given by:

$$-\mathrm{div}\,\boldsymbol{v}_{wr}dV = -(1+e)\,\mathrm{div}\,\boldsymbol{v}_{wr}dV_s \tag{5.7}$$

where $\boldsymbol{v}_{wr}$ is the flux velocity of the liquid phase measured relative to the soil skeleton. The continuity equation for the water is therefore given based on Equations 5.6 and 5.7 as:

$$(1+e)\,\mathrm{div}\,\boldsymbol{v}_{wr} + S_r\frac{de}{dt} + S_r\frac{d\boldsymbol{u}_d}{dt}\nabla e + e\frac{dS_r}{dt} + e\frac{d\boldsymbol{u}_d}{dt}\nabla S_r = 0. \tag{5.8}$$

By considering the mass balance equation for the solid fraction within an infinitesimal element of space of the soil domain, it is shown in Appendix A (see Equation A.10) that:

[1]Eulerian and Lagrangian derivatives coincide if small displacements are assumed. However, a hypothesis of small displacements is different from the one of small strains assumed throughout this thesis, as large values of displacements can occur in circumstances where small strains are present. In this work the possibility of large displacements is explicitly contemplated and, therefore, a distinction is made between Eulerian and Lagrangian derivatives. In particular this possibility is considered in the light of the numerical simulations of pressuremeter tests presented in Chapter 7 where large values of displacements are calculated.

$$\frac{d\boldsymbol{u}_d}{dt}\boldsymbol{\nabla}e + \frac{de}{dt} + (1+e)\frac{d\epsilon_v}{dt} = 0. \tag{5.9}$$

Using Equation 5.9, it is possible to rewrite Equation 5.8 as:

$$\operatorname{div}\boldsymbol{v}_{wr} - S_r\frac{d\epsilon_v}{dt} + n\frac{dS_r}{dt} + n\frac{d\boldsymbol{u}_d}{dt}\boldsymbol{\nabla}S_r = 0 \tag{5.10}$$

where n is the porosity and $d\epsilon_v/dt$ is the volumetric strain rate (compression positive).

Following the same logic, the equation of air continuity, written in terms of the flux velocity of the gas phase relative to the soil skeleton, $\boldsymbol{v}_{ar}$ is:

$$\operatorname{div}\boldsymbol{v}_{ar} + \frac{\boldsymbol{v}_{ar}\boldsymbol{\nabla}\rho_a}{\rho_a} + (1-S_r)\left(\frac{n}{\rho_a}\left(\frac{d\rho_a}{dt} + \frac{d\boldsymbol{u}_d}{dt}\boldsymbol{\nabla}\rho_a\right) - \frac{d\epsilon_v}{dt}\right) - n\frac{dS_r}{dt} - n\frac{d\boldsymbol{u}_d}{dt}\boldsymbol{\nabla}S_r = 0 \tag{5.11}$$

where ρ_a is the air density (coinciding with the gas density due to the assumption that air is the only species present in the gas phase). Comparing Equation 5.11 with Equation 5.10, the additional terms in Equation 5.11 arise as a result of the air compressibility.

If the advective flux of the dissolved air has to be taken into account, the air continuity expression of Equation 5.11 is rewritten in the following form:

$$\operatorname{div}(\boldsymbol{v}_{ar} + H\boldsymbol{v}_{wr}) + \frac{(\boldsymbol{v}_{ar} + H\boldsymbol{v}_{wr})\boldsymbol{\nabla}\rho_a}{\rho_a} + (1-(1-H)S_r)\left(\frac{n}{\rho_a}\left(\frac{d\rho_a}{dt} + \frac{d\boldsymbol{u}_d}{dt}\boldsymbol{\nabla}\rho_a\right) - \frac{d\epsilon_v}{dt}\right) - n(1-H)\frac{dS_r}{dt} - n(1-H)\frac{d\boldsymbol{u}_d}{dt}\boldsymbol{\nabla}S_r = 0 \tag{5.12}$$

where H is Henry's coefficient of solubility. The terms involving $H\boldsymbol{v}_{wr}$ and the introduction of the factors $(1-H)$ additional to Equation 5.11 arise as a result of the advective flux of dissolved air in the liquid phase.

Extended versions of the water and air continuity expressions, which account for the presence of water vapour in the gas phase, are derived by means of a "compositional" approach by Olivella, Carrera, Gens and Alonso [77] (who also included the complication of a soluble salt component). These expressions reduce to Equations 5.10 and 5.12 for

the simplified conditions considered here. The same authors (see Olivella, Gens, Carrera and Alonso [80]), however, seem to neglect the terms corresponding to $n(d\boldsymbol{u}_d/dt)\nabla S_r$ in Equation 5.10 and to $-n(1-H)(d\boldsymbol{u}_d/dt)\nabla S_r$ and $(1-(1-H)S_r)(n/\rho_a)(d\boldsymbol{u}_d/dt)\nabla\rho_a$ in Equation 5.12 in the numerical implementation of the water and air continuity expressions within the finite element code "CODE_BRIGHT" [67].

Extended versions of the water and air continuity expressions are also derived by Lewis and Schrefler [79], by considering the balance of mass for each phase (they also consider exchange of species between phases due to the presence of water vapour in the gas phase and take into account the compressibility of liquid and solid phases, but on the other hand they neglect the presence of dissolved air in the liquid phase). The expressions presented by Lewis and Schrefler [79] reduce, for the simple problem considered here, to forms which differ from Equations 5.10 and 5.11. This is due to their assumption of small displacements of the solid phase, which means that the term $n(d\boldsymbol{u}_d/dt)\nabla S_r$ in Equation 5.10 is neglected; due to the same assumption the two terms $-n(d\boldsymbol{u}_d/dt)\nabla S_r$ and $(1-S_r)(n/\rho_a)(d\boldsymbol{u}_d/dt)\nabla\rho_a$ present in Equation 5.11 are also absent in their formulation. In deriving the final forms of the equations of water and air continuity, Lewis and Schrefler [79] also neglect, on the basis of the small displacements assumption, the terms containing ∇e in the intermediate forms of the equations of water, air and solid continuity, such as, for example, the term $S_r(d\boldsymbol{u}_d/dt)\nabla e$ appearing in the expression of water continuity given by Equation 5.8. As shown above, however, these terms are rigorously absent from the final form of the equations of water and air continuity as they disappear when the intermediate forms of the equations of water and air continuity are combined with the corresponding equation for the solid fraction. Therefore a less restrictive hypothesis than the one assumed by Lewis and Schrefler [79] can be postulated in order to eliminate all the gradient terms from the equations of water and air continuity, as it is sufficient to hypothesise that only the terms containing the gradient of degree of saturation and air density are negligible.

Equations 5.10 and 5.12 are the water and air continuity equations expressed in terms of relative flux velocities of the liquid and gas phases with respect to the soil skeleton, $\boldsymbol{v}_{wr}$

and $\boldsymbol{v}_{ar}$. Alternatively, the continuity equations can be derived in terms of the absolute flux velocities, $\boldsymbol{v}_{wa}$ and $\boldsymbol{v}_{aa}$, giving:

$$\text{div } \boldsymbol{v}_{wa} + S_r \frac{dn}{dt} + n \frac{dS_r}{dt} = 0 \tag{5.13}$$

$$\text{div } (\boldsymbol{v}_{aa} + H\boldsymbol{v}_{wa}) + \frac{(\boldsymbol{v}_{aa} + H\boldsymbol{v}_{wa})\nabla \rho_a}{\rho_a} + (1-(1-H)S_r)\left(\frac{n}{\rho_a}\frac{d\rho_a}{dt} + \frac{dn}{dt}\right) - n(1-H)\frac{dS_r}{dt} = 0. \tag{5.14}$$

In the original version of code "Compass", as in many examples in the literature, Equations 5.13 and 5.14 were incorrectly combined with Darcy's law, whereas Darcy's law actually provides expressions for the relative flux velocities of the liquid and gas phases $\boldsymbol{v}_{wr}$ and $\boldsymbol{v}_{ar}$, and should therefore be combined with Equations 5.10 and 5.12. This follows an historical pattern in modelling of saturated problems, where Biot [81] correctly presented the saturated version of Equation 5.10, whereas Terzaghi [73] incorrectly combined the saturated version of Equation 5.13 with Darcy's law.

Comparison of Equations 5.13 and 5.14 with Equations 5.10 and 5.12 shows that the continuity equations expressed in terms of absolute flux velocities differ from the equations expressed in terms of relative flux velocities in two respects:

1. the term $-S_r(d\epsilon_v/dt)$ in Equation 5.10 is replaced by $S_r(dn/dt)$ in Equation 5.13; similarly the term $-(1-(1-H)S_r)(d\epsilon_v/dt)$ in Equation 5.12 is replaced by $(1-(1-H)S_r)(dn/dt)$ in Equation 5.14;

2. the term $n(d\boldsymbol{u}_d/dt)\nabla S_r$ in Equation 5.10 is absent from Equation 5.13; similarly the terms $-n(1-H)(d\boldsymbol{u}_d/dt)\nabla S_r$ and $(1-(1-H)S_r)(n/\rho_a)(d\boldsymbol{u}_d/dt)\nabla \rho_a$ in Equation 5.12 are absent from Equation 5.14.

In the original version of code "Compass" (and probably in many other numerical codes), the first of these errors involved in using Equations 5.13 and 5.14 was subsequently corrected by wrongly assuming (without explicitly stating in the relevant documentation) that $dn/dt = -d\epsilon_v/dt$, whereas in fact $dn/dt = -(1-n)(d\epsilon_v/dt) - (d\boldsymbol{u}_d/dt)\nabla n$ (see

Equation A.9 in Appendix A). This follows the incorrect logic presented by Terzaghi [73]. For saturated conditions, this would result in correct formulation of the governing flow equation. For unsaturated conditions, however, the formulation is still incorrect, because of the absence of the term $n(d\boldsymbol{u}_d/dt)\nabla S_r$ in Equation 5.13 and of the terms $-n(1-H)(d\boldsymbol{u}_d/dt)\nabla S_r$ and $(1-(1-H)S_r)(n/\rho_a)(d\boldsymbol{u}/dt)\nabla\rho_a$ in Equation 5.14.

In this work the forms of the continuity equations expressed in terms of flux velocities relative to the soil skeleton (Equations 5.10 and 5.12), have been implemented in code "Compass". Details of the numerical implementation of the additional terms described in item number 2 above, are given in Section 5.4.4. A simple numerical analysis is also presented in Section 6.2 in order to demonstrate the potential significance of the errors described.

5.3 Overview of code "Compass"

In this section an overview of the methodology of discretization and computational procedure adopted in code "Compass" is given and the original contributions of the author's work will be highlighted. Some of the aspects discussed here refer to the code "Compass" in its original version and, therefore, do not represent an innovative aspect. This discussion is, however, useful in order to better understand the issues presented in the subsequent sections.

5.3.1 Discretized form of the governing equations

The governing differential equations (Equations 5.1, 5.10 and 5.12) presented in Section 5.2 have to be expressed, in order to be solved numerically, in terms of field variables whose variation with space and time, given the boundary conditions, has to be determined by integration. The chosen field variables are the displacement vector, $\boldsymbol{u}_d$, the pore water pressure (scalar), u_w and the pore air pressure (scalar), u_a. The set of governing equations expressed in terms of field variables are presented below for the case of an elasto-plastic stress-strain relationship (the Alonso, Gens and Josa [1] model was present in the original version of "Compass") and for the case of a unique relationship between degree of satura-

tion, net stresses and suction (the state surface expression of Lloret and Alonso [22] given by Equation 2.41 was present in the original version of "Compass") :

$$\frac{\partial}{\partial x_j}\frac{d\overline{\sigma}_{ij}}{dt}+\frac{\partial}{\partial x_i}\frac{du_a}{dt}-\frac{db_i}{dt}=0 \quad \text{with } i,j=\{x,y,z\} \tag{5.1bis}$$

$$\operatorname{div} \boldsymbol{v}_{wr} + (S_r \boldsymbol{m}^T \mathbf{B} + n\boldsymbol{\nabla} S_r)\frac{d\boldsymbol{u}_d}{dt} + n g_2 \frac{du_a}{dt} - n g_2 \frac{du_w}{dt} + n\,\boldsymbol{g}_1{}^T \frac{d\overline{\boldsymbol{\sigma}}}{dt} = 0 \tag{5.15}$$

$$\begin{aligned}\operatorname{div}(\boldsymbol{v}_{ar} + H\boldsymbol{v}_{wr}) + \frac{(\boldsymbol{v}_{ar} + H\boldsymbol{v}_{wr})\boldsymbol{\nabla}\rho_a}{\rho_a} + ((1-(1-H)S_r)(\frac{n}{\rho_a}\boldsymbol{\nabla}\rho_a - \boldsymbol{m}^T\mathbf{B}) - \\ n(1-H)\boldsymbol{\nabla}S_r)\frac{d\boldsymbol{u}_d}{dt} + ((1-(1-H)S_r)\frac{n}{\rho_a}\beta - n(1-H)g_2)\frac{du_a}{dt} + \\ n(1-H)g_2\frac{du_w}{dt} - n(1-H)\boldsymbol{g}_1{}^T\frac{d\overline{\boldsymbol{\sigma}}}{dt} = 0\end{aligned} \tag{5.16}$$

where $\mathbf{B}$ is the differential operator of strains (defined using the convention of compression positive), $\overline{\boldsymbol{\sigma}}$ is the net stress vector, β is the constant relating air density to air pressure (from the gas law), the vector $\boldsymbol{m}$ is given by $(1\ 1\ 1\ 0\ 0\ 0)^T$, and $g_2 = \partial S_r/\partial s$, $\boldsymbol{g}_1 = \partial S_r/\partial\overline{\boldsymbol{\sigma}}$ are, respectively, the derivatives of the state surface expression for degree of saturation with respect to suction and the net stress vector. The equilibrium condition given by Equation 5.1, is expressed in its general three-dimensional form which reduces according to the type of bi-dimensional analysis (plane-strain, axi-symmetric, plane-stress) performed. Similarly the differential operator of strains, $\mathbf{B}$ differs according to the type of bi-dimensional analysis and the definitions of $\mathbf{B}$ for the plane-strain and axi-symmetric regimes are given in Section 5.4.5.

The net stress rate $d\overline{\boldsymbol{\sigma}}/dt$ for an elasto-plastic constitutive model may be expressed in terms of the rates of the field variables and the plastic strain rate $d\boldsymbol{\epsilon}^p/dt$ by using the constitutive relationship:

$$\frac{d\overline{\boldsymbol{\sigma}}}{dt} = \mathbf{D}\left(\mathbf{B}\frac{d\boldsymbol{u}_d}{dt} - \frac{1}{3}A_s\,\boldsymbol{m}^T\left(\frac{du_a}{dt} - \frac{du_w}{dt}\right) - \frac{d\boldsymbol{\epsilon}^p}{dt}\right) \tag{5.17}$$

where $\mathbf{D}$ is the elastic stiffness matrix and A_s is the elastic volumetric compressibility of the soil due to a change in suction. The terms containing the relative flux velocities, $\boldsymbol{v}_{wr}$

and v_{ar}, in Equations 5.15 and 5.16 may be expressed in terms of the field variables pore water pressure u_w and pore air pressure u_a by using the generalized Darcy's law for the liquid and gas flows. In the same way the terms containing the air density, ρ_a, can be related to the pore air pressure field variable, u_a by means of the gas law for the isothermal case.

According to the finite element method, the system of governing differential equations above may be rewritten, using a shape function approximation for the variation of the field variables. In this way the system of governing equations above are expressed in terms of the nodal unknowns of the field variables. These vectors of nodal unknowns are: $\hat{\boldsymbol{u}}_d$, the vector of nodal displacement unknowns, $\hat{\boldsymbol{u}}_a$, the vector of nodal pore air pressure unknowns and $\hat{\boldsymbol{u}}_w$, the vector of nodal pore water pressure unknowns. This approximated system of governing differential equations is then transformed into an algebraic system of equations in the nodal unknowns of the field variables by using the Galerkin weighted residual approach for discretization with respect to space and a finite difference approximation for discretization with respect to time. The details of the discretization procedure with respect to space are not given here and the interested reader can refer to the work of Ramesh [82]. The final discretized form of the system of governing equations is given by:

$$\boldsymbol{\mathcal{K}} \begin{bmatrix} \hat{\boldsymbol{u}}_w \\ \hat{\boldsymbol{u}}_a \\ \hat{\boldsymbol{u}}_d \end{bmatrix} + \boldsymbol{\mathcal{C}} \begin{bmatrix} \frac{\Delta \hat{\boldsymbol{u}}_w}{\Delta t} \\ \frac{\Delta \hat{\boldsymbol{u}}_a}{\Delta t} \\ \frac{\Delta \hat{\boldsymbol{u}}_d}{\Delta t} \end{bmatrix} = \boldsymbol{\mathcal{T}} + \boldsymbol{\mathcal{R}} \tag{5.18}$$

where $\boldsymbol{\mathcal{K}}$ and $\boldsymbol{\mathcal{C}}$ are, respectively, the so-called stiffness matrix and mass matrix, the vector $\boldsymbol{\mathcal{T}}$ is the flux vector and the vector $\boldsymbol{\mathcal{R}}$ is the residual vector (due to the assumption of an elasto-plastic model for the soil). The symbol $\Delta \bullet / \Delta t$ denotes a finite difference approximation for the temporal derivative of the vectors of nodal unknowns.

The matrices $\boldsymbol{\mathcal{K}}$, $\boldsymbol{\mathcal{C}}$ and the vectors $\boldsymbol{\mathcal{T}}$, $\boldsymbol{\mathcal{R}}$ are defined as:

$$\boldsymbol{\mathcal{K}} = \begin{bmatrix} \boldsymbol{\mathcal{K}}_f \\ \hline \boldsymbol{\mathcal{K}}_u \end{bmatrix} = \left[\begin{array}{ccc} \mathbf{K}_{ww} & 0 & 0 \\ \mathbf{K}_{aw} & \mathbf{K}_{aa} & 0 \\ \hline 0 & 0 & 0 \end{array}\right] \tag{5.19}$$

$$\mathcal{C} = \begin{bmatrix} \mathcal{C}_f \\ \hline \mathcal{C}_u \end{bmatrix} = \left[\begin{array}{ccc} \mathbf{C}_{ww} & \mathbf{C}_{wa} & \mathbf{C}_{wu} \\ \mathbf{C}_{aw} & \mathbf{C}_{aa} & \mathbf{C}_{au} \\ \hline \mathbf{C}_{uw} & \mathbf{C}_{ua} & \mathbf{C}_{uu} \end{array}\right] \tag{5.20}$$

$$\mathcal{T} = \left[\begin{array}{c|c} \mathcal{T}_f & \mathcal{T}_u \end{array} \right]^T = \left[\begin{array}{cc|c} t_w & t_a & t_u \end{array} \right]^T \tag{5.21}$$

$$\mathcal{R} = \left[\begin{array}{c|c} \mathcal{R}_f & \mathcal{R}_u \end{array} \right]^T = \left[\begin{array}{cc|c} \psi_w & \psi_a & \phi_u \end{array} \right]^T \tag{5.22}$$

where the sub-matrices and sub-vectors arising from the flux equations have been distinguished from the ones relating to the equilibrium equation. The first subscript of the terms appearing on the right hand side of Equations 5.19, 5.20, 5.21 and 5.22 indicates the type of governing equation which is referred to: w for the equation of water continuity, a for the equation of air continuity and u for the equation of equilibrium. The second subscript, when present, indicates to which type of unknown the term is applied to: w for the vector of nodal pore water pressure unknowns, a for the vector of pore air pressure unknowns and u for the vector of nodal displacement unknowns. The symbology adopted follows approximately the one employed by Ramesh [82] for the original version of code "Compass". There are, however, some differences between the definitions of these terms presented by Ramesh [82] and implemented in the original version of code "Compass", and the definitions proposed in this work and implemented in the amended version of the code. These differences are explained below.

1. The terms due to presence of water vapour within the gas phase are neglected in this work. This is an acceptable approximation for the problems considered here as explained in Section 5.2.

2. The finite difference approximation for the time derivatives of the nodal unknowns in the discretized equations of water and air flows (see Equation 5.18) is accomplished in this work by employing a second-order fully implicit scheme. In the original version of code "Compass" the temporal derivatives of nodal unknowns of pore air

pressure and pore water pressure were instead discretized by using a first-order fully implicit approximation. The reason for moving to the second-order scheme and the discretized form for these temporal derivatives are discussed in Section 5.4.1.

3. The residual flux terms $\boldsymbol{\psi}_w$ and $\boldsymbol{\psi}_a$, which were absent in the original version of code "Compass", are considered here (see Equation 5.22). When an elasto-plastic constitutive model for the soil is employed in conjunction with a state surface expression for degree of saturation introducing a dependency on the net stress state (as the state surface expression of Equation 2.41 proposed by Lloret and Alonso [22] and implemented in the original version of "Compass"), the residual flux terms $\boldsymbol{\psi}_w$ and $\boldsymbol{\psi}_a$ must be included in the discretized form of the two equations of flow, analogous to the residual force term $\boldsymbol{\phi}_u$ (Equation 5.22) in the equilibrium equation. The presence of residual flux terms should also be considered if variation of degree of saturation with net stress and suction is represented by an elasto-plastic relationship, such as the one presented in Chapter 4. The reasons for the presence of residual flux terms, their definitions (for both cases of state surface and elasto-plastic relationship for degree of saturation) and relevant numerical implementation will be further discussed in Sections 5.4.2 and 5.4.3.

4. The terms $\mathbf{C}_{wu}$ and $\mathbf{C}_{au}$ have been modified in this work. The term $\mathbf{C}_{wu}$ considered here takes into account the presence of the discretized form of the term $n(d\boldsymbol{u}_d/dt)\nabla S_r$ in Equation 5.10, which was neglected in the original version of code "Compass". Analogously the definition of $\mathbf{C}_{au}$ considered in this work includes the discretized form of the terms $-n(1-H)(d\boldsymbol{u}_d/dt)\nabla S_r$ and $(1-(1-H)S_r)(n/\rho_a)(d\boldsymbol{u}_d/dt)\nabla\rho_a$ in Equation 5.12. The discretized forms of the new terms introduced in this work are presented in Section 5.4.4.

Due to the choice of a fully implicit scheme for the discretization with respect to time in the time derivatives in the equations of water and air flows, the algebraic system given by Equation 5.18 is a non linear system with the coefficient matrices, $\boldsymbol{\mathcal{K}}_f$, $\boldsymbol{\mathcal{C}}_f$ and the residual flux terms vector, $\boldsymbol{\mathcal{R}}_f$ depending on the nodal unknowns. The flux vector, $\boldsymbol{\mathcal{T}}$,

instead, is constant and depends only on the boundary conditions applied. Therefore, the system has to be solved using an iterative technique and, in the code "Compass", a fully implicit Picard iteration scheme (see Celia, Bouloutas and Zarba [83]) is employed. This involves sequential estimation of the nodal unknowns, $\hat{\boldsymbol{u}}_d$, $\hat{\boldsymbol{u}}_a$ and $\hat{\boldsymbol{u}}_w$ from the system of Equation 5.18. The system is solved as a linear system, using the latest estimate for the coefficient matrices $\boldsymbol{\mathcal{K}}_f$, $\boldsymbol{\mathcal{C}}_f$ and the residual terms vector $\boldsymbol{\mathcal{R}}_f$. The new estimate of the nodal unknowns is used to calculate $\boldsymbol{\mathcal{K}}_f$, $\boldsymbol{\mathcal{C}}_f$ and $\boldsymbol{\mathcal{R}}_f$ in the next iteration.

An iterative convergency algorithm at Gauss point level must also be employed for the integration of the elasto-plastic stress strain relationship adopted in "Compass" (i.e. the Alonso, Gens and Josa [1] model). Each iteration of this convergency algorithm involves the estimation of the increment of plastic strain rate in a given time step. The calculated increment of plastic strain rate is used to compute the residual terms of vector, $\boldsymbol{\mathcal{R}}$ (Equation 5.22) which are applied to the system of algebraic equations given by Equation 5.18 in the next iteration. The stress-strain convergency algorithm adopted in code "Compass" is discussed further in the next section.

5.3.2 Visco-plastic stress-strain convergency algorithm

The convergency algorithm at Gauss point level used within "Compass" for the elasto-plastic stress-strain relationship of Alonso, Gens and Josa [1] simulates an artificial visco-plastic process which takes place during a pseudo-time interval until the stress state is converged back onto the yield surface. In the generic l^{th} iteration of the generic k^{th} time step, the algebraic system of Equation 5.18 is solved. The residual term vector $\boldsymbol{\mathcal{R}}$ of Equation 5.22 is composed of the residual terms computed in the previous iteration. The solution of the system of Equation 5.18 gives an estimate of the increment of the nodal unknowns vectors with respect to the previous iteration, $\delta(\Delta\hat{\boldsymbol{u}}_d)^{k,l}$, $\delta(\Delta\hat{\boldsymbol{u}}_a)^{k,l}$ and $\delta(\Delta\hat{\boldsymbol{u}}_w)^{k,l}$ defined as:

$$\delta(\Delta\hat{\boldsymbol{u}}_d)^{k,l} = \hat{\boldsymbol{u}}_d^{k,l} - \hat{\boldsymbol{u}}_d^{k,l-1}, \quad \delta(\Delta\hat{\boldsymbol{u}}_a)^{k,l} = \hat{\boldsymbol{u}}_a^{k,l} - \hat{\boldsymbol{u}}_a^{k,l-1}, \quad \delta(\Delta\hat{\boldsymbol{u}}_w)^{k,l} = \hat{\boldsymbol{u}}_w^{k,l} - \hat{\boldsymbol{u}}_w^{k,l-1}. \quad (5.23)$$

From the calculated values of the increments of nodal unknowns a "trial" net stress rate vector is calculated as:

$$\frac{\delta\left(\Delta\overline{\sigma}\right)^{k,l}}{\Delta t}_{trial} = \mathbf{D}\left(\hat{\mathbf{B}}\frac{\delta\left(\Delta\hat{\boldsymbol{u}}_d\right)^{k,l}}{\Delta t} - \frac{1}{3}A_s\,\boldsymbol{m}^T\mathbf{N}\left(\frac{\delta\left(\Delta\hat{\boldsymbol{u}}_a\right)^{k,l}}{\Delta t} - \frac{\delta\left(\Delta\hat{\boldsymbol{u}}_w\right)^{k,l}}{\Delta t}\right)\right) \tag{5.24}$$

where $\mathbf{N}$ is the shape function vector, $\hat{\mathbf{B}}$ is the strain matrix (obtained by applying the differential operator of strain $\mathbf{B}$ to the shape function vector, $\mathbf{N}$). The term "rate" used for the definition of Equation 5.24 has no physical meaning and it simply indicates a variation of the stress state during the convergency algorithm. From Equation 5.24 the "trial" net stress vector is calculated as:

$$\overline{\boldsymbol{\sigma}}^{k,l}_{trial} = \overline{\boldsymbol{\sigma}}^{k,l-1}_{corrected} + \frac{\delta\left(\Delta\overline{\sigma}\right)^{k,l}}{\Delta t}_{trial}\Delta t \tag{5.25}$$

where $\overline{\boldsymbol{\sigma}}^{k,l-1}_{corrected}$ indicates the net stress vector at the end of the previous iteration (the meaning of the subscript "corrected" will be explained later). The computed "trial" net stress vector in order to be acceptable must comply with the yield criterion expressed by the analytical condition $\mathcal{F} \leq 0$ within a given tolerance.
Therefore, when

$\mathcal{F}(\overline{\boldsymbol{\sigma}}^{k,l}_{trial}, s^{k,l}_{trial}, \overline{p}_o^{*k,l-1}) \leq 0 \rightarrow$ "trial" stress state is compatible with yield criterion

$\mathcal{F}(\overline{\boldsymbol{\sigma}}^{k,l}_{trial}, s^{k,l}_{trial}, \overline{p}_o^{*k,l-1}) > 0 \rightarrow$ "trial" stress state is incompatible with yield criterion

where $\mathcal{F}(\overline{\boldsymbol{\sigma}}^{k,l}_{trial}, s^{k,l}_{trial}, \overline{p}_o^{*k,l-1})$ is the yield function of the Alonso, Gens and Josa [1] (see Section 2.4) computed for the "trial " net stress state $\overline{\boldsymbol{\sigma}}^{k,l}_{trial}$, for the "trial" value of suction $s^{k,l}_{trial}$ and for the value of the hardening parameter at the end of the previous iteration $\overline{p}_o^{*k,l-1}$. The tolerance assumed for the compatibility of the stress state with the yield criterion is explained in Section 5.4.2. If the "trial" stress state is compatible with the yield criterion, this is assumed as the stress state at the end of the time step and no further procedures are needed.

If the "trial" net stress state lies outside the yield locus, an iterative routine is needed to converge it back to the yield locus. An artificial visco-plastic strain rate vector, $(d\boldsymbol{\epsilon}^{vp}/dt)^{k,l}$

is calculated as:

$$\frac{d\boldsymbol{\epsilon}^{vp\,k,l}}{dt} = \gamma \left\langle \Phi(\mathcal{F}) \right\rangle \frac{\partial \mathcal{Q}^{k,l}}{\partial \overline{\boldsymbol{\sigma}}} (\overline{\boldsymbol{\sigma}}^{k,l}_{trial}, s^{k,l}_{trial}, \overline{p}^{*k,l-1}_{o}) \tag{5.26}$$

where γ is a fluidity parameter controlling the plastic flow rate (an input parameter for the code), $\langle \bullet \rangle$ is the Macaulay operator, Φ is a positive increasing function (see Owen and Hinton [84]) and $\mathcal{Q}$ is the plastic potential for the Alonso, Gens and Josa [1] model (Equation 2.35). The flow vector, $(\partial \mathcal{Q}/\partial \overline{\boldsymbol{\sigma}})^{k,l}$ in Equation 5.26 is calculated at the "trial" stress state. On the basis of the artificial visco-plastic strain rate vector, $(d\boldsymbol{\epsilon}^{vp}/dt)^{k,l}$ given by Equation 5.26 a "corrected" net stress rate vector can be computed as:

$$\frac{\delta \left(\Delta \overline{\boldsymbol{\sigma}}\right)^{k,l}}{\Delta t}_{corrected} = \frac{\delta \left(\Delta \overline{\boldsymbol{\sigma}}\right)^{k,l}}{\Delta t}_{trial} - \gamma \left\langle \Phi(\mathcal{F}) \right\rangle \mathbf{D} \frac{\partial \mathcal{Q}^{k,l}}{\partial \overline{\boldsymbol{\sigma}}}. \tag{5.27}$$

From this the "corrected" net stress vector is calculated as:

$$\overline{\boldsymbol{\sigma}}^{k,l}_{corrected} = \overline{\boldsymbol{\sigma}}^{k,l-1}_{corrected} + \frac{\delta \left(\Delta \overline{\boldsymbol{\sigma}}\right)^{k,l}}{\Delta t}_{corrected} \Delta t. \tag{5.28}$$

The increment of plastic volumetric strain, $\Delta \epsilon_v^{p\,k,l}$ during the current iteration is given by:

$$\delta \left(\Delta \epsilon_v^p\right)^{k,l} = \boldsymbol{m}^T \frac{d\boldsymbol{\epsilon}^{vp\,k,l}}{dt} \Delta t. \tag{5.29}$$

This increment of plastic volumetric strain, according to the Alonso, Gens and Josa [1] model, is related to a change of the hardening parameter $\overline{p}^*_o$ (see Equation 2.27). Therefore the updated value of the hardening parameter is given by:

$$\overline{p}^{*k,l}_{o} = \overline{p}^{*k,l-1}_{o} \exp \frac{v^{k,l-1}\, \delta \left(\Delta \epsilon_v^p\right)^{k,l}}{(\lambda(0) - \kappa)} \tag{5.30}$$

where $v^{k,l-1}$ is the specific volume at the end of the previous iteration and $\lambda(0)$ and κ are parameters in the Alonso, Gens and Josa [1] model (see Section 2.4). While the "trial" net stress given by Equation 5.25 satisfied the equilibrium equation, the "corrected" one given by Equation 5.28 will not fulfill the equilibrium condition any more, due to the occurrence of plastic strain. This means that the vector of the rate of internal forces, $\boldsymbol{\iota}^{k,l}$ is not equal to the vector of the rate of external forces, $\boldsymbol{t}^k_u$ (see Equation 5.21). The vector

$\iota^{k,l}$ is calculated by integration of the product of the transpose of the strain matrix, $\hat{\mathbf{B}}^T$ and the total stress rate vector over the spatial domain. The total stress rate vector is given by:

$$\frac{\Delta\boldsymbol{\sigma}^{k,l}}{\Delta t} = \frac{\overline{\boldsymbol{\sigma}}^{k,l}_{corrected} - \overline{\boldsymbol{\sigma}}^{k,0}}{\Delta t} + \frac{\hat{\boldsymbol{u}}_a^{k,l} - \hat{\boldsymbol{u}}_a^{k,0}}{\Delta t} \tag{5.31}$$

where the superscripts $(k, 0)$ indicate that the value considered is computed at the beginning of the k^{th} time step. The term "rate" for the definition above has this time a physical meaning (i.e. the variation of the total stress state over an interval of time), unlike the cases of Equations 5.24 and 5.27 where the term "rate" was used simply to indicate a variation of the stress state during the convergency algorithm. The residual force term, ${\boldsymbol{\phi}_u}^{k,l}$, defined in Equation 5.22 is then calculated as:

$$\boldsymbol{\phi}_u^{k,l} = \boldsymbol{t}_u^k - \iota^{k,l}. \tag{5.32}$$

This residual force term is then applied in the next iteration to the equation of equilibrium. The vector of rate of external forces, $\boldsymbol{t}_u^k$ defined in Equation 5.21 is, instead, applied to the equation of equilibrium only in the first iteration of each time step and is considered equal to the null vector in the subsequent iterations. The occurence of plastic strains, in the generic l^{th} iteration of the generic k^{th} time step, and the consequent evaluation of the "corrected" net stress state given in Equation 5.28, means that the continuity conditions for water and air are also not satisfied any more. This is true for either a state surface expression for S_r involving dependency on the net stress state (such as the one proposed by Lloret and Alonso [22]) or the new form of relationship for S_r described in Chapter 4. Consequently, residual flux terms, $\boldsymbol{\psi}_a$ and $\boldsymbol{\psi}_w$, must be included in the water and air flow equations as well as the residual force term in the equilibrium equation. A detailed description of the reasons for these residual flux terms together with their definitions are given in Sections 5.4.2 and 5.4.3, for the cases of the state surface of S_r by Lloret and Alonso [22] and the new relationship for S_r presented in Chapter 4, respectively.

Convergence is achieved at the l^{th} iteration of the k^{th} time step if the following criteria are satisfied:

1. The "trial" stress state, given by the "trial" net stress vector $\overline{\sigma}^{k,l}_{trial}$ and the "trial" suction, $s^{k,l}_{trial}$ lies within a "tolerance zone" outside the yield locus. This criterion is one of the modifications to the convergency algorithm of code "Compass" performed by the author and it is discussed further in Section 5.4.2.

2. The equilibrium equation is satisfied ($\boldsymbol{\iota}^{k,l} = \boldsymbol{t}^{k}_{u}$) within a given tolerance. This means that at each node the vectors of rate of internal forces, $\boldsymbol{\iota}^{k,l}$ and of external forces, $\boldsymbol{t}^{k}_{u}$ must satisfy the following condition:

$$|t^{k}_{i,j} - \iota^{k,l}_{i,j}| \leq \tau_1 |t^{k}_{i,j}| \tag{5.33}$$

   where $i = \{x, y\}$ denotes the x and y components of the nodal force rate and j is the node number. The tolerance factor, τ_1 is assumed equal to 10^{-4}.

3. Each nodal unknown has to satisfy the condition:

$$|\hat{u}^{k,l}_{i,j} - \hat{u}^{k,l-1}_{i,j}| \leq \tau_2 |\Delta\hat{u}^{k,l-1}_{i,j}| \tag{5.34}$$

   where $i = \{w, a, x, y\}$ denotes the type of unknown (the subscripts x and y indicate the x and y components of displacement) and j is the node number. The tolerance factor, τ_2 is assumed equal to 10^{-3}

On the basis of the numerical analyses performed in this work it was found that the fluidity parameter γ, introduced in Equation 5.26, has a great influence on the stability of the convergency algorithm and is more important than the choice of the number of increments during plastic loading. It is worth noting that this fluidity parameter does not have any physical meaning but is just a numerical parameter which affects the iterative process for convergency. In particular, it controls the magnitude of both the "correction" of the "trial" net stress state and of the hardening of the yield locus which take place in each iteration. Smaller values of fluidity parameter would tend to result in a requirement for a greater number of iterations but would give a more stable convergency process. It is believed that the cause of instability when using a high value of fluidity parameter is the problem known as "numerical unloading". This happens when, during the convergency

process, a Gauss point, which was deforming plastically, becomes elastic again due to a redistribution of stresses in the surrounding region and, therefore, accumulates spurious plastic strains. Numerical unloading, which takes place in the so-called path dependent state determination algorithms (such as the visco-plastic algorithm presented above), can cause deterioration of the solution with oscillations and even divergence (see Marques [85]). This problem is avoided by choosing a small value of the fluidity parameter, γ, because the increased number of iterations allows for a higher redistribution of stresses before convergency is achieved.

5.4 Modifications to code "Compass"

In the previous sections the modifications to the original version of code "Compass" performed in this work have been outlined and the theoretcal background related to the changes in the formulation of the continuity equations of water and air has been covered. This section provides a discussion of further issues relating to the modifications performed and to the numerical aspects of these changes.

5.4.1 Temporal discretization and resulting algebraic system of equations

In Section 5.3.1 the discretized form of the system of governing equations implemented in code "Compass" for a flow-deformation problem in unsaturated soils was described. For the generic l^{th} iteration of the generic k^{th} time step, the approximation for the temporal derivatives of nodal unknowns in the discretized continuity equations of water and air flows (Equation 5.18) is achieved in this work through a second-order backward finite difference scheme, given by:

$$\frac{\Delta \hat{\boldsymbol{u}}_j}{\Delta t}^{k,l} = \frac{\hat{\boldsymbol{u}}_j^{k,l} - \frac{4}{3}\hat{\boldsymbol{u}}_j^{k-1} + \frac{1}{3}\hat{\boldsymbol{u}}_j^{k-2}}{\frac{2}{3}\Delta t} \quad \text{with} \quad j = \{a, w, d\}. \tag{5.35}$$

This represents a change to the original version of the code where a first order backward approximation scheme was implemented, having the form:

$$\frac{\Delta \hat{\boldsymbol{u}}_j}{\Delta t}^{k,l} = \frac{\hat{\boldsymbol{u}}_j^{k,l} - \hat{\boldsymbol{u}}_j^{k-1}}{\Delta t} \quad \text{with} \quad j = \{a, w, d\}. \tag{5.36}$$

The reason for this change is explained later in this section. For the discretized form of the equilibrium equation (Equation 5.18) the approximation for the increment (denoted with the symbol δ) of temporal derivatives of nodal unknowns in the generic l^{th} iteration of the generic k^{th} time step, is accomplished through the following first order forward scheme, which is the same scheme originally implemented in code "Compass":

$$\frac{\delta\left(\Delta \hat{\boldsymbol{u}}_j\right)^{k,l}}{\Delta t} = \frac{\hat{\boldsymbol{u}}_j^{k,l} - \hat{\boldsymbol{u}}_j^{k,l-1}}{\Delta t} \quad \text{with} \quad j = \{a, w, d\}. \tag{5.37}$$

Therefore, taking into account the notation introduced in Equations 5.19, 5.20, 5.21 and 5.22, the following algebraic system, to be solved in the generic l^{th} iteration of the generic k^{th} time step, is obtained:

$$\begin{aligned}
&\boldsymbol{\mathcal{K}}_f{}^{k,l-1} \begin{bmatrix} \hat{\boldsymbol{u}}_w^{k,l} \\ \hat{\boldsymbol{u}}_a^{k,l} \\ \hat{\boldsymbol{u}}_d^{k,l} \end{bmatrix} + \boldsymbol{\mathcal{C}}_f{}^{k,l-1} \begin{bmatrix} \frac{\Delta \hat{\boldsymbol{u}}_w}{\Delta t}^{k,l} \\ \frac{\Delta \hat{\boldsymbol{u}}_a}{\Delta t}^{k,l} \\ \frac{\Delta \hat{\boldsymbol{u}}_d}{\Delta t}^{k,l} \end{bmatrix} = \boldsymbol{\mathcal{T}}_f{}^{k} + \boldsymbol{\mathcal{R}}_f{}^{k,l-1} \\
&\boldsymbol{\mathcal{K}}_u{}^{k,l-1} \begin{bmatrix} \hat{\boldsymbol{u}}_w^{k,l} \\ \hat{\boldsymbol{u}}_a^{k,l} \\ \hat{\boldsymbol{u}}_d^{k,l} \end{bmatrix} + \boldsymbol{\mathcal{C}}_u{}^{k,l-1} \begin{bmatrix} \frac{\delta\left(\Delta \hat{\boldsymbol{u}}_w\right)^{k,l}}{\Delta t} \\ \frac{\delta\left(\Delta \hat{\boldsymbol{u}}_a\right)^{k,l}}{\Delta t} \\ \frac{\delta\left(\Delta \hat{\boldsymbol{u}}_d\right)^{k,l}}{\Delta t} \end{bmatrix} = \boldsymbol{\mathcal{T}}_u{}^{k} + \boldsymbol{\mathcal{R}}_u{}^{k,l-1}.
\end{aligned} \tag{5.38}$$

The superscript on the symbols of the mass matrix $\boldsymbol{\mathcal{C}}$, stiffness matrix $\boldsymbol{\mathcal{K}}$ and residual vector $\boldsymbol{\mathcal{R}}$ indicates that these are evaluated using the values of the nodal unknowns computed in the previous iteration. In the system given by Equation 5.38 the following vectors of nodal unknowns are chosen as the ones to be solved for the l^{th} iteration of the k^{th} time step:

$\hat{\boldsymbol{u}}_w^{k,l}$ for the pore water pressure

$\hat{\boldsymbol{u}}_a^{k,l}$ for the pore air pressure

$\delta\left(\Delta\hat{\boldsymbol{u}}_d\right)^{k,l}$ for the displacement.

Consequently, by taking into account Equations 5.35 and 5.37 and by rewriting the nodal displacements and the second order approximations for the temporal derivative of nodal displacements as:

$$\hat{\boldsymbol{u}}_d^{k,l} = \hat{\boldsymbol{u}}_d^{k,l-1} + \delta\left(\Delta\hat{\boldsymbol{u}}_d\right)^{k,l} \tag{5.39}$$

$$\frac{\Delta\hat{\boldsymbol{u}}_d}{\Delta t}^{k,l} = \frac{\hat{\boldsymbol{u}}_d^{k,l-1} + \delta\left(\Delta\hat{\boldsymbol{u}}_d\right)^{k,l} - \frac{4}{3}\hat{\boldsymbol{u}}_d^{k-1} + \frac{1}{3}\hat{\boldsymbol{u}}_d^{k-2}}{\frac{2}{3}\Delta t} \tag{5.40}$$

the system given by Equation 5.38 can be expressed in the following form, where, on the left hand side, only the terms containing the unknowns to be solved for in each iteration are present:

$$\begin{bmatrix} \boldsymbol{\mathcal{K}}_f{}^{k,l-1} + \frac{3}{2\Delta t}\boldsymbol{\mathcal{C}}_f{}^{k,l-1} \\ \boldsymbol{\mathcal{K}}_u{}^{k,l-1} + \frac{1}{\Delta t}\boldsymbol{\mathcal{C}}_u{}^{k,l-1} \end{bmatrix} \begin{bmatrix} \hat{\boldsymbol{u}}_a^{k,l} \\ \hat{\boldsymbol{u}}_w^{k,l} \\ \delta\left(\Delta\hat{\boldsymbol{u}}_d\right)^{k,l} \end{bmatrix} = \begin{bmatrix} \boldsymbol{\mathcal{E}}_f{}^{k,l-1} \\ \boldsymbol{\mathcal{E}}_u{}^{k,l-1} \end{bmatrix} + \begin{bmatrix} \boldsymbol{\mathcal{T}}_f{}^{k} \\ \boldsymbol{\mathcal{T}}_u{}^{k} \end{bmatrix} + \begin{bmatrix} \boldsymbol{\mathcal{R}}_f{}^{k,l-1} \\ \boldsymbol{\mathcal{R}}_u{}^{k,l-1} \end{bmatrix} \tag{5.41}$$

where the two vectors $\boldsymbol{\mathcal{E}}_f{}^{k,l-1}$ and $\boldsymbol{\mathcal{E}}_u{}^{k,l-1}$ appearing on the right side of the system in Equations 5.41 are given by:

$$\boldsymbol{\mathcal{E}}_f{}^{k,l-1} = -\boldsymbol{\mathcal{K}}_f{}^{k,l-1} \begin{bmatrix} 0 \\ 0 \\ \hat{\boldsymbol{u}}_d^{k,l-1} \end{bmatrix} - \frac{3}{2\Delta t}\boldsymbol{\mathcal{C}}_f{}^{k,l-1} \begin{bmatrix} -\frac{4}{3}\hat{\boldsymbol{u}}_w^{k-1} + \frac{1}{3}\hat{\boldsymbol{u}}_w^{k-2} \\ -\frac{4}{3}\hat{\boldsymbol{u}}_a^{k-1} + \frac{1}{3}\hat{\boldsymbol{u}}_a^{k-2} \\ +\hat{\boldsymbol{u}}_d^{k,l-1} - \frac{4}{3}\hat{\boldsymbol{u}}_d^{k-1} + \frac{1}{3}\hat{\boldsymbol{u}}_d^{k-2} \end{bmatrix} \tag{5.42}$$

$$\boldsymbol{\mathcal{E}}_u{}^{k,l-1} = -\boldsymbol{\mathcal{K}}_u{}^{k,l-1} \begin{bmatrix} 0 \\ 0 \\ \hat{\boldsymbol{u}}_d^{k,l-1} \end{bmatrix} - \frac{1}{\Delta t}\boldsymbol{\mathcal{C}}_u{}^{k,l-1} \begin{bmatrix} -\hat{\boldsymbol{u}}_w^{k,l-1} \\ -\hat{\boldsymbol{u}}_a^{k,l-1} \\ 0 \end{bmatrix}. \tag{5.43}$$

The definition of the vector, $\boldsymbol{\mathcal{E}}_f{}^{k,l-1}$ given by Equation 5.42 differs from the one employed in the original version of code"Compass", due to the different discretization assumed in

this work for the temporal derivatives in the equations of water and air flows. For the same reason the matrix $\boldsymbol{C}_f^{k,l-1}$ is multiplied by the coefficient 3/2 in Equation 5.42 and 5.41 whereas in the original version of the code this coefficient was absent. The resulting system given by Equation 5.41 has to be solved using an iterative process which combines a fully implicit Picard iteration scheme (see Celia, Bouloutas and Zarba [83]) for the solution of the equations of water and air flows and a visco-plastic algorithm for the integration of the elasto-plastic stress-strain relationship.

The reason for the choice of a second-order finite difference approximation of the temporal derivatives of nodal unknowns instead of a first-order one, is that this approximation has proven (see Bouloutas [86]) to give improved performance for mass conservation in the two equations of flow when a "capacitative" approach is employed. The "capacitative" approach for the flow equations, used in this work, consists of expressing the storage terms in the flow equations (see Equations 5.10 and 5.12) in terms of the field unknowns (see Equations 5.15 and 5.16) by using the chain rule of derivation. Solutions of coupled flow-deformation problems in unsaturated soils, achieved using the "capacitative" approach and a first-order backward finite difference for the temporal derivatives of nodal unknowns, have been shown to produce unacceptably large mass balance errors for many sample calculations (see for example Celia, Bouloutas and Zarba [83]).

Conversely the "conservative" approach (see Celia, Bouloutas and Zarba [83], Allen and Murphy [87], Olivella, Gens, Carrera and Alonso [80]) discretizes directly the storage terms in the flow equations (Equations 5.10 and 5.12) without reducing them in terms of temporal derivatives of field unknowns. This approach combined with a first-order backward finite difference scheme in time, has proven to alleviate the mass balance problems discussed above. The "capacitative" approach implemented in the original version of code "Compass" was kept in the present work, however, in order to improve mass balance, it was combined with a second-order finite difference approximation for time derivatives, as discussed earlier in this section. For the sample calculations performed in this work, however, no significant differences were observed between the first-order and second-order finite difference schemes and mass balance was acceptable in both cases.

5.4.2 Improvement of the convergency algorithm

In this section two different aspects relating to the improvement of the stress-strain convergency algorithm originally implemented in code "Compass" are discussed. First the necessity of considering residual flux terms in the equations of flow, analogous to residual force terms in the equation of equilibrium, is demonstrated. The definition of these residual flux terms, neglected in the original version of the code, and the relevant numerical implementation, are presented. Subsequently, the first of the three convergence criteria introduced in Section 5.3.2 is illustrated. This criterion differs from the one adopted in the original version of the code and the reasons for this change are discussed.

When an elasto-plastic constitutive model is implemented within a finite element code, generally an iterative convergency algorithm is employed for each elasto-plastic load step to correct the stress state back onto the yield surface. For coupled flow-deformation analyses of saturated soils this convergency process is due to the dependency of the effective stress rate on the plastic strain rate in the equilibrium equation. This produces in each iteration a residual force term which is applied as a load to the equilibrium equation in the next iteration. A convergency algorithm for the elasto-plastic model of Alonso, Gens and Josa [1] within the equilibrium equation was implemented in the original version of code "Compass" and an outline of this convergency algorithm was given in Section 5.3.2.

For coupled flow-deformation analyses of unsaturated soils, the rate of degree of saturation, dS_r/dt in the water and air flows equations (Equations 5.10 and 5.12) may also depend on the net stress rate, $d\overline{\sigma}/dt$ through, for example, a state surface relationship. Such dependency was present in the original version of code "Compass", where the state surface expression for degree of saturation of Lloret and Alonso [22], given by Equation 2.41, was implemented. Consequently, the rate of degree of saturation, dS_r/dt in the water and air flows equations depends on the plastic strain rate, $d\epsilon^p/dt$ through the constitutive relationship of Equation 5.17. This explains the occurrence of residual flux terms in the flow equations as well as residual forces in the equilibrium equation. By discretizing with respect to space Equations 5.15 and 5.16, as already described in Section 5.3.1, and by assuming for the plastic strain rate $d\epsilon^p/dt$ a finite difference approximation in time, the

two residual flux terms, ψ_w and ψ_a, components of the residual vector $\mathcal{R}$ of Equation 5.22, are computed as:

$$\psi_w = \int_\Omega \mathbf{N}^T n \boldsymbol{g}_1{}^T \mathbf{D} \frac{\Delta \boldsymbol{\epsilon}^p}{\Delta t} \, d\Omega \tag{5.44}$$

$$\psi_a = -\int_\Omega \mathbf{N}^T n(1-H) \boldsymbol{g}_1{}^T \mathbf{D} \frac{\Delta \boldsymbol{\epsilon}^p}{\Delta t} \, d\Omega \tag{5.45}$$

where $\mathbf{N}$ is the shape functions vector, n is the porosity, $\mathbf{D}$ is the elastic matrix, $\boldsymbol{g}_1 = \partial S_r / \partial \overline{\boldsymbol{\sigma}}$, $\boldsymbol{\epsilon}^p$ is the vector of plastic strains and Ω is the space domain. The sign of the residual flux terms above differs from that of the same terms presented in the paper by Gallipoli, Karstunen and Wheeler [58] (where occurence of dissolved air in the liquid phase was also ignored) because in that work a positive convention for tensile stresses and strains was assumed. Consistent with the approach followed for the discretization of the temporal derivatives of nodal unknowns in the discretized continuity equations of water and air flows (Equation 5.18), a second-order finite difference approximation in time for the plastic strain rate in Equations 5.44 and 5.45 is employed, giving for the generic l^{th} iteration of the generic k^{th} time step:

$$\frac{\Delta \boldsymbol{\epsilon}^{p\,k,l}}{\Delta t} = \frac{\boldsymbol{\epsilon}^{p,k,l-1} - \frac{4}{3}\boldsymbol{\epsilon}^{p,k-1} + \frac{1}{3}\boldsymbol{\epsilon}^{p,k-2}}{\frac{2}{3}\Delta t}. \tag{5.46}$$

Therefore the residual flux terms in the generic l^{th} iteration of the generic k^{th} time step are expressed in the algebraic equation system of Equation 5.41, as:

$${\psi_w}^{k,l} = \int_\Omega \mathbf{N}^T \left(n \boldsymbol{g}_1{}^T \mathbf{D} \right)^{k,l-1} \frac{\Delta \boldsymbol{\epsilon}^{p\,k,l}}{\Delta t} \, d\Omega \tag{5.47}$$

$${\psi_a}^{k,l} = -\int_\Omega \mathbf{N}^T (1-H) \left(n \boldsymbol{g}_1{}^T \mathbf{D} \right)^{k,l-1} \frac{\Delta \boldsymbol{\epsilon}^{p\,k,l}}{\Delta t} \, d\Omega. \tag{5.48}$$

In the computation of the above integrals a 3×3 Gauss rule was adopted and, therefore, all the factors under the integral symbol must be evaluated at the sampling Gauss points within each element. The shape function vector $\mathbf{N}$ can be readily evaluated at the Gauss points. The other factors under the integral depend on the net stress vector $\overline{\boldsymbol{\sigma}}$, suction

s, plastic strain vector $\boldsymbol{\epsilon}^p$, and hardening parameter $\overline{p}_o^*$. In particular the porosity n depends on the values of net stresses, suction and hardening parameter according to the Alonso, Gens and Josa [1] model, $\boldsymbol{g}_1$ depends on the values of net stresses and suction according to the Lloret and Alonso [22] state surface expression for degree of saturation, $\mathbf{D}$ depends on the values of net stresses according to the Alonso, Gens and Josa [1] model, and the finite approximation in time for plastic strain rate depends on the plastic strain values. Numerical integration of the factors under the integral is, therefore, immediate as most of the quantities they depend on (namely net stress vector, plastic strain vector and hardening parameter) are defined at the Gauss points. Suction, however, is a nodal variable, but it can be easily computed at the Gauss point locations using a shape function approximation.

The presence of the residual flux terms defined above must be considered if the state surface for degree of saturation includes dependency on the net stress state (see Equation 2.41). If there is no dependency of S_r on net stress state (e.g. if $d = 0$ in the state surface expression selected in Equation 2.41), then $\boldsymbol{g}_1 = \mathbf{0}$ in Equations 5.44 and 5.45 and the residual flux terms vanish. The presence of residual flux terms should also be considered if variation of degree of saturation with net stress and suction is represented by an elasto-plastic framework, such as the one presented in Chapter 4. In this case, however, the definitions of the residual flux terms differ from those presented in Equations 5.44 and 5.45 and will be given in Section 5.4.3. The ideas presented above apply to any finite element code implementing unsaturated coupled flow-deformation analyses by using an elasto-plastic constitutive model for the soil and employing a convergency algorithm, irrespective of the type of convergency algorithm used.

A numerical simulation was performed in order to assess the influence of residual flux terms on numerical predictions. The results of this simulation showed that substantial errors may arise if these residual flux terms are omitted. These results are presented in detail in Section 6.3.

The other modification concerning the convergency algorithm relates to the implementation of a new convergency criterion (the first of the three convergency criteria intro-

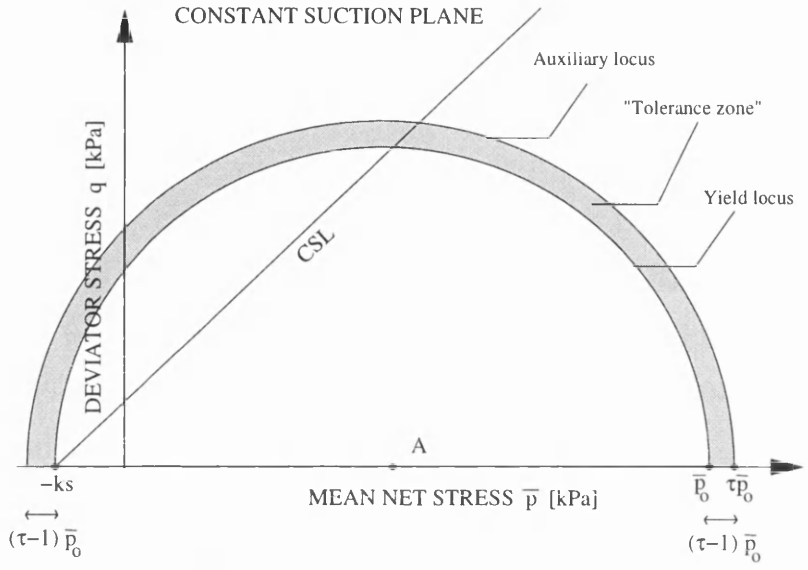

Figure 5.1: "Tolerance zone" for the convergency criterion

duced in Section 5.3.2). This criterion assumes that, during the convergency process, the net stress state is converged back onto the yield surface and, therefore, is an acceptable net stress state, when it is confined within a "tolerance zone" delimited by the current yield curve in the $(q, \overline{p})$-plane at constant suction and an auxiliary curve lying outside the yield locus. The amplitude of this "tolerance zone" is decided by the user through the input of a control parameter. The auxiliary curve chosen for delimiting the "tolerance zone" is an expanded yield curve, as shown in Figure 5.1, and the magnitude of the expansion is controlled by the tolerance factor $\tau > 1$ to be input by the user, which muliplies the hardening parameter, $\overline{p}_o$ of the yield curve in the $(q, \overline{p})$-plane at constant suction. The auxiliary curve is identified by the additional condition that the centres of the the auxiliary and yield curves on the mean net stress axis (point A in Figure 5.1) coincide.

The equations of the yield locus and of the auxiliary locus are given respectively by:

$$\mathcal{F} = q^2 - M^2(\overline{p}_o - \overline{p})(\overline{p} + ks) = 0 \qquad (2.33bis)$$

$$\mathcal{G} = q^2 - M^2(\tau\overline{p}_o - \overline{p})(\overline{p} + (\tau - 1)\overline{p}_o + ks) = 0. \qquad (5.49)$$

In the generic l^{th} iteration of the generic k^{th} time step, the convergency criterion is satisfied

by the "trial" net stress state (see Section 5.3.2) if the following condition is met:

$$\mathcal{G}(\overline{\sigma}^{k,l}_{trial}, s_{trial}, \overline{p}_o^{*k,l-1}) \leq 0. \tag{5.50}$$

If the condition given by Equation 5.50 is satisfied, this means that the "trial" net stress state is bounded within a "tolerance zone" (see Figure 5.1) which has an amplitude determined by the value of the tolerance factor τ. In this work 1.0001 was assumed as a typical value for the tolerance factor τ.

The convergency criterion presented above was implemented in the code by the author as a replacement of another criterion, present in the original version of "Compass". The previous criterion assumed that, during the convergency process, the net stress state was converged back onto the yield locus, when the following condition on the visco-plastic strain rate $(d\epsilon^{vp}/dt)^{k,l}$, given by Equation 5.26, was satisfied (see Thomas and He [43]):

$$\left| \frac{d\epsilon^{vp\,k,l}}{dt} \right| \leq \tau \tag{5.51}$$

where τ is a tolerance factor. This criterion was abandoned in this work because the requirement that the norm of the visco-plastic strain rate vector has to be smaller than a given tolerance does not represent a valid test on the convergency of the net stress state. The visco-plastic strain rate vector, in each iteration, depends also on the fluidity parameter, γ (see Equation 5.26), which is an input parameter used to control the stability of the convergency algorithm. If a very small value for the fluidity parameter γ is chosen, very small values of the visco-plastic strain rate are calculated in each iteration. Therefore the criterion of Equation 5.51 might be satisfied when the net stress state is still far from being converged back onto the yield locus. In contrast, the fulfilment of the criterion proposed by the author (Equation 5.50) guarantees that the net stress state is confined at the end of the convergency process within a "tolerance zone", adjacent to the yield locus, whose amplitude may be defined a priori.

5.4.3 Implementation of the S_r relationship proposed in Chapter 4

In this section issues associated with the numerical implementation of the new relationship for degree of saturation proposed in Chapter 4 in code "Compass", are discussed. The new relationship postulates a link between degree of saturation S_r, suction s, and specific volume v, having the form:

$$S_r = \left(\frac{1}{1+(\phi\,(v-1)\psi s)^n}\right)^m \qquad (4.5bis)$$

where ϕ, ψ, m and n are model parameters. The relationship of Equation 4.5 is implemented in "Compass" in combination with the elasto-plastic model of Alonso, Gens and Josa [1], which predicts the change of specific volume with changing stress state and stress history. This relationship is able to model the variation of degree of saturation in an elasto-plastic fashion, consistent with the rest of the stress-strain model. This means that the temporal derivative of degree of saturation in the continuity equations of water and air flows (Equations 5.10 and 5.12) can be split into two contributions, one due to reversible changes of degree of saturation (elastic derivative), ${dS_r}^e/dt$, and one due to irreversible changes (plastic derivative), ${dS_r}^p/dt$:

$$\frac{dS_r}{dt} = \frac{{dS_r}^e}{dt} + \frac{{dS_r}^p}{dt}\,. \qquad (5.52)$$

The elastic derivative can be expressed in terms of the vector of net stress rate, $d\overline{\sigma}/dt$ and suction rate ds/dt through the relationship:

$$\frac{{dS_r}^e}{dt} = {\boldsymbol{g}_1}^T\frac{d\overline{\sigma}}{dt} + g_2\frac{ds}{dt} \qquad (5.53)$$

where $\boldsymbol{g}_1$ and g_2 are respectively the derivative of the reversible part of the change of degree of saturation with respect to the net stress vector and suction. These terms are defined as:

$$\boldsymbol{g}_1 = g_3\frac{\partial\Delta v^e}{\partial\overline{\sigma}} \qquad (5.54)$$

and

$$g_2 = g_4 + g_3\frac{\partial\Delta v^e}{\partial s} \qquad (5.55)$$

where $g_3 = \partial S_r/\partial v$ and $g_4 = \partial S_r/\partial s$ are the partial derivative of Equation 4.5 with respect to specific volume and suction while $\partial \Delta v^e/\partial \overline{\boldsymbol{\sigma}}$ and $\partial \Delta v^e/\partial s$ are the partial derivative of the elastic variation of the specific volume with respect to the net stress vector and suction. These definitions of $\boldsymbol{g}_1$ and g_2 are different from those adopted for the case of the state surface originally implemented in "Compass", where the terms $\boldsymbol{g}_1$ and g_2 are the derivatives of the total change of degree of saturation with respect to net stress state and suction rather than the derivatives of the reversible part of the change of degree of saturation.

From the proposed relationship of degree of saturation (Equation 4.5), the explicit forms of the two partial derivatives with respect to specific volume and suction, g_3 and g_4 can be obtained as:

$$g_3 = -\frac{mn\psi}{v-1}\,\frac{\left(\phi(v-1)^{\psi}s\right)^n}{\left(1+\left(\phi(v-1)^{\psi}s\right)^n\right)^{m+1}} \tag{5.56}$$

and

$$g_4 = -mn\,\frac{\left(\phi(v-1)^{\psi}\right)^n s^{n-1}}{\left(1+\left(\phi(v-1)^{\psi}s\right)^n\right)^{m+1}}. \tag{5.57}$$

Similarly, based on the Alonso, Gens and Josa [1] model the the two partial derivatives of the elastic variation of the specific volume $\partial \Delta v^e/\partial \overline{\boldsymbol{\sigma}}$ and $\partial \Delta v^e/\partial s$ can be calculated (see Equation 2.18) as:

$$\frac{\partial \Delta v^e}{\partial \overline{\boldsymbol{\sigma}}} = -\frac{\kappa}{3\overline{p}}\,\boldsymbol{m}^T \tag{5.58}$$

and

$$\frac{\partial \Delta v^e}{\partial s} = -\frac{\kappa_s}{s+p_{atm}} \tag{5.59}$$

where κ and κ_s are parameters in the Alonso, Gens and Josa [1] model (see Section 2.4). Combination of Equations 5.56 and 5.58 with Equation 5.54 and Equations 5.56, 5.57 and 5.59 with Equation 5.55, yields the following explicit forms of the terms $\boldsymbol{g}_1$ and g_2 for the case when the proposed relationship for degree of saturation is employed in conjunction with the elasto-plastic stress-strain model of Alonso, Gens and Josa [1]:

$$\boldsymbol{g}_1 = \frac{mn\psi}{v-1} \frac{\left(\phi(v-1)^{\psi} s\right)^n}{\left(1+(\phi(v-1)^{\psi} s)^n\right)^{m+1}} \frac{\kappa}{3\overline{p}} \boldsymbol{m}^T \tag{5.60}$$

and

$$g_2 = mn \frac{\left(\phi(v-1)^{\psi}\right)^n s^{n-1}}{\left(1+(\phi(v-1)^{\psi} s)^n\right)^{m+1}} \frac{\kappa_s}{s+p_{atm}}. \tag{5.61}$$

The plastic derivative, $dS_r{}^p/dt$, can be expressed in terms of the temporal derivative of the plastic changes of specific volume:

$$\frac{dS_r{}^p}{dt} = g_3 \frac{d\Delta v^p}{dt}. \tag{5.62}$$

Taking into account Equations 5.52, 5.53 and 5.62, the continuity equations of water and air flows, expressed in terms of field variables, become for the case of the new relationship for degree of saturation:

$$\operatorname{div} \boldsymbol{v}_{wr} + (S_r \boldsymbol{m}^T \mathbf{B} + n \boldsymbol{\nabla} S_r) \frac{d\boldsymbol{u}_d}{dt} + n g_2 \frac{du_a}{dt} - n g_2 \frac{du_w}{dt} + n \boldsymbol{g}_1{}^T \frac{d\overline{\boldsymbol{\sigma}}}{dt} + n g_3 \frac{d\Delta v^p}{dt} = 0 \tag{5.63}$$

$$\begin{aligned} \operatorname{div}(\boldsymbol{v}_{ar} + H\boldsymbol{v}_{wr}) + \frac{(\boldsymbol{v}_{ar} + H\boldsymbol{v}_{wr})\boldsymbol{\nabla}\rho_a}{\rho_a} + ((1-(1-H)S_r)(\frac{n}{\rho_a}\boldsymbol{\nabla}\rho_a - \boldsymbol{m}^T\mathbf{B}) - \\ n(1-H)\boldsymbol{\nabla}S_r)\frac{d\boldsymbol{u}_d}{dt} + ((1-(1-H)S_r)\frac{n}{\rho_a}\beta - n(1-H)g_2)\frac{du_a}{dt} + \\ n(1-H)g_2\frac{du_w}{dt} - n(1-H)\boldsymbol{g}_1{}^T\frac{d\overline{\boldsymbol{\sigma}}}{dt} - n(1-H)g_3\frac{d\Delta v^p}{dt} = 0. \end{aligned} \tag{5.64}$$

The differences between the continuity equations presented above and the ones, valid for the case of the state surface originally implemented in "Compass", given by Equations 5.15 and 5.16 are due to the changed definition for the terms $\boldsymbol{g}_1$ and g_2 and the presence of the additional terms $ng_3(d\Delta v^p/dt)$ and $-n(1-H)g_3(d\Delta v^p/dt)$ in Equations 5.63 and 5.64 respectively, due to the irreversible changes of degree of saturation. The continuity equations above are discretized with respect to space and time, as already explained in Section 5.3.1, and reduce to an algebraic system in the nodal unknowns of field variables. This algebraic system differs from the one derived for the case of the state

surface expression of Lloret and Alonso [22] originally implemented in "Compass" in the following respects:

1. The sub-matrix $\boldsymbol{C}_f$ of the mass matrix $\boldsymbol{C}$ (Equation 5.20) takes into account the new expressions for the terms $\boldsymbol{g}_1$ and g_2 given by Equations 5.60 and 5.61. The new expressions for the terms $\boldsymbol{g}_1$ and g_2 also appear in the definitions of the residual flux terms, $\boldsymbol{\psi}_w$ and $\boldsymbol{\psi}_a$ (components of the residual vector $\boldsymbol{\mathcal{R}}$ of Equation 5.22) which are given later in this section.

2. The definitions of the residual flux terms, $\boldsymbol{\psi}_w$ and $\boldsymbol{\psi}_a$, must also take into account the discretized form of the terms $ng_3(d\Delta v^p/dt)$ and $-n(1-H)g_3(d\Delta v^p/dt)$ appearing in Equations 5.63 and 5.64 respectively.

Discretization with respect to space and time of Equations 5.63 and 5.64 yields the following expressions for the two residual flux terms $\boldsymbol{\psi}_w$ and $\boldsymbol{\psi}_a$ valid for the case when the relationship for degree of saturation of Equation 4.5 is employed:

$$\boldsymbol{\psi}_w = \int_\Omega \mathbf{N}^T n \left(\boldsymbol{g}_1{}^T \mathbf{D} \frac{\Delta \boldsymbol{\epsilon}^p}{\Delta t} + g_3 \frac{\Delta v^p}{\Delta t} \right) d\Omega \tag{5.65}$$

$$\boldsymbol{\psi}_a = -\int_\Omega \mathbf{N}^T n(1-H) \left(\boldsymbol{g}_1{}^T \mathbf{D} \frac{\Delta \boldsymbol{\epsilon}^p}{\Delta t} + g_3 \frac{\Delta v^p}{\Delta t} \right) d\Omega \tag{5.66}$$

where $\mathbf{N}$ is the shape functions vector, $\mathbf{D}$ is the elatic matrix, $\boldsymbol{\epsilon}^p$ is the vector of plastic strains and Ω is the space domain. The finite difference approximation for the temporal derivative of the plastic change of specific volume, $\Delta v^p/\Delta t$, can be rewritten in terms of the natural logarithm of the hardening parameter $\Delta(\ln \overline{p}_o^*)/\Delta t$, by using the hardening law (see Equation 2.27) of the Alonso, Gens and Josa [1] model:

$$\frac{\Delta v^p}{\Delta t} = -(\lambda(0) - \kappa) \frac{\Delta(\ln \overline{p}_o^*)}{\Delta t} \tag{5.67}$$

where $\lambda(0)$ and κ are parameters in the Alonso, Gens and Josa [1] model (see Section 2.4). Consequently, the residual flux terms $\boldsymbol{\psi}_w$ and $\boldsymbol{\psi}_a$ of Equations 5.65 and 5.66 are rewritten as:

$$\psi_w = \int_\Omega \mathbf{N}^T n \left(\boldsymbol{g}_1{}^T \mathbf{D} \frac{\Delta \boldsymbol{\epsilon}^p}{\Delta t} - g_3(\lambda(0) - \kappa) \frac{\Delta(\ln \overline{p}_o^*)}{\Delta t} \right) d\Omega \tag{5.68}$$

$$\psi_a = - \int_\Omega \mathbf{N}^T n(1 - H) \left(\boldsymbol{g}_1{}^T \mathbf{D} \frac{\Delta \boldsymbol{\epsilon}^p}{\Delta t} - g_3(\lambda(0) - \kappa) \frac{\Delta(\ln \overline{p}_o^*)}{\Delta t} \right) d\Omega. \tag{5.69}$$

The finite difference approximation in time, $\Delta(\ln \overline{p}_o^*)/\Delta t$, in Equations 5.68 and 5.69 is represented, consistently with the approach followed for the discretization of temporal derivatives of nodal unknowns in the discretized continuity equations for water and air flows (Equation 5.18), by a second-order finite difference scheme. This is given, for the generic l^{th} iteration of the generic k^{th} time step, by:

$$\frac{\Delta(\ln \overline{p}_o^*)^{k,l}}{\Delta t} = \frac{\ln \overline{p}_o^{*k,l-1} - \frac{4}{3} \ln \overline{p}_o^{*k-1} + \frac{1}{3} \ln \overline{p}_o^{*k-2}}{\frac{2}{3} \Delta t}. \tag{5.70}$$

Therefore the residual flux terms, ψ_w and ψ_a, (for the generic l^{th} iteration of the generic k^{th} time step) to be considered in the algebraic system of Equation 5.41, are given by:

$$\psi_w = \int_\Omega \mathbf{N}^T \left(\left(n \boldsymbol{g}_1{}^T \mathbf{D} \right)^{k,l-1} \frac{\Delta \boldsymbol{\epsilon}^{p\,k,l}}{\Delta t} - (n g_3)^{k,l-1} (\lambda(0) - \kappa) \frac{\Delta(\ln \overline{p}_o^*)^{k,l}}{\Delta t} \right) d\Omega \tag{5.71}$$

$$\psi_a = - \int_\Omega \mathbf{N}^T (1 - H) \left(\left(n \boldsymbol{g}_1{}^T \mathbf{D} \right)^{k,l-1} \frac{\Delta \boldsymbol{\epsilon}^{p\,k,l}}{\Delta t} - (n g_3)^{k,l-1} (\lambda(0) - \kappa) \frac{\Delta(\ln \overline{p}_o^*)^{k,l}}{\Delta t} \right) d\Omega. \tag{5.72}$$

A numerical computation of the integrals above, employing a 3×3 Gauss rule, is performed in code "Compass". The factors under the integral symbol, therefore, have to be sampled at Gauss points. This is readily accomplished, as already illustrated for the case of the integrals in Equations 5.47 and 5.48, because these factors depend directly or indirectly on quantities defined at Gauss points (i.e. the net stress vector $\overline{\boldsymbol{\sigma}}$, specific volume v and hardening parameter $\overline{p}_o^*$) or on nodal variables (i.e. suction, s) which may be evaluated at Gauss points using a shape function approximation.

The ideas presented above are applicable to any finite element code implementing the relationship for degree of saturation given by Equation 4.5 in combination with an elasto-plastic model predicting the variation of specific volume and employing a convergency

algorithm, irrespective of the type of convergency algorithm used. In order to validate the implementation of the relationship for degree of saturation of Equation 4.5, in combination with the Alonso, Gens and Josa [1] model, into code "Compass", three benchmark problems, for which the analytical solution was known, were numerically simulated. These numerical simulations modelled the following notional triaxial laboratory tests already described in Chapter 4:

1. A fully drained test at constant suction of 100 kPa, involving isotropic compression from an initial isotropic normally consolidated state of $\overline{p} = 50$ kPa to $\overline{p} = 100$ kPa, followed by shearing to critical state at constant mean net stress.

2. A fully drained test at constant suction of 100 kPa, involving isotropic compression from an initial isotropic normally consolidated state of $\overline{p} = 180$ kPa to $\overline{p} = 400$ kPa, followed by elastic isotropic unloading to $\overline{p} = 100$ kPa.

3. A fully undrained (with respect to the liquid phase) test involving shearing to a critical state, starting from an initial isotropic normally consolidated state of $\overline{p} = 100$ kPa and $s = 100$ kPa. The shearing of the sample is performed by increasing the axial net stress whilst keeping the radial net stress constant.

These three numerical tests are a complete set of analyses for validating the implementation of the relationship for degree of saturation proposed in Chapter 4 within code "Compass". The first test assesses the performance of the code when elasto-plastic deformations occur in a fully drained condition (i.e. no coupling between the equilibrium equation and the continuity equations for water and air flows). The unloading stage of the second test assesses the performance of the code when purely elastic deformation take place under fully drained conditions. The third test gives an indication on the correctness of the implementation for cases when coupling between the equilibrium equation and the continuity equation of water flow takes place.

Figure 5.2 presents the comparisons between numerical and analytical results for the three tests described above. The numerical solution matches perfectly the analytical one in all three cases, confirming the correctness of the implementation of the relationship for

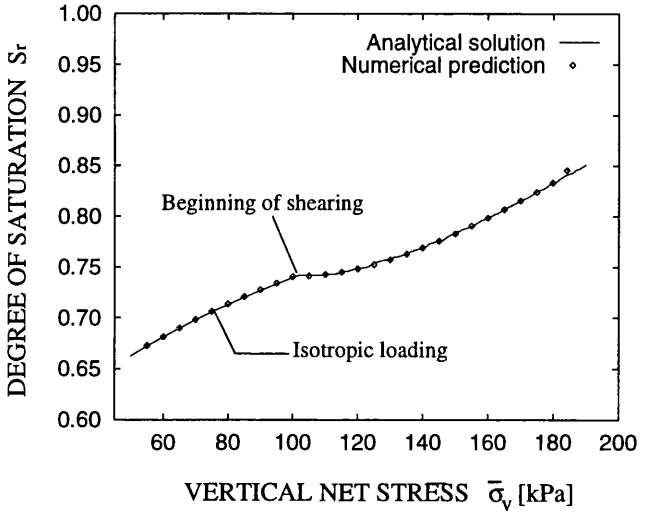

(a)

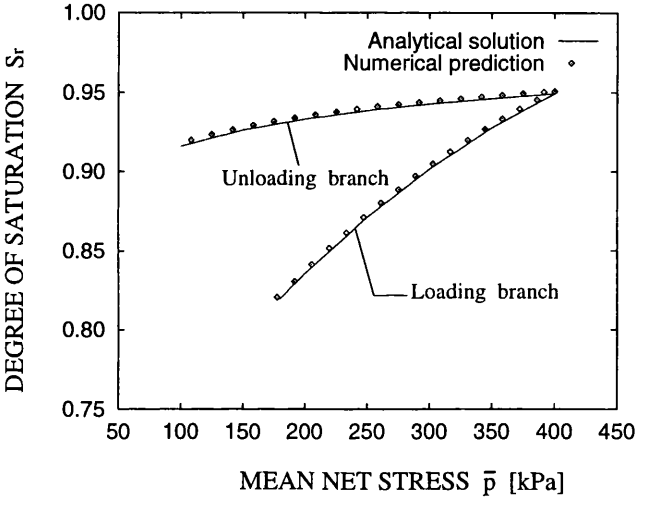

(b)

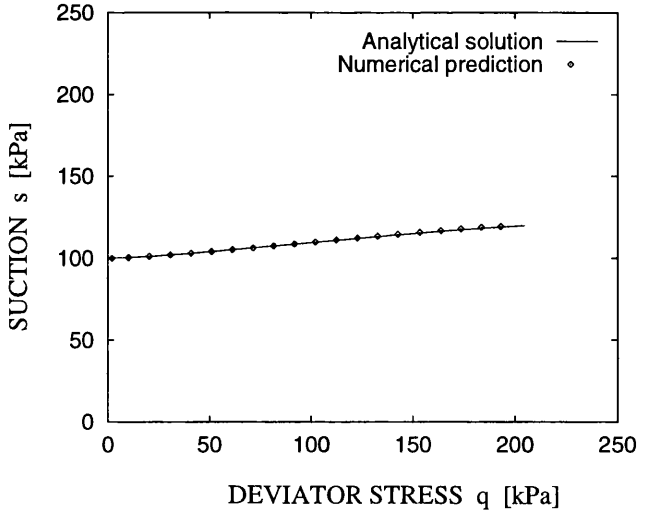

(c)

Figure 5.2: Comparison between numerical and analytical predictions. (a) Benchmark test 1 (b) Benchmark test 2 (c) Benchmark test 3

degree of saturation given by Equation 4.5 in code "Compass". The mechanical parameters for the Alonso, Gens and Josa [1] model, which have been used for the analytical and numerical predictions, are the ones defined in Chapter 3 and reported in Table 3.2. The model parameters used for the relationship for degree of saturation are the ones defined in Section 4.3 and reported in Table 4.2. The analytical solutions presented here were computed for comparing the predictions of the new relationship for degree of saturation with experimental data in Section 4.4. For the numerical simulations, the mesh used was the same one employed for the other axi-symmetric numerical analyses presented in Chapter 6 (see Figure 6.1).

5.4.4 Implementation of the terms containing ∇S_r and $\nabla \rho_a$

As mentioned in Section 5.3.1, one of the modifications to the original version of code "Compass" made in this work, was the inclusion in the algebraic system of governing equations (Equation 5.18) of the discretized form of the terms in the continuity equations for water and air containing ∇S_r and $\nabla \rho_a$. These are: the term $n(d\boldsymbol{u}_d/dt)\nabla S_r$ in Equation 5.10 and the terms $-n(1-H)(d\boldsymbol{u}_d/dt)\nabla S_r$ and $(1-(1-H)S_r)(n/\rho_a)(d\boldsymbol{u}_d/dt)\nabla \rho_a$ in Equation 5.12. The inclusion of these terms affects the definition of the sub-matrices $\mathbf{C}_{wu}$ and $\mathbf{C}_{au}$ of the mass matrix $\boldsymbol{C}$ (Equation 5.20). In this section some numerical aspects relating to the implementation of these terms within code "Compass" are discussed.

By employing the finite element method for discretizing Equations 5.15 and 5.16 with respect to space and by applying the Galerkin weighted residual approach together with a finite difference approximation in time for the temporal derivatives of the displacement vector, the following discretized forms are obtained:

$$n\frac{d\boldsymbol{u}_d}{dt}\nabla S_r = \int_\Omega \mathbf{N}^T n \nabla S_r \mathbf{N}\, d\Omega \, \frac{\Delta \hat{\boldsymbol{u}}_d}{\Delta t} \tag{5.73}$$

$$-n(1-H)\frac{d\boldsymbol{u}_d}{dt}\nabla S_r = -\int_\Omega \mathbf{N}^T n(1-H) \nabla S_r \mathbf{N}\, d\Omega \, \frac{\Delta \hat{\boldsymbol{u}}_d}{\Delta t} \tag{5.74}$$

$$(1-(1-H)S_r)\frac{n}{\rho_a}\frac{d\boldsymbol{u}_d}{dt}\nabla \rho_a = \int_\Omega \mathbf{N}^T (1-(1-H)S_r)\frac{n}{\rho_a} \nabla \rho_a \mathbf{N}\, d\Omega \, \frac{\Delta \hat{\boldsymbol{u}}_d}{\Delta t} \tag{5.75}$$

where $\hat{\boldsymbol{u}}_d$ is the vector of nodal unknowns of displacement and Ω is the space domain. The finite difference approximation in time $\Delta\hat{\boldsymbol{u}}_d/\Delta t$ is achieved through the second-order backward scheme (fully implicit) given by Equation 5.35.

In the generic l^{th} iteration of the generic k^{th} time step, the changes to the algebraic system of governing equations (Equation 5.18) with respect to the original version of code "Compass", due to the incorporation of the terms given in Equations 5.73, 5.74 and 5.75 can be summarized as follows:

1. The sub-matrix $\mathbf{C}_{wu}^{k,l-1}$ of the mass matrix $\boldsymbol{\mathcal{C}}^{k,l-1}$ (Equation 5.20) includes the term $\int_\Omega \mathbf{N}^T(n\boldsymbol{\nabla}S_r)^{k,l-1}\mathbf{N}\,d\Omega$.

2. The sub-matrix $\mathbf{C}_{au}^{k,l-1}$ of the mass matrix $\boldsymbol{\mathcal{C}}^{k,l-1}$ (Equation 5.20) includes the terms $-\int_\Omega \mathbf{N}^T(n(1-H)\boldsymbol{\nabla}S_r)^{k,l-1}\mathbf{N}\,d\Omega$ and $\int_\Omega \mathbf{N}^T((1-(1-H)S_r)(n/\rho_a)\boldsymbol{\nabla}\rho_a)^{k,l-1}\mathbf{N}\,d\Omega$.

The integrals above are numerically computed in code "Compass" using a 3×3 Gauss rule. The factors under the integrals therefore have to be sampled at Gauss points and this is not as straightforward as in the cases of the numerical integration of the residual flux terms given by Equations 5.47, 5.48, 5.71 and 5.72. In the integrals above there are factors which did not appear in the integrals defining the residual flux terms. These are: the degree of saturation S_r, the air density ρ_a, the gradient of air density $\boldsymbol{\nabla}\rho_a$ and the gradient of degree of saturation $\boldsymbol{\nabla}S_r$.

The evaluation of degree of saturation S_r and air density ρ_a at Gauss points is immediate as these factors depend directly or indirectly on quantities defined at Gauss points (i.e. the net stress vector $\overline{\boldsymbol{\sigma}}$ and the specific volume v) or on nodal variables (i.e. pore air pressure u_a and suction s) which may be evaluated at Gauss points using a shape function approximation. In particular, the degree of saturation depends on suction s and the net stress vector $\overline{\boldsymbol{\sigma}}$ for the case of the state surface expression of Lloret and Alonso [22] or on suction s and specific volume v for the relationship proposed in Chapter 4, while the air density depends on the air pressure u_a through the gas law for the isothermal case.

The first of the two gradient factors, $\boldsymbol{\nabla}\rho_a$, is also evaluated at Gauss points taking into account the dependency of the air density ρ_a on the pore air pressure u_a (through

application of the gas law under isothermal conditions) with u_a at Gauss points, in turn, expressed as a function of the nodal unknowns of pore air pressure by means of a shape function approximation. This factor is, therefore, rewritten as:

$$\nabla {\rho_a}^{k,l-1} = \beta \nabla \mathbf{N} \left(\hat{\boldsymbol{u}}_a^{k,l-1} + p_{atm} \right) \tag{5.76}$$

where β is the constant relating air density to the absolute value of air pressure (from the gas law) and the evaluation of the gradient factor $\nabla \mathbf{N}$ at the Gauss sampling points is readily accomplished by calculating the values of the cartesian derivatives of the shape functions at the locations of the Gauss points.

The numerical sampling at Gauss points of the other gradient factor, ∇S_r requires a more laborious approach. The degree of saturation is a quantity defined at Gauss points due to its dependency on the net stress vector $\overline{\sigma}$ for the case of the state surface expression of Lloret and Alonso [22] and on the specific volume v for the case of the relationship for S_r proposed in Chapter 4, as both these quantities are defined at Gauss points. Consequently, in order to calculate the gradient of degree of saturation, it is necessary to extrapolate from the discrete values at the Gauss points a continuous function describing the variation of this quantity over the soil domain. Moreover such function must possess the property of being continuous at the inter-element boundaries shared between two elements which are part of the same material zone of the soil domain. This is achieved by assuming for the degree of saturation a shape function approximation which is the same one employed to model the variation over the soil domain of the field variables (i.e. displacement, pore water pressure and pore air pressure). The variation of the degree of saturation is, therefore, approximated as:

$$S_r = \mathbf{N} \hat{\boldsymbol{S}}_r \tag{5.77}$$

where $\mathbf{N}$ is the shape functions vector and $\hat{\boldsymbol{S}}_r$ are the nodal values of degree of saturation. These nodal values are computed by fitting element-wise the assumed form of variation for degree of saturation (Equation 5.77) to the Gauss points values using a least square method. This approach follows the technique proposed by Hinton and Campbell [88] for

the local smoothing of discontinuous finite element functions (in particular they refer to local smoothing of the stress field when a 2×2 Gauss rule is employed). As this technique is based on fitting locally (element-wise) the proposed shape function approximation to the Gauss points values, it does not produce unique values of degree of saturation at nodes. Nodal averages must, therefore, be calculated as continuity of the degree of saturation needs to be guaranteed on inter-element boundaries which are contained within the same material zone. The factor ∇S_r occurring in sub-matrices $\mathbf{C}_{wu}^{k,l-1}$ and $\mathbf{C}_{au}^{k,l-1}$ may, therefore, be rewritten in the form:

$$\nabla S_r{}^{k,l-1} = \nabla \mathbf{N}\, \hat{\boldsymbol{S}}_r^{k,l-1} \tag{5.78}$$

where the gradient of shape function $\nabla \mathbf{N}$ can be readily evaluated at the Gauss sampling points.

A simple numerical study was performed in order to assess the consequences of neglecting terms involving ∇S_r and $\nabla \rho_a$ in the continuity equations (as was done in the original version of code "Compass"). The results of this analysis are presented in detail in Section 6.2.

5.4.5 Plane-strain regime for elasto-plastic deformations

In this section the formulation of the plane-strain deformation regime for an elasto-plastic unsaturated soil is presented and the aspects of incorrect modelling in the original version of code "Compass" are highlighted. These inconsistencies are also thought to be present in other finite element codes due to historical reasons.

For an elasto-plastic unsaturated soil, the total strain rate vector, $d\boldsymbol{\epsilon}/dt$, is made up of three components:

$$\frac{d\boldsymbol{\epsilon}}{dt} = \frac{d\boldsymbol{\epsilon}^{\sigma e}}{dt} + \frac{d\boldsymbol{\epsilon}^{se}}{dt} + \frac{d\boldsymbol{\epsilon}^{p}}{dt} \tag{5.79}$$

where $d\boldsymbol{\epsilon}^{\sigma e}/dt$ is the elastic strain rate vector due to a change in the net stresses, $d\boldsymbol{\epsilon}^{se}/dt$ is the elastic strain rate vector due to a change in suction and $d\boldsymbol{\epsilon}^{p}/dt$ is the plastic strain

rate vector. The incremental stress-strain relationship linking net stress rate $d\overline{\sigma}/dt$ to the elastic strain rate vector due to a change in net stresses, $d\epsilon^{\sigma e}/dt$ is given by:

$$\frac{d\overline{\sigma}}{dt} = \mathbf{D}\,\frac{d\epsilon^{\sigma e}}{dt} \tag{5.80}$$

where $\mathbf{D}$ is the elastic tangent stiffness matrix. The other two strain rate vectors which contribute to the total strain rate in Equation 5.79 are given by:

$$\frac{d\epsilon^{se}}{dt} = \frac{1}{3}\,A_s\,\boldsymbol{m}^T\,\frac{ds}{dt} \tag{5.81}$$

$$\frac{d\epsilon^{p}}{dt} = \frac{d\lambda}{dt}\,\frac{\partial \mathcal{Q}}{\partial \overline{\sigma}} \tag{5.82}$$

where A_s is the elastic volumetric compressibility of the soil due to a change in suction, the vector $\boldsymbol{m}$, already defined in Equation 2.4, is $(1\ 1\ 1\ 0\ 0\ 0)^T$, $d\lambda/dt$ is the plastic multiplier and $\mathcal{Q}$ is the plastic potential.

Equations 5.79, 5.80, 5.81 and 5.82 have to be simultaneously satisfied at each material point within the soil domain together with the consistency condition which imposes that, during plastic flow, the stress state must lie on the yield locus. This means that the net stress rate vector $d\overline{\sigma}/dt$ and the suction rate ds/dt must satisfy the following incremental form of the consistency equation:

$$d\mathcal{F}(\overline{\sigma}, s, \overline{p}_o^*) = 0 \tag{5.83}$$

where $\overline{p}_o^*$ is the hardening parameter. This set of equations represents the general formulation of the elasto-plastic constitutive model for unsaturated soil. It introduces a non-linear relationship in an incremental form between the net stress rate vector, $d\overline{\sigma}/dt$, the total strain rate vector, $d\epsilon/dt$, and the rate of suction, ds/dt. When the general formulation given above is applied to the particular case of plane-strain deformation, the out-of-plane component of the total strain rate vector, $d\epsilon/dt$ must be fixed at zero. Therefore for the plane-strain case where z is the out-of-plane direction, if compressive strains are assumed as positive, the total strain rate vector, $d\epsilon/dt$ is given by:

$$\frac{d\epsilon}{dt} = \left(\frac{d\epsilon_x}{dt} \quad \frac{d\epsilon_y}{dt} \quad \frac{d\epsilon_z}{dt} \quad \frac{d\gamma_{xy}}{dt} \quad \frac{d\gamma_{yz}}{dt} \quad \frac{d\gamma_{zx}}{dt}\right)^T =$$
$$= \left(-\frac{\partial}{\partial x}\frac{du_x}{dt} \quad -\frac{\partial}{\partial y}\frac{du_y}{dt} \quad 0 \quad \left(\frac{\partial}{\partial y}\frac{du_x}{dt} + \frac{\partial}{\partial x}\frac{du_y}{dt}\right) \quad 0 \quad 0\right)^T \tag{5.84}$$

where du_x/dt and du_y/dt are the in-plane components of the displacement rate vector. If the stress component $\overline{\sigma}_z$ is a principal stress component, then the two components $(d\lambda/dt)(\partial\mathcal{Q}/\partial\tau_{zx})$ and $(d\lambda/dt)(\partial\mathcal{Q}/\partial\tau_{yz})$ of the plastic strain rate vector of Equation 5.82 are equal to zero and the plastic strain rate vector is defined as:

$$\frac{d\epsilon^p}{dt} = \left(\frac{d\epsilon_x^p}{dt} \quad \frac{d\epsilon_y^p}{dt} \quad \frac{d\epsilon_z^p}{dt} \quad \frac{d\gamma_{xy}^p}{dt} \quad \frac{d\gamma_{yz}^p}{dt} \quad \frac{d\gamma_{zx}^p}{dt}\right)^T =$$
$$= \left(\frac{d\lambda}{dt}\frac{\partial\mathcal{Q}}{\partial\overline{\sigma}_x} \quad \frac{d\lambda}{dt}\frac{\partial\mathcal{Q}}{\partial\overline{\sigma}_y} \quad \frac{d\lambda}{dt}\frac{\partial\mathcal{Q}}{\partial\overline{\sigma}_z} \quad \frac{d\lambda}{dt}\frac{\partial\mathcal{Q}}{\partial\tau_{xy}} \quad 0 \quad 0\right)^T. \tag{5.85}$$

In the original version of code "Compass" the plane-strain assumption was implemented incorrectly by imposing the condition of nullity not only on the out-of-plane component of the total strain rate vector, $d\epsilon/dt$, but also on the out-of-plane components of each of the three individual strain rate contributions represented in Equation 5.79. This incoconsistency is believed to also be present in other finite element codes (see, for example, Gatmiri, Tavakoli, Moussavi and Delage [45]) and this is due to the history of the development of finite element programs, which have often been improved by adding new features to existing versions. As a result, parts of a code which were correct in previous versions have often been imported into a newer version of the code without carrying out all the changes which were required. In particular, the first versions of finite element programs included only a linear-elastic constitutive model. In this case the plane-strain condition can be independently imposed on the total strain vector or on the elastic strain vector, because these two coincide. When plastic behaviour was introduced, the constitutive model used most frequently for geomaterials was the elastic-perfectly plastic Mohr-Coulomb model with an associated flow rule. In this case the out-of-plane component of the plastic strain vector is always zero, if it is assumed that the out-of-plane stress remains the intermediate principal stress throughout the analysis, because the plastic potential is independent of the

intermediate principal stress. When, subsequently, more sophisticated constitutive models and plastic flow rules were introduced, it was possible that the assumption of nullity of the out-of-plane component of the plastic strain vector was erroneously retained.

In the case of unsaturated soil there is a third contribution to the total strain vector due to the elastic deformation caused by a change in suction. When the pre-existing codes were extended to include constitutive models for unsaturated soil, the elastic contribution of strain due to change in suction had to be introduced and, in some implementations the out-of-plane component of this contribution was assumed to be null for the plane-strain deformation.

In order to assess the potential significance of these errors, simple numerical studies were performed with both the original and the amended version of code "Compass". The results of these studies are presented in Section 6.4 where two different implementations for the plane-strain deformation regime are compared. The first one (version A) is the correct one and has been described previously in this section, the second one (version B), which corresponds to the original version of "Compass", is based on the assumption that the out-of-plane component of each single contribution of the total strain rate vector, $d\boldsymbol{\epsilon}/dt$, in Equation 5.79 is null. Version B of the plane-strain formulation therefore assumes that the total strain rate vector, $d\boldsymbol{\epsilon}/dt$, is still defined according to Equation 5.79, but the two contributions given by $d\boldsymbol{\epsilon}^{se}/dt$ and $d\boldsymbol{\epsilon}^{p}/dt$ are now incorrectly defined as:

$$\frac{d\boldsymbol{\epsilon}^{se}}{dt} = \frac{1}{2} A_s \boldsymbol{n}^T \frac{ds}{dt} \tag{5.86}$$

$$\begin{aligned} \frac{d\boldsymbol{\epsilon}^{p}}{dt} &= \left(\frac{d\epsilon_x^p}{dt} \quad \frac{d\epsilon_y^p}{dt} \quad \frac{d\epsilon_z^p}{dt} \quad \frac{d\gamma_{xy}^p}{dt} \quad \frac{d\gamma_{yz}^p}{dt} \quad \frac{d\gamma_{zx}^p}{dt} \right)^T = \\ &= \left(\frac{d\lambda}{dt} \frac{\partial \mathcal{Q}}{\partial \overline{\sigma}_x} \quad \frac{d\lambda}{dt} \frac{\partial \mathcal{Q}}{\partial \overline{\sigma}_y} \quad 0 \quad \frac{d\lambda}{dt} \frac{\partial \mathcal{Q}}{\partial \tau_{xy}} \quad 0 \quad 0 \right)^T \end{aligned} \tag{5.87}$$

where A_s, $d\lambda/dt$ and $\mathcal{Q}$ have been previously defined and the auxiliary vector $\boldsymbol{n}$ is $(1\ 1\ 0\ 0\ 0\ 0)^T$. Equation 5.87 violates the plastic flow rule.

The unnecessary constraints on the out-of-plane components of the two strain rate vectors, $d\boldsymbol{\epsilon}^{se}/dt$, and, $d\boldsymbol{\epsilon}^{p}/dt$ incorrectly imposed by Equations 5.86 and 5.87, cause the

out-of plane component of the elastic strain rate vector due to a change in net stresses, $d\epsilon^{\sigma e}/dt$, to be equal to zero and, as a result, the out-of-plane component of the net stress rate vector, $d\overline{\sigma}/dt$ is related to the other two in-plane components through the relationship:

$$\frac{d\overline{\sigma}_z}{dt} = \nu \left(\frac{d\overline{\sigma}_x}{dt} + \frac{d\overline{\sigma}_y}{dt} \right) \tag{5.88}$$

where ν is the Poisson's ratio of the soil skeleton. This well-known relationship is valid when the plane-strain condition is applied to elastic deformation for saturated soils. It is possible that Equation 5.88 has sometimes been confused with the definition of the plane-strain condition itself. For plane-strain behaviour of an unsaturated soil, Equation 5.88 is, however, only true for the specific case of elastic behaviour at a constant value of suction.

In Chapter 7 the improved version of code "Compass", implementing the new relationship for degree of saturation proposed in Chapter 4 (Equation 4.5), is applied to the study of an axi-symmetric boundary value problem, namely the modelling of pressuremeter tests in unsaturated soils. Equations 5.79, 5.80, 5.81, 5.82 and 5.83 given above, represent the generic expression of the elasto-plastic constitutive relationship between net stresses, suction and strain rates and are still valid for the axi-symmetric case. The constitutive relationship for the case of axi-symmetric deformation differs from the plane-strain case only in the definition of the total strain rate vector. In particular, Equation 5.84 is replaced for the axi-symmetric deformation regime with compressive strains assumed as positive, by:

$$\begin{aligned} \frac{d\boldsymbol{\epsilon}}{dt} &= \left(\frac{d\epsilon_x}{dt} \quad \frac{d\epsilon_y}{dt} \quad \frac{d\epsilon_z}{dt} \quad \frac{d\gamma_{xy}}{dt} \quad \frac{d\gamma_{yz}}{dt} \quad \frac{d\gamma_{zx}}{dt} \right)^T = \\ &= \left(-\frac{\partial}{\partial x}\frac{du_x}{dt} \quad -\frac{\partial}{\partial y}\frac{du_y}{dt} \quad -\frac{1}{x}\frac{du_x}{dt} \quad \left(\frac{\partial}{\partial y}\frac{du_x}{dt} + \frac{\partial}{\partial x}\frac{du_y}{dt} \right) \quad 0 \quad 0 \right)^T \end{aligned} \tag{5.89}$$

where du_x/dt and du_y/dt are, respectively, the radial and axial components of the displacement rate vector and x is the radial distance from the axis of symmetry.

Chapter 6

Demonstration of effects of changes to code "Compass"

6.1 Introduction

This chapter demonstrates the significance of the various changes and improvements to code "Compass" performed by the author, by presenting results of numerical simulations of simple boundary value problems. A detailed description of the modifications carried out by the author was given in Chapter 5. The simulations presented in this chapter are summarized below.

1. Section 6.2 shows the significance of incorrectly combining absolute flux velocities (rather than flux velocities relative to the soil skeleton) with Darcy's law in the two equations of flow (as occurred in the original version of code "Compass" and also other examples in the literature). The detailed description of the errors in the flow equations present in the original version of the code was given in Section 5.2, while issues relating to the numerical implementation of the additional terms arising from the correct expression of the flow equations were discussed in Section 5.4.4. The demonstration presented in Section 6.2 involves the simulation of an isotropic loading test on a cylindrical sample of soil with an initial gradient of suction over the sample height.

2. Section 6.3 demonstrates the significance of the errors arising when residual flux terms in the flow equations are neglected during the iterative convergency algorithm

for the elasto-plastic stress-strain model (as discussed in Section 5.4.2). This demonstration involves the simulation of undrained (with respect to the liquid phase) isotropic loading of a cylindrical sample.

3. Section 6.4 investigates the effect of the amendments carried out by the author to the incorrect plane-strain formulation which was implemented in the original version of the code and which is believed to be present also in other examples in the literature (see Section 5.4.5). This involved the simulations of drained biaxial loading tests and wetting tests at constant in-plane net stresses on a rectangular specimen under bi-dimensional plane-strain conditions.

4. Section 6.5 shows the influence of changing the model for variation of degree of saturation from the state surface expression of Lloret and Alonso [22] (Equation 2.41), implemented in the original version of code "Compass", to the improved elasto-plastic relationship proposed by the author in Chapter 4. This involved the simulation of a two-stage test on a cylindrical sample of soil: isotropic compression followed by shearing in triaxial compression. In each stage the loading was applied relatively rapidly, and this was then followed by a consolidation phase.

6.2 Effect of errors in the equations of water and air flows

The equations of continuity of water and air were derived in terms of liquid and gas flux velocities relative to the soil skeleton in Section 5.2. This is the form in which these equations should be formulated if the flux velocities are to be related to the relevant potential gradient through Darcy's law. In the original version of code "Compass", as in many other examples in literature, the continuity equations expressed in terms of absolute flux velocities were, however, employed in conjunction with the assumption of Darcy's law for the absolute flux velocities. This generated two types of errors, as described in detail in Section 5.2.

To demonstrate the potential significance of these errors a numerical analysis was performed. An isotropic loading test on a cylindrical sample with a height of 50 mm and

radius of 25 mm was simulated. The values used for the mechanical parameters within the constitutive model of Alonso, Gens and Josa [1] were those established in Chapter 3 and reported in Table 3.2. The constitutive model for degree of saturation used was the elasto-plastic relationship proposed by the author in Chapter 4 (Equation 4.5) and the values of the relevant model parameters were those reported in Table 4.2. The coefficients of water permeability k_w and air permeability k_a were assumed to vary with degree of saturation according to the reduced form of the relationships proposed by Brooks and Corey [47] given by Equations 3.5 and 3.6. The values chosen for the relevant model parameters in the permeability relationships were those reported in Table 3.8.

Axi-symmetric analyses were performed, with the finite element mesh shown in Figure 6.1. Quadrilateral eight-noded isoparametric elements were used, with the same shape functions for all the nodal unknowns. The analyses were performed with the following three different versions of the water and air continuity equations:

1. Equations of continuity of water and air correctly expressed in terms of relative flux velocities (Equations 5.10 and 5.12).

2. Equations of continuity of water and air incorrectly expressed in terms of absolute flux velocities (Equations 5.13 and 5.14). This assumption results in two different types of errors, as described in Section 5.2. The first type of error applies equally to saturated or unsaturated conditions, and is often (as it was in the original version of code "Compass") corrected by an additional compensating mistake which follows the incorrect logic of Terzaghi [73]. The second type of error applies exclusively to the unsaturated case and it is related to the distinction between Lagrangian and Eulerian temporal derivatives of degree of saturation and air density.

3. Equations of continuity of water and air expressed in terms of absolute flux velocities (Equations 5.13 and 5.14) but with dn/dt incorrectly replaced by $-d\epsilon_v/dt$. This corresponds to the original version of code "Compass" (and probably of many other numerical codes) where the first type of error involved in using Equations 5.13 and 5.14 is subsequently rectified by the above incorrect assumption (see Section 5.2).

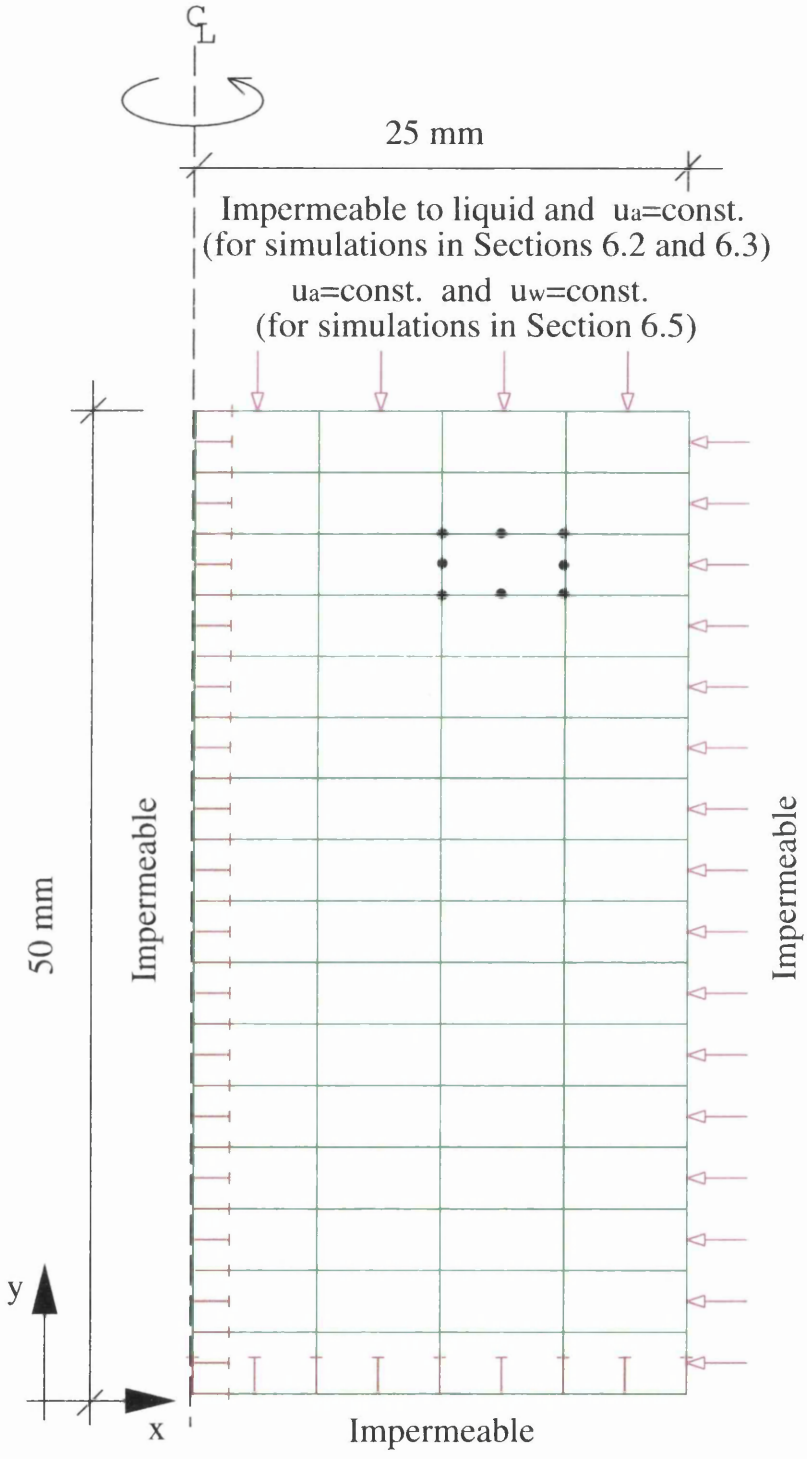

Figure 6.1: Finite element mesh and boundary conditions for axi-symmetric simulations

The presence of this compensating error would result in correct formulation of the governing flow equation for the saturated case. For unsaturated conditions, however, the formulation is still incorrect, due to the presence of the second type of error involved in using Equations 5.13 and 5.14.

The initial net stress state was assumed to be isotropic, with the mean net stress at 20 kPa throughout the sample and suction varying linearly from zero at the bottom of the sample to 700 kPa at the top of the sample. This was achieved with total stresses of 20 kPa (relative to atmospheric pressure) applied on all boundaries, pore air pressure at atmospheric value throughout the sample and pore water pressure varying from 0 to -700 kPa (relative to atmospheric value) from the bottom to the top of the sample. An example with an initial gradient of suction (and hence S_r) over the sample height was chosen in order to maximize the possible effect of the terms containing the gradient of degree of saturation, which is present in the correct formulations of Equations 5.10 and 5.12 but is missing in the incorrect versions of Equations 5.13 and 5.14. The initial value selected for the hardening parameter, $\overline{p}_o^*$, in the Alonso, Gens and Josa [1] model was 30 kPa, so that the initial stress state was inside the yield surface for all points in the sample. The numerical simulation involved rapid isotropic loading, with total normal stresses on both the cylindrical boundary and the top boundary increased from 20 kPa to 620 kPa over a period of 10 minutes, followed by subsequent equalization of pore pressures over a period of 4 hours. Throughout loading and equalization no drainage of liquid was allowed across any boundary, whereas drainage of gas was allowed at the top of the sample where the value of pore air pressure was imposed at atmospheric pressure (see Figure 6.1). Inspection of the results showed that the pore air pressure remained essentially constant at the atmospheric value throughout the sample at all times in the simulation (because of the high compressibility and permeability of the air phase). The simulation effectively represented initial undrained loading (with respect to the water phase) followed by internal redistribution of water (to equalize the suction throughout the sample).

The predicted distributions of suction across the sample at the end of loading and at times of 24 minutes and 4 hours after the end of loading are reported in Figure 6.2. The

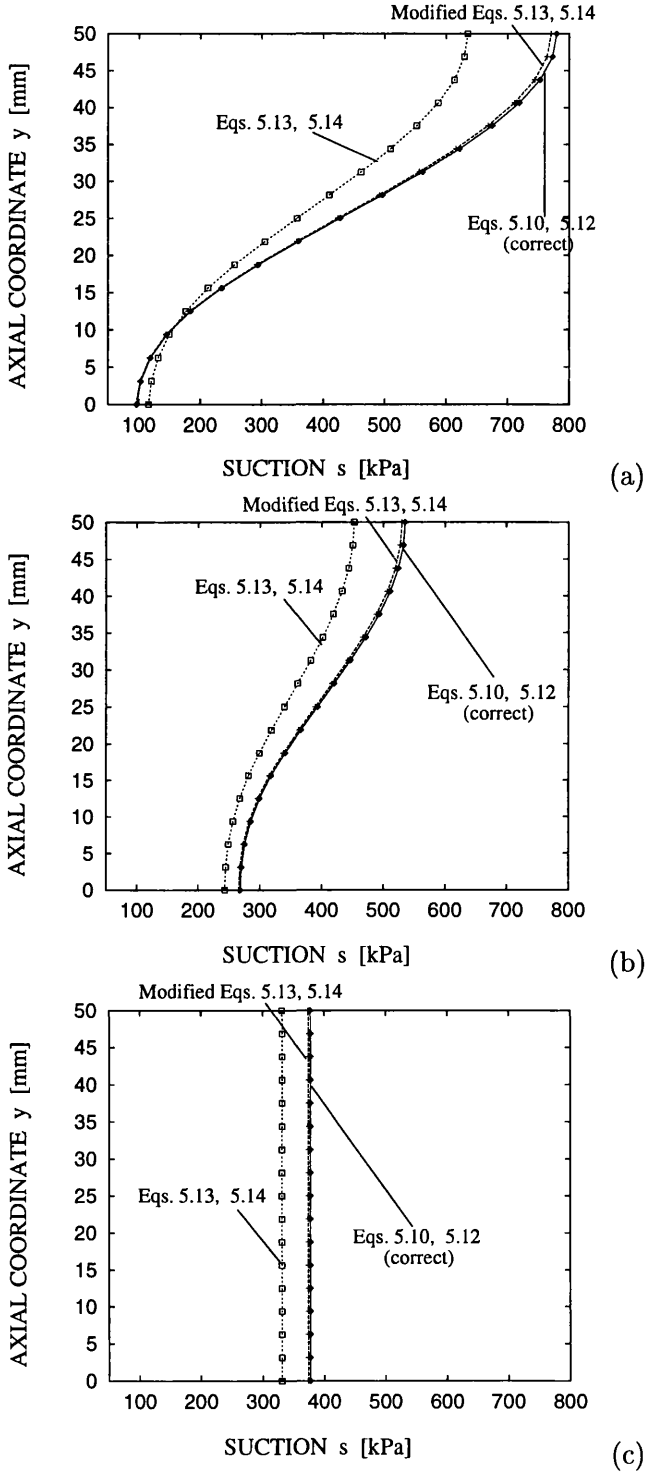

Figure 6.2: Suction across the sample: (a) at the end of loading, (b) 24 minutes after the end of loading, (c) 4 hours after the end of loading

correct results in Figure 6.2 are those predicted using the continuity equations expressed in terms of relative flux velocities (Equations 5.10 and 5.12). Inspection of Figure 6.2 reveals that incorrect use of the continuity equations expressed in terms of absolute flux velocities (Equations 5.13 and 5.14) would result in significant errors in the predicted changes of suction generated during undrained loading and that substantial errors remain even in the final equilibrium situation after internal equalization of suction. Much of this error is corrected if dn/dt is incorrectly replaced by $-d\epsilon_v/dt$ in Equations 5.13 and 5.14 (see Figure 6.2), as appears to be done in several existing finite element codes. It is, however, clearly an unsatisfactory situation, with potential for mistakes, if the published literature or documentation on such codes arrives at this result by two incorrect statements which happen, when combined, to give an approximately correct result.

The differences in Figure 6.2 between the results obtained with the modified versions of Equations 5.13 and 5.14 and those obtained with Equations 5.10 and 5.12 are attributable to the term $n(d\boldsymbol{u}_d/dt)\nabla S_r$ in the water continuity expression of Equation 5.10 (for this example, the additional terms in the air continuity expression of Equation 5.12 have no influence, because the pore air pressure remains constant throughout the sample at all times). The correct inclusion of this term results in a predicted value of suction at the end of loading which is about 9 kPa greater at the top of the sample and 1 kPa greater at the bottom of the sample than the corresponding predictions from the modified forms of the continuity equations where the gradient terms are neglected. These differences are relatively small in comparison with the absolute values of suction involved in this example. However, if these differences are compared with the changes of suction generated by the application of load, they are seen to be significant. For example, at the top of the specimen the error in computed suction of 9 kPa, arising from neglecting the term involving the gradient of S_r, is approximately 12% of the correctly computed increase of suction due to loading (an increase of 79 kPa from 700 kPa to 779 kPa). The differences in predicted values of suction attributable to the term $n(d\boldsymbol{u}_d/dt)\nabla S_r$ in Equation 5.10 remain small during the consolidation stage and correspond to a value of approximately 3 kPa after attainment of internal equalization of suction. For the specific example presented here

the influence of the term $n(du_d/dt)\nabla S_r$ in Equation 5.10 on the computed results does not seem to have significance for practical purposes. There could, however, be other loading conditions or combinations of parameter values where the influence was more significant, and a cautious approach would therefore be to include the additional terms in Equations 5.10 and 5.12. This does not appear to be the case in most existing codes for unsaturated soils.

A similar example to that shown here was presented by Gallipoli, Karstunen and Wheeler [58]. In that work, however, the state surface expression of Lloret and Alonso [22] was employed to model the variation of degree of saturation instead of the elasto-plastic relationship developed in Chapter 4. The conclusions arising from both examples were qualitatively the same. It should be noted that the numerical results for the example presented in the paper by Gallipoli, Karstunen and Wheeler [58] were affected by a minor error introduced by the author inadvertently into code "Compass", which influenced the results of those analyses where the stress state was not homogeneous over the soil domain (as the example presented in that paper). This fault was subsequently detected and, after having corrected the code, the re-computation of the analysis showed that the conclusions presented in that paper were still entirely valid.

6.3 Effect of residual flux terms

In Section 5.4.2 it was shown that, if the degree of saturation depends on the net stresses and if an elasto-plastic constitutive model for the mechanical behaviour is employed together with a stress-strain convergency algorithm, then residual flux terms arise in the two equations of flow during the convergency process for the constitutive model in each elasto-plastic time step, analogous to the role of residual forces in the equilibrium equation. These residual flux terms were missing in the original version of code "Compass", and they were subsequently incorporated by the author.

A numerical simulation was performed in order to assess the influence of residual flux terms on numerical predictions. The numerical study simulated an isotropic loading test on a cylindrical sample having the dimensions shown in Figure 6.1.

The mesh used for the axi-symmetric analysis was the same as for the example presented in Section 6.2 (see Figure 6.1), although for this case a coarser mesh could have been used due to the homogeneity of the predicted net stress state and pore pressures distribution across the sample.

The constitutive models for the stress-strain behaviour and the permeability relationships were the same as for the example presented in Section 6.2 and the relevant model parameter values are reported in Tables 3.2 and 3.8. The variation of degree of saturation was, however, modelled by the state surface expression of Lloret and Alonso [22] (Equation 2.41), as implemented in the original version of code "Compass", rather than by the elasto-plastic relationship proposed by the author in Chapter 4 (Equation 4.5). This was done to emphasize that neglecting the residual flux terms could cause errors even when using a state surface expression for degree of saturation (if this incorporated dependence on mean net stress), to highlight the possible occurrence of errors in previous simulations involving the original version of code "Compass" or other codes presented in the literature.

For the state surface expression for degree of saturation two different sets of parameters values were proposed in Chapter 3: one set, reported in Table 3.6, matching behaviour on the normal compression lines (when behaving plastically), the other set, reported in Table 3.7, selected as a compromise between elastic and plastic behaviour. In the numerical analyses presented in this section the soil was in an overconsolidated state prior to loading and most of the stress path during loading was inside the elastic domain. Therefore the second set of parameters values, reported in Table 3.7, was used for the state surface expression of Lloret and Alonso [22] (Equation 2.41).

The initial net stress state was assumed to be uniform and isotropic, with a mean net stress of 120 kPa, pore air pressure at atmospheric value and pore water pressure at -200 kPa (relative to atmospheric) throughout the sample. This gave an initial value of suction of 200 kPa throughout the sample. The initial value of the hardening parameter, $\overline{p}_o^*$ was 50 kPa, so that the value of isotropic yield stress $\overline{p}_o$ at a suction of 200 kPa was approximately 180 kPa. The loading process consisted of an increase of the applied total normal stress from 120 kPa to 220 kPa on both the cylindrical boundary and the top

boundary over a period of 1 hour. The boundary conditions for liquid and gas flows were the same as for the example described in Section 6.2 (see Figure 6.1) i.e. all boundaries were impermeable with respect to liquid flows, whereas drainage of gas was allowed at the top boundary. The results showed again that the pore air pressure remained practically constant at atmospheric pressure throughout the sample, whereas changes of pore water pressure were generated uniformly throughout the sample during loading.

The numerical analysis was performed with two different versions of the code: one including the presence of residual flux terms in the equations of continuity of water and air, as defined in Equations 5.44 and 5.45, and another one without the residual flux terms. Results are shown in Figures 6.3, 6.4, 6.5 and 6.6, where the variations of four quantities over the time of loading are reported: vertical displacement measured at the top of the sample, suction, degree of saturation and water content. The last three quantities were constant throughout the sample.

Inspection of the results shows that the differences between the two cases in terms of vertical displacement are relatively small, whereas greater discrepancies are present for the variation of suction, degree of saturation and water content. For the two plots of suction and degree of saturation (Figures 6.4 and 6.5) a clear discontinuity in the slope of the curve, marking the onset of yielding, is evident when residual fluxes are considered, whereas no discontinuity is apparent when residual fluxes are neglected. For the plot of the variation of water content (see Figure 6.6), the case when residual fluxes are considered correctly predicts no variation of water content, as would be expected since the analysis simulates an undrained test with respect to the liquid phase. In contrast, the case where residual fluxes are neglected, incorrectly predicts a change of water content after occurrence of yielding.

Further analyses were carried out by introducing a stronger dependency of the degree of saturation on the mean net stress (by selecting a higher value for the parameter d in Equation 2.41) and the results obtained from the version without residual flux terms predicted more dramatically erroneous variation of the water content after yielding and also displacements were significantly in error. Furthermore, when the parameter d in

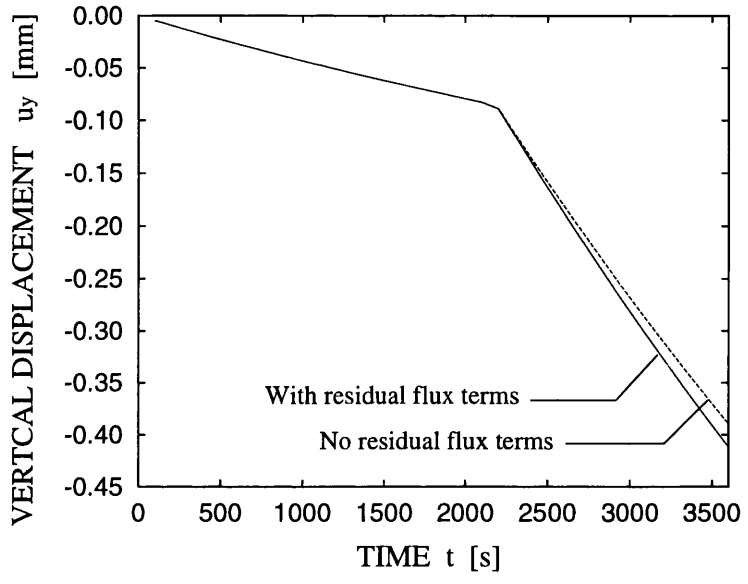

Figure 6.3: Vertical displacement at the top of the sample

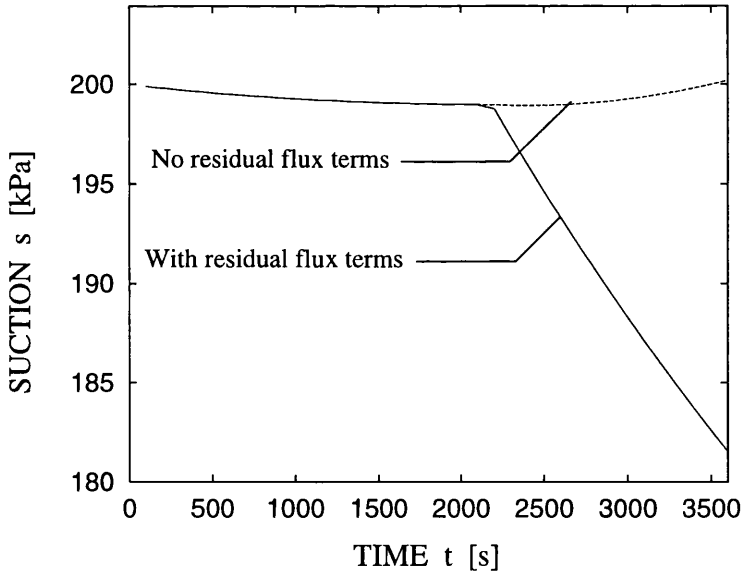

Figure 6.4: Variation of suction

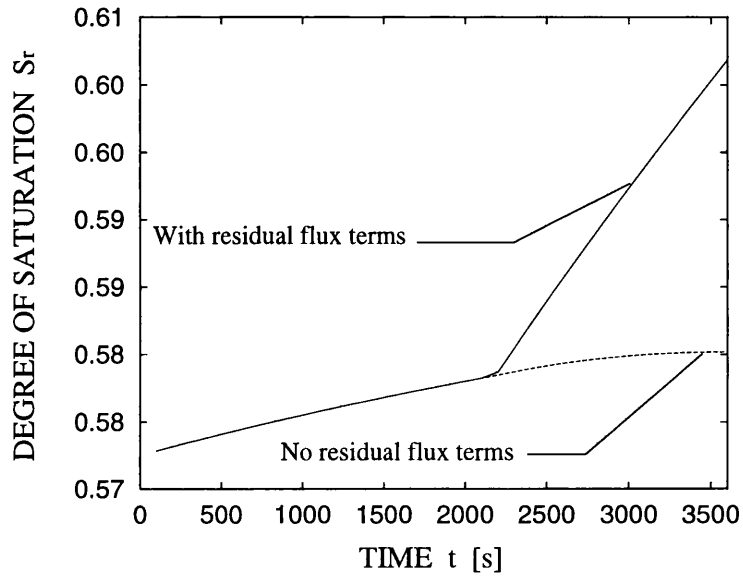

Figure 6.5: Variation of degree of saturation

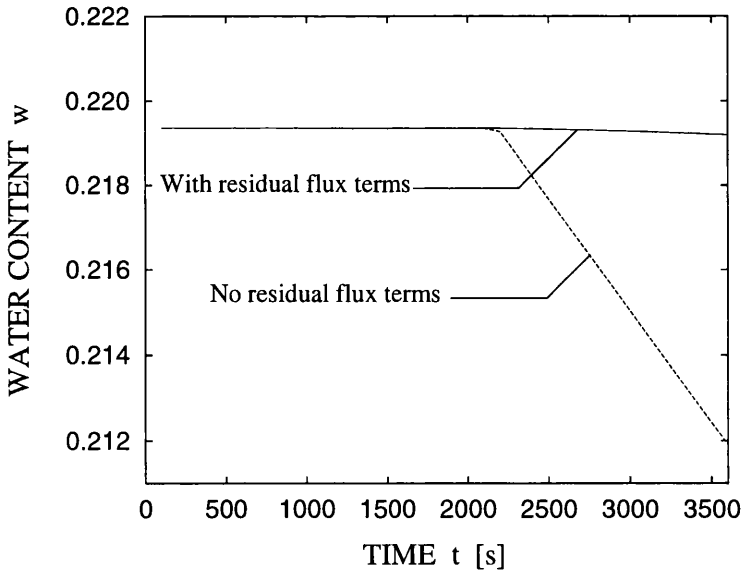

Figure 6.6: Variation of water content

Equation 2.41 was about 10 times larger than the value shown in Table 3.7, the code failed to converge if residual flux terms were omitted.

The results shown above indicate that, when a state surface for degree of saturation incorporating dependency on mean net stress is employed, the omission of residual flux terms in the stress-strain convergency algorithm induces errors in the predictions or even failure of the code. As explained in Section 5.4.3, similar residual flux terms also arise when the new relationship for degree of saturation developed in Chapter 4 is employed in combination with a stress-strain convergency algorithm. Also in this case omission of residual terms can produce significant errors in the predictions.

6.4 Effect of errors in plane-strain formulation

Section 5.4.5 described two different versions of the plane-strain implementation for an unsaturated soil with elasto-plastic mechanical behaviour: the first one was the correct formulation (Version A) whereas the second one (Version B) incorrectly assumed that the out-of-plane component of each single contribution of the total strain rate vector, $d\epsilon/dt$, in Equation 5.79 was null. The incorrect formulation was implemented in the original version of code "Compass" and has been corrected by the author in the version of the code used in this work. This erroneous formulation of the plane-strain regime is also believed to be implemented in other finite element codes (see, for example, Gatmiri, Tavakoli, Moussavi and Delage [45]) due to the history of the development of finite element programs, as explained in Section 5.4.5.

In order to assess the potential significance of these errors, simple numerical analyses were performed with both the incorrect implementation (Version B) and the correct implementation (Version A) of the plane-strain deformation regime. The numerical analyses simulated a bi-dimensional plane-strain problem having a rectangular geometry with height of 50 mm and width of 25 mm (see Figure 6.7). The two types of numerical analyses were: (a) wetting of the soil with the vertical and horizontal in-plane net stresses held constant and equal and (b) simultaneous increase of both vertical and horizontal net stresses (maintaining the two equal) while holding the suction constant. Each simulation

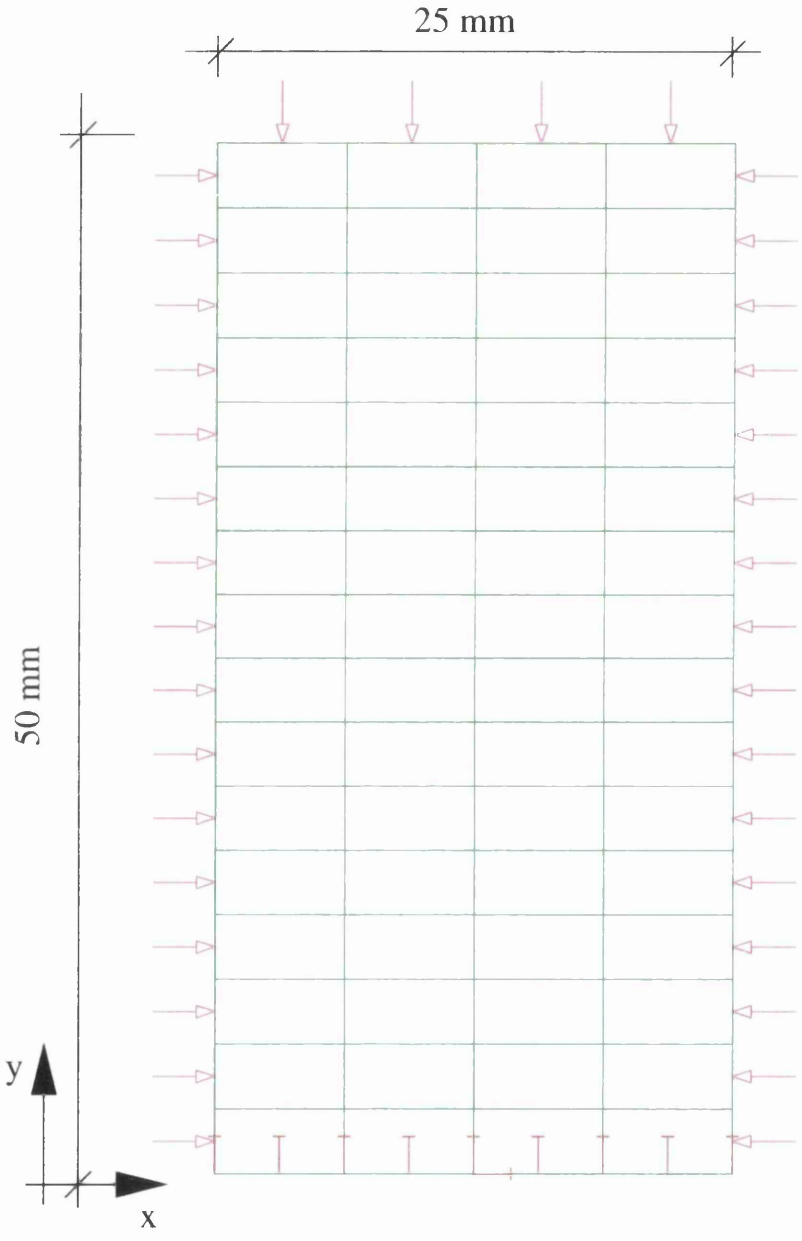

Figure 6.7: Finite element mesh and boundary conditions for plane-strain simulations

was modelled as fully drained; this means that the pore air pressure and the pore water pressure were imposed at all nodes within the mesh and they were constant for the in-plane loading (case (b)) whereas their variation was controlled for the wetting example (case (a)). The reason for performing drained analyses by imposing the variation of pore pressures at nodes is the saving of computational time as this choice avoids the coupling between the equation of equilibrium and the equations of flow. For the purpose of these analyses the coupling with the flow equations is not needed and the use of the equilibrium equation is sufficient to demonstrate the differences between the correct and the incorrect plane-strain formulations. The stress-strain behaviour with the relevant parameter values were the same as for the other simulations of this chapter (see Section 6.2). The choice of constitutive model for the variation of degree of saturation had no significance for the purpose of this example because the analysis was fully drained (i.e. pore water pressure and pore air pressure varyied in a pre-determined fashion at all nodes), as explained above.

Plane-strain analyses were performed by using the mesh shown in Figure 6.7. The mesh geometry is the same as the one of the mesh employed for the axi-symmetric analyses of this chapter (see Figure 6.1). In this case, again, a coarser discretization could have been employed due to the homogeneity of the predicted net stress state and pore pressure distribution over the soil sample.

Wetting case Figure 6.8 shows the projections of three different wetting paths on the $(s, \overline{p})$-plane for the correct version of the plane-strain formulation (Version A) and for the incorrect one (Version B). The initial net stress state was assumed to be isotropic (i.e. with the out-of-plane net stress $\overline{\sigma}_z$ equal to the two in-plane net stresses $\overline{\sigma}_x$ and $\overline{\sigma}_y$) and equal to 100 kPa, 250 kPa, or 400 kPa. The starting value of suction was taken as 200 kPa in all three simulations. In all cases the in-plane net stresses $\overline{\sigma}_x$ and $\overline{\sigma}_y$ were held constant during wetting. With the correct formulation (version A) the mean net stress, $\overline{p}$, varied during wetting, because of changes induced in the out-of-plane net stress, $\overline{\sigma}_z$, which arose in order to maintain the plane-strain condition. In contrast, version B incorrectly predicts no change of out-of plane net stress, $\overline{\sigma}_z$ and hence no change of mean net stress.

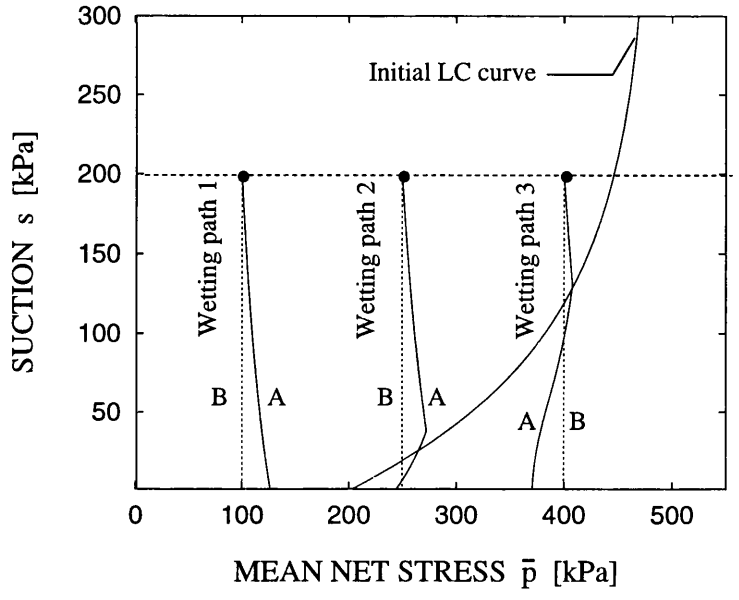

Figure 6.8: Projections on the $(s, \bar{p})$-plane of computed wetting paths

Figure 6.9 shows the vertical displacement measured at the top of the sample for the three wetting paths. In each figure a comparison is made between the correct and incorrect plane-strain formulations. Figure 6.9 (a) shows that even when the wetting path remains in the elastic region the two versions give substantially different results. In particular, the incorrect version (version B) tends to overestimate the wetting-induced swelling of the soil. Inspection of Equation 5.86 shows that in version B the vertical component, $d\epsilon_y^{se}/dt$ of the elastic strain rate vector due to a change in suction, $d\boldsymbol{\epsilon}^{se}/dt$ is incorrectly predicted as:

$$\frac{d\epsilon_y^{se}}{dt} = \frac{1}{2} A_s \frac{ds}{dt} \tag{6.1}$$

where A_s is the elastic volumetric compressibility of the soil due to a change in suction. In contrast, for this type of elastic wetting path under constant in-plane net stresses the value of $d\epsilon_y^{se}/dt$ is correctly given by version A as:

$$\frac{d\epsilon_y^{se}}{dt} = (1+\nu)\frac{1}{3} A_s \frac{ds}{dt}. \tag{6.2}$$

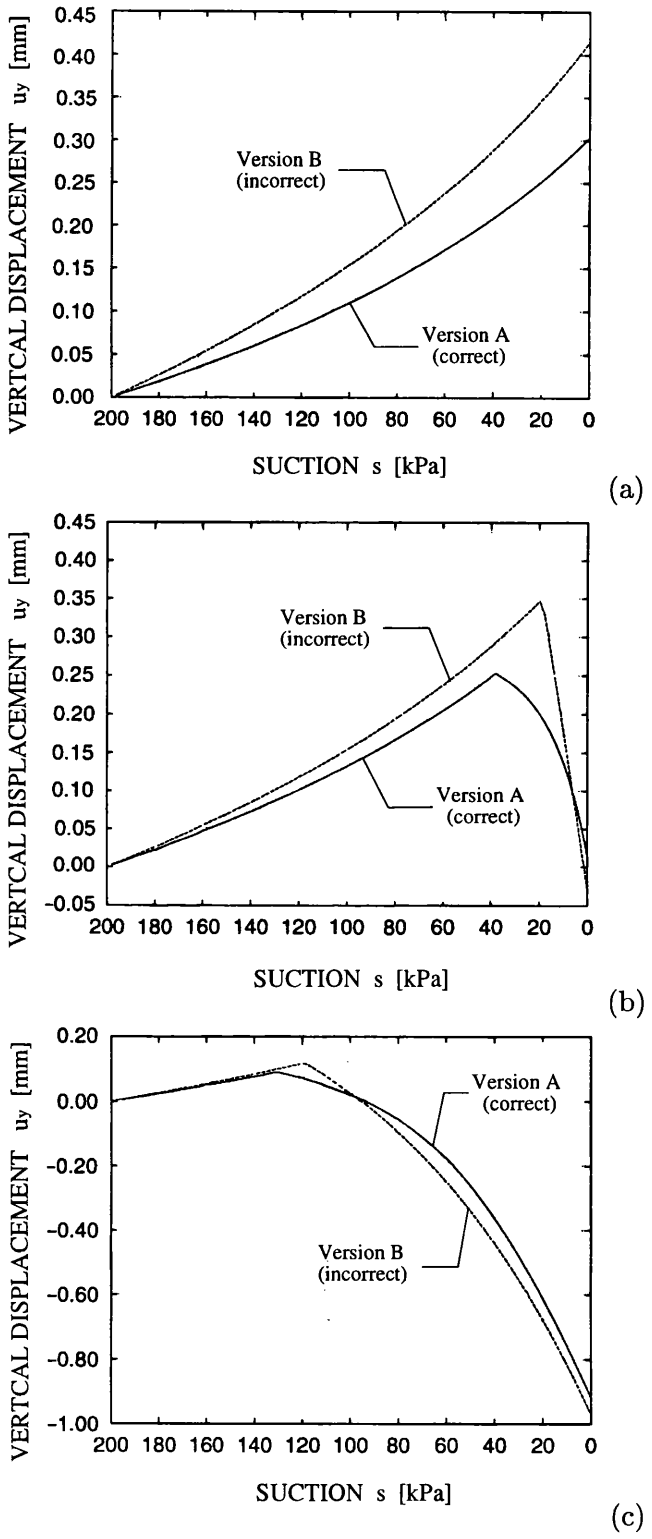

Figure 6.9: Vertical displacement at the top of the sample versus suction for: (a) wetting path 1, (b) wetting path 2, (c) wetting path 3

Equations 6.1 and 6.2 coincide only if the Poisson's ratio, ν is equal to 0.5. It is also evident from Figure 6.9 (b) that the correct and the incorrect versions of the code predict that yielding will occur at different values of suction. This is a consequence of the fact that the stress paths in the elastic region are different. In particular, the correct formulation predicts an increase in mean net stress whereas in the incorrect one the mean net stress remains constant (see Figure 6.8). Moreover, in the correct version a deviatoric component of net stress arises due to the change in the out-of-plane net stress: therefore in this case the yield point is not situated on the LC yield curve for isotropic stress states.

When plastic deformations occur (see Figures 6.9 (b) and (c)) the incorrect version tends to overestimate the collapse of the soil produced by a decrement of suction. For large wetting-induced plastic deformation (see Figure 6.9 (c)) the two curves seem to become parallel and the percentage error due to the use of the incorrect version becomes less significant as the magnitude of the collapse strains increases.

Biaxial in-plane loading case Figure 6.10 shows the projections of the two constant suction biaxial in-plane loading stress paths on the $(s, \overline{p})$-plane for both correct and incorrect plane-strain formulations. In this case the projections of the stress paths for the two formulations coincide (although a small difference is present in the final values of mean net stress, $\overline{p}$ achieved in the two cases) and, for clarity, they have been plotted slightly separated in Figure 6.11. Each simulation was carried out at a constant value of suction of either 100 kPa or 0 kPa (fully saturated). The initial net stress state was isotropic with $\overline{\sigma}_x$, $\overline{\sigma}_y$ and $\overline{\sigma}_z$ all equal to 100 kPa. Loading was then performed by increasing $\overline{\sigma}_x$ and $\overline{\sigma}_y$ at the same rate to final values of 400 kPa.

Figure 6.11 shows the vertical displacement measured at the top of the sample for the two stress paths. Each figure presents a comparison between the correct and incorrect versions of the plane-strain formulation. It is clear that the two versions give exactly the same results when the soil behaves elastically. This is because the component of the elastic strain rate vector due to change in suction, $d\boldsymbol{\epsilon}^{se}/dt$, which was present in the wetting paths, is absent and the total strain rate vector, $d\boldsymbol{\epsilon}/dt$,

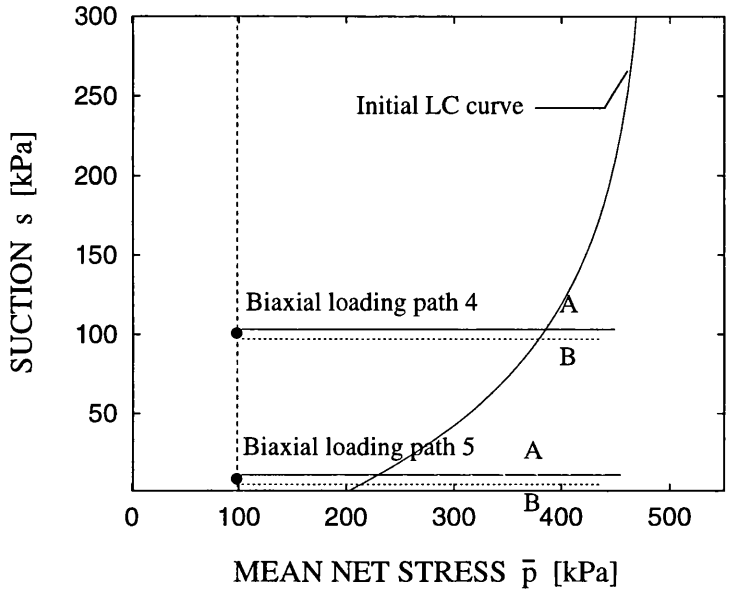

Figure 6.10: Projections on the $(s, \bar{p})$-plane of computed biaxial in-plane loading paths

coincides with the elastic strain rate vector due to a change in the net stress state, $d\boldsymbol{\epsilon}^{\sigma e}/dt$ (see Section 5.4.5).

In the plastic field the incorrect version tends to overestimate the compression of the soil produced by an increment of the in-plane stress. This tendency, however, is less evident when large plastic strains occur and, again, the two curves become almost parallel. The percentage error produced by the use of the incorrect formulation (Version B) therefore becomes less important for large values of plastic strains. This also suggests that the incorrect formulation could be difficult to detect in numerical codes implementing the traditional models for saturated soils, as can be deduced from the results of the simulation of loading test in saturated conditions (see Figure 6.11 (b)).

6.5 Effect of the improved modelling of the variation of S_r

In this section the numerical simulation of a notional laboratory test is described in order to investigate the differences in the predictions of the stress-strain response, the variation of suction and the variation of water content computed by using two different models for reproducing the variation of degree of saturation. The models considered are the

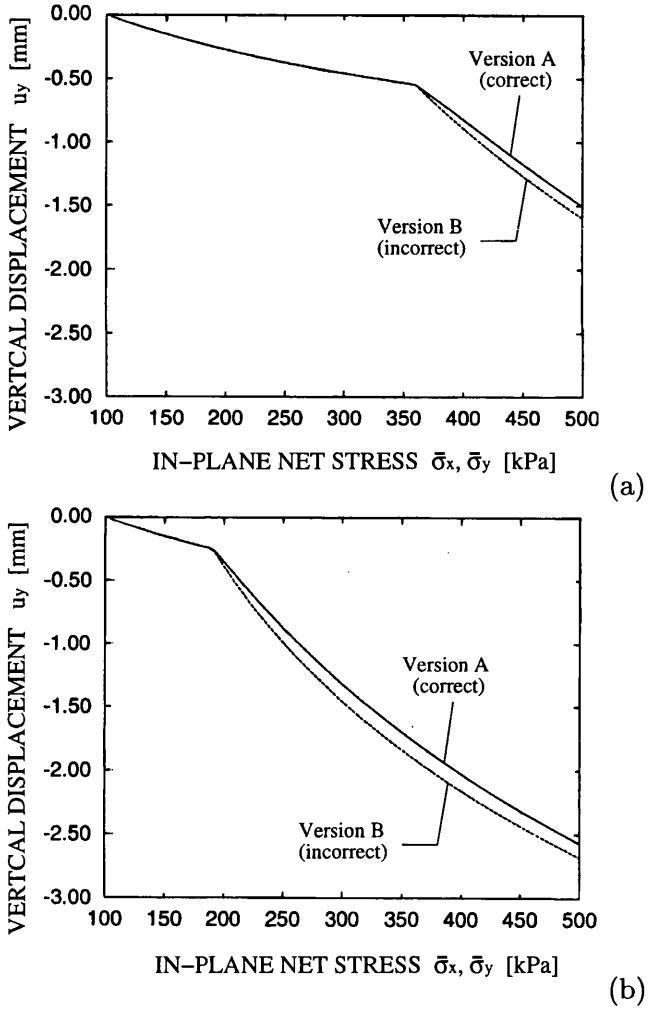

Figure 6.11: Vertical displacement at the top of the sample versus in-plane normal net stress for: (a) biaxial loading path 4, (b) biaxial loading path 5

state surface expression (Equation 2.41) of Lloret and Alonso [22] and the elasto-plastic relationship (Equation 4.5) proposed by the author in Chapter 4.

The analysis simulates a notional test on a cylindrical unsaturated soil sample involving two rapid loading stages, each one followed by a consolidation phase at constant applied stresses. The first loading process involved isotropic compression whereas the second one consisted of shearing in triaxial compression at constant mean total stress. This example was chosen to demonstrate the effects of the use of the new relationship for degree of saturation (rather than the state surface approach) for both isotropic loading and pure shearing. The simulation of the two rapid loading stages, where strong coupling of flow and deformation occurs, gives an indication of the significantly different mechanical response induced by the particular choice of constitutive model for degree of saturation. On the other hand, the results from the two subsequent consolidation stages provide information on the differences which still remain at the end of the drainage process when the distribution of suction has reached a steady state situation. The simulation of consolidation stages also gives some indication of the influence of each of the two constitutive models for degree of saturation on the consolidation time needed to reach internal equalization of suction.

The stress-strain model and the permeability relationships with the relevant parameter values were the same as those assumed for the previous simulations in this chapter (see Section 6.2). As mentioned above, the two models employed for the variation of degree of saturation were the state surface expression (Equation 2.41) of Lloret and Alonso [22], implemented in the original version of code "Compass", and the elasto-plastic relationship (Equation 4.5), proposed in Chapter 4 and implemented in code "Compass" by the author as explained in Section 5.4.3. For the state surface expression both the sets of parameters values defined in Chapter 3 were employed in the simulation. The first set (set 1), to be used in those cases where substantial plastic strains occur, was reported in Table 3.6 whereas the second set (set 2), suggested for analyses where much of the stress path remains inside the yield surface, was presented in Table 3.7. For the elasto-plastic relationship for the variation of degree of saturation the parameter values were those defined in Chapter 4

and reported in Table 4.2.

Axi-symmetric analyses were performed by using the same mesh employed in Sections 6.2 and 6.3, shown in Figure 6.1.

The initial net stress state was assumed to be isotropic, with a mean net stress of 80 kPa and a suction of 100 kPa throughout the sample. This value of suction was obtained by taking the pore air pressure at atmospheric value and the pore water pressure at -100 kPa (relative to atmospheric). The initial value of the hardening parameter, $\overline{p}_o^*$ was 70 kPa which resulted in a value of the isotropic yield stress, $\overline{p}_o$ at a suction of 100 kPa of approximately 180 kPa and hence an overconsolidated condition for the initial state of the sample. The first (isotropic) loading process lasted 10 minutes and involved an increase of the applied total stress (on both the cylindrical boundary and the top boundary) from 80 kPa to 230 kPa. This was followed by a consolidation phase of 24 hours at constant applied stress. The second (shearing) loading process started at the end of the previous consolidation stage and again lasted 10 minutes. It consisted of increasing the axial stress by 100 kPa whilst at the same time decreasing the radial stress by 50 kPa, resulting in an increment of deviator stress of 150 kPa whilst maintaining the mean total stress constant. This was followed by a second consolidation phase of 24 hours.

Throughout the two loading stages and the following consolidation phases, drainage of air and water was allowed at the top boundary, where values of pore air pressure and pore water pressure were fixed, respectively, at atmospheric pressure and -100 kPa (see Figure 6.1), resulting in an imposed value of suction of 100 kPa. All other boundaries were impermeable to both liquid and gas flows. Inspection of the results revealed that in this analysis, as in Sections 6.2 and 6.3, the pore air pressure remained sensibly constant at the atmospheric value at any point within the sample and at any time during the simulation.

Results for the rapid isotropic loading process are shown in Figure 6.12, where the variation of suction (computed at the undrained base of the sample) and the vertical displacement (computed at the top of the sample) are plotted for the three different cases of modelling of variation of degree of saturation.

Inspection of Figure 6.12 reveals that, during the initial elastic phase of loading, the

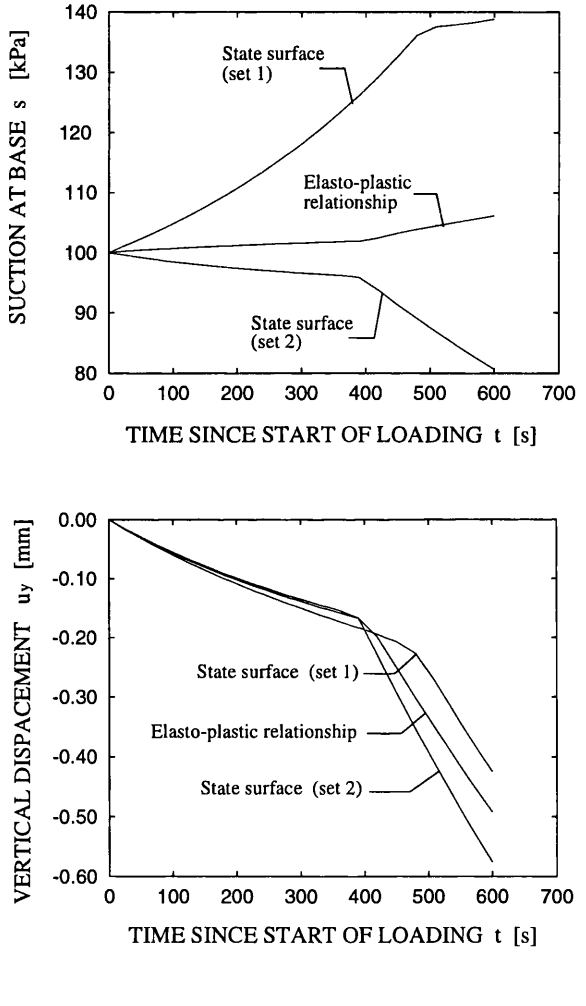

Figure 6.12: Rapid isotropic loading: (a) variation of suction at base of sample, (b) vertical displacement at top of sample

predicted variations of suction and displacement from the state surface approach using the second set of parameter values (elastic) give reasonable agreement with the results from the improved elasto-plastic relationship for degree of saturation. After the onset of yielding (marked by a discontinuity of slope in all three plots), however, it is the state surface approach using the first set of parameter values (plastic) that match better the subsequent changes of suction and displacement predicted by the improved elasto-plastic formulation for degree of saturation. These results confirm that the state surface expression is able to match reasonably well the predictions of the elasto-plastic relationship either in the elastic or in the elasto-plastic domain if an appropriate set of parameter values is used. It is not possible, however, to predict results which are in agreement with those computed by the elasto-plastic relationship throughout the whole range of loading (covering both the elastic and elasto-plastic parts of the test) by adopting a unique set of parameter values for the state surface expression.

Figure 6.13 shows the variation of suction (at the base of the sample) and vertical displacement (at the top of the sample) during the subsequent consolidation stage. Inspection of Figure 6.13 (a) indicates that internal equalization of suction is achieved for the simulation employing the elasto-plastic relationship for degree of saturation and for the simulation using the state surface expression with set 1 parameter values (plastic). In contrast, for the case where set 2 parameter values (elastic) are used for the state surface expression, the computed value of suction at the end of the consolidation stage is approximately 7 kPa less than the final equilibrium value of 100 kPa. In this case, therefore, the excess pore water pressure generated from the previous loading stage is still not completely dissipated. This result suggests that the use of the state surface approach can predict times of consolidation which are noticeably different compared to those predicted by the elasto-plastic relationship for degree of saturation. This result is caused by the different values of degree of saturation predicted in the two cases which, in turn, produces noticeably different values of coefficient of liquid permeability according to the relationship given by Equation 3.5.

At the end of the consolidation process the analysis with the state surface expression using set 1 parameter values (plastic) and the analysis with the elasto-plastic relationship

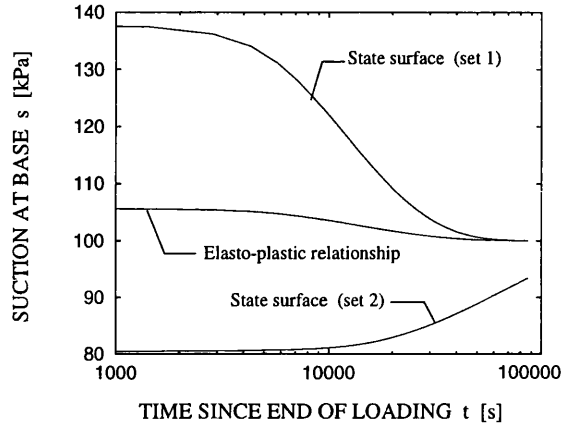

(a)

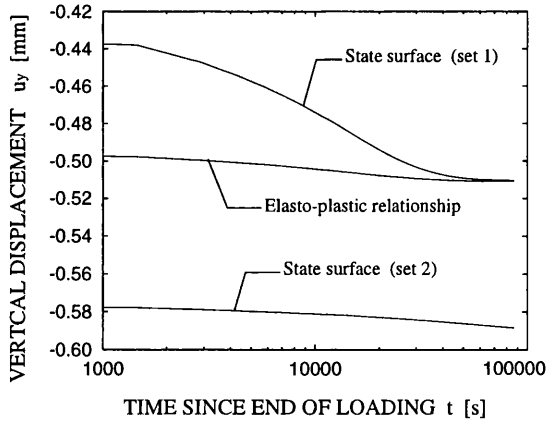

(b)

Figure 6.13: Consolidation phase after isotropic loading: (a) variation of suction at base of sample, (b) vertical displacement at top of sample

for degree of saturation predict the same final settlement (see Figure 6.13 (b)). This is because at the end of the consolidation process identical values of suction and mean net stress are achieved and the position of the LC yield curve is the same in the two cases. In these two cases, an increase in suction is predicted during initial rapid isotropic loading (see Figure 6.12 (a)) and this leads to a subsequent decrease of suction during the consolidation phase (see Figure 6.13 (a)). Expansion of the LC yield curve is, therefore, occurring during the consolidation phase, with the final stress state lying on the yield curve. In contrast, for the analysis with the state surface expression using set 2 parameter values (elastic), a decrease in suction is predicted during initial rapid isotropic loading (see Figure 6.12 (a)) and this leads to a subsequent increase of suction during the consolidation phase (see Figure 6.13 (a)). This means that the final stress state, at the end of consolidation, lies inside the LC yield curve. Greater expansion of the yield curve has, therefore occurred in this case than in the other two cases, with the consequence that the final value of predicted settlement is about 15% greater (see Figure 6.12 (b)). Therefore, even at the end of the consolidation stage when excess pore water pressures are completely dissipated, significantly different values of displacements can be predicted depending on whether the state surface approach or the improved elasto-plastic relationship for degree of saturation is used. This is because the final drained condition at the end of consolidation is attained in the two cases by following different stress paths which can involve different amounts of plastic strain.

Results for the rapid shearing stage are shown in Figure 6.14. For the analysis using the state surface expression with set 1 parameter values (plastic) and for the analysis using the elasto-plastic relationship for degree of saturation, the stress state at the start of shearing lies on the yield locus and, therefore, elasto-plastic strains occur from the start of loading in both these analyses. This is not the case for the state surface expression using set 2 parameter values (elastic) which starts from a stress state lying inside the yield locus. Therefore in this case, there is an initial purely elastic phase, followed by a yield point which is clearly marked by a discontinuity in the slope of the curves reported in Figures 6.14 (a) and (b). Figure 6.14 (a) shows different patterns of suction variation

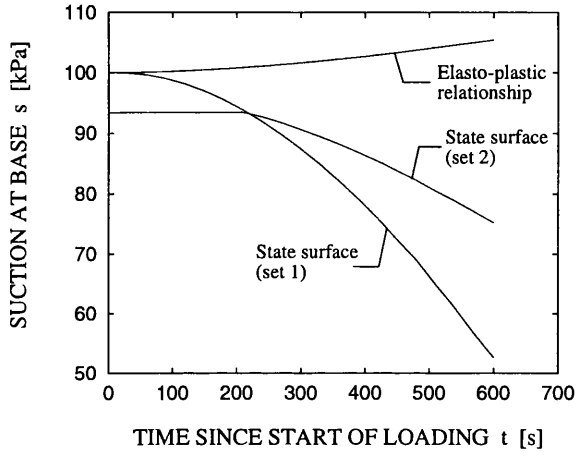

(a)

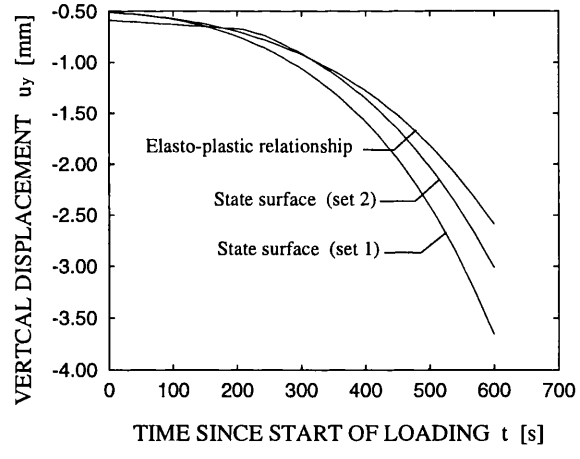

(b)

Figure 6.14: Rapid shearing: (a) variation of suction at base of sample, (b) vertical displacement at top of sample

depending whether the state surface approach for degree of saturation or the elasto-plastic relationship for degree of saturation is employed. In particular, with the state surface approach, for both sets of parameter values, the computed results indicate a decrease of suction, which is more significant than the corresponding increase in suction observed with the elasto-plastic relationship. The different predictions of suction variation affect the mechanical response: significantly greater values of displacements are computed at the top of the sample when the state surface approach for degree of saturation is used, as shown in Figure 6.14 (b).

Figure 6.15 shows the variation of suction (at the base of the sample) and vertical displacement (at the top of the sample) during the consolidation stage following shearing. It is again noticeable that with the state surface approach using set 2 parameter values (elastic), equalization of suction is incomplete after 24 hours (see Figure 6.15 (a)), because lower values of degree of saturation are predicted than for the two other analyses, and this results in lower values of liquid permeability. The vertical displacements observed during consolidation (see Figure 6.15 (b)) are given by elastic shrinkage (associated with an increase of suction during consolidation) for the two analyses employing the state surface expression, and by elasto-plastic collapse (associated with a decrease of suction during consolidation) for the analysis employing the elasto-plastic relationship. The location of the LC yield curve (i.e. the value of the hardening parameter $\overline{p}_o^*$) at the end of consolidation is different in all three cases, and hence all three predict different final settlements. For the two cases using the state surface approach the final stress state lies inside the LC yield curve and the location of the yield curve at the end of consolidation corresponds to the position achieved at the end of the rapid shearing stage. In contrast, for the analysis employing the elasto-plastic relationship, the final stress state lies on the LC yield curve. Inspection of Figure 6.15 (b) reveals that the analysis employing the state surface expression using set 1 parameter values (plastic) estimates a final vertical displacement that is almost 40% greater than that predicted by the analysis employing the elasto-plastic relationship for degree of saturation. This overestimation is reduced to approximately 13% if the state surface expression using set 2 parameter values (elastic) is employed.

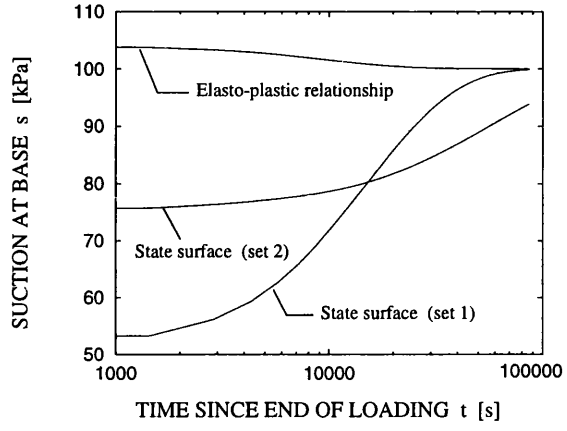

(a)

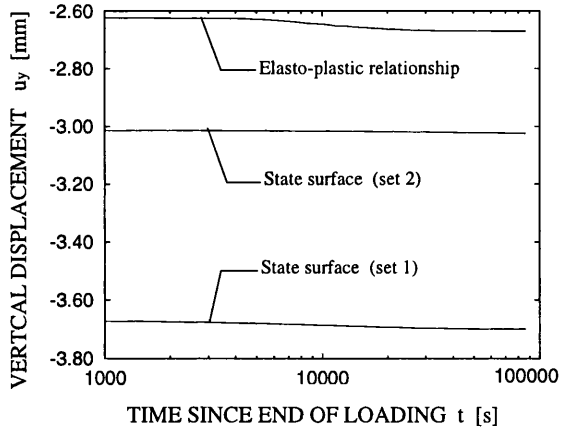

(b)

Figure 6.15: Consolidation phase after shearing: (a) variation of suction at base of sample, (b) vertical displacement at top of sample

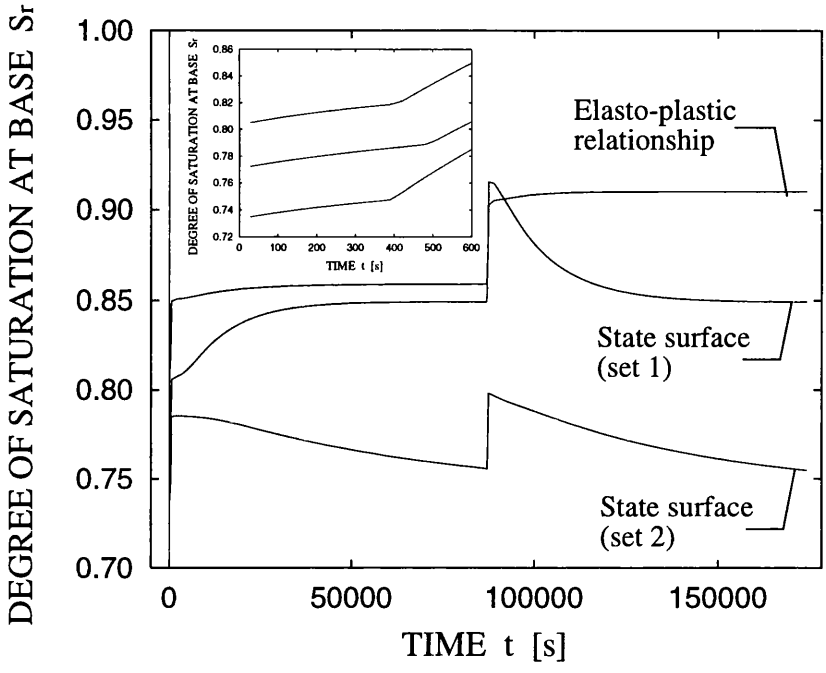

Figure 6.16: Variation of degree of saturation at base of sample during all 4 test stages

Figures 6.16 and 6.17 show the variations of degree of saturation and water content with time at the base of the sample throughout the whole test. In Figure 6.16 the almost instantaneous changes of degree of saturation refer to the two rapid loading stages (an expanded view of the first rapid isotropic loading stage is also included in the figure). Each of these sharp changes is followed by a gradual variation of degree of saturation with time which refers to the subsequent consolidation phases. Inspection of Figure 6.16 reveals that the values of degree of saturation predicted by the three simulations at the start of the test are noticeably different. The difference of predictions between the state surface relationship using set 1 parameter values (plastic) and the elasto-plastic relationship reduces at the end of the first consolidation stage. This is an expected result as the parameter values in both these relationships were selected on the basis of laboratory test data defining the isotropic normal compression lines and, in both analyses, the same isotropic normally consolidated stress state is predicted at the end of the first consolidation stage. However, at the end of the second consolidation process (after shearing), significantly different values of degree of

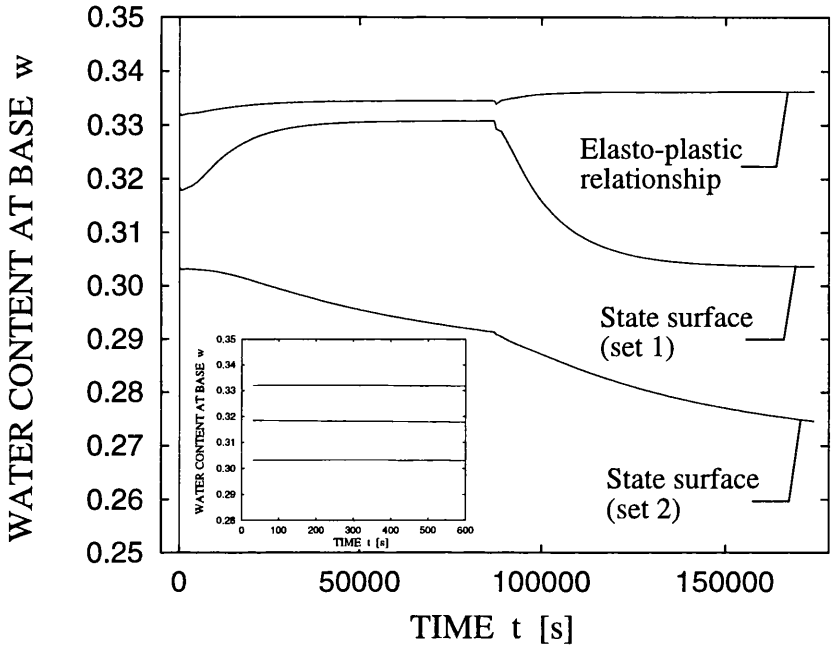

Figure 6.17: Variation of water content at base of sample during all 4 test stages

saturation are again predicted in all the three cases.

In each of the two analyses employing the state surface expression the value of degree of saturation predicted at the end of the second consolidation phase (after shearing) is similar to that occurring at the end of the first consolidation phase (after isotropic loading). This is explained by the fact that, at these two times, similar values of mean net stress and suction are attained within the soil sample and the stress states differ only in the value of the deviator stress. As the assumed state surface expression for degree of saturation does not involve any dependency on the deviator stress, similar values of degree of saturation occur at these two times.

Inspection of Figure 6.17 shows that the analysis employing the elasto-plastic relationship for degree of saturation predicts much smaller variations of water content throughout the test than the predictions from the other two simulations. For the degree of saturation variation, noticeably different values of water content are predicted at the beginning of the test by the three models. The differences between the predicted values of water content

from the analysis using the state surface expression with set 1 parameter values (plastic) and the corresponding predictions when using the elasto-plastic relationship for degree of saturation reduce at the end of the first consolidation phase, for the same reason as explained for the variation of the degree of saturation. Again, however, significantly different values of water content are predicted in all three analyses at the end of the second consolidation phase. Finally, the expanded view of the variation of water content during the first isotropic loading, shown in Figure 6.17, reveals that water content remains essentially constant throughout this phase of the test, suggesting that fully undrained conditions occur at the base of the sample during the two rapid loading stages.

6.6 Concluding remarks

In this chapter the significance of the various improvements incorporated in code "Compass" by the author has been assessed by performing numerical analyses of very simple boundary value problems, such as simulations of the behaviour of soil specimens under specified stress paths. In each analysis the results computed by using the improved version of the code have been compared with those obtained from an appropriate earlier version of the code without the relevant change. The changes made by the author to code "Compass" are believed to have general relevance, as they refer to issues which also apply to other finite element codes presented in the literature.

In Section 6.2 a numerical example was presented in order to investigate the consequence of incorrectly relating, in the two equations of continuity of water and air, the absolute flux velocities of the liquid and gas phases (rather than the flux velocities relative to the soil skeleton) to the relevant potential gradient through the Darcy's law. This inconsistency was present in the original version of code "Compass" and a similar incorrect assumption can also be found in other examples in the literature. The incorrect and correct formulations of the flow equations, implemented respectively in the original and improved versions of code "Compass", were used to simulate a problem involving isotropic loading of a cylindrical soil specimen. The results showed substantial differences in the predicted changes of suction during undrained loading and subsequent consolidation, with

noticeable errors remaining even at the end of the consolidation process. It was also shown that much of this error can be corrected if the term dn/dt in the equations of continuity expressed in terms of absolute flux velocities is replaced by $-d\epsilon_v/dt$, as appears to be done in several finite element codes even if not explicitely stated in the relevant documentation. The remaining omission of terms such as $n(d\boldsymbol{u}_d/dt)\nabla S_r$ in the water continuity equation and $-n(1-H)(d\boldsymbol{u}_d/dt)\nabla S_r$ and $(1-(1-H)S_r)(n/\rho_a)(d\boldsymbol{u}_d/dt)\nabla\rho_a$ in the air continuity equation produced errors in the prediction of suction which were relatively small if compared with the absolute values of suction in this example. These errors, however, were not insignificant if compared with the change of suction generated during undrained loading. Moreover, there may be other circumstances where the influence of this omission becomes more significant than in the particular example chosen in this work.

A numerical study was presented in Section 6.3 in order to explore the importance of the changes to the convergency algorithm of code "Compass" performed by the author. In particular it was shown in Section 5.4.2 that, if an elasto-plastic stress-strain model is employed together with a stress-strain convergency algorithm, and if the degree of saturation depends on net stress state (through, for example, a state surface expression or an elasto-plastic relationship for degree of saturation), residual flux terms must be included in the flow equations during the convergency process within each elasto-plastic time step, as well as residual force terms in the equilibrium equation. The expressions for the residual flux terms in the two flow equations for the case when a state surface approach for degree of saturation is employed, were derived in Section 5.4.2 (analogous definitions were also given in Section 5.4.3 for the case when the new elasto-plastic relationship for degree of saturation, proposed by the author in Chapter 4, is employed). The numerical study showed that substantial errors may arise if these residual flux terms are omitted. Further analyses not presented in this work also indicated that, if parameter values different from those adopted in this example were chosen for the state surface expression (introducing a stronger dependency of degree of saturation on the mean net stress), more significant errors were predicted and, in some cases, the code failed to converge if residual flux terms were omitted.

In Section 6.4 a numerical analysis was presented in order to assess the significance of the corrections to the plane-strain deformation regime for an elasto-plastic unsaturated soil originally implemented in code "Compass". The incorrect formulation present in the original version of code "Compass" can also be found in other examples in the literature due to historical reasons related to the development of finite element programs (see Section 5.4.5). The numerical analysis compared the incorrect and correct formulations of the plane-strain deformation regime for a wetting stress path (with in plane net stresses held constant) and a biaxial in-plane loading stress path (at constant suction). For wetting, the incorrect version tends to overestimate substantially the swelling of the soil in the elastic phase. It also tends to overestimate the collapse compression due to a decrease of suction in the plastic phase. This effect, however, is more evident for small values of plastic strains whereas for large values of plastic strains the correctly predicted and incorrectly predicted suction-displacement curves seem to become parallel. For constant suction biaxial in-plane loading, the two versions give identical results in the elastic field. When plastic strains occur the incorrect version predicts greater deformations for the same increment of in-plane net stress. This tendency is, however, less evident than in the wetting case and, for large values of plastic strains, the predicted load-displacement curves again become almost parallel. The incorrect formulation could be difficult to detect in numerical codes implementing traditional models for saturated soil, as can be deduced from the results of the simulation of the biaxial in-plane loading test at zero suction.

In Section 6.5 the simulation of a notional laboratory test was presented in order to compare the predictions of displacement, variation of suction and variation of water content obtained by the improved elasto-plastic modelling of the variation of degree of saturation proposed in Chapter 4, with the corresponding predictions computed by using the state surface approach for degree of saturation implemented in the original version of code "Compass". The test consisted of a rapid isotropic loading stage followed by a subsequent consolidation phase, and then a rapid shearing stage, again followed by a subsequent consolidation phase. The results from the rapid isotropic loading stage showed that, if the loading path involves an initial elastic section followed by yielding and a subsequent elasto-

plastic section, it is not possible while using a single set of parameter values in a state surface expression for degree of saturation, to obtain a reasonable match through the whole loading process to the results predicted by using the improved elasto-plastic relationship for degree of saturation. This result confirms the limitations of the state surface approach for the prediction of degree of saturation already highlighted in Chapters 2 and 3.

During the rapid loading stages presented in Section 6.5, simulations employing different models for the variation of degree of saturation produced significantly different predictions of suction changes. This in turn influenced the stress path followed by the soil, causing noticeably different responses in the strain behaviour. For example, at the end of the consolidation phase after isotropic loading the vertical displacement at the top of the sample computed by the state surface expression using set 2 parameter values (i.e. the set to be used in those analyses where much of the stress paths remain inside the yield locus) was approximately 15% greater than the case where the elasto-plastic relationship for degree of saturation was employed. This difference was even more significant at the end of the second consolidation phase (after shearing), where the state surface expression using set 1 parameter values (i.e. the set to be used in those analyses where substantial plastic strains occur) estimated a vertical displacement that was almost 40% greater than the one computed by the elasto-plastic relationship for degree of saturation. Another interesting result was that the analysis with the elasto-plastic relationship for degree of saturation predicted relatively small variation of water content throughout the various test stages, whereas substantially larger changes were predicted by the state surface expression for degree of saturation. This was because the elasto-plastic model for degree of saturation predicts much smaller changes of suction during undrained loading than the state surface relationship. Finally, significantly different consolidation times were computed for the complete dissipation of the excess pore water pressure generated by the rapid loading stages if the state surface equation using set 2 parameter values was employed. This is clearly a consequence of the relationship between the coefficient of liquid permeability and the degree of saturation (see Equation 3.5). When the elasto-plastic relationship for degree of saturation is employed, or the state surface expression with set 1 parameter values,

greater values of degree of saturation and consequently greater values of the coefficient of liquid permeability are predicted than in the case where the state surface expression with set 2 parameter values is used, which explains the shorter time needed for consolidation.

Chapter 7

FE modelling of pressuremeter tests in unsaturated soils

7.1 Introduction

This chapter describes how the code "Compass" (improved as discussed in Chapter 5) was used to analyse a boundary value problem. The chosen boundary value problem was the expansion of a pressuremeter device in an unsaturated soil.

In Chapters 5 and 6 the results of simple numerical analyses, such as simulations of laboratory tests, were presented in order to qualitatively assess the implications of the changes carried out by the author to code "Compass" and to validate the correctness of these modifications. In the present chapter the numerical study of pressuremeter tests in unsaturated soil is presented to demonstrate the application of the improved version of code "Compass" to the analysis of a more complex boundary value problem. A comparison is also presented between the numerical predictions obtained with the state surface equation for degree of saturation (Equation 2.41) of Lloret and Alonso [22] (implemented in the original version of the code) and those computed with the elasto-plastic relationship proposed by the author in Chapter 4.

In Section 7.2 the basic features of the pressuremeter testing technique are summarized and a brief overview of previous work related to finite element simulations of pressuremeter tests in saturated soils is given. The study presented in this chapter is the first finite element coupled flow-deformation analysis of pressuremeter tests in unsaturated soil and

the objectives of this work are discussed in detail in Section 7.3. The numerical modelling of the problem is described in detail in Sections 7.4 to 7.7.

7.2 Pressuremeter test: introduction to the technique and overview of previous FE analyses

Pressuremeter testing is a method of ground investigation used to determine the mechanical properties of a soil and the in-situ value of horizontal stress at a particular depth within a soil deposit. During a pressuremeter test a cylindrical probe, with an expandable flexible membrane on the surface of its test section, is inserted within a borehole in the ground. Once the pressuremeter probe has been positioned at the test location, the membrane is expanded, applying a uniform pressure to the walls of the borehole. The applied pressure and the amount of expansion are plotted as a cavity pressure against cavity expansion curve, which is interpreted either for determining mechanical properties and in-situ stress state of the soil or for directly determining design parameters.

Various pressuremeter testing techniques exist and these differ essentially in the procedure adopted for the insertion of the pressuremeter probe in the ground. The two main categories are:

1. Pre-bored pressuremeter tests (PBP). In this type of test the probe is lowered inside a pre-bored hole which has a slightly bigger diameter than the probe itself.

2. Self-bored pressuremeter tests (SBP). In this type of test the probe is equipped with a drilling system. The idea is that the probe bores its own way to the test location by progressively replacing the ground removed by drilling. This technique is designed to minimize the level of disturbance to the surrounding soil.

The cavity pressure-cavity expansion curve recorded during the test can be interpreted subsequently by means of analytical or numerical methods in order to determine the mechanical properties of the soil. The analytical methods are based on fitting a theoretical solution, derived for the case of an infinitely long cylindrical cavity expanding in an unbounded homogenous medium, to the experimental cavity pressure-cavity expansion

curve. For saturated soils, analytical solutions for the problem of the expansion of an infinitely long cylindrical cavity are available for different types of constitutive relationships. By fitting the analytical solution to the experimental curve it is possible to determine the value of the model parameters relevant to the constitutive model assumed in the analytical derivation. An alternative method consists of modelling the pressuremeter expansion process by means of numerical techniques such as the finite element method. This approach, though more laborious than the previous one, can lead to increased accuracy in the definition of the theoretical expansion curve because it can account for the real geometry of the pressuremeter device. Moreover, while closed form analytical solutions of the cavity expansion problem are available only for a limited number of stress-strain relationships, the numerical approach allows a wider range of constitutive models for the soil to be considered. Finally, the use of numerical techniques allows the modelling of the coupling between flow and deformations, providing a tool which can take into account the effect of rate of loading on the test results and which can provide information on the response after expansion when a consolidation process takes place (e.g. holding tests).

A number of numerical studies of pressuremeter testing and cylindrical cavity expansion in saturated soil have been presented in the literature. Although in some applications the finite difference method was employed (see, for example, Pyrah, Anderson and Hashim [89]), the majority of these studies use the finite element technique. Some of them are simulations of fully drained tests in terms of effective stresses (see for example Fahey and Carter [90]) or fully undrained in terms of total stresses (see for example Houlsby and Carter [91], Zentar, Moulin and Hicher [92]), others model cases where coupling of flow and deformation takes place (see, for example, Fioravante, Jamiolkowski and Lancellotta [93], Charles, Yu and Sheng [94]). Often an objective of these studies is to fit the numerical simulations to experimental pressuremeter test data in order to determine the values of the mechanical parameters of the soil (i.e. the mechanical parameters relevant to the constitutive models employed for the numerical simulations), as in the work presented by Fahey and Carter [90] and Fioravante, Jamiolkowski and Lancellotta [93]. In some other papers numerical simulations have been employed to investigate the effect of the

finite length of the pressuremer device on the interpretation of the experimental cavity pressure-cavity expansion curve (Houlsby and Carter [91], Charles, Yu and Sheng [94], Zentar, Moulin and Hicher [92]).

The application of the pressuremeter technique to unsaturated soils is still highly tentative, because of difficulty in the interpretation of test results, and important questions relating to the numerical or analytical modelling of such tests are still to be answered. The only application of the finite element technique to the study of pressuremeter tests in unsaturated soil published to date is due to Consoli, Schnaid and Mantaras [95]. In this work it was assumed that the expansion of the pressuremeter device is a fully drained process so that the value of suction within the soil remains constant during the test. This hypothesis simplifies the problem, because it avoids the need for fully coupled flow-deformation analyses. In addition, it allows the same constitutive models employed for drained analyses in saturated soils to be used for unsaturated soils, based on the assumption that unsaturated soils at constant suction behave qualitatively in the same way as saturated soil in drained conditions. Therefore, the same stress-strain relationship may be used in the two cases (as long as a dependency of the model parameters on the level of suction is accounted for).

7.3 Objectives of the work

The work presented in this chapter is a study of pressuremeter tests in unsaturated soil based on coupled flow-deformation finite element analyses. This is achieved by employing constitutive models (stress-strain and degree of saturation relationships) which are specific to unsaturated soils and take into account explicitly the variation of suction.

One objective of this work is to demonstrate the capability of the version of code "Compass" improved by the author, when applied to the study of a boundary value problem in unsaturated soil involving coupling of flow and deformation. This particular boundary value problem (the pressuremeter test) was chosen for a number of reasons. Firstly, the pressuremeter test is a closer representation of a bi-dimensional problem occurring in geotechnical engineering than any plane-strain analysis which is a bi-dimensional approximation of a true three-dimensional geotechnical case. Secondly, the pressuremeter test is

a similar process to the expansion of an infinitely long cylindrical cavity in an unbounded medium, for which rigorous analytical solutions are available for several types of constitutive models. Consequently in one of the analyses performed in this work, which simulates a pressuremeter test in overconsolidated soil producing an entirely elastic response in the early stage of the expansion process (see Section 7.7), the analytical solution for the expansion of a cylindrical cavity in a monophase linear elastic material can be used to assess the correctness of the computed predictions. Finally, the pressuremeter has the potential to be a useful in-situ testing technique for determining unsaturated soil parameters if a satisfactory method of test interpretation can be developed, and an objective of this study is to improve current understanding of pressuremeter tests in unsaturated soils, to assist interpretation of test results.

With reference to the final point, a number of numerical simulations illustrated in this chapter investigate the effect of different rates of expansion on the coupling between flow and deformations during pressuremeter expansion in an unsaturated soil. Suction monitored pressuremeter tests in unsaturated granite residual soils of southern Brazil by Schnaid and co-workers (private communication) seem to validate the assumption of constant values of suction in the zone of soil around the cavity during pressuremeter expansion. In these tests, constant values of suction were measured by tensiometers at radial distances from the borehole axis of 30 cm and 60 cm. The hypothesis of fully drained conditions, on which some proposed numerical and analytical methods of interpretation are based (see Consoli, Schnaid and Mantaras [95], Schnaid and da Silva [96]) may, however, be acceptable under particular circumstances (e.g. fissured soils) but it is debatable as a general assumption. Further investigation was needed, therefore, to explore under what circumstances the expansion process could be considered as fully drained.

Results from numerical simulations of pressuremeter tests at different rates of expansion are presented in Section 7.6 in order to explore the range of conditions for which it is acceptable to consider the pressuremeter test as a drained process. This work does not represent, however, a full parametric study and the results are restricted to the constitutive models, set of model parameters values and initial stress state assumed in these numerical

analyses. Further research on this topic is needed in order to extend this work and propose a complete relationship (accounting for the influence of each parameter of the constitutive models and of the initial stress state) which could be used in practical situations to assess whether it is appropriate to treat a pressuremeter expansion test in an unstaurated soil as a drained process.

Another objective of this study is to explore the effect that the different relationships for describing the variation of degree of saturation have on simulations of pressuremeter tests in unsaturated soils. In particular two different options were considered: the state surface expression for degree of saturation of Lloret and Alonso [22] which was implemented in the original version of code "Compass", and the new elasto-plastic relationship for degree of saturation proposed in Chapter 4 and implemented by the author in code "Compass" as described in Chapter 5.

The study of the influence of rate of expansion on the coupling between flow and deformations during pressuremeter tests was undertaken for a normally consolidated unsaturated soil. A single analysis of pressuremeter expansion in an overconsolidated unsaturated soil is presented in Section 7.7.

7.4 Problem definition

7.4.1 Pressuremeter device and test procedure

The type of pressuremeter test modelled was a self-boring pressuremeter test (SBP). The problem was modelled according to the geometry and dimensions of the Cambridge self-boring pressuremeter (CSBP) as developed at Cambridge University in 1971 (see Wroth and Hughes [97]). This device has a radius, R_o, of 42 mm and a ratio between the length and the radius of the expanding section equal approximately to 12. A schematic representation of the Cambridge self-boring pressuremeter is shown in Figure 7.1 and a detailed description of the device and method of operation is given by Clarke [98].

This type of pressuremeter test is simpler to model than a pre-bored pressuremeter test, which would require also the modelling of the process of excavation of the borehole in order to reproduce the changes of the in-situ net stresses and suction produced by

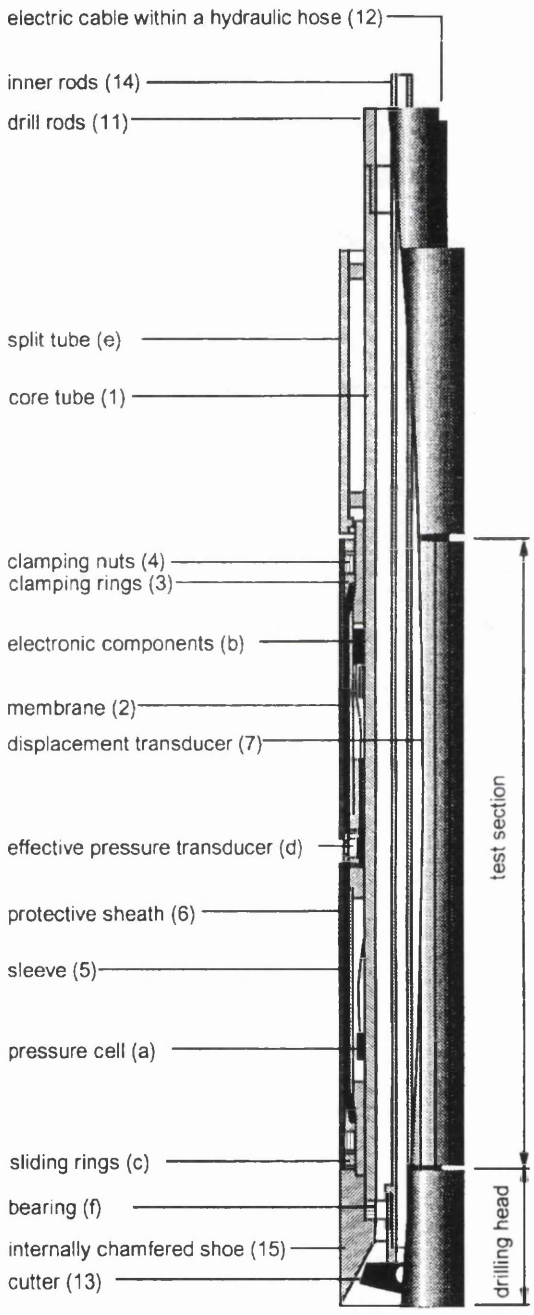

Figure 7.1: Schematic representation of the Cambridge self-boring pressuremeter (after Clarke [98])

excavation.

Even for self-boring pressuremeter tests, the installation process can produce an alteration to the in-situ distribution of suction and net-stresses as the probe advances. The importance of this effect depends on the installation procedure adopted and it was neglected in this study in the interest of simplicity.

7.4.2 Material parameters and in-situ stress state

The set of material parameters used in the simulations was the same as used in the other numerical examples presented in this thesis. The selection of the values of these material parameters is described in details in Chapters 3 and 4.

The parameter values for the stress-strain relationship of Alonso, Gens and Josa [1] are reported in Table 3.2. Two differences regarding the modelling of the elastic behaviour were, however, introduced. Firstly, a constant value of Poisson's ratio, $\nu = 0.3$, was assumed instead of a constant value of 10 MPa for the shear modulus, G. This involved a modification to the original version of code "Compass", where the elastic behaviour was described in terms of the shear modulus. The modification was considered appropriate as it was observed that, with $G = 10$ MPa, negative values of Poisson's ratio were occurring in a localized zone of soil at the extremities of the pressuremeter membrane, which resulted in a highly unrepresentative elastic mode of deformation. Negative values of Poisson's ratio were caused by a significant decrease in the value of mean net stress at the extremities of the membrane resulting in a very low value of the bulk modulus. Clearly, the choice of a constant value of Poisson's ratio has the drawback of implying a non-conservative "elastic" relationship, because the shear modulus depends on the mean net stress (see Zytynski, Randolph, Nova and Wroth [99]). This choice seemed, however, a more realistic option. A constant value of Poisson's ratio was also assumed in other finite element studies of pressuremeter tests in saturated soil using Cam-Clay type models, such as the one by Charles, Yu and Sheng [94].

The second difference was that a lower limit value of the bulk modulus, K, of 200 kPa was enforced in the code. This change was achieved by modifying the original implementation in code "Compass" of the elastic part of the constitutive model of Alonso, Gens and

Josa [1]. The modification was dictated by the need to avoid an ill-conditioned system of equations when values of mean net stress close to zero were attained in very localized regions of the soil domain located at the two extremities of the pressuremeter membrane (where elastic unloading took place). The ill-conditioning was due to the prediction, according to the Alonso, Gens and Josa [1] model, of values of bulk modulus and specific volume tending respectively to zero and infinity when the value of mean net stress tended to zero.

The parameter values for the degree of saturation relationship presented in Chapter 4 (Equation 4.5) are reported in Table 4.2.

The initial distributions of net stress and suction were assumed constant throughout the soil domain. In all the numerical analyses in normally consolidated soil the same initial net stress state was assumed: the vertical net stress was equal to 100 kPa and the horizontal net stresses (radial and circumferential net stress) were calculated as 60 kPa by using a coefficient of earth pressure at rest, K_{nc} of 0.6. The coefficient of earth pressure at rest, K_{nc} was computed according to the Jâky's simplified formula [100] ($K_{nc} = 1 - \sin\phi'$) for normally consolidated saturated soils, by assuming an angle of friction, ϕ' of 23 degrees. This value of the angle of friction is consistent with the value of M reported in Table 3.2 for triaxial compression stress paths. The chosen in-situ net stress state corresponds to a soil depth between 5 and 6 metres. An initial suction of 200 kPa was taken in all the numerical analyses by assuming a pore air pressure of zero (relative to atmospheric pressure) and a pore water pressure of -200 kPa (relative to atmospheric pressure). Atmospheric pressure was assumed to be 100 kPa and the only influence of this is in the compressibility of the gas phase.

For the soil in normally consolidated conditions, a value of 15.6 kPa was calculated for the hardening parameter, $\overline{p}_o^*$ from the values of net stresses and suction given above. This value was obtained by calculating first the isotropic yield stress, $\overline{p}_o$ from the analytical expression of the elliptical yield curve in constant suction planes (Equation 2.33) by using values of suction and net stresses equal to those in-situ (as the in-situ stress state was on the yield locus). Subsequently this value of $\overline{p}_o$ together with the in-situ value of suction

were input in the analytical expression of the LC yield curve (Equation 2.26) in order to obtain the above value for the hardening parameter, $\overline{p}_o^*$.

In practice net stresses are likely to increase with depth and suction is also likely to vary with depth. The assumption of constant initial values of net stresses and suction over the whole mesh allowed a clearer interpretation of the effects of pressuremeter expansion, as the spatial variations of net stresses and suction were entirely attributable to the expansion process. This assumption involved a maximum error in the estimate of the in-situ net stress state at the top and bottom of the mesh of between 15% and 20%.

7.4.3 Mesh and boundary conditions

The pressuremeter expansion was modelled as a bi-dimensional axi-symmetric problem by using the finite element meshes shown in Figure 7.2. A coarse (Figure 7.2 (a)) and a fine (Figure 7.2 (b)) mesh were initially tested in order to ensure the adequacy of the refinement adopted in the zones where the highest gradients of displacement and suction were expected (i.e. at the pressuremeter-soil interface and at the extremities of the pressuremeter membrane). Quadrilateral eight-noded isoparametric elements were used, with the same shape functions for all the nodal unknowns (displacement, pore air pressure and pore water pressure). The coarse mesh was divided into 240 elements with a total of 781 nodes whereas the fine mesh had 312 elements with a total of 1007 nodes.

In the majority of bi-dimensional (i.e. axi-symmetric) finite element studies of pressuremeter tests presented in the literature (see, for example, Charles, Yu and Sheng [94], Fioravante, Jamiolkowski and Lancellotta [93], Houlsby and Carter [91], Zentar, Moulin and Hicher [92]), symmetry is assumed about the horizontal plane passing through the middle of the pressuremeter membrane and, therefore, only half of the mesh shown in Figure 7.2 is analysed. This assumption neglects the finite length of the pressuremeter below the membrane and models the body of the pressuremeter as extending above and below the membrane to infinity. This was not assumed in this work where the finite length of the pressuremeter below the membrane was explicitly taken into account. The results showed that differences of the predicted net stress state could be observed in the two zones above and below the membrane due to the finite length of the device. This, however, was

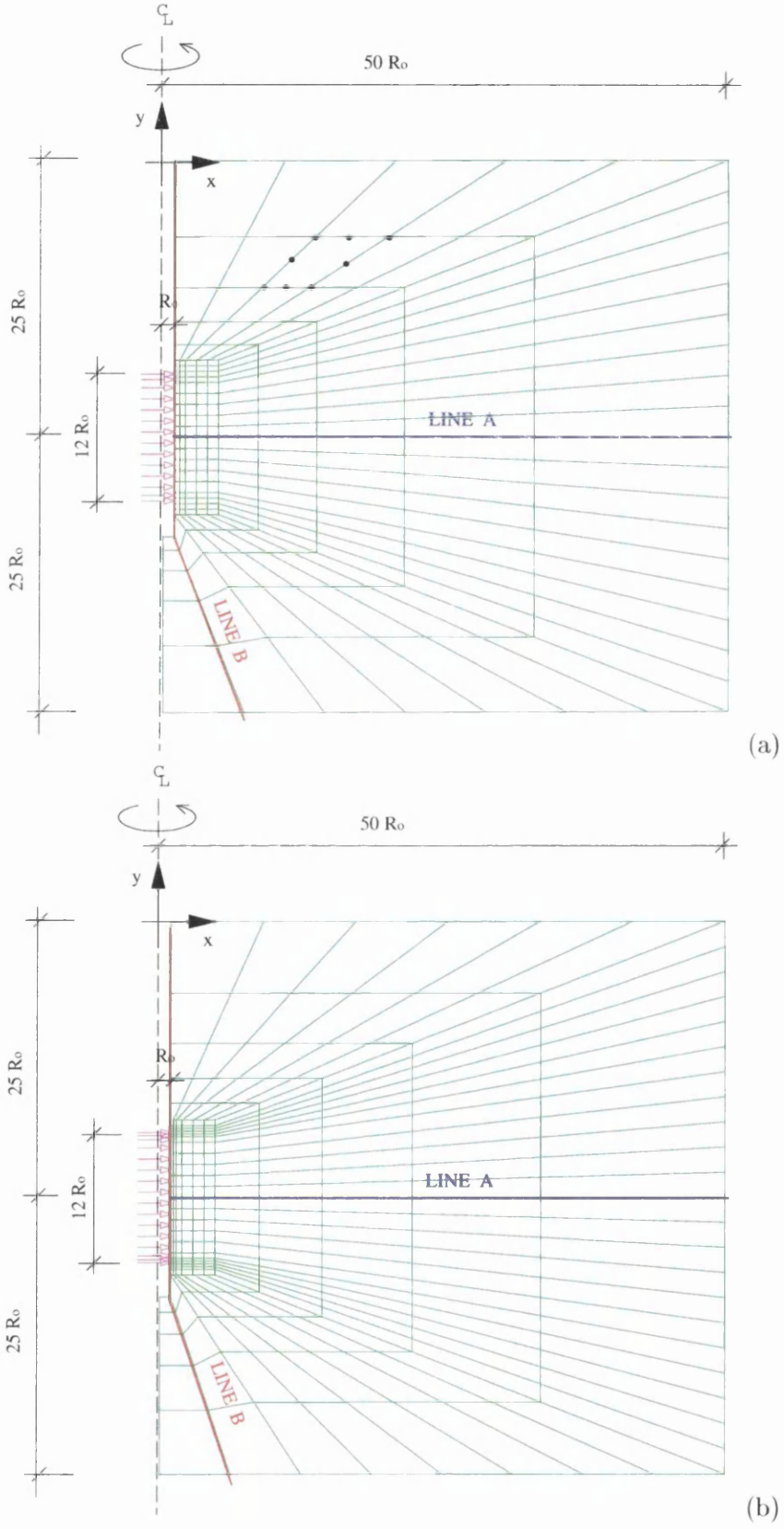

Figure 7.2: Finite element mesh for pressuremeter test simulation: (a)coarse mesh (b)fine mesh

a localized effect and it is believed not to affect significantly the response measured at the mid-height of the pressuremeter.

Figure 7.2 (a) shows that the top and bottom boundaries of the mesh were at a distance of 25 times the probe radius, R_o from the mid-height of the pressuremeter membrane and the outer boundary was at a distance of 50 times R_o from the centre-line. Similar distances of the mesh boundaries were chosen by Fioravante, Jamiolkowski and Lancellotta [93] for their coupled flow-deformation numerical model in saturated soils. On these boundaries displacements in the perpendicular directions were prevented whilst the values of pore air pressure and pore water pressure were fixed at their intial values (see Figures 7.3 and 7.4).

The assumed boundaries were sufficiently far away from the pressuremeter to avoid any influence on the numerical predictions, as was confirmed by inspection of the results obtained in all the analyses performed. This was consistent with a previous numerical study by Houlsby and Carter [91], which showed that the effect of the free surface on the results of pressuremeter tests in saturated cohesive soils is practically negligible if the test takes place at a depth greater than 10 times the pressuremeter diameter.

Modelling of the boundary condition at the interface between the pressuremeter body and the soil must take into account the geometry of the pressuremeter device. Above and below the membrane the pressuremeter consists of two cylindrical steel sections of the same diameter as the deflated testing section (see Figure 7.1) which prevent inward displacements of the soil during the expansion process.

The rigorous modelling of the boundary condition at the pressuremeter body in the zones above and below the membrane is difficult to achieve in finite element analyses. The two steel sections above and below the pressuremeter membrane prevent the possibility of the soil moving radially towards the borehole but they do not impose any restraint on the outward radial displacements. Therefore a varying boundary condition should be ideally imposed at the interface between the steel sections and the soil. While the radial net stress at this interface is greater than zero, the boundary condition should be a displacement-controlled one imposing a restraint of zero radial displacement. For the liquid and gas flows, an impermeable boundary should be assumed. When the radial net stress attains a

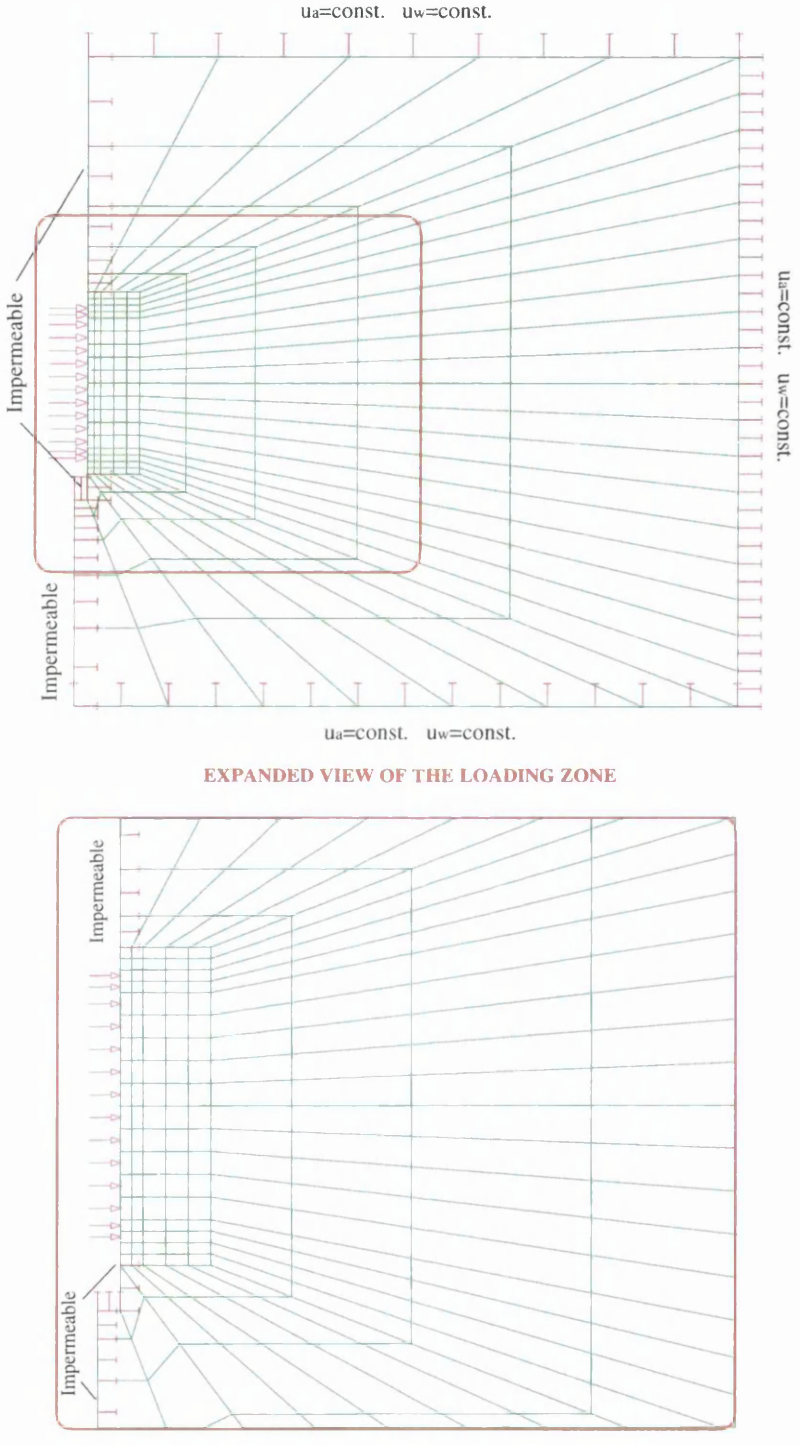

Figure 7.3: Pressuremetr body modelled as impermeable displacement-controlled boundary

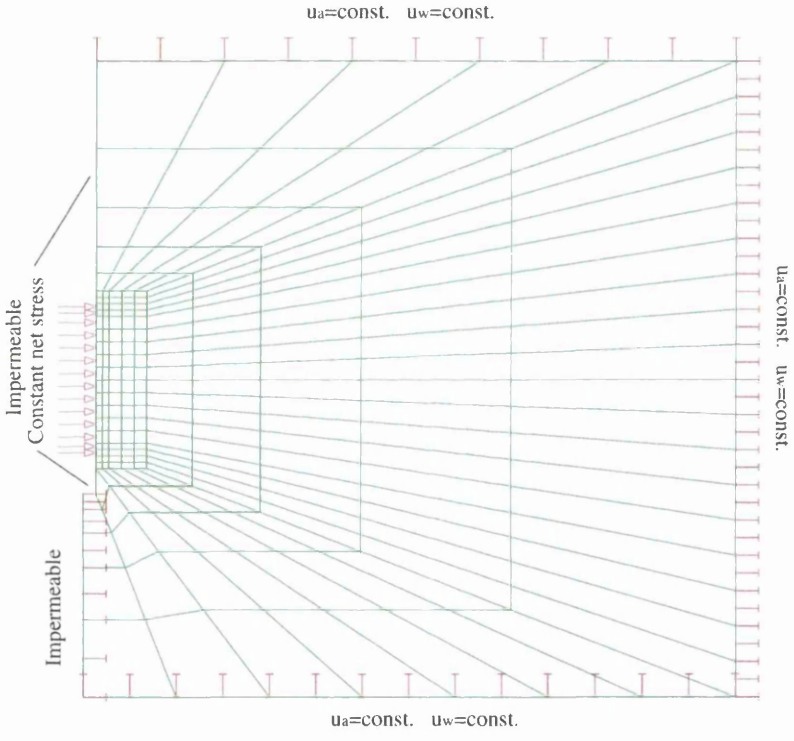

Figure 7.4: Pressuremeter body modelled as impermeable stress-controlled boundary

value of zero any further reduction of its value is not possible as tension cannot occur at the interface between the soil and steel sections. Separation of the soil from the probe will therefore occur and the type of boundary condition changes from displacement-controlled to stress-controlled (with an imposed value of radial net stress of zero). For the boundary conditions on the liquid and gas flows, additional hypotheses on the presence of liquid and gas in the space between the probe and soil after separation need to be introduced. The problem becomes even more complex if the occurrence of friction between the probe and the soil has to be considered. A further difficulty arises if the simplifying assumption of a top steel section extending up to the soil surface is not made. In this case the geometry of the borehole above the the steel section and the conditions at the borehole wall (i.e. the presence of casing, drilling fluid etc.) should be taken explicitly into account.

Due to the complexities outlined above, in previous finite element simulations of pressuremeter tests two different simplified options for modelling the boundary condition at the interface between pressuremeter body and soil have been used. One option regards the pressuremeter body as a stress-controlled boundary with the imposed radial net stress equal to the in-situ value. This sort of assumption was made by Fioravante, Jamiolkowski and Lancellotta [93] in terms of constant in-situ radial effective stress for their study in saturated conditions. Alternatively, the pressuremeter body can be regarded as a displacement-controlled boundary with perpendicular displacements prevented, as proposed by Houlsby and Carter [91] and Charles, Yu and Sheng [94]. In both cases the boundary is modelled as impermeable with respect to liquid and gas flows. These two types of boundary conditions at the pressuremeter body are summarized in Figures 7.3 and 7.4 and they have both been tested in this work.

In the displacement-controlled case (see Figure 7.3), the radial displacements of the first two elements above and below the loading section were not restrained and a stress-controlled boundary condition (with radial net stress equal to the in-situ value) was instead assumed. This was suggested by the observation that, for the analysis performed with a stress-controlled boundary condition, noticeable outward radial displacements took place at the boundaries of these elements.

7.4.4 Influence of mesh updating

All the numerical analyses that were performed, were continued to cavity strains, ϵ_c between 10% and 15% where the cavity strain is defined as:

$$\epsilon_c = \frac{a - a_o}{a_o} \tag{7.1}$$

with a and a_o respectively the current and initial radius of the cavity measured at the mid-height of the pressuremeter membrane. The attained large values of cavity strain suggested that the simulation of the pressuremeter expansion had to be regarded as a large displacement problem and, consequently, the importance of mesh updating was investigated. The introduction of mesh updating allowed the geometrical non-linearity of the problem to be taken into account without representing, however, a full large-strain formulation.

In order to investigate the importance of mesh updating a pressuremeter test was simulated by applying an increment of cavity pressure from 60 kPa (the initial in-situ horizontal total stress) to 190 kPa varying linearly over a period of 900 seconds. The increment of the applied cavity pressure was limited to 130 kPa because, in some simulations, a further increase would have caused the predicted stress path in a restricted zone at the extremities of the membrane to hit the yield envelope on the dry side after a previous elastic unloading. This was intentionally avoided because it caused computational problems due to the fact that code "Compass" is not designed to deal with strain softening and the consequent strain localization problems. Other examples of finite element simulations of pressuremeter tests in the literature, where Cam-Clay type models have been used in conjunction with a convergency algorithm, also tend to be limited to values of cavity strain similar to those achieved in this work (whereas real pressuremeter tests are typically taken to cavity strains of about 40%).

The loading process was split into 50 load increments each of them extending over a time interval of 18 seconds. The pressuremeter body above and below the membrane was modelled as a stress-controlled impermeable boundary, as explained above, and the coarse mesh of Figure 7.2 (a) was employed. The relationship for the variation of degree of satu-

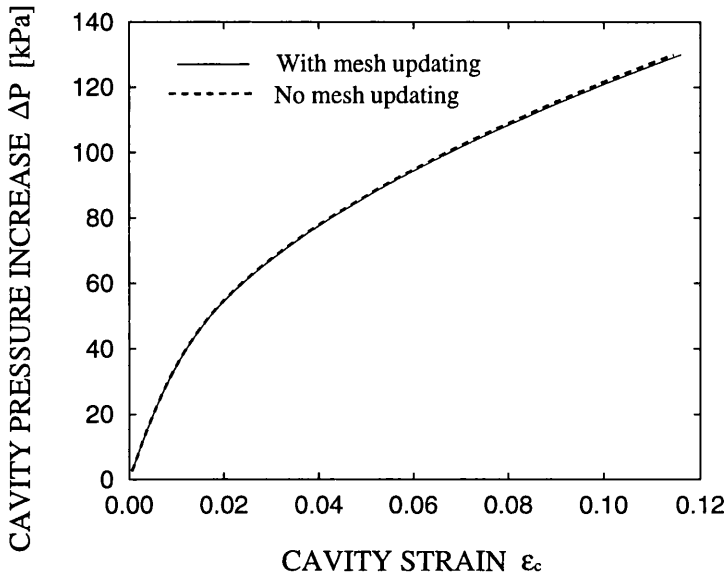

Figure 7.5: Influence of mesh updating on the predicted cavity pressure-cavity strain curve

ration was the one proposed in Chapter 4 (Equation 4.5). Two analyses were performed: in one analysis the nodal coordinates of the mesh were updated at the beginning of each time step according to the displacements that occurred in the previous stages while in the other the mesh configuration was the same for each time step. The results of the computations are shown in Figures 7.5 and 7.6 where the variation of cavity strain and suction (measured at the surface of the pressuremeter at the mid-height of the membrane) with the applied cavity pressure are plotted. Inspection of Figure 7.5 suggests that the cavity pressure-cavity strain curve is approximately the same in both cases regardless of whether mesh updating is employed or not. The difference between the two analyses would be expected, however, to increase if the expansion process were taken further. A more noticeable difference was observed between the two cases for the prediction of the suction variation at the mid-height of the pressuremeter membrane (see Figure 7.6). Although mesh updating appeared to be not essential for the analyses presented in this chapter, this feature was retained in the subsequent simulations as it did not require a substantial increse of computational effort.

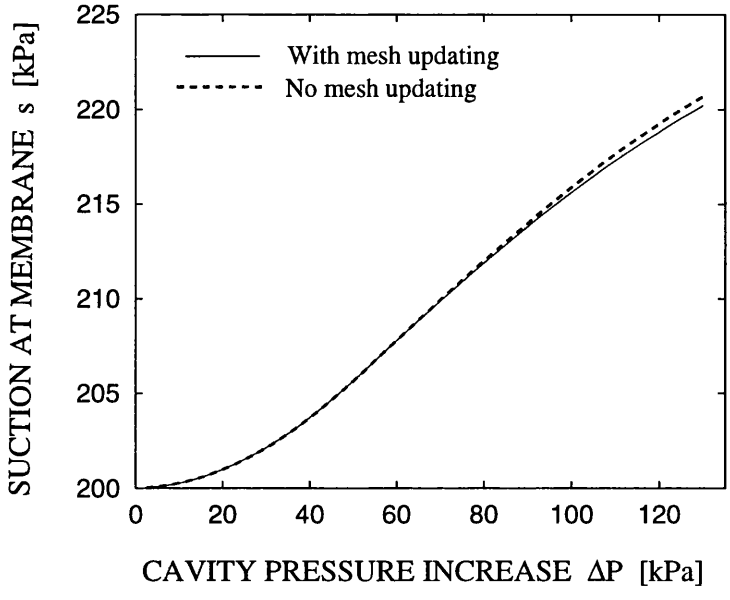

Figure 7.6: Influence of mesh updating on the predicted cavity pressure-suction curve

7.4.5 Influence of boundary conditions on pressuremeter body

Similar analyses to those performed to investigate mesh updating were carried out in order to explore the influence of the two possible boundary conditions at the pressuremeter body. In one analysis a stress-controlled impermeable (with respect to both liquid and gas flows) boundary was assumed, with radial net stress equal to the in-situ value, as shown in Figure 7.4). In the other analysis the pressuremeter body was modelled as an impermeable boundary with displacement in the perpendicular direction prevented (see Figure 7.3) while no restraints were imposed on vertical displacements.

The results of the simulations for the two different boundary conditions are illustrated in Figures 7.7, 7.8 and 7.9, which show contour plots of mean net stress, $\overline{p}$, deviator stress, q, and suction, s, at the end of loading, with the values of the contour lines indicated in Pa. Inspection of Figures 7.7, 7.8 and 7.9 reveals that the predicted spatial distributions of $\overline{p}$, q and s were very similar in both cases. Some differences can be noticed in the zone of soil just below the pressuremeter. When a displacement-controlled boundary condition was adopted, higher values of mean net stress and deviator stress were calculated. This

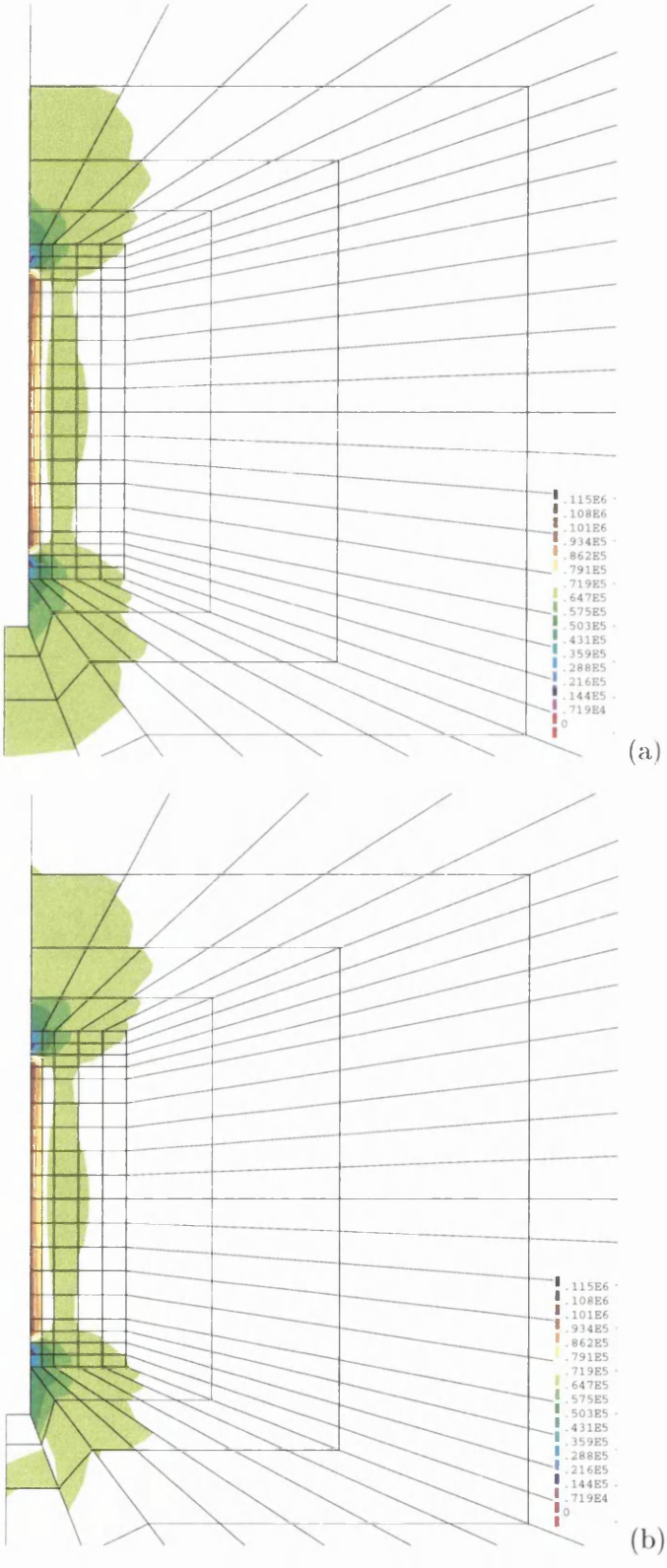

Figure 7.7: Contour plots of mean net stress at the end of loading: (a)stress-controlled boundary (b)displacement-controlled boundary

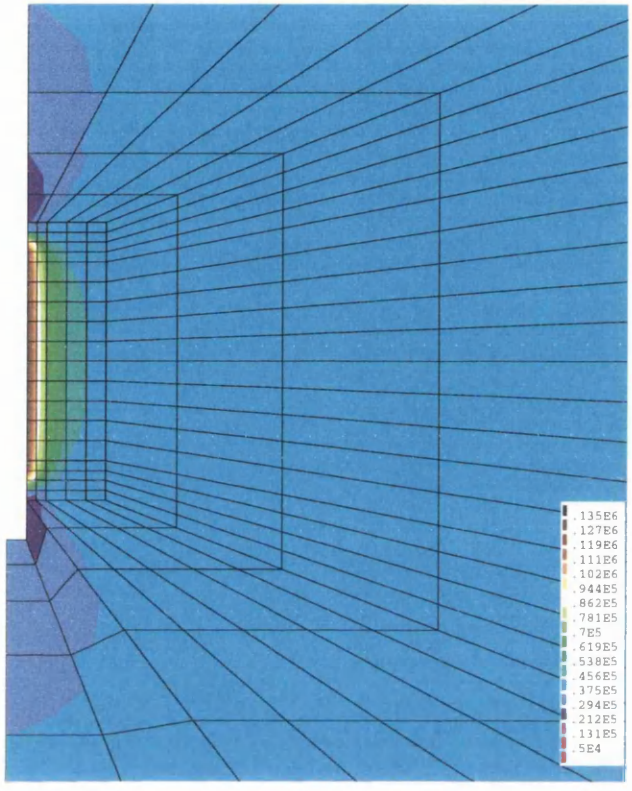

(a)

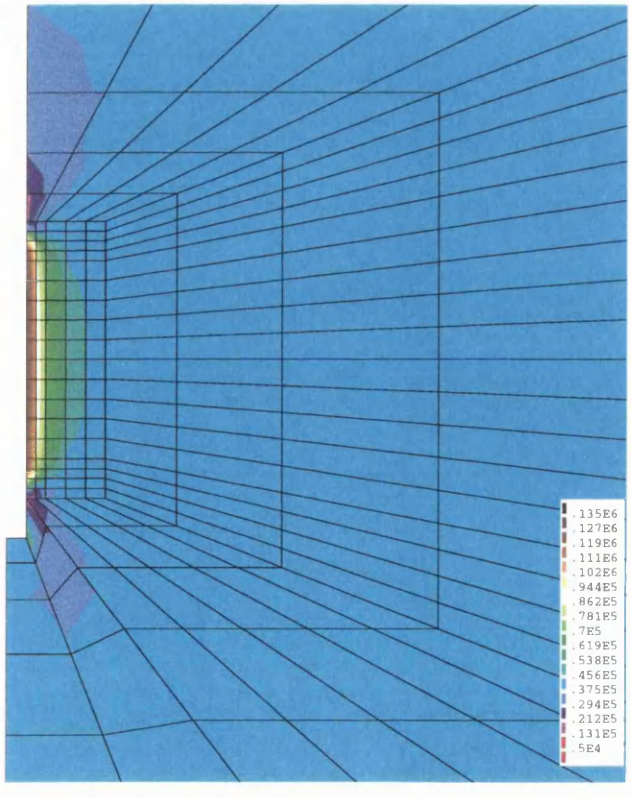

(b)

Figure 7.8: Contour plots of deviator stress at the end of loading: (a)stress-controlled boundary (b)displacement-controlled boundary

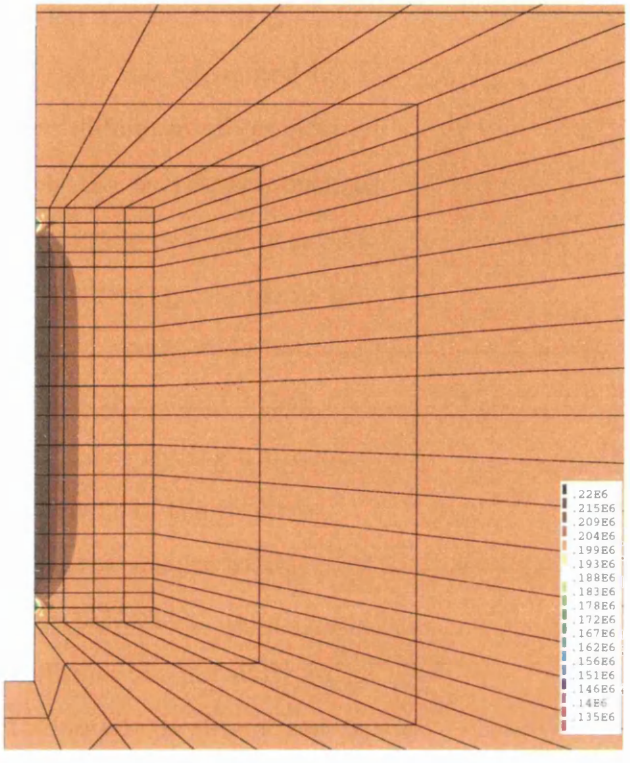

(a)

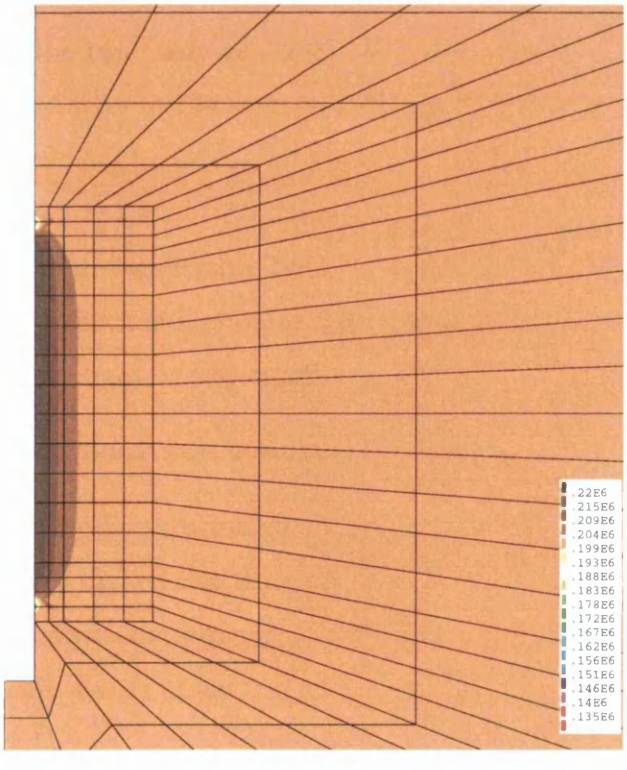

(b)

Figure 7.9: Contour plots of suction at the end of loading: (a)stress-controlled boundary (b)displacement-controlled boundary

was due to the fact that the heave of the soil at the bottom of the borehole, observed in the stress-controlled case, was prevented by the restraints imposed in the displacement-controlled case. Such difference of prediction is, however, a localized effect which does not affect significantly the overall response of the test. The predicted curves of cavity pressure against cavity strain and cavity pressure against cavity suction, though not shown here for brevity, were indistinguishable in the two cases. In all the following analyses a displacement-controlled impermeable boundary, as shown in Figure 7.3, was assumed at the pressuremeter body above and below the membrane, because this seemed closer to the real condition occurring during a pressuremeter test and also because it reduced the number of nodal unknowns of the problem.

The insensitivity of the results to the particular boundary condition adopted for the pressuremeter body is believed to be a consequence of a combination of factors such as the unsaturated condition, the normally consolidated state of the soil and the particular constitutive model adopted. It should not therfore be assumed that this result is valid for all finite element simulations of pressuremeter tests. For example, more pronounced differences between the two analyses described above would be expected for the case of an undrained pressuremeter test in saturated soil where no change in volume of the soil is permitted.

Results in Figures 7.7, 7.8 and 7.9 demonstrate that the in-situ values of net stresses and suction are restored considerably before reaching the boundaries of the mesh. This confirms that the top, bottom and outer boundaries of the mesh are sufficiently distant from the pressuremeter to avoid any significant influence on the computed results.

7.4.6 Mesh refinement and loading discretization

Mesh refinement and loading discretization were next investigated. In the first case two different analyses were carried out using the coarse and fine mesh shown in Figure 7.2. The results of the analyses are presented in Figures 7.10 and 7.11, which show curves of cavity pressure against cavity strain and cavity pressure against suction (measured at the pressuremeter boundary at the mid-height of the pressuremeter membrane). Inspection of Figure 7.10 reveals that, for the prediction of the cavity pressure-cavity strain relationship,

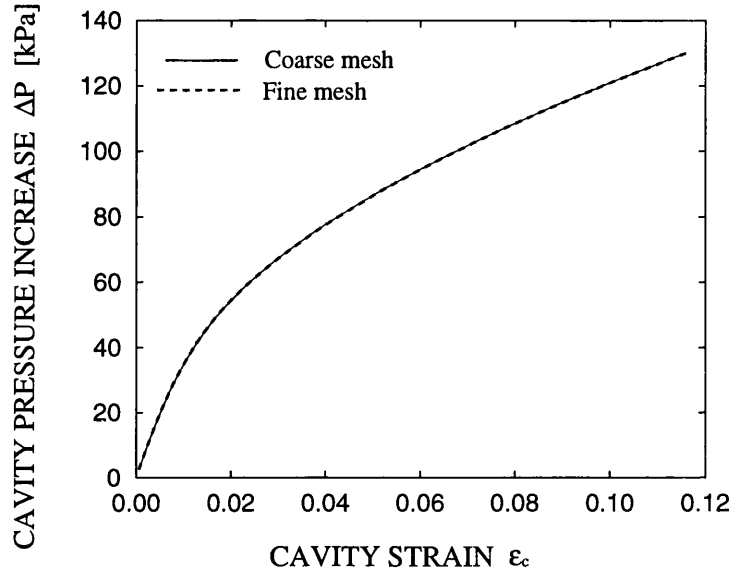

Figure 7.10: Influence of mesh refinement on the predicted cavity pressure-cavity strain curve

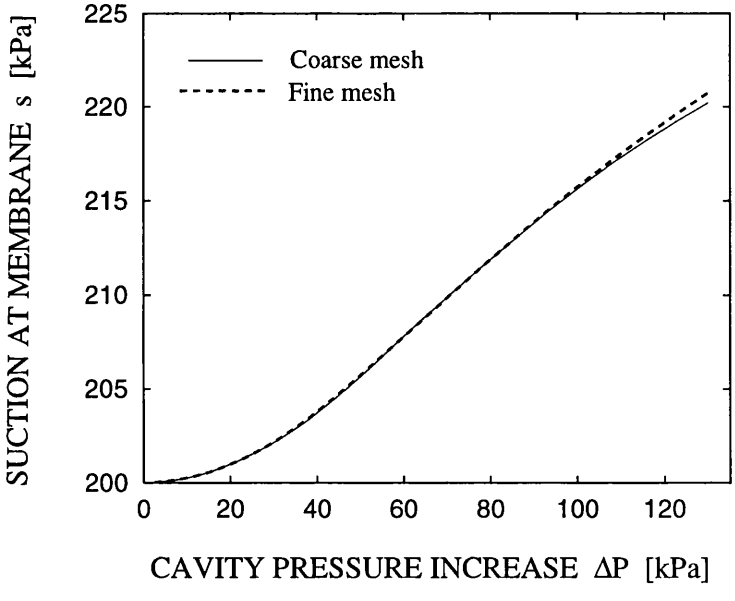

Figure 7.11: Influence of mesh refinement on the predicted cavity pressure-suction curve

the use of the mesh with a finer discretization in the zones of higher spatial gradients of the unknowns, does not produce any discernible change. Figure 7.11 shows that, for the prediction of suction variation at the pressuremeter body (at the mid-height of the pressuremeter), the use of the finer mesh resulted in a change of approximately 2% in the computed value of suction at the end of loading compared to the analysis where the coarse mesh was used. The distribution of net stresses and suction within the soil domain, although the comparison is not shown here in the interest of brevity, was also predicted by the coarse mesh with acceptable accuracy. The coarse mesh was hence adopted for all the subsequent analyses, because the greater computational effort required by the use of the fine mesh was not considered justifiable by the relatively small increase of accuracy achieved.

For the investigation of loading discretization, two different analyses were carried out. In one analysis the loading process over an interval of time of 900 seconds, was split into 50 increments, each one applied over a time interval of 18 seconds. The other one involved 100 load steps, each one taking place over a time interval of 9 seconds. The results of the calculations for both cases are presented in Figures 7.12 and 7.13 which show curves of cavity pressure against cavity strain and cavity pressure against suction at the membrane respectively. Inspection of Figure 7.12 and 7.13 shows that, for both predictions, the results obtained are insensitive to the loading discretization adopted. A choice of 50 loading increments was, therefore, considered acceptable and employed for all subsequent analyses.

7.4.7 Summary of specifications for the "standard" analysis

In the previous sections the specifications for a "standard" analysis, which has been shown to provide numerically reliable results, have been defined. These specifications are summarized in Table 7.1. The finite element analyses presented further in this chapter rely on the specifications of the "standard" analysis as a basis. In each of the following finite element analyses only one of the specifications reported in Table 7.1 is varied according to the particular aspect being investigated.

In the following part of this section, the results computed for the "standard" analysis

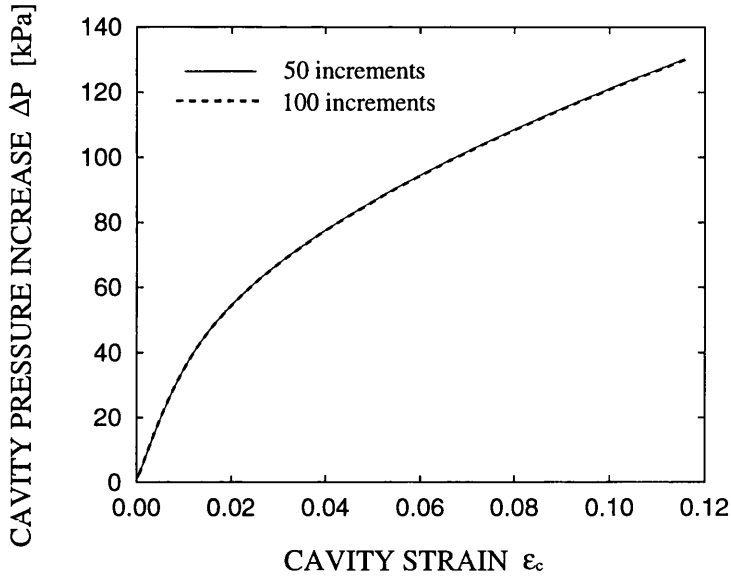

Figure 7.12: Influence of loading discretization on the predicted cavity pressure-cavity strain curve

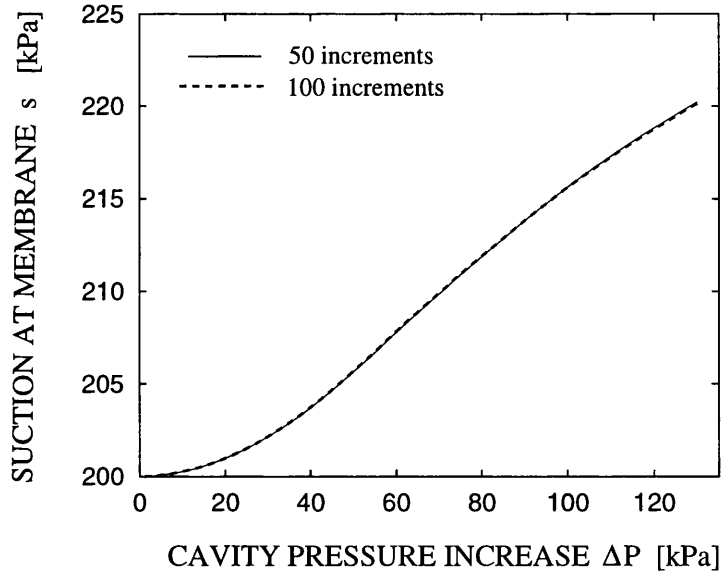

Figure 7.13: Influence of loading discretization on the predicted cavity pressure-suction curve

CONSTITUTIVE MODELS	
Stress-strain model	Alonso, Gens and Josa [1][1]
Stress-strain model parameters	reported in Table 3.2[1]
Degree of saturation relationship	Equation 4.5 (elasto-plastic relationship)
Degree of saturation relationship parameters	reported in Table 4.2
Air and water permeability relationships	Equations 3.6, 3.5 (Brooks and Corey [47])
Permeability relationships parameters	reported in Table 3.8
PROBLEM GEOMETRY AND INITIAL STRESS STATE	
Finite element mesh	shown in Figure 7.2 (a)
Mesh updating	yes
Initial vertical net stress	100 kPa
Initial horizontal net stress	60 kPa
Initial pore air pressure	0 (relative to atmospheric)
Initial pore water pressure	-200 kPa (relative to atmospheric)
Initial hardening parameter ($\bar{p}_o^*$)	15.6 kPa (normally consolidated state)
LOADING AND BOUNDARY CONDITIONS	
Applied increase of cavity pressure	130 kPa over a period of time of 900 s
Loading discretization	50 increments of 18 s
Other boundary conditions	shown in Figure 7.3

[1] A value of Poisson's ratio ν equal to 0.3 was used instead of a constant value of shear modulus G and a lower limit value of bulk modulus K equal to 200 kPa was assumed (see Section 7.4.2).

Table 7.1: Specifications of the "standard" analysis

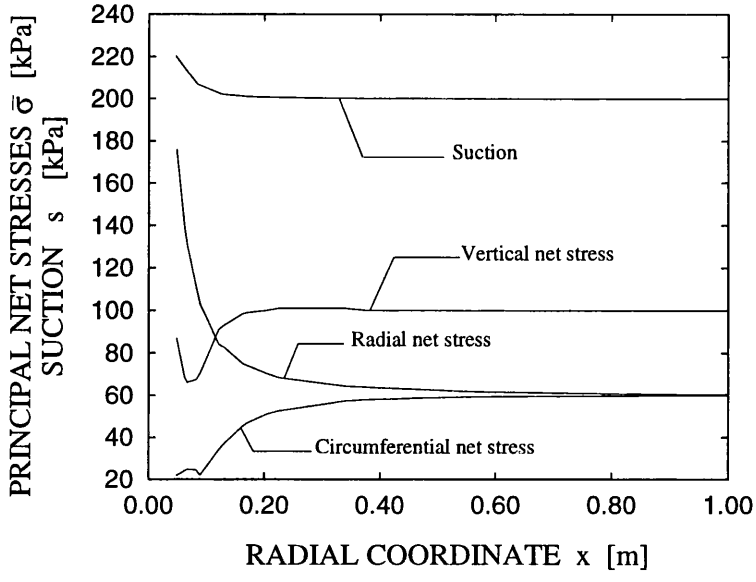

Figure 7.14: Radial variation of suction and principal net stresses at the end of expansion

are used to illustrate some significant aspects which are common to all the pressuremeter simulations performed. Figure 7.14 shows the variation of suction and principal net stresses along the radius at mid-height of the pressuremeter membrane at the end of the expansion process (at a cavity strain between 11% and 12%). In particular, the variation of suction refers to the nodes lying on the line A shown in Figure 7.2 (a), whereas the principal net stresses are computed along the closest radial alignment of Gauss points above line A. Inspection of Figure 7.14 reveals that the variation of suction from the initial value (200 kPa) is limited to a zone of soil extending to a radial distance from the borehole axis of about 0.20 m. For the net stress state the in-situ values of stresses are restored at a radial distance of about 0.50 m. This numerical result agrees with experimental data from suction monitored pressuremeter tests in unsaturated granite residual soils of southern Brazil by Schnaid and co-workers (private communication) where constant suction was measured during expansion by tensiometers at radial distances from the borehole axis of 30 cm and 60 cm. This result also confirms that the in-situ values of suction and principal net stresses are restored significantly before the outer boundary of the mesh, which is located at a radial coordinate of 2.125 m.

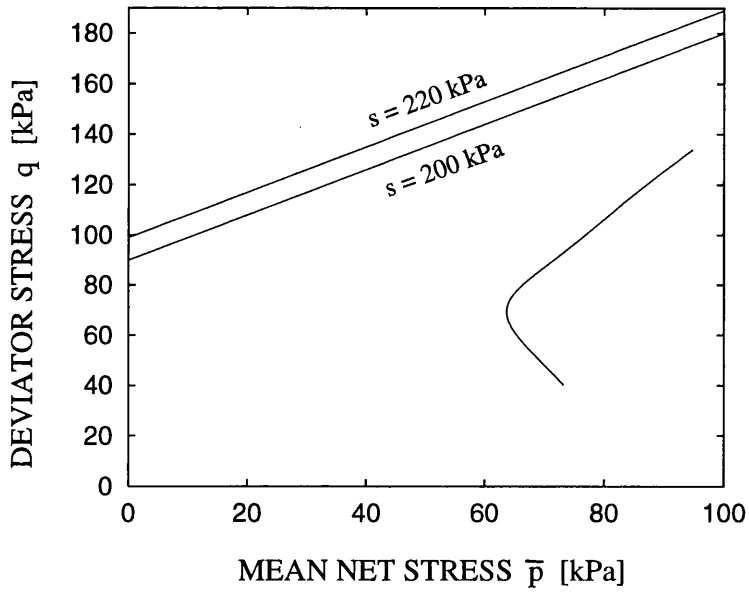

Figure 7.15: Projection on the $(q, \overline{p})$-plane of the predicted stress path at the pressuremeter boundary at the mid-height of the pressuremeter membrane

Figure 7.15 shows the projection of the stress path on the $(q, \overline{p})$-plane, computed at the closest Gauss point to the mid-height of the pressuremeter membrane above line A together with the two critical state lines corresponding to suctions of 200 kPa and 220 kPa, which are, respectively, the in-situ value and the approximate maximum value of suction attained during the expansion. Inspection of Figure 7.15 indicates that, for the magnitude of cavity strains simulated in this work, the stress path at the pressuremeter boundary is still far from critical state. Given that the zone immediately adjacent to the pressuremeter boundary is where shearing is most intense, it is clear that (at the mid-height of the pressuremeter) none of the soil has approached anywhere close to shear failure. At a cavity strain of approximately 12% the expansion process is therefore nowhere near the cavity limit pressure (which corresponds to a condition with a substantial anulus of soil reaching shear failure). The large cavity strain of about 12% is, in the simulations presented here, a consequence of large pre-failure plastic shear and volumetric strains resulting from the Cam-Clay type of elasto-plastic model, rather than an indication of widespread shear failure and an impending limit pressure.

This result provides an explanation for the significant lower magnitudes of cavity pressure computed by the present analysis (at given values of cavity strain) than the analytical solution provided by Yu and Houlsby [101] for an infinitely long cylindrical cavity expanding in a cohesive-frictional soil. In the latter study the behaviour of the soil is assumed linearly elastic until the shear failure is reached and, until the soil closest to the pressuremeter reaches shear failure, only elastic shear straining takes place (because the mean stress remains constant). After the attainment of shear failure, yielding of the soil takes place with a flow rule given by a prescribed dilation angle. In contrast, in this study, elasto-plastic deformations take place from the beginning of the expansion process, as the mechanical behaviour of the soil is modelled through a Cam-Clay type model (i.e. the Alonso, Gens and Josa [1] model) and the initial state of the soil is normally consolidated. Therefore significant plastic volumetric and shear strains occur well before critical state is attained and this causes a noticeably less stiff soil response than in the Yu and Houlsby [101] analysis.

7.5 Effect of the modelling of the variation of S_r

This section describes the investigation of the effect of changing the modelling of the variation of degree of saturation from the state surface expression of Lloret and Alonso [22] (Equation 2.41), originally implemented in code "Compass", to the relationship proposed in Chapter 4 (Equation 4.5), implemented in code "Compass" by the author.

Two different analyses are compared. One analysis was carried out according to the specifications of the "standard" analysis as reported in Table 7.1. The other analysis employed the state surface of Lloret and Alonso [22] (Equation 2.41) instead of the elasto-plastic relationship presented in Chapter 4 (Equation 4.5).

In the numerical analysis presented in this section the soil is initially in a normally consolidated state and the stress paths for most of the soil domain during pressuremeter expansion, involve elasto-plastic deformation. Therefore the first of the two sets of parameter values for the state surface expression of Lloret and Alonso [22] defined in Section 3.3 was used (see Table 3.6).

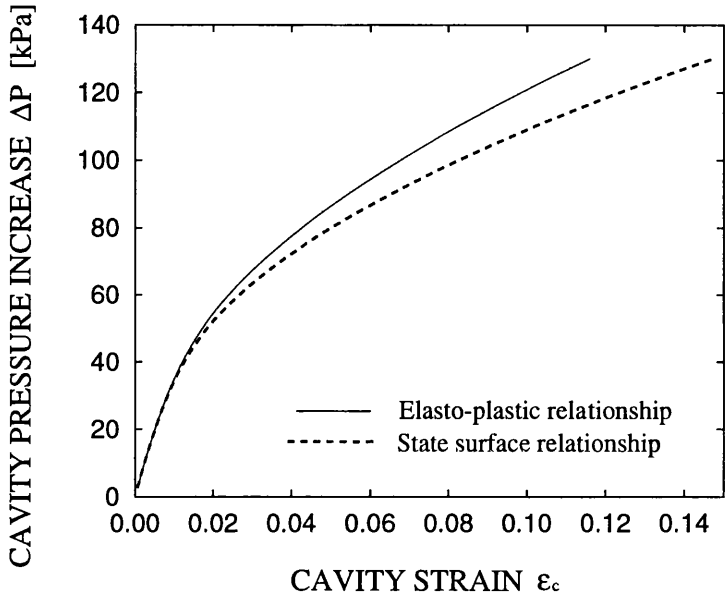

Figure 7.16: Influence of modelling of variation of S_r on the predicted cavity pressure-cavity strain curve

The predicted relationships of cavity pressure against cavity strain and cavity pressure against suction (measured at the pressuremeter boundary at the mid-height of the membrane) for the two analyses are respectively shown in Figures 7.16 and 7.17. Inspection of Figures 7.16 and 7.17 indicates that the results measured at the pressuremeter boundary are significantly influenced by the model used to represent the variation of degree of saturation. When improved modelling of the variation of degree of saturation is introduced, by using the elasto-plastic relationship proposed in this thesis, the predicted pattern of variation of suction at the pressuremeter boundary is the opposite to that predicted with the state surface relationship, as it shows an increase of suction with increasing cavity pressure instead of a decrease (Figure 7.17). This result is in accordance with the predicted variations of suction during rapid isotropic loading and rapid shearing for the case of the simple analysis described in Section 6.5 (see Figures 6.12 (a) and 6.14 (a)). Inspection of Figures 6.12 (a) and 6.14 (a) indicates that, when the elasto-plastic relationship for degree of saturation is employed, the numerical analysis predicts an increase of suction

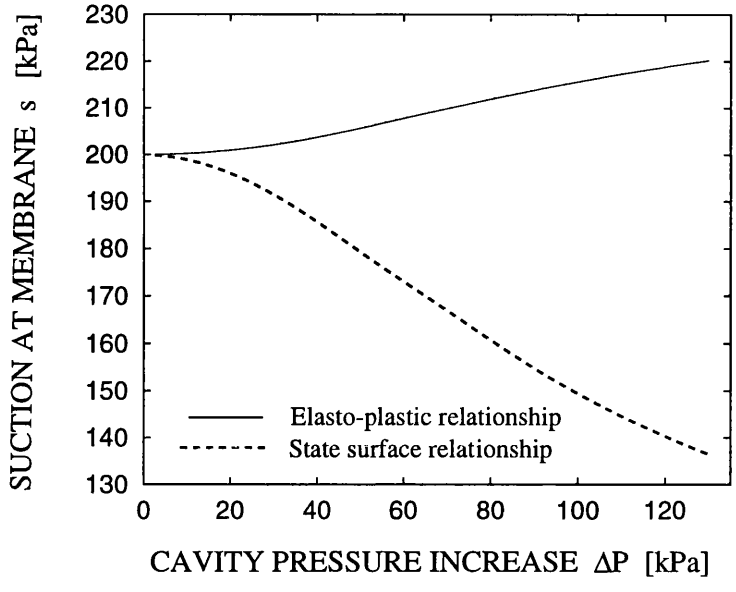

Figure 7.17: Influence of modelling of variation of S_r on the predicted cavity pressure-suction curve

both during rapid isotropic loading and during rapid pure deviatoric loading. Similarly, for the pressuremeter simulation of this section, the predicted increase of suction at the mid-height of the pressuremeter boundary corresponds to a computed stress path consistent with that of the simple analysis. Close to the mid-height of the pressuremeter boundary the predicted stress path presents an initial small decrease of mean net stress counterbalanced by a greater increase towards the end of the expansion and a much more significant increment of deviator stress (see Figure 7.15). For the case of the state surface expression of Lloret and Alonso [22] using the parameters values of Table 3.6 (set 1), the results presented in Figures 6.12 (a) and 6.14 (a) (set 1) indicate the occurrence of an increase of suction during rapid isotropic loading whilst a decrease of suction is computed during rapid deviator loading. The drop in suction predicted by the state surface expression during the pressuremeter expansion is explained by the fact that the computed stress path close to the mid-height of the pressuremeter boundary is dominated by an increase of deviator stress whereas relatively small changes of mean net stress are observed.

Another difference shown in Figure 7.17 between the two types of modelling for the

variation of degree of saturation is that the increase of suction at the end of loading predicted with the new relationship is significantly smaller than the corresponding decrease of suction predicted with the state surface relationship.

The improvements to the modelling of variation of degree of saturation influence significantly not only the predicted variation of suction but also the stress-strain behaviour of the soil. Figure 7.16 shows that, when the state surface expression is used for modelling the variation of degree of saturation, the predicted cavity strain at a cavity pressure increase of 130 kPa is overpredicted by approximately 27% with respect to the case when the elasto-plastic relationship proposed in this thesis is employed. The difference of deformations observed in the analyses is clearly due to the dependency of the stress-strain model adopted (i.e. Alonso, Gens and Josa [1] model) on the value of suction. The most substantial differences should therefore be expected in those cases where strong coupling between flow and deformation occurs. For the limit condition of a fully drained test the numerical results computed by employing two different models for variation of degree of saturation would be expected to coincide and the only difference between the two cases would be the predicted distribution of degree of saturation over the soil domain.

In Figures 7.18, 7.19 and 7.20 the contour plots of mean net stress, deviator stress and suction (values indicated in Pa) at the end of loading process are shown for the case when the state surface expression is employed. The corresponding contour plots for the case when the elasto-plastic relationship for degree of saturation is employed are the "standard" ones shown in Figures 7.7 (b), 7.8 (b) and 7.9 (b). Comparison of Figures 7.18 and 7.19 with Figures 7.7 (b), and 7.8 (b) reveals that the predictions of the spatial distributions of mean net stress and deviator stress are similar for both cases. When the state surface expression is employed, the values of mean net stress and deviator stress calculated close to the pressuremeter boundary are respectively greater and smaller than those from the analysis performed by assuming the elasto-plastic relationship for degree of saturation. This occurs because the values of vertical net stress and circumferential net stress computed close to the pressuremeter boundary by using the state surface expression are greater than the corresponding values computed using the elasto-plastic relationship.

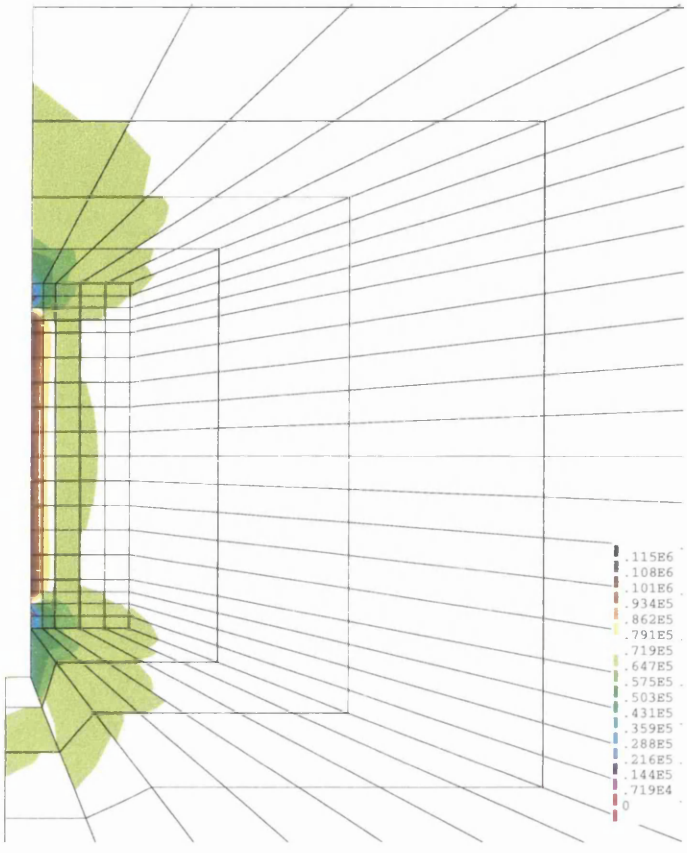

Figure 7.18: Contour plot of mean net stress at the end of loading computed by using the state surface expression for S_r

These differences, however, are restricted to a zone of soil immediately adjacent to the pressuremeter and the predicted net stress state quickly becomes very similar in the two cases with increasing radial distance from the loaded area.

Comparison of the contour plots of suction shown in Figures 7.20 and 7.9 (b) indicates that the predicted spatial distributions of suction at the end of loading are very different in the two cases. In particular, the state surface expression predicts a decrease of suction everywhere in the zone of soil affected by the pressuremeter expansion whereas the elasto-plastic relationship for degree of saturation predicts an increase of suction almost everywhere in the zone of soil affected by the test. In a very restricted area of soil adjacent to the top and bottom extremities of the pressuremeter membrane a drop in suction below the in-situ value is predicted by the analysis employing the elasto-plastic relationship

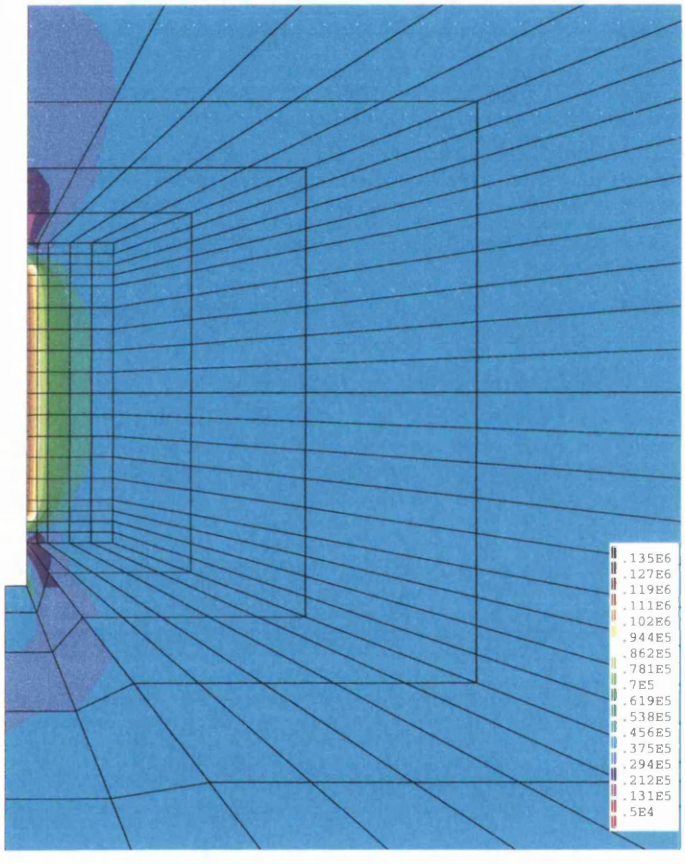

Figure 7.19: Contour plot of deviator stress at the end of loading computed by using the state surface expression for S_r

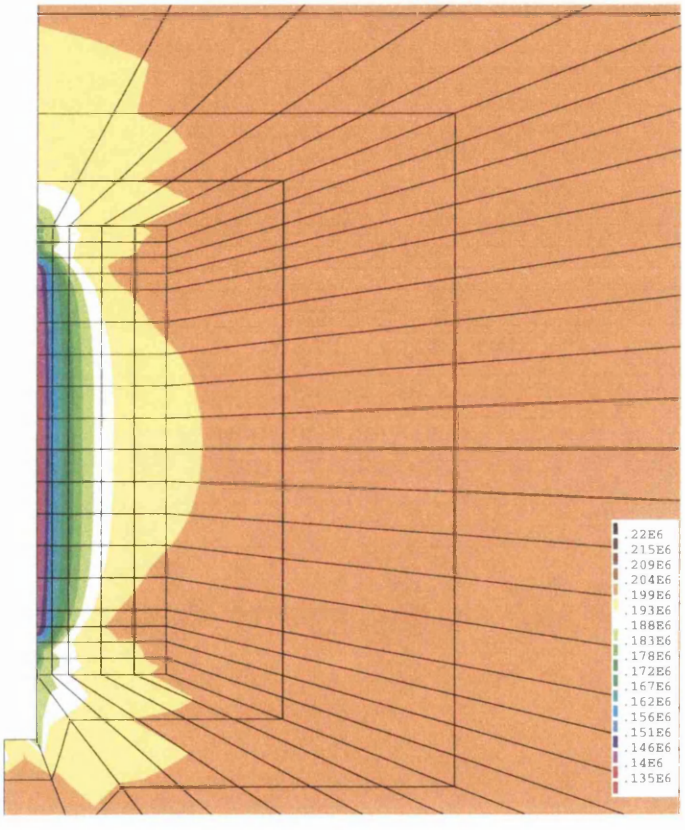

Figure 7.20: Contour plot of suction at the end of loading computed by using the state surface expression for S_r

for degree of saturation. This is clearly shown in Figure 7.21 (a) where the variation of suction along the pressuremeter boundary (line B in Figure 7.2 (a)) is presented. This very localized drop in suction is explained by the dependency of degree of saturation on specific volume introduced by the elasto-plastic relationship (Equation 4.5). As the soil experiences significant swelling at the extremities of the pressuremeter membrane, due to a marked decrease of mean net stress, the degree of saturation tends to drop as predicted by Equation 4.5. Therefore, due to the almost undrained condition at which expansion takes place (see next section), such decrease must be compensated by a fall of suction in order to obtain acceptable values of water content.

Figure 7.21 (b) shows the variation of suction along the pressuremeter boundary at the end of the expansion process when the state surface expression is employed. The presence of oscillations of the predicted value of suction in the zone immediately below the pressuremeter membrane suggests that the mesh refinement may not be adequate in this area. Inspection of Figure 7.21 (a) reveals that an analogous instability, although less pronounced, may also be detected for the case when the elasto-plastic relationship for degree of saturation is employed (immediately below the zone presenting the sharp drop in suction at the bottom of the pressuremeter membrane).

Figure 7.21 (c) shows the variation of suction along a radius at the mid-height of the pressuremeter membrane (line A in Figure 7.2 (a)) at the end of the expansion process for both types of degree of saturation relationship. Inspection of Figure 7.21 (c) confirms that in both cases the change of suction caused by the pressuremeter expansion is restricted to a zone of soil close to the pressuremeter and the in-situ value of suction is restored considerably before the outer boundary of the mesh (located at a radial coordinate of 2.125 m).

7.6 Effect of loading rate

This section reports an investigation of the effect of different rates of loading applied by the pressuremeter membrane to the cavity wall. The numerical results presented in the previous sections suggest that the simulation of the "standard" analysis cannot be

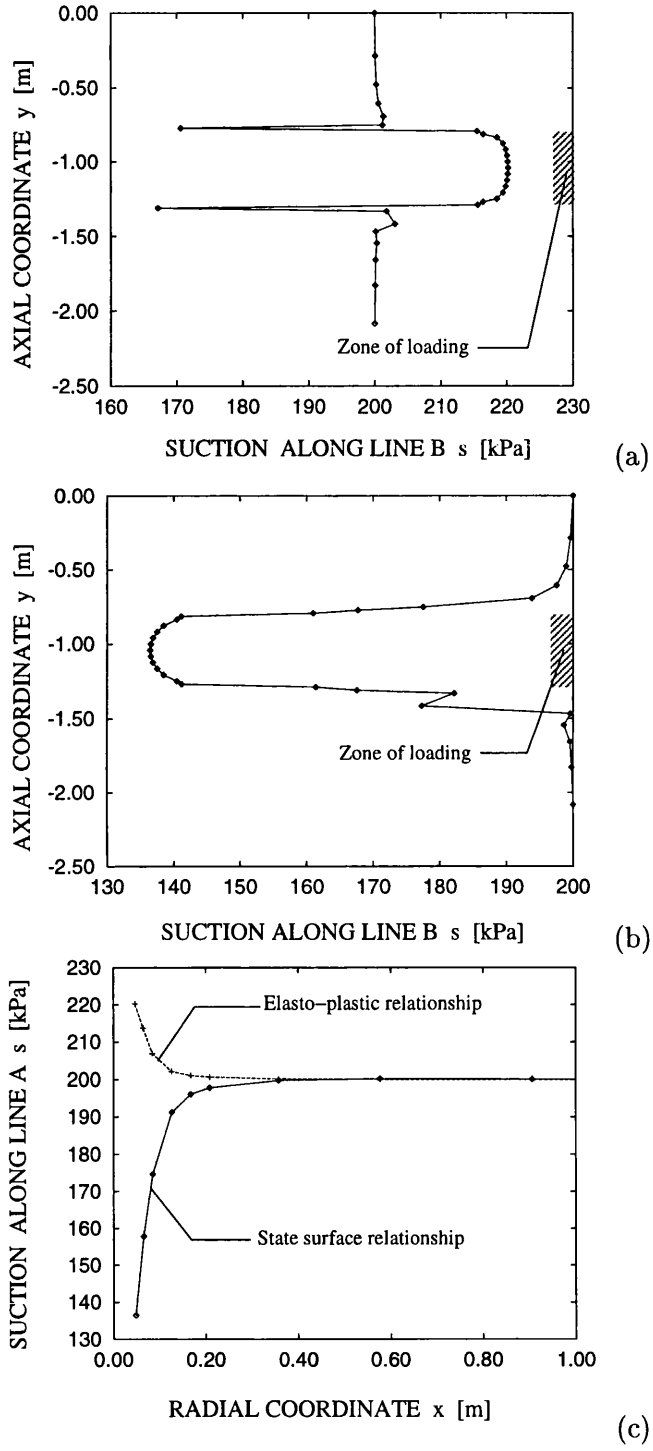

Figure 7.21: Variation of suction along: (a)line B (Figure 7.2 (a)) for the elasto-plastic relationship (b)line B for the state surface relationship (c)line A for both relationships

regarded as a fully drained process. Coupling between flow and deformation occurs as indicated by the variation of suction measured around the borehole wall. The loading rate adopted in the "standard" analysis was constant and corresponded to an ultimate increase of cavity pressure of 130 kPa over a period of 900 s (15 minutes). This loading rate can be regarded as similar to the one employed during a pressuremeter test carried out according to the Ménard method specification, as explained below.

The Ménard method (see Clarke [98]) requires an expansion of the pressuremeter membrane which doubles the initial volume of the test pocket. This is equivalent to the attainment of a cavity strain of approximately 41%. The prescribed test procedure is stress-controlled with 7 to 15 increments of cavity pressure up to the cavity strain of 41%. Each pressure increase is held constant for a time interval of 1 minute and the reading of the cavity expansion, taken at the end of this period, is used for the definition of the cavity pressure-cavity strain curve. This implies that the duration of a pressuremeter test carried out according to the Ménard method requirements, should be between 7 and 15 minutes (to a cavity strain of 41%). Given the non-linear nature of the cavity pressure-cavity strain curve, a cavity strain of 12% (corresponding to the end of loading in the "standard" analysis presented earlier) would typically be achieved in 4-10 minutes in a test performed according to the Ménard method specifications. The rate of expansion represented by the "standard" analysis is therefore about half the typical rate of a Ménard test.

The results from the "standard" analysis (which show significant variations of suction generated during pressuremeter expansion) indicate therefore, that a pressuremeter test carried out according to the Ménard specifications in an unsaturated soil having similar properties to those assumed in the "standard" analysis, should not be regarded as a fully drained process.

In order to assess the effect of rate of loading, other analyses were performed by applying the same increase of cavity pressure (130 kPa) over different periods of time. In each analysis the loading rate was assumed constant throughout the expansion process. The only parameter which was varied with respect to the "standard" analysis (see Table 7.1) was the period of time over which loading took place while all the other specifications were

the same. The following five other loading time were employed: 90 s (1.5 minute), 9000 s (2.5 hours), 90000 s (≈1 day), 900000 s (≈10 days), 9000000 s (≈104 days).

Figure 7.22 shows the variations of pore water pressure, pore air pressure and suction computed during the pressuremeter expansion at the pressuremeter boundary at the mid-height of the pressuremeter membrane for different times of loading. Inspection of Figure 7.22 (a) suggests that the pressuremeter test, carried out adopting a rate of loading similar to the one suggested by the Ménard specifications, can be regarded as an almost fully undrained process with respect to the liquid phase. A much longer time of loading of the order of 100 days must be assumed in order to avoid the build up of any substantial excess cavity pore water pressure during the test.

The loading rate adopted for pressuremeter tests in partly saturated residual soils by Schnaid and co-workers (private communication) at Universidade Federal do Rio Grande do Sul, Brazil is significantly slower than the one adopted in tests performed according to the Ménard specifications. In their work the ultimate cavity strain of 41% is attained in a period of time between 1 and 2 hours instead of between 7 and 15 minutes as suggested by the Ménard method. The loading rate adopted by Schnaid and co-workers is of the same order of magnitude as the rate of loading employed for the numerical analysis which simulates a test duration of 9000 s. However, such loading rate, although sensibly slower than the one suggested by the Ménard method, would still produce a soil response closer to a fully undrained behaviour with respect to the liquid phase than to a fully drained one. Therefore there may be cases, as the numerical results of this study indicate, where the execution of fully drained pressuremeter tests in unsaturated soils is not a realistic option.

For the two test simulations employing faster rates of loading (i.e. 90 s and 900 s) a clear, although very small, increase of pore air pressure at the pressuremeter boundary can be observed in Figure 7.22 (b), indicating a moderate degree of coupling between gas flow and deformation (for all slower rates of loading the test is effectively fully drained with respect to the gas phase). This increase of pore air pressure at the pressuremeter boundary in the fastest tests implies that the difference between the variations of suction

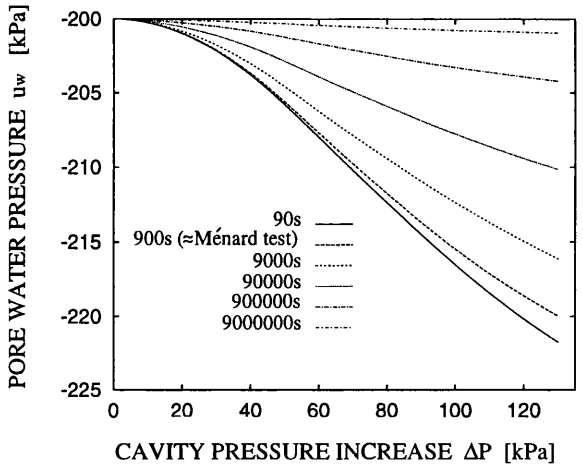

(a)

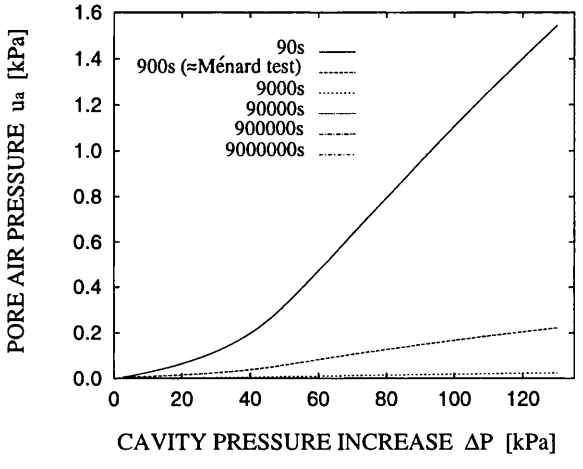

(b)

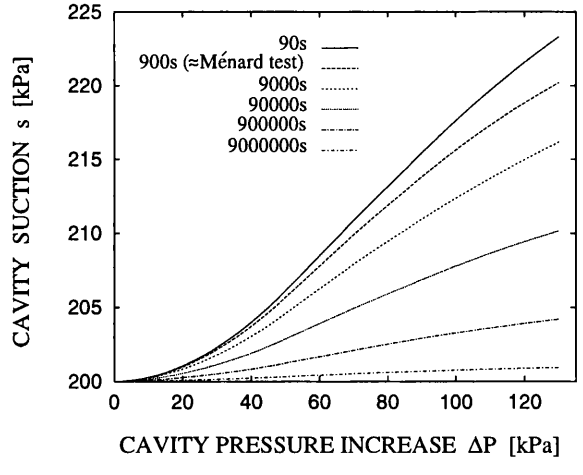

(c)

Figure 7.22: Influence of time of loading on the predicted (a)cavity pressure-pore water pressure curve, (b)cavity pressure-pore air pressure curve and (c)cavity pressure-suction curve, all computed at the mid-height of the pressuremeter membrane

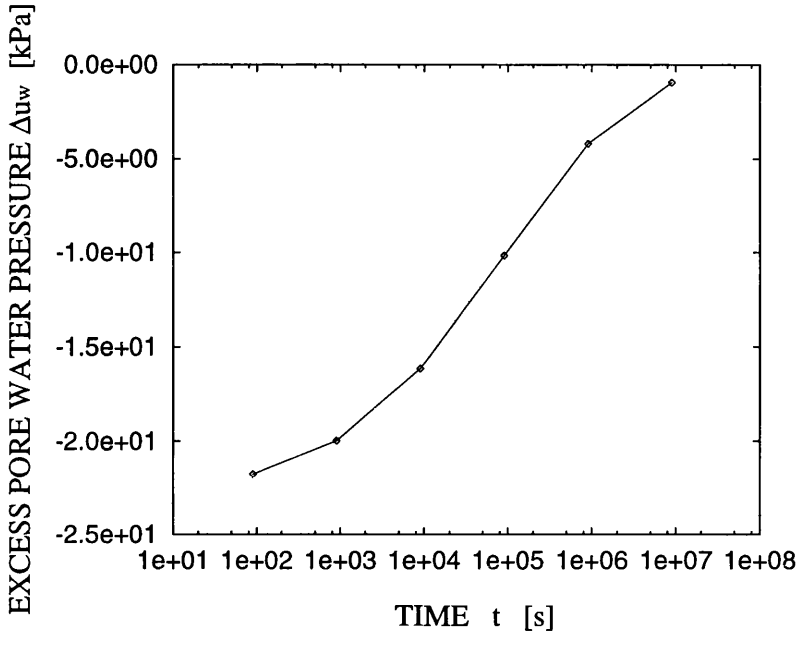

Figure 7.23: Influence of time of loading on the excess pore water pressure computed at the end of loading at the mid-height of the pressuremeter boundary

at the pressuremeter boundary computed for these two rate of loading (Figure 7.22 (c)) is greater than the difference between the two corresponding variations of pore water pressure (Figure 7.22 (a)).

Figure 7.23 presents the predictions of the excess pore water pressure at the end of loading, computed at the pressuremeter boundary at the mid-height of the pressuremeter membrane, for the six different rates of loading. The S-shaped curve shown in Figure 7.23 confirms that the two analyses simulating the fastest and slowest rates of loading are approaching respectively the limit conditions of fully undrained and fully drained expansions (with respect to the liquid phase).

Figure 7.24 shows the cavity pressure-cavity strain relationship computed for different times of loading. The curves presented in Figure 7.24 vary over a range of loading rates which covers the whole spectrum of conditions from fully undrained to fully drained. Nevertheless inspection of Figure 7.24 reveals that the rate of loading does not affect significantly the overall cavity pressure-cavity strain response measured during the test. This

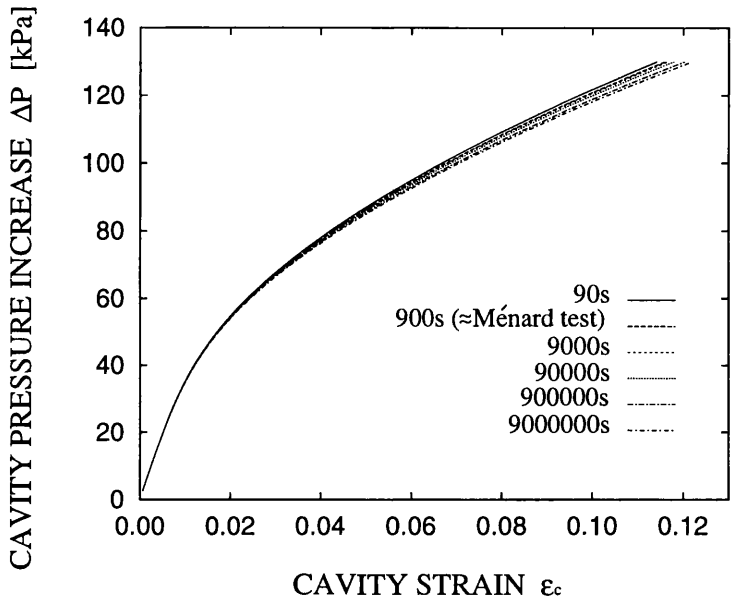

Figure 7.24: Influence of time of loading on the predicted cavity pressure-cavity strain curve

is a significant result as it indicates that, in some circumstances, it is reasonable to regard the results from pressuremeter tests, which are in reality almost undrained with respect to the liquid phase, as if these tests were fully drained processes. In other words, numerical and analytical methods proposed for the interpretation of the cavity pressure-cavity strain curve from a fully drained pressuremeter expansion, based on solutions for drained pressuremeter tests in saturated soils (see Consoli, Schnaid and Mantaras [95], Schnaid and da Silva [96]), may be applicable to tests carried out at significantly faster rates of loading. If this result, obtained for the initial conditions and material properties specified in the "standard" analysis, could be shown to be valid under more general circumstances, this would provide a justification to the extension to unsaturated soils of methods of interpretation of pressuremeter tests proposed for drained conditions in the saturated case.

A significantly stronger dependency of the predicted cavity pressure-cavity strain relationship on the rate of loading should be expected when the state surface expression of Lloret and Alonso [22] (Equation 2.41) is employed for predicting the variation of degree of

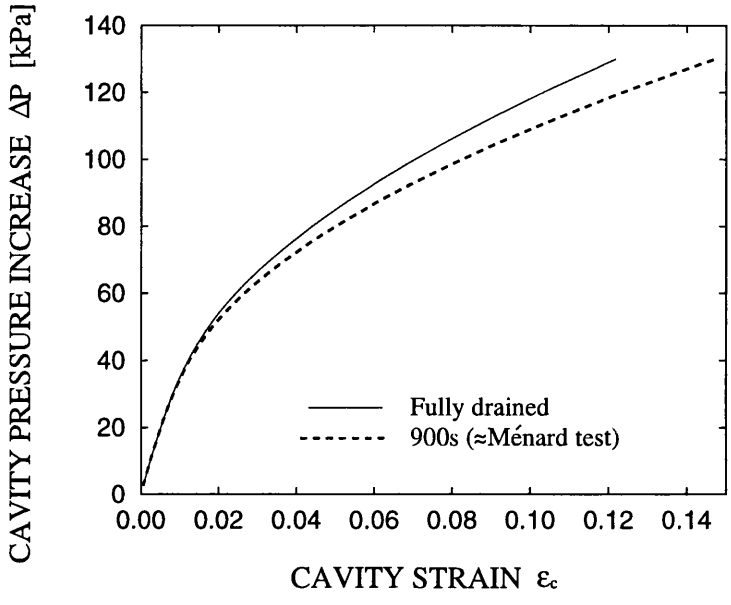

Figure 7.25: Influence of time of loading on the predicted cavity pressure-cavity strain curve (state surface equation used to model the variation of S_r)

saturation. This can be inferred by inspection of Figure 7.25 where a comparison is shown between the cavity pressure-cavity strain relationship for a loading time of 900 s computed by using the state surface expression (the same as the one shown in Figure 7.16) with the predicted cavity pressure-cavity strain relationship for a loading time of 9000000 s shown in Figure 7.24, which simulates a practically fully drained pressuremeter expansion. The computed stress-strain response for a fully drained problem is independent of the model assumed for the variation of degree of saturation. Therefore, the cavity pressure-cavity strain curve for a loading time of 9000000 s shown in Figure 7.24 coincides with the curve which would be predicted by using the state surface expression for a fully drained pressuremeter expansion.

The sensitivity of the strain response to the loading rate is expected to depend on the initial suction. In the saturated limit (zero suction) greater excess pore water pressure would be predicted during the expansion process than in the unsaturated case presented here. Therefore, as the initial suction tends from 200 kPa to zero, greater excess pore water

pressure and, consequently, greater excess suction should also be computed. Moreover, the Alonso, Gens and Josa [1] stress-strain model, employed in the simulations, suggests that, for a smaller value of in-situ suction than that assumed, the cavity pressure-cavity strain curves at different loading rates should exhibit greater differences than those shown Figure 7.24, as the stress-strain behaviour of the soil becomes more sensitive to suction changes.

Due to the complexity of the constitutive models employed a complete parametric study would be required in order to determine under what conditions it would be acceptable to idealize the stress-strain response from pressuremeter expansion in an unsaturated soil as fully drained (constant suction). This issue, however, is not within the scope of the present work and it will be investigated in future research.

7.7 Effect of overconsolidation

In this section the effect of overconsolidation on the predicted results of pressuremeter tests in unsaturated soils is considered.

Numerical results from two different analyses are presented in this section. One of these analyses was carried out according to the specifications of the "standard" case (see Table 7.1) simulating a pressuremeter test carried out in normally consolidated soil. The other, instead, assumed a soil in overconsolidated conditions. The analysis for the overconsolidated case combines an initial fully elastic response (i.e. occurrence of only elastic strains at any point throughout the soil domain) with a subsequent elasto-plastic behaviour as the expansion process is taken beyond the point when irreversible deformations begin to occur at the pressuremeter boundary. A value of 2 was chosen for the overconsolidation ratio, defined as the ratio between the maximum vertical net stress experienced by the soil in its past stress history and the current vertical net stress. The further assumption of a constant value of suction during the whole previous soil history was also introduced in the interest of simplicity.

The assumption of an overconsolidated soil involved the definition of initial in-situ values for the hardening parameter, $\overline{p}_o^*$ and the horizontal net stresses, $\overline{\sigma}_h$ (radial and

circumferential net stresses) which were different to those assumed for the normally consolidated soil in the "standard" analysis.

The maximum vertical net stress, $\overline{\sigma}_v^{nc}$ of the soil during its past history was calculated as $OCR\,\overline{\sigma}_v = 200$ kPa where $\overline{\sigma}_v = 100$ kPa is the current vertical net stress and $OCR = 2$ is the overconsolidation ratio. The attainment in the past of this vertical net stress corresponded to a normally consolidated condition. The horizontal net stress, $\overline{\sigma}_h^{nc} = 120$ kPa acting at that moment could, therefore, be calculated by assuming for the coefficient of earth pressure at rest, K_{nc}, the same value of 0.6 as in the "standard" analysis. This value of K_{nc} was calculated by using Jâky's simplified formula [100] for saturated normally consolidated soils. The past net stress state, defined by the principal stresses $\overline{\sigma}_v^{nc}$ and $\overline{\sigma}_h^{nc}$, and the concomitant value of suction (equal to the in-situ value of 200 kPa due to the assumption of constancy during the previous soil history) were then used to calculate the hardening parameter, $\overline{p}_o^*$, for the soil prior to the pressuremeter expansion by using the Alonso, Gens and Josa [1] model. In particular the principal net stresses above were used to calculate the mean net stress, $\overline{p}$ and the deviator stress, q which, together with the value of suction, s, were input in Equation 2.33 for calculating $\overline{p}_o$. This value was then used for obtaining a value of 38.8 kPa for the hardening parameter, $\overline{p}_o^*$, by employing the analytical expression of the LC yield curve (Equation 2.26).

The value of the coefficient of earth pressure at rest in the overconsolidated condition, K_o was evaluated by considering an elastic unloading path at zero lateral strain, from the normally consolidated state corresponding to the past maximum verical net stress. Due to the assumption of constant suction during the previous soil history, this yielded the following expression for the coefficient of earth pressure at rest in an overconsolidated soil, K_o:

$$K_o = K_{nc}\,OCR - \frac{\nu}{1-\nu}(OCR - 1) \tag{7.2}$$

where ν is the Poisson's ratio, assumed in this work equal to 0.3. Therefore from Equation 7.2 a value of 0.8 was calculated for the coefficient of earth pressure, K_o corresponding to an overconsolidation ratio of 2.

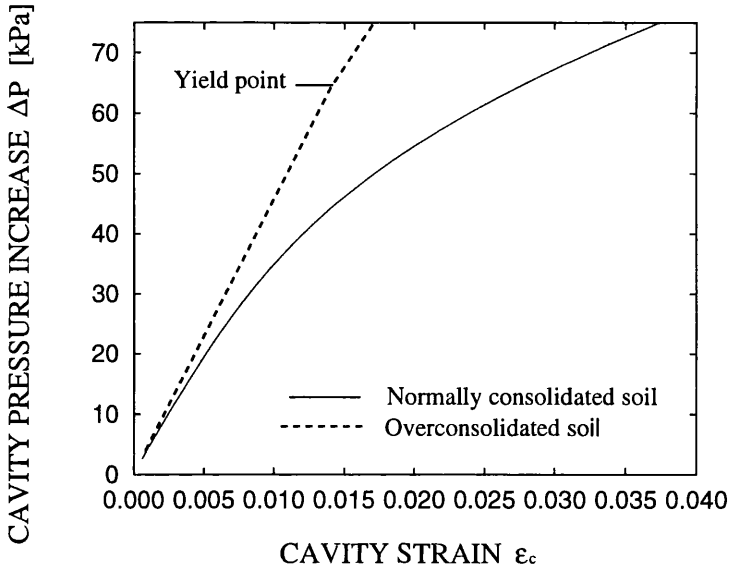

Figure 7.26: Influence of overconsolidation on the predicted cavity pressure-cavity strain curve (initial elastic stage)

Due to the stiffer response of the overconsolidated soil, a value of 200 kPa, larger than in the normally consolidated case, was chosen for the increase of the applied cavity pressure during expansion in order to attain an ultimate cavity strain of a similar magnitude to the one achieved in the normally consolidated case. All the other specifications for the simulation carried out in overconsolidated soil were the same as the ones adopted for the "standard" analysis.

Figures 7.26 and 7.27 show the curves of cavity pressure-cavity strain and cavity pressure-suction at the pressuremeter boundary during the first elastic stage of the test in overconsolidated soil (yielding occurs for an increase of the applied cavity pressure of 64 kPa) together with the corresponding curves referring to the normally consolidated soil ("standard" analysis). In the overconsolidated case the first part of the expansion process corresponds to purely elastic soil behaviour at any point throughout the domain.

Inspection of Figure 7.26 suggests for the overconsolidated soil a linear elastic response despite the non-linear elastic law of the Alonso, Gens and Josa [1] model which assumes a dependency on the mean net stress of the Young's modulus and a dependency on suction

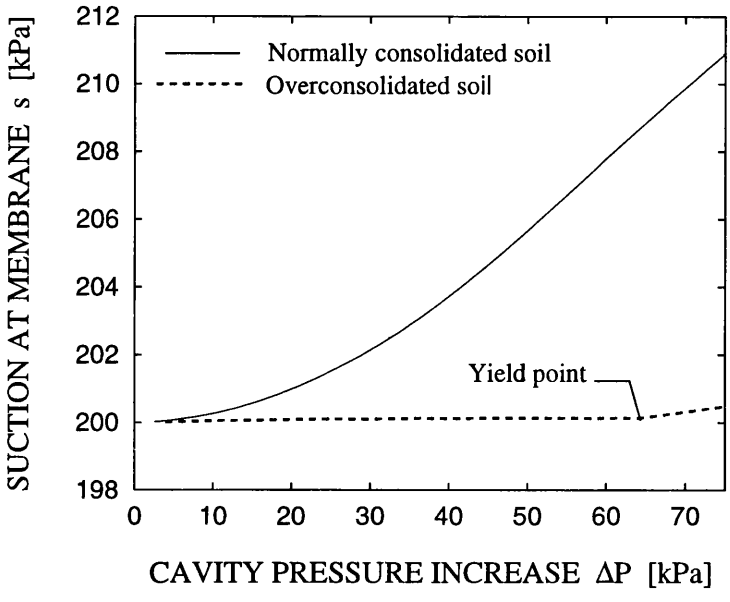

Figure 7.27: Influence of overconsolidation on the predicted cavity pressure-suction curve (initial elastic stage)

of the volumetric stiffness relative to a change in suction. The linear elastic behaviour can be explained by the prediction, in this phase of the test, of constant values of mean net stress and suction equal to their in-situ values at almost any point within the soil domain. This feature is clearly shown in Figure 7.28 where the contour plots of suction and mean net stress at the end of the initial elastic stage are presented. Although small localized variations can be observed at the extremities of the membrane, the values of mean net stress and suction appear to be uniform over the rest of the domain and equal to the initial values of 87 kPa and 200 kPa respectively.

On the basis of this prediction, it can be deduced that a similar result, apart from minor effects due to the variations of mean net stress and suction at the membrane extremities, would be obtained by simulating the same test in a single phase linear elastic medium with a Young's modulus equal to that computed by the Alonso, Gens and Josa [1] model for the initial values of net stresses. This circumstance is also confirmed by the results shown in Figure 7.29 where the predicted variations of vertical, radial and circumferential

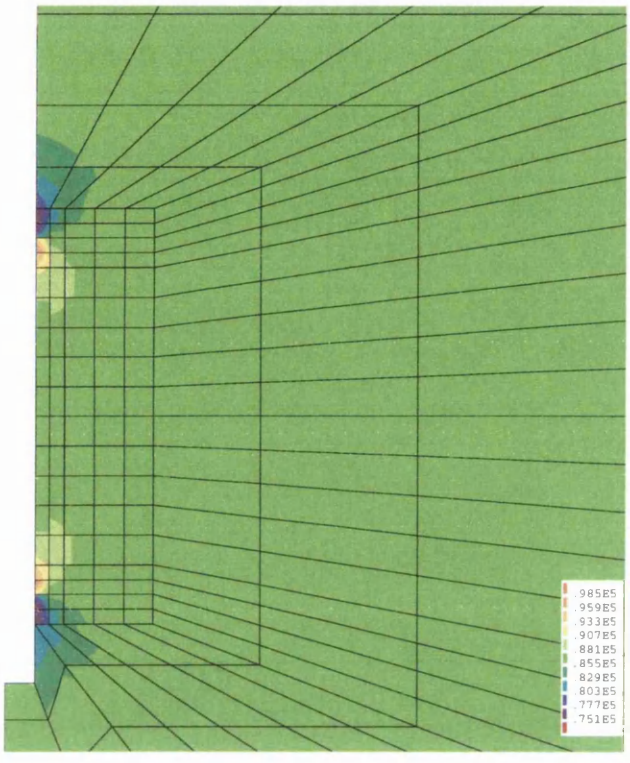

(a)

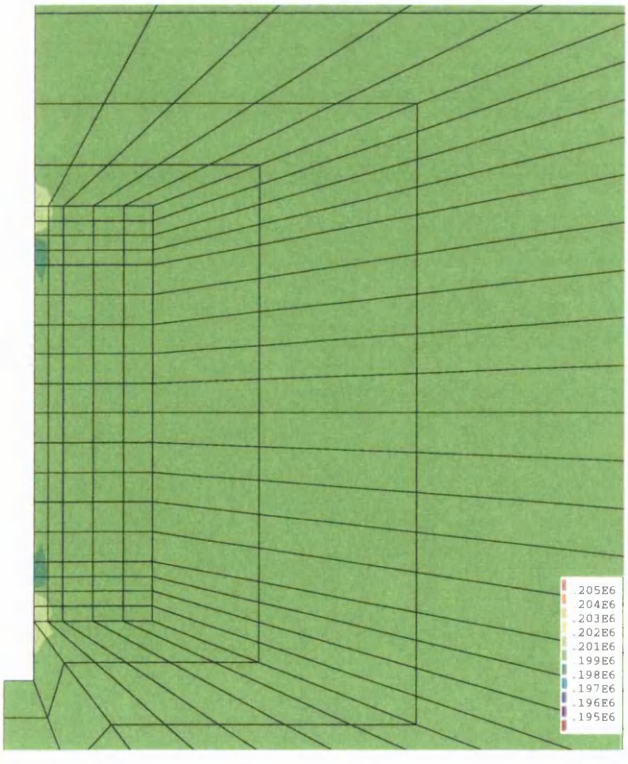

(b)

Figure 7.28: Contour plots at the end of the initial elastic stage of: (a)mean net stress (b)suction

net stresses at the two closest Gauss points to the middle of the pressuremeter membrane are presented. In this zone the soil is subjected to a similar mode of deformation as in the case of the expansion of an infinitely long cylindrical cavity. Indeed, the computed net stress variation matches the linear pattern predicted by the analytical solution of an infinitely long cylindrical cavity expanding in a single phase linear elastic material.

This is not a surprising result as an analogous conclusion can be rigorously drawn for the similar problem of the expansion of an infinitely long cylindrical cavity in a medium obeying the elastic law of the Alonso, Gens and Josa [1] model. In this case it is not difficult to show that, if a relationship for degree of saturation not depending on deviator stress is employed[1], the stress-strain response can be calculated using the solution for a single phase linear elastic medium. In the linear elastic solution, the value of the Young's modulus is given by the Alonso, Gens and Josa [1] model for a stress state corresponding to the initial in-situ value. It is also possible to show that no changes in suction occur during expansion.

Figures 7.30 and 7.31 show the curves of cavity pressure-cavity strain and cavity pressure-suction at the pressuremeter boundary during the whole test for both the overconsolidated and normally consolidated cases. As shown in Figure 7.30, a value of cavity strain of about 14% is attained for the ultimate pressure of 200 kPa indicating, as expected, a stiffer response than in the normally consolidated case. Clearly this implies, for the overconsolidated case, a higher value of the modified limit pressure, defined by the Ménard specifications as the cavity pressure corresponding to a value of 41% cavity strain.

Examination of Figure 7.31 confirms that no changes in suction are predicted during the elastic phase of expansion. Even after yielding, smaller increases of suction than in the normally consolidated case are observed. This is despite the fact that the increase of applied cavity pressure during the elasto-plastic part of the expansion process is larger than in the normally consolidated case and the loading rate is about 1.5 times faster. This result suggests that, for an overconsolidated soil, the effect of rate of loading on

[1]For elastic deformation this condition is met by both the relationships for degree of saturation considered in this work: the state surface expression of Lloret and Alonso [22] (Equation 2.41) and the elasto-plastic relationship proposed in Chapter 4 (Equation 4.5).

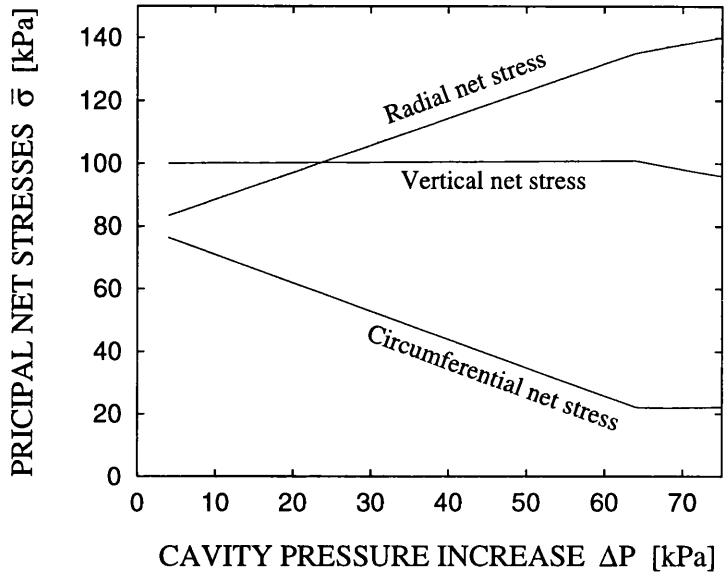

Figure 7.29: Variation of net stress state at the mid-height at the pressuremeter (initial elastic stage)

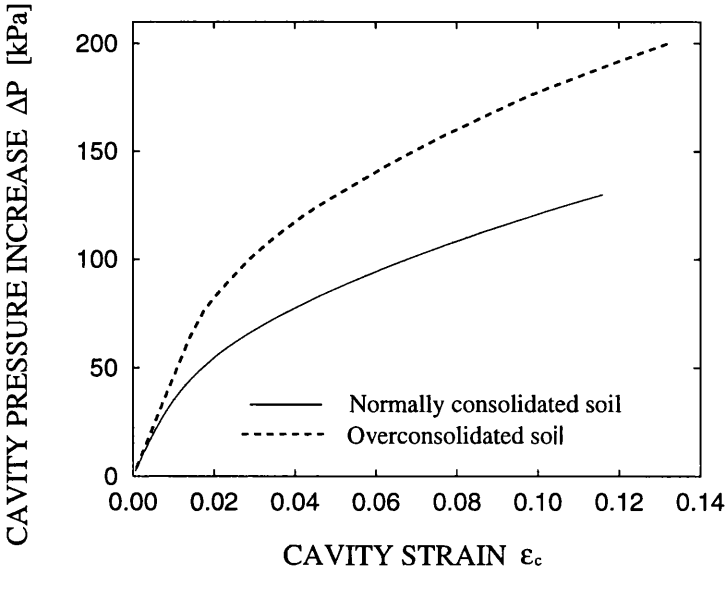

Figure 7.30: Influence of overconsolidation on the predicted cavity pressure-cavity strain curve (whole test)

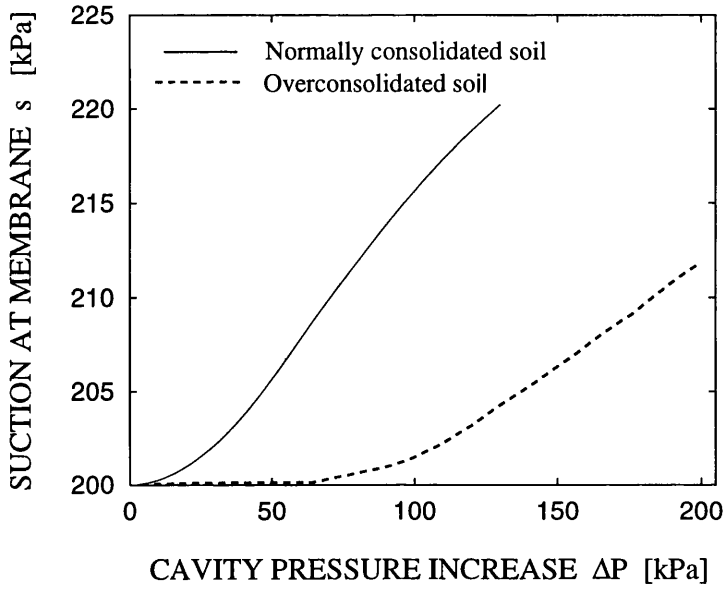

Figure 7.31: Influence of overconsolidation on the predicted cavity pressure-suction curve (whole test)

the predicted cavity pressure-cavity strain relationship is even less important than for a normally consolidated soil.

7.8 Concluding remarks

In this chapter the finite element code "Compass", improved by the author as described in Chapter 5, has been applied to the simulation of pressuremeter tests in unsaturated soil.

The simulations presented in this chapter reproduce pressuremeter expansions up to values of cavity strain ranging between 12% and 15%, involving occurrence of elasto-plastic strains and coupling of flow and deformation. The results demonstrate the potential of the enhanced code to be applied to the study of more complex problems than the ones illustrated in Chapters 5 and 6. They also demonstrate the importance of adequate modelling of the variation of degree of saturation for the study of a boundary value problem. The results calculated by using the improved relationship for the variation of degree of saturation proposed in this thesis, are significantly different to those computed by assuming

the state surface expression implemented in the original version of the code. The results obtained from this study also allowed a number of issues relating to pressuremeter tests in unsaturated soil to be explained.

Preliminary work was carried out in order to define a "standard" analysis which provided numerically reliable results. This case formed a basis for exploring different features of the pressuremeter problem by varying in each analysis only one of the "standard" specifications according to the aspect being investigated.

The effect of the rate of loading on the occurrence of coupling between flow and deformation has been assessed. For a normally consolidated soil with parameter values similar to those reported Table 7.1, it has been shown that a very slow rate of increasing cavity pressure, with a test duration of the order of 100 days, would be needed in order to achieve a fully drained response with respect to the liquid phase. When a test with a duration of about 15 minutes is simulated, similar to the rate which would be employed for a pressuremeter test performed according to the Ménard specifications, the numerical results predict that the soil behaviour is very close to fully undrained. Even for a slower rate of loading (a test duration of 150 minutes), of the same order of magnitude as the one used by Schnaid and co-workers (private communication) for pressuremeter tests in southern Brazil, the soil response is closer to fully undrained than to fully drained.

However, during a fully undrained test a relatively small increase of pore water pressure was computed at the pressuremeter boundary, where the maximum variation of pore water pressure is attained. This meant that the cavity strain-cavity pressure relationships calculated for a range of loading rates from fully undrained to fully drained, were all very similar. This is a significant result, as it allows the use of numerical and analytical methods of interpretation proposed for drained pressuremeter tests in saturated soils to be extended also to unsaturated cases. This extension is based on the hypothesis that the mechanical behaviour of unsaturated soils in drained conditions is qualitatively similar to the saturated one and, therefore, the same stress-strain relationships may be used in the two cases as long as a dependency of the mechanical parameters on the level of suction is accounted for.

The relative insensitivity of the stress-strain response to the rate of loading is believed to be partly a consequence of the initial value of suction. On the basis of the Alonso, Gens and Josa [1] model, it is reasonable to expect a stronger dependency on rate of loading when smaller values of initial suction are assumed. The results obtained are strictly valid only for the set of parameters values employed in the simulations. This work does not aim, therefore, to give a general answer to the problem of the interpretation of pressuremeter tests in unsaturated soil. Further research is needed in order to carry out a full parametric study of the various factors involved.

Another important result is that the observed insensitivity of the predicted cavity pressure-cavity strain curve to the the rate of loading is partly a consequence of the use of the elasto-plastic relationship (Equation 4.5) proposed in Chapter 4 for the prediction of the variation of degree of saturation. When the state surface expression (Equation 2.41) of Lloret and Alonso [22] is employed (as in the original version of code "Compass"), noticeably larger differences between curves at different rates of loading are predicted. For the same rate of loading, the two relationships for degree of saturation predict significantly different responses in terms of cavity pressure-cavity strain and cavity pressure-suction at pressuremeter boundary curves. The patterns of suction variation in the two cases are opposite, as the elasto-plastic relationship suggests an increase of suction while the state surface expression indicates a decrease. These results confirm the critical role of improved modelling of the variation of degree of saturation for accurate predictions of the values of suction and deformations in a boundary value problem.

Results also showed that any significant variation of suction from the initial in-situ value (200 kPa) is limited to a restricted cylinder of soil around the probe (with a radius from the borehole axis of less than 20 cm). For the net stress state, the in-situ values are restored at a radial distance of about 50 cm. This numerical result agrees with experimental data from suction monitored pressuremeter tests in unsaturated granite residual soils of southern Brazil by Schnaid and co-workers (private communication) where constant values of suction were measured during expansion by tensiometers at radial distances from the borehole axis of 30 cm and 60 cm.

An analysis simulating a pressuremeter test in overconsolidated soil was also performed. The first part of this analysis predicts a fully elastic response at any point throughout the soil domain and a linear cavity pressure-cavity strain relationship. The linearity of the stress-strain response is explained by the constant values of mean net stress and suction computed during the elastic phase of expansion at any point throughout the soil domain, apart from localized variations observed at the extremities of the pressuremeter membrane. Under these circumstances the non-linear elastic relationship of the Alonso, Gens and Josa [1] model coincides with a linear elastic law where the Young's modulus is equal to the initial one (calculated for the in-situ net stress state). This results provides a validation of the correctness of the predictions computed by the code because an analogous conclusion can be rigorously drawn for the ideal case of an infinitely long cylindrical cavity expanding in an unbounded unsaturated medium obeying the non-linear elastic law of the Alonso, Gens and Josa [1] model and an isotropic relationship for the variation of degree of saturation. In this case no variation of suction is predicted and the stress-strain response can be calculated by using the solution available for single phase linear elastic medium, with a Young's modulus corresponding to the initial stress state of the soil.

If the whole test is considered (including the subsequent elasto-plastic phase of expansion), the predicted cavity pressure-cavity strain relationship for the oveconsolidated soil shows a stiffer response than the corresponding normally consolidated soil, indicating, as expected, higher values of the modified limit pressure (defined according to the specifications of the Ménard test) for overconsolidated soils. The cavity pressure-suction relationship predicts no changes of suction during the initial elastic expansion while an increase is computed after yielding. Comparison with the results of the simulation in normally consolidated soil for a loading time of 900 s indicates that a smaller increase in suction is predicted at the end of the expansion process for the overconsolidated case. This occurs despite the fact that the increase of cavity pressure during the elasto-plastic phase of expansion is larger than in the normally consolidated case and the loading rate is 1.5 times faster. This result, therefore, indicates that overconsolidation tends to reinforce even further the conclusion that the predicted stress-strain response is insensitive to the

rate of loading.

Chapter 8

Conclusions and suggestions for further research

8.1 Conclusions

The work presented in this thesis relates to three main areas: the constitutive modelling of unsaturated soils; the improvement of a numerical tool (i.e. the finite element code "Compass") for studying boundary value problems in unsaturated soils; and initial application of the numerical code to pressuremeter testing in unsaturated soils.

8.1.1 Constitutive modelling

On the constitutive side, the main contribution of this work is the formulation of a new relationship for degree of saturation, S_r, which introduces a relationship between degree of saturation, suction and specific volume (see Chapter 4). This form of relationship attempts to take into account the influence of the arrangement of voids in an unsaturated soil on the soil-water characteristic curve by introducing dependency on the specific volume. The use of the plastic component of the change of specific volume instead of the specific volume was also considered. Dependency on specific volume was chosen, however, because this has the advantage of relating quantities directly measured in the laboratory. Therefore, a general relationship for a given soil can be defined, which could then be combined with any particular stress-strain model predicting the variation of specific volume.

It was shown that, if an elasto-plastic stress-strain model is assumed, the proposed relationship is capable of predicting both reversible (in the elastic domain) and irreversible

(in the elasto-plastic domain) variations of degree of saturation, resulting in an elasto-plastic relationship for degree of saturation. The proposed relationship also provides a means of predicting the variation of degree of saturation observed during shearing of unsaturated soil samples in the laboratory.

This development represents a significant improvement over the traditional approach of a unique relationship (i.e. a state surface) between degree of saturation, suction and mean net stress adopted previously for the study of coupled flow-deformation problems in unsaturated soils. The limitations of the state surface approach were qualitatively described in Section 2.5.1, and these are largely overcome by the new relationship proposed in this thesis. A quantitative assessment of the errors involved in using a state surface expression for degree of saturation was also presented in Section 3.3 by comparing experimental results with the predictions obtained by using the state surface expression of Lloret and Alonso [22] (Equation 2.41).

The relationship for degree of saturation proposed in this thesis is, however, unable to reproduce the feature of hydraulic hysteresis observed during wetting-drying cycles. In this case the irreversible changes of degree of saturation are not caused by the occurrence of irreversible changes in the arrangement of soil voids but they are related to irreversibility in the process of water draining into or out of voids, caused by differences in the geometry of the air-water interfaces during wetting and drying (see Section 2.5.3). For example, hydraulic hysteresis can occur during wetting-drying cycles at constant net stress taking place within the yield locus, where irreversible changes of specific volume (i.e. changes of void arrangement) are not present.

Based on the equation proposed by van Genuchten [48] (Equation 2.42), an explicit form for the relationship between degree of saturation, suction and specific volume was presented in Section 4.3 to fit the normal compression and critical state data from laboratory tests on compacted Speswhite Kaolin performed by Sivakumar [13]. The proposed analytical expression is, however, only one possibility and different choices for the relationship between degree of saturation, suction and specific volume can be envisaged on the basis of other experimental evidence.

The model predictions in terms of variation of degree of saturation were compared with experimental results from several types of tests on compacted Speswhite Kaolin carried out by Sivakumar [13] and Zakaria [15]. The experimental data covered a wide range of stress paths, including isotropic loading to normally consolidated states (at various different values of suction), isotropic unloading and re-loading, wetting under isotropic stress states, and various forms of suction controlled shearing. In all the experimental tests, however, suction was varied monotonically, so any influence of hydraulic hysteresis was excluded. The predictions were computed by combining the proposed relationship for degree of saturation with the two elasto-plastic stress-strain models of Alonso, Gens and Josa [1] and Wheeler and Sivakumar [3]. Generally, a very good agreement with the experimental results was achieved. The best agreement was usually obtained when the Wheeler and Sivakumar [3] model was combined with the proposed relationship for degree of saturation. This is explained by the fact that the Wheeler and Sivakumar [3] model is better able to match the variation of specific volume of Speswhite Kaolin than the model of Alonso, Gens and Josa [1].

In the numerical analyses described in the thesis, the constitutive relationship assumed for the stress-strain behaviour was the elasto-plastic model of Alonso, Gens and Josa [1]. On the basis of the experimental data for compacted Speswhite Kaolin provided by Sivakumar [13] and Zakaria [15], a set of soil parameter values (assumed in all the relevant computations presented in the thesis) were selected (see Chapter 3). One significant point relates to the choice of a value greater than 1 for the parameter r, whereas Alonso, Gens and Josa [1] in the development of their model suggested values smaller than 1. It was shown that the choice of a value of r greater than 1 is consistent with the prediction of realistic shapes for the LC yield curves if it is combined with a value of the reference pressure, p^c sensibly higher than the range of values of interest for the hardening parameter, $\overline{p}_o^*$.

8.1.2 Improvements to code "Compass"

On the numerical side, the thesis describes the improvements and developements undertaken by the author on the finite element code "Compass" (originally developed by Prof.

H.R. Thomas and co-workers at the University of Cardiff).

The changes undertaken by the author on code "Compass" relate to the following different issues.

1. The relationship between degree of saturation, suction and specific volume proposed in this thesis was implemented in code "Compass". The correctness of this implementation was confirmed by the agreement between numerical and analytical computations for three benchmark problems simulating notional laboratory tests involving a wide variety of possible soil responses: from purely elastic to elasto-plastic, from fully drained conditions to coupled flow-deformation.

   The numerical simulation of another notional laboratory test involving coupling of flow and deformation was performed in order to assess the difference of predictions obtained by using the state surface approach for degree of saturation (originally implemented in "Compass") and the new elasto-plastic relationship for degree of saturation combined with the elasto-plastic model of Alonso, Gens and Josa [1]. The results showed that the use of the state surface expression with an adequate set of parameters values can give similar results to those computed with the elasto-plastic relationship for degree of saturation either in the elastic or in the elasto-plastic domain. It is not possible, however, to obtain an agreement in both domains by using a single set of parameter values for the state surface expression. Clearly this is caused by the inability of the state surface approach to take into account the effect of yielding on the variation of degree of saturation.

   The differences between the predictions of the two relationships for degree of saturation were not limited to the prediction of the variation of degree of saturation (or water content). Significantly different results were also computed for the mechanical response and the consolidation time during the equalization stages subsequent to loading. The first effect is a consequence of the different suction variations computed by the two models during undrained or partially drained loading, which results in different stress paths. For the example studied, the displacements were noticeably overestimated in the case when the state surface approach for degree of saturation

was employed. The second effect is a consequence of the link between liquid permeability and degree of saturation. In the case where the elasto-plastic relationship was employed, significantly greater values of liquid permeability were calculated due to greater values of degree of saturation, and this accelerated the process of dissipation of excess pore water pressure.

2. The equations of water and air continuity in code "Compass" were corrected by expressing them in terms of flux velocities of the liquid and gas phases relative to the soil skeleton. In the original code, as in other examples in the literature, these equations involved absolute flux velocities, which were incorrectly related to the gradients of hydraulic or pneumatic head by using Darcy's law. This is incorrect, because Darcy's law postulates a relationship between the flux velocities relative to the soil skeleton and the gradient of the relevant potential. The use of Darcy's law in combination with the absolute flux velocities produces two different types of errors. The first error, which affects analyses under either saturated or unsaturated conditions, is the introduction of the derivative dn/dt instead of $-d\epsilon_v/dt$ in both the equations of water and air continuity. The second error, which only has any influence for unsaturated conditions, is the omission (in both equations) of terms containing the gradient of degree of saturation and the gradient of air density. The first error, although present in the documentation of the original version of code "Compass", was subsequently corrected by the authors of the original version by making the compensating error in the implementation of the continuity equations of incorrectly assuming $dn/dt = -d\epsilon_v/dt$ (following an historical error made by Terzaghi [73]). It is possible that this compensating error is also present in the numerical implementations of the other examples in the literature where the incorrect combination of Darcy's law with absolute flux velocities is stated in the documentation.

   A numerical study was presented simulating a notional laboratory test in order to assess the effect of the incorrect combination of Darcy's law with absolute flux velocities. The results showed significant differences between the correct and incorrect formulations for the predicted values of suction during undrained loading. The errors

due to the use of the incorrect formulation also remained at the end of consolidation. It was also shown that these differences are almost completely eliminated if the compensating error of assuming $dn/dt = -d\epsilon_v/dt$ is introduced. The omission of terms containing the gradients of degree of saturation and air density affected the predicted values of suction by a relatively small amount compared with the absolute values of suction involved in the particular example considered. The errors due to this omission were, however, not insignificant if compared with the changes of suction induced by loading.

3. Modificatitions were carried out to the convergency algorithm for the elasto-plastic model of Alonso, Gens and Josa [1].

   Firstly, residual flux terms, which had been omitted in the original version of code "Compass", were included. These terms arise in the two equations of water and air continuity during the convergency process at constitutive level, analogous to residual forces in the equation of equilibrium. In general, if a relationship for degree of saturation that includes dependency on the net stresses is used together with a convergency algorithm for an elasto-plastic stress-strain model, these residual flux terms must be taken into account during the convergency process at constitutive level. Definitions of the residual flux terms were given both for the case of a state surface relationship for degree of saturation and for the case of the proposed new elasto-plastic relationship for degree of saturation.

   The second modification consisted of changing one of the three convergency criteria present in the original code. The proposed criterion introduces a tolerance zone surrounding the yield envelope with an amplitude defined by the user. During the convergency algorithm the stress state is regarded as converged back onto the yield locus if it lies within this tolerance zone. The new criterion replaced that implemented in the original version of the code, which imposed a restriction on the visco-plastic strain rate in order to test for convergency of the stress state. This, however, did not represent a valid test for convergency as the visco-plastic strain rate depends also on the fluidity parameter, γ which is an input parameter used to

control the speed and the stability of the convergency process.

A numerical study simulating a notional laboratory test was performed in order to explore the consequences of neglecting the residual flux terms during the convergency algorithm. The computations showed that the omission of these terms resulted in substantial errors in the predictions. It was also observed that, for particular choices of parameter values in a state surface equation for degree of saturation, the code was unable to converge when residual flux terms were not taken into account.

4. The error in the implementation of the plane-strain deformation regime for elasto-plastic unsaturated soils in the original version of code "Compass" was corrected. The original formulation incorrectly imposed the condition of nullity on the out-of-plane component of each of the three contributions to the total strain rate vector (i.e. the elastic strain rate vector due to a change in the net stresses, the elastic strain rate vector due to a change in suction and the plastic strain rate vector). In the plane-strain deformation regime, however, only the out-of-plane component of the total strain rate vector must be equal to zero. Such inconsistency, present in the original implementation of "Compass", appears to be present also in other examples published in the literature and is probably due to the history of the development of finite element programs.

   Using both the correct and the incorrect formulations of the plane-strain deformation regime, numerical simulations of two types of notional bi-axial tests were performed in order to assess the significance of the errors caused by the incorrect formulation. First, three different wetting paths were simulated and the results showed that, for a given decrease of suction, the incorrect version tended to overestimate both the elastic swelling and the elasto-plastic collapse-compression after the onset of yielding. Second, two in-plane loading paths at constant suction were simulated. In this case the correct and the incorrect version predicted the same results in the elastic domain but, after the onset of yielding, the incorrect version tended to overestimate the compression of the soil sample due to an increase of the applied load. In both types of test simulations the overestimation of the elasto-plastic compressive strain,

due to a decrease of suction or an increase of in-plane stresses, was more evident at small values of plastic strains, whereas at large values of plastic strains the stress-strain curves predicted by the two versions seemed to become parallel. Moreover the relatively small differences between the results calculated by the correct and incorrect versions for the in-plane loading simulation at a constant suction of zero (saturated conditions) explains why this type of error was difficult to detect in codes implementing traditional models for saturated problems.

5. A program was coded interfacing the input and output of code "Compass" to the commercial software FEMGEN/FEMVIEW [66] for graphical pre- and post-processing of data.

6. The option of performing mesh updating (i.e. updating of nodal coordinates) at the beginning of each time step according to the displacements that occurred in the previous stages of the analysis, was introduced within code "Compass". This modification allows geometrical non-linearity to be taken into account in those cases where large values of displacement occur. This does not represent, however, a full large-strain formulation of the problem. This option was introduced as it was considered necessary for the simulation of the pressuremeter tests presented in Chapter 7, where large values of displacement are computed at the pressuremeter membrane during the expansion process.

8.1.3 Application to pressuremeter testing

The application of code "Compass" to the simulation of pressuremeter tests in unsaturated soil demonstrated the potential of the code, as enhanced in this work, for analysing boundary value problems involving elasto-plastic strains, coupled flow-deformation and large values of displacement. The study also provided some initial insight into the interpretation of the results from pressuremeter tests in unsaturated soils.

Several simulations of pressuremeter tests in normally consolidated unsaturated Speswhite Kaolin were carried out at different rates of loading, with the duration of the test ranging from 90 s to 9000000 s. The variation of pore water pressure predicted at the pressure-

meter membrane (where the maximum variation of pore water pressure is attained) showed that fully drained conditions (with respect to liquid) could only occur during very slow tests, which would not be feasible in reality. The simulation of a test performed at similar loading rate as a standard Ménard test, suggested that the soil response was close to fully undrained with respect to liquid flow. Even for a slower rate as that used by Schnaid and co-workers (private communications) for tests in unsaturated residual soils of southern Brazil, the behaviour is closer to fully undrained than fully drained. For the gas phase, however, only in the two fastest tests (with loading rates respectively similar to that of a Ménard test and one order of magnitude faster) it was possible to detect any degree of coupling between deformation and the gas flow and, in all cases, the computed variation of pore air pressure was relatively small.

Despite the fact that a complete range of conditions, from fully undrained to fully drained with respect to the liquid flow, was considered, the computed variation of pore water pressure, and hence suction, at the pressuremeter membrane was relatively small in all simulations. This, in turn, meant that similar cavity pressure-cavity strain relationships were predicted, irrespective of the rate of loading. This result seems to suggest that it is possible to interpret pressuremeter tests in unsaturated soils, even if carried out at rate of loading involving undrained soil response (as for example Ménard tests), by using analytical and numerical methods proposed for fully drained tests. In particular, methods developed for interpreting fully drained tests in saturated soils could be applied to the unsaturated case, simply by selecting parameter values that are appropriate to the initial in-situ value of suction in the soil. The conclusion that the pressuremeter response in an unsaturated soil is relatively insensitive to rate of loading is, however, at this stage limited to the particular conditions considered in this work, namely the assumed in-situ soil state (net stresses, suction and normally consolidated state) and the chosen set of parameters values. A wider parametric study is needed in order to explore whether the conclusions above are more generally applicable.

One simulation of a pressuremeter test was also carried out using the state surface equation for degree of saturation originally implemented in code "Compass". In this

case the results predicted that suction at the pressuremeter membrane decreased during expansion, whereas the analyses employing the improved elasto-plastic variation of degree of saturation showed a small increase of suction. The results from the analysis employing the state surface relationship for degree of saturation also showed a significantly stronger dependency of the cavity pressure-cavity strain response on the rate of loading. Therefore, the conclusion that the rate of loading has a relatively small effect on the pressuremeter response is partly a consequence of the new degree of saturation relationship. This confirms the vital role of accurate modelling of the degree of saturation in obtaining a realistic hydro-mechanical response for boundary value problems.

One simulation of a pressuremeter expansion in an overconsolidated unsaturated soil predicted even smaller variation of suction at the pressuremeter membrane than in the equivalent normally consolidated soil. Prior to yielding the suction remained absolutely costant, consistent with analytical results for the expansion of an infinitely long cylinder in an elastic soil. Consequently, pressuremeter expansion in overconsolidated unsaturated soils is likely to be even less sensitive to rate of loading than in normally consolidated unsaturated soils.

8.2 Suggestions for further research

The model proposed in this thesis for representing the variation of degree of saturation in an elasto-plastic fashion is a significant improvement over the approch used in the past for modelling the variation of degree of saturation (i.e. a state surface). Further research, however, is needed for taking into account the other crucial aspect of hydraulic hysteresis. This can be achieved by following two different routes. The first approach is similar to that used in this thesis for describing the elasto-plastic variation of degree of saturation. It consists of developing an hysteretic constitutive model for the variation of degree of saturation which does not affect the drained mechanical behaviour of the soil. In this case, the proposed hysteretic model can be used as an extension to any existing stress-strain relationship for unsaturated soils. Following this approach, an initial proposal for modelling hydraulic hysteresis was made by Vaunat, Romero and Jommi [102]. The

second approach is more complete as it aims to take into account the link between the variation of degree of saturation and the drained stress-strain response of the soil. This approach, therefore, requires the development of a model which combines the drained mechanical behaviour and the variation of degree of saturation in a unique framework. In this direction, Buisson and Wheeler [103] presented some preliminary ideas in order to take into account the influence of the hydraulic hysteresis on the hydro-mechanical behaviour of unsaturated soils. Their qualitative framework is based on the consideration of the distinct mechanisms governing volume changes in gas filled voids and liquid filled voids.

On the numerical side, further improvements may be undertaken on code "Compass". An algorithm should be implemented in the code to deal with the transition from unsaturated to saturated conditions and vice-versa. The transition to saturated conditions could be simulated by imposing that, after a zero value of suction is attained, the pore air pressure in the equilibrium equation (Equation 5.1) is equal to the pore water pressure and the degree of saturation in the equations of liquid and gas flows (Equations 5.10 and 5.12), is equal to 1. The equation of gas flow should still be used in the saturated zone (due to the presence of dissolved air) for calculating a notional value of the pore air pressure. The process of desaturation starts when the notional value of pore air pressure (which is smaller than pore water pressure value while the soil is saturated) becomes equal to the value of pore water pressure.

Moreover, future achievements on the side of constitutive modelling for the variation of degree of saturation (e.g. modelling of hydraulic hysteresis) should be implemented in the code in order to enhance the accuracy of this tool for the hydro-mechanical analysis of boundary value problems in unsaturated soils.

Finally, another improvement recommended to be made to the code is the implementation of the option for simulating processes of excavation and construction, which is an important feature for the application of the code to practical engineering problems. In the current version of the code the processes of excavation and construction can only be simulated by reducing or increasing with time the applied loads on the boundary of the

soil domain. This is, however, a crude approximation as the stress path induced by excavation or construction is unknown and should be computed as a result of the finite element analysis.

The results obtained from the simulation of pressuremeter tests in unsaturated soils suggest that there is scope for further research. The small sensitivity of the computed cavity pressure-cavity strain response to the rate of loading is a result which is due to the particular in-situ stress state, past stress history and set of model parameters chosen for the simulations in this thesis. In order to achieve conclusions having more general validity it would be necessary to perform a full parametric study of the problem, taking into account the variation of each factor which has a significant effect on the outcome of the analysis. It is possible that for different conditions from those assumed in this thesis a stronger dependency of the stress-strain response on the rate of loading could be obtained and, therefore, a methodology should be proposed for detecting under which circumstances the pressuremeter expansion can be regarded as a fully drained (constant suction) process.

Appendix A

Solid fraction mass balance equation

The solid fraction mass balance equation is derived here using an Eulerian approach. This means that the mass balance of soil is applied to an infinitesimal element of space (the control volume) within the soil domain. This infinitesimal element of space having a constant volume dV, is shown in Figure A.1 and the volume of the solid fraction, dV_s, within this control volume is given by:

$$dV_s = (1 - n)dV \tag{A.1}$$

where n is the porosity.

The rate of change of the solid fraction volume within the control volume is obtained

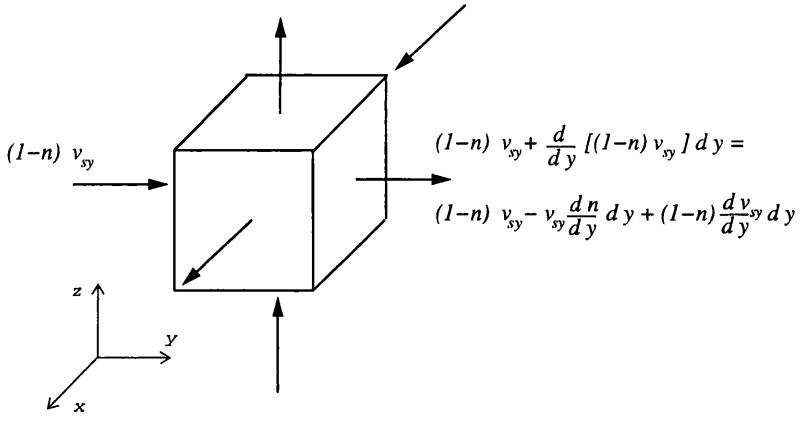

Figure A.1: Infinitesimal control volume for the mass balance of the solid fraction

by differentiating Equation A.1 with respect to time, giving an Eulerian derivative:

$$\frac{d(dV_s)}{dt} = -\frac{dn}{dt}dV. \tag{A.2}$$

A change of porosity within the control volume can be caused by two different physical processes. One is the occurence of deformation of the soil skeleton and the other is the rigid motion of the solid skeleton (having a spatial gradient of porosity) through the control volume. Thus:

$$\frac{dn}{dt} = \left(\frac{dn}{dt}\right)_d + \left(\frac{dn}{dt}\right)_t \tag{A.3}$$

where $(dn/dt)_d$ is the component of the rate of change of n due to soil deformation and $(dn/dt)_t$ is the component due to rigid motion. The distinction between these two different contributions to dn/dt is important because only the part $(dn/dt)_d$ can be related to the volumetric strain rate, through the relationship:

$$\left(\frac{dn}{dt}\right)_d = -(1-n)\left(\frac{d\epsilon_v}{dt}\right) \tag{A.4}$$

where ϵ_v is the volumetric strain rate (compression positive). Therefore the rate of change of the solid fraction volume may be rewritten, by distinguishing between these two contributions to the porosity change rate and by using Equation A.4, as:

$$\frac{d(dV_s)}{dt} = -\left[\left(\frac{dn}{dt}\right)_t - (1-n)\left(\frac{d\epsilon_v}{dt}\right)\right] dV. \tag{A.5}$$

If the solids are assumed to be incompressible, the mass balance of the solid fraction requires that the rate of change of the solid fraction volume within the control volume, given by Equation A.5, must be equal to the net influx of solids through the element boundaries. Figure A.1 shows the inflow and outflow of solids per unit area through the two faces of an infinitesimal element that are perpendicular to the y axis (where v_{sy} in Figure A.1 represents the component of absolute flux velocity of the soil skeleton in the y direction). Consideration of similar fluxes in the x and z directions results in the following expression for the net influx I of solids through the element boundaries:

$$I = -\left(-\frac{d\boldsymbol{u}_d}{dt}\nabla n + (1-n)\mathrm{div}\,\boldsymbol{v}_{sa}\right)dV \tag{A.6}$$

where $\boldsymbol{v}_{sa}$ is the absolute velocity vector of the solid fraction and $\boldsymbol{u}_d$ is the displacement vector for the soil skeleton. Equation A.6 can be rewritten in an alternative form:

$$I = -\left(-\frac{d\boldsymbol{u}_d}{dt}\nabla n - (1-n)\frac{d\epsilon_v}{dt}\right)dV. \tag{A.7}$$

The continuity equation for the solid fraction is therefore derived by equating $d(dV_s)/dt$ from Equations A.5 with I from Equation A.7, to give:

$$\frac{d\boldsymbol{u}_d}{dt}\nabla n + \left(\frac{dn}{dt}\right)_t = 0. \tag{A.8}$$

Using Equations A.3 and A.4 to replace $(dn/dt)_t$, Equation A.8 can be rewritten as:

$$\frac{d\boldsymbol{u}_d}{dt}\nabla n + \frac{dn}{dt} + (1-n)\frac{d\epsilon_v}{dt} = 0. \tag{A.9}$$

Equation A.9 can be rewritten in terms of void ratio, e instead of porosity, n, to give:

$$\frac{d\boldsymbol{u}_d}{dt}\nabla e + \frac{de}{dt} + (1+e)\frac{d\epsilon_v}{dt} = 0. \tag{A.10}$$

Appendix B

Published papers

D. Gallipoli. Numerical modelling of unsaturated soils and application to pressuremeter testing. In *Proceedings BGS Young Geotechnical Engineers' Conference, Newcastle*, 1998.

D. Gallipoli, M. Karstunen and S.J. Wheeler. Plane-strain modelling for unsaturated soil. In *Proceedings European Conference on Numerical Methods in Geotechnical Engineering, Udine*, pages 463–472, 1998.

D. Gallipoli, M. Karstunen and S.J. Wheeler. A note on modelling coupled flow-deformation in unsaturated soils. In *Proceedings International Symposium on Numerical Models in Geomechanics, Graz*, pages 255–262, 1999.

D. Gallipoli, M. Karstunen and S.J. Wheeler. Numerical modelling of pressuremeter tests in unsaturated soil. In *Proceedings International Conference on Computer Methods and Advances in Geomechanics, Tucson*, accepted for publication, 2001.

D. Gallipoli, M. Karstunen and S.J. Wheeler. An improved relationship for modelling irreversible changes of degree of saturation within an unsaturated soil. To be submitted to *Géotechnique.*

References

[1] E.E. Alonso, A. Gens, and A. Josa. A constitutive model for partially saturated soils. *Géotechnique*, 40(3):405–430, 1990.

[2] E.E. Alonso, A. Gens, and D.W. Hight. Special problem soils. general report. In *Proceedings European Conference Soil Mechanics and Foundation Engineering, Dublin*, volume 3, pages 1087–1146, 1987.

[3] S.J. Wheeler and V. Sivakumar. An elasto-plastic critical state framework for unsaturated soil. *Géotechnique*, 45(1):35–53, 1995.

[4] A.W. Bishop. The principle of effective stress. *Tek. Ukeblad*, 39:859–863, 1959.

[5] J.B.E. Jennings and J.B. Burland. Limitations to the use of effective stresses in partially saturated soils. *Géotechnique*, 12(2):125–144, 1962.

[6] S. Kato, H. Matsuoka, and D.A. Sun. A constitutive model for unsaturated soil based on extended smp. In *Proceedings International Conference on Unsaturated Soils, Paris*, volume 2, pages 739–744, 1995.

[7] S.J. Wheeler and D. Karube. State of the art report - constitutive modelling. In *Proceedings International Conference on Unsaturated soils, Paris*, volume 3, pages 1323–1356, 1995.

[8] D.G. Fredlund and N.R. Morgenstern. Stress state variables for unsaturated soils. *Journal of Geotechnical Engineering, ASCE*, 103(GT5):447–466, 1977.

[9] Y. Khogo. A consolidation analysis method for unsaturated soils coupled with an elasto-plastic model. In *Proceedings International Conference on Unsaturated Soils, Paris*, volume 2, pages 1085–1093, 1995.

[10] A. Modaressi, N. Abou-Bekr, and J.J. Fry. Unified approach to model partially saturated and saturated soil. In *Proceedings International Conference on Unsaturated Soils, Paris*, volume 3, 1995.

[11] G.T. Houlsby. The work input to an unsaturated granular material. *Géotechnique*, 47(1):193–196, 1997.

[12] J.H. Dudley. Review of collapsing soils. *Journal of SMFD Division, ASCE*, 96(SM3):925–947, 1970.

[13] V. Sivakumar. *A Critical State Framework for Unsaturated Soil.* PhD thesis, University of Sheffield, UK, 1993.

[14] A. Josa. *Un modelo elasto-plastico para suelos no saturados.* PhD thesis, Universitata Politecnica de Catalunya, Barcelona, Spain, 1988.

[15] I. Zakaria. *Yielding of unsaturated soil.* PhD thesis, University of Sheffield, UK, 1995.

[16] J.L. Justo, A. Delgado, and J. Ruiz. The influence of stress-path in the collapse-swelling of soils at the laboratory. In *Proceedings International Conference on Expansive Soils, Adelaide*, pages 67–71, 1984.

[17] V. Escario and J. Sáez. Measurement of the properties of swelling and collapsing soils under controlled suction. In *Proceedings International Conference on Expansive Soils, Haifa*, pages 195–200, 1973.

[18] Yudhbir. Collapsing behaviour of residual soils. In *Proceedings Southeast Asian Geotechnical Conference, Hong-Kong*, pages 915–930, 1982.

[19] E.E. Alonso, A. Gens, A. Lloret, and D.Q. Yang. Experimental behaviour of highly expansive double-structure clay. In *Proceedings International Conference on Unsaturated Soils, Paris*, volume 1, pages 11–16, 1995.

[20] P. Delage, M. Audiguier, Y. Cui, and M.D. Howat. Microstructure of compacted silt. *Canadian Geotechnical Journal*, 33:150–158, 1996.

[21] E.L. Matyas and H.S. Radhakrishna. Volume change characteristics partially saturated soils. *Géotechnique*, 18(4):432–448, 1968.

[22] A. Lloret and E.E. Alonso. State surfaces for partially saturated soils. In *Proceedings International Conference Soil Mechanics and Foundation Engineering, San Francisco*, volume 2, pages 557–562, 1985.

[23] D.G. Fredlund and N.R. Morgenstern. Constitutive relations for volume change in unsaturated soils. *Canadian Geotechnical Journal*, 13(3):261–273, 1976.

[24] D.G. Fredlund, N.R. Morgenstern, and R.A. Widger. The shear strength of unsaturated soils. *Canadian Geotechnical Journal*, 15(3):313–321, 1978.

[25] Massachusetts Institute of Technology. An instrument for the in situ measurement of the properties of soft clays. Technical Report No. 1 to U.S. Army Engineers Waterways Experimental Station, Vicksburg, Mississippi, The Soil Engineering Division, Department of Civil Engineering, Massachusetts Institute of Technology, USA, 1963. Contract No. DA-22-079-eng-288.

[26] A.W. Bishop, I. Alpan, G.E. Blight, and I.B. Donald. Factors controlling the strength of partly saturated cohesive soils. In *Research Conference on Shear Strength of Cohesive Soils, ASCE, Boulder, University of Colorado*, 1960.

[27] J.K.M. Gan, D.G. Fredlund, and H. Rahardjo. Determination of the shear strength parameters of an unsaturated soil using the direct shear test. *Canadian Geotechnical Journal*, 25:500–510, 1988.

[28] V. Escario and J. Sáez. The shear strength for partly saturated soils. *Géotechnique*, 36(3):453–456, 1986.

[29] V. Escario and J.F.T. Jucá. Strength and deformation of partly saturated soils. In *Proceedings International Conference Soil Mechanics and Foundation Engineering, Rio de Janeiro*, volume 1, pages 43–46, 1989.

[30] T.M.P. de Campos and C.W. Carrillo. Direct shear testing on an unsaturated soil from Rio de Janeiro. In *Proceedings International Conference on Unsaturated Soils, Paris*, volume 1, pages 31–38, 1995.

[31] E.E. Drumright and J.D. Nelson. The shear strength of unsaturated tailings sand. In *Proceedings International Conference on Unsaturated Soils, Paris*, volume 1, pages 45–50, 1995.

[32] S.A. Röhm and O.M. Vilar. Shear strength of an unsaturated sandy soil. In *Proceedings International Conference on Unsaturated Soils, Paris*, volume 1, pages 189–193, 1995.

[33] S.J. Wheeler and V. Sivakumar. Influence of compaction procedure on the mechanical behaviour of an unaturated compacted clay: shearing and constitutive modelling (part 2). Submitted for publication to Géotechnique.

[34] K.H. Roscoe and J.B. Burland. *Engineering plasticity.* CUP, Cambridge, UK, 1968. (eds. J. Heyman and F.A. Leckie).

[35] Y.J. Cui and P. Delage. Yielding and plastic behaviour of an unsaturated compacted silt. *Géotechnique*, 46(2):291–311, 1996.

[36] I. Zakaria, S.J. Wheeler, and W.F. Anderson. Yielding of unsaturated compacted kaolin. In *Proceedings International Conference on Unsaturated soils, Paris*, volume 1, pages 223–228, 1995.

[37] Y.J. Cui, P. Delage, and N. Sultan. An elasto-plastic model for compacted soils. In

Proceedings International Conference on Unsaturated Soils, Paris, volume 2, pages 703–709, 1995.

[38] S.J. Wheeler and V. Sivakumar. Critical state concepts for unsaturated soil. In *Proceedings International Conference Expansive Soils, Dallas*, volume 1, pages 167–172, 1992.

[39] S.J. Wheeler and V. Sivakumar. *Predictive soil mechanics.* Thomas Telford, London, UK, 1993. (eds. G.T. Houlsby and A.N. Schofield).

[40] A. Maatouk, S. Leroueil, and P. La Rochelle. Yielding and critical state of a collapsible unsaturated silty soil. *Géotechnique*, 45(3):465–477, 1995.

[41] A. Lloret, A. Gens, F. Batlle, and E.E. Alonso. Flow and deformation analysis of partially saturated soils. In *Proceedings European Conference Soil Mechanics and Foundation Engineering, Dublin*, volume 2, pages 565–568, 1987.

[42] E.E. Alonso, F. Batlle, A. Gens, and A. Lloret. Consolidation analysis of partially saturated soils. application to earthdam construction. In *Proceedings International Conference on Numerical Methods in Geomechanics, Innsbruck*, 1988.

[43] H.R. Thomas and Y. He. Modelling the behaviour of unsaturated soil using an elasto-plastic constitutive model. *Géotechnique*, 48(5):589–603, 1998.

[44] K. Nesnas and I.C. Pyrah. A two dimensional finite element consolidation model for unsaturated soil. In *Proceedings European Conference on Numerical Methods in Geotechnical Engineering, Udine*, pages 357–366, 1998.

[45] B. Gatmiri, S. Tavakoli, J. Moussavi, and P. Delage. Numerical approach of elasto-plastic consolidation of unsaturated soils. In *Proceedings International Conference on Unsaturated Soils, Paris*, volume 2, pages 1057–1064, 1995.

[46] A. Gens, J. Vaunat, and A. Ledesma. Analysis of hydration of an engineered barrier in a radioactive waste repository scheme using an elasto-plastic model. In *Proceedings*

International Conference on Unsaturated Soils, Paris, volume 2, pages 1065–1073, 1995.

[47] R.H. Brooks and A.T. Corey. Hydraulic properties of porous media. *Hydrol. Paper no.3, Civil Engineering Dep., Colorado State Univ., Fort Collins*, 1964.

[48] M.Th. van Genuchten. A closed-form equation for predicting the hydraulic conductivity of unsaturated soil. *Soil Sci. Soc. Am. J.*, 44:892–898, 1980.

[49] D.G. Fredlund and A. Xing. Equations for the soil-water characteristic curve. *Canadian Geotechnical Journal*, 31:521–532, 1994.

[50] S.L. Barbour. Nineteenth Canadian Geotechnical Colloquium: The soil-water characteristic curve: a historical perspective. *Canadian Geotechnical Journal*, 35, 1998.

[51] S.J. Wheeler. Inclusion of specific water volume within an elasto-plastic model for unsaturated soil. *Canadian Geotechnical Journal*, 33(1):42–57, 1996.

[52] D. Croney. The movement and distribution of water in soils. *Géotechnique*, 3(1):1–16, 1952.

[53] R.K. Schofield. The pf of the water in soil. In *Transactions 3rd International Congress Soil Science*, volume 2, pages 37–48, 1935.

[54] W.R. Gardner. Some steady state solutions of the unsaturated moisture flow equation with application to evaporation from a water table. *Soil Science*, 85:228–232, 1958.

[55] A.T. Corey. The interrelation between gas and oil relative permeabilities. *Producer's Monthly*, 19(1), 1954.

[56] D.G. Fredlund and H. Rahardjo. *Soil mechanics for unsaturated soils.* John Wiley & Sons, Inc., New York, 1993.

[57] D. Gallipoli, M. Karstunen, and S.J. Wheeler. Plane-strain modelling for unsaturated soil. In *Proceedings European Conference on Numerical Methods in Geotechnical Engineering, Udine*, pages 463–472, 1998.

[58] D. Gallipoli, M. Karstunen, and S.J. Wheeler. A note on modelling coupled flow-deformation in unsaturated soils. In *Proceedings International Symposium on Numerical Models in Geomechanics, Graz*, pages 255–262, 1999.

[59] G.E. Blight. Flow of air through soils. *Journal of Soil Mechanics and Foundation Engineering Division, ASCE*, 97(SM4):607–624, 1971.

[60] D.G. Fredlund, A. Xing, and S. Huang. Predicting the permeability function for unsatuarted soils using the soil-water characteristic curve. *Canadian Geotechnical Journal*, 31:533–546, 1994.

[61] N.T. Burdine. Relative permeability calculations from pore-size distribution data. *Petr. Trans., Am. Inst. Mining Metall. Eng.*, 198:71–77, 1953.

[62] Y. Mualem. A new model for predicting the hydraulic conductivity of unsaturated porous media. *Water Resources Research*, 12:513–522, 1976.

[63] D.G. Fredlund, A. Xing, M.D. Fredlund, and S.L. Barbour. The relationship of the unsaturated soil shear strength to the soil-water characteristic curve. *Canadian Geotechnical Journal*, 33:440–448, 1996.

[64] R. Horn, T. Baumgartl, W. Gräsle, and B.G. Richards. Stress induced changes of hydraulic properties in soils. In *Proceedings International Conference on Unsaturated Soils, Paris*, volume 1, pages 123–127, 1995.

[65] V. Sivakumar and S.J. Wheeler. Influence of compaction procedure on the mechanical behaviour of an unaturated compacted clay: wetting and isotropic compression (part 1). submitted for publication to Géotechnique.

[66] Femsys Limited, Leicester, UK. *FEMGV4, User Manual*, November 1996.

[67] S. Olivella. *Nonisothermal multiphase flow of brine and gas through saline media.* PhD thesis, Universitata Politecnica de Catalunya, Barcelona, Spain, 1988.

[68] D. Gawin, P. Baggio, and B.A. Schrefler. Coupled heat, water and gas flow in deformable porous media. *International Journal for Numerical Methods in Fluids*, 20:969–987, 1995.

[69] N.M. Safai and G.F. Pinder. Vertical and horizontal land deformation in a desaturating porous medium. *Advances Water Resources*, 2:19–25, 1979.

[70] R.H. Brooks and A.T. Corey. Properties of porous media affecting fluid flow. *Journal Irrig. Drain. Division, ASCE*, 92(IR2):61–68, 1966.

[71] H.R. Thomas and Y. He. Analysis of coupled heat, moisture and air transfer in a deformable unsaturated soil. *Géotechnique*, 45(4):677–689, 1995.

[72] B. Gatmiri and P. Delage. Nouvelle formulation de la surface d'état en indice des vides pour un modèle non linéaire élastique des sols non saturés–code u-dam. In *Proceedings International Conference on Unsaturated Soils, Paris*, volume 2, pages 1049–1056, 1995.

[73] K. Terzaghi. *Theoretical soil mechanics.* John Wiley & Sons, Inc., New York, 1943.

[74] J.R. Philip and D.A. de Vries. Moisture movement in porous materials under temperature gradients. *Transactions American Geophysical Union*, 38(2):222–232, 1957.

[75] D.A. de Vries. Simultaneous transfer of heat and moisture in porous media. *Transactions American Geophysical Union*, 39(5):909–916, 1958.

[76] D.A. Philip. The concept of diffusion applied to soil water. *Proceedings of the National Academy of Sciences of India*, 24A:93–104, 1955.

[77] S. Olivella, J. Carrera, A. Gens, and E.E. Alonso. Nonisothermal multhiphase flow of brine and gas through saline media. *Transport Porous Media*, 15:271–293, 1994.

[78] S. Panday and M.Y. Corapcioglu. Reservoir transport equations by compositional approach. *Transport Porous Media*, 4:369–393, 1989.

[79] R.W. Lewis and B.A. Schrefler. *The finite element method in the static and dynamic deformation and consolidation of porous media.* John Wiley & Sons, Ltd, Chichester, UK, 1998.

[80] S. Olivella, A. Gens, J. Carrera, and E.E. Alonso. Numerical formulation for a simulator (code-bright) for the coupled analysis of saline media. *Engineering Computations*, 13(7):87–112, 1996.

[81] M.A. Biot. General theory of three-dimensional consolidation. *Journal of Applied Physics*, 12:155–165, 1941.

[82] A. Ramesh. *Modelling the thermo/hydraulic/mechanical behaviour of unsaturated soil using an elasto-plastic constitutive relationship.* PhD thesis, University of Cardiff, UK, 1996.

[83] M.A. Celia, E.T. Bouloutas, and R.L. Zarba. A general mass-conservative numerical solution for the unsaturated flow equation. *Water Resources Research*, 26(7):1483–1496, 1990.

[84] D.R.J. Owen and E. Hinton. *Finite Elements in Plasticity: Theory and Practice.* Pineridge Press, Swansea, UK, 1980.

[85] J. M. M. C. Marques. Stress computation in elastoplasticity. *Engineering Computations*, 1:42–51, 1984.

[86] E. T. Bouloutas. *Improved numerical approximations for flow and transport in the unsaturated zone.* PhD thesis, Department Civil Engineering, Massachusetts Institute of Technology, 1989.

[87] M.B. Allen and C.L. Murphy. A finite-element collocation method for variably saturated flow in two space dimensions. *Water Resources Research*, 22(11):1537–1542, 1986.

[88] E. Hinton and J.S. Campbell. Local and global smoothing of discontinuous finite element functions using a least squares method. *International Journal for Numerical Methods in Engineering*, 8:461–480, 1974.

[89] I.C. Pyrah, W.F. Anderson, and R. Hashim. Finite difference simulation of cylindrical cavity expansion. In *Proceedings International Symposium on Numerical Models in Geomechanics, Montreal*, pages 661–668, 1997.

[90] M. Fahey and J.P. Carter. A finite-element study of the pressuremeter test in sand using a nonlinear elastic-plastic model. *Canadian Geotechnical Journal*, 30(2):348–362, 1993.

[91] G.T. Houlsby and J.P. Carter. The effects of pressuremeter geometry on the results of tests in clay. *Géotechnique*, 43(4):567–576, 1993.

[92] R. Zentar, G. Moulin, and P.Y. Hicher. Numerical analysis of pressuremeter test in soil. In *Proceedings European Conference on Numerical Methods in Geotechnical Engineering, Udine*, pages 593–600, 1998.

[93] V. Fioravante, M. Jamiolkowski, and R. Lancellotta. An analysis of pressuremeter holding test. *Géotechnique*, 44(2):227–238, 1994.

[94] M. Charles, H.S. Yu, and D. Sheng. Finite element analysis of pressuremeter tests using critical state soil models. In *Proceedings International Symposium on Numerical Models in Geomechanics, Graz*, pages 645–650, 1999.

[95] N.C. Consoli, F. Schnaid, and F.M. Mantaras. Numerical analysis of pressuremeter tests and its application to the design of shallow foundations. In *Proceedings International Workshop on Applications of Computational Mechanics in Geotechnical Engineering, Rio de Janeiro*, pages 25–34, 1997.

[96] F. Schnaid and G.F. da Silva. Ensaios presiométricos em um solo não saturado da região sul do Brasil. In *Anais Simpósio Brasileiro de Solos Não Saturados, Rio de Janeiro*, 1997.

[97] C.P. Wroth and J.M.O. Hughes. An instrument for the in situ measurement of the properties of soft clays. Technical Report CUED/D, Soils TR 13, University of Cambridge, UK, 1972.

[98] B.G. Clarke. *Pressuremeter in geotechnical design.* Blackie Academic & Professional, Glasgow, UK, 1995.

[99] M. Zytynski, M.F. Randolph, R. Nova, and C.P. Wroth. Short communication on modelling the unloading-reloading behaviour of soils. *International Journal for Numerical and Analytical Methods in Geomechanics*, 2:87–94, 1978.

[100] J. Jâky. Pressure in silos. In *Proceedings International Conference Soil Mechanics and Foundation Engineering*, volume 1, pages 103–107, 1948.

[101] H.S. Yu and G.T. Houlsby. Finite cavity expansion in dilatant soils: loading analysis. *Géotechnique*, 41(2):173–183, 1991.

[102] J. Vaunat, E. Romero, and C. Jommi. An elastoplastic hydro-mechanical model for unsaturated soils. In *Proceedings International Workshop on Unsaturated Soils: Experimental Evidence and Theoretical Approaches, Trento*, 2000.

[103] R.M. Buisson and S.J. Wheeler. The inclusion of hydraulic hysteresis in an alternative framework for unsaturated soils. In *Proceedings International Workshop on Unsaturated Soils: Experimental Evidence and Theoretical Approaches, Trento*, 2000.